FIGURE 4.1.5.2-55 TRANSONIC DRAG DUE TO LIFT
(a)   A TAN Λ_{LE} = 0
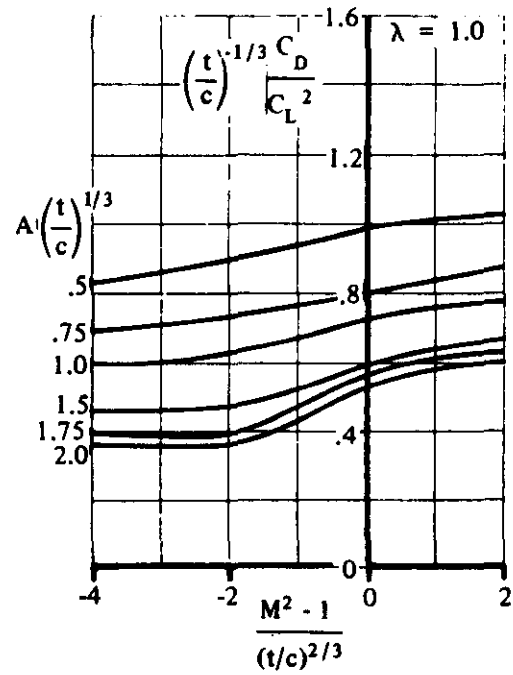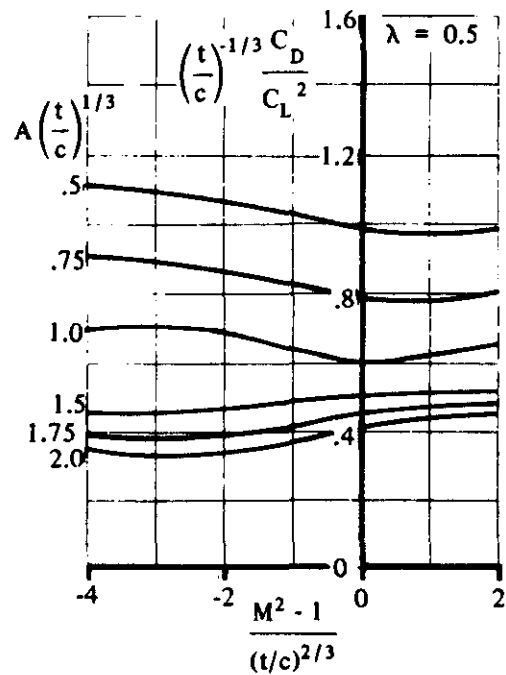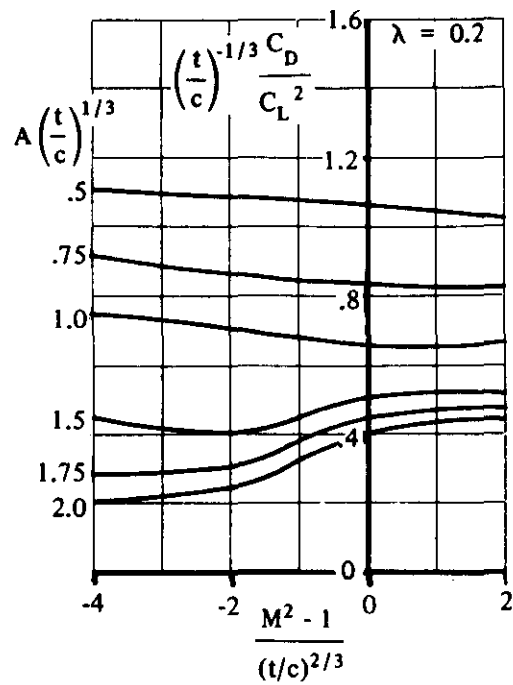
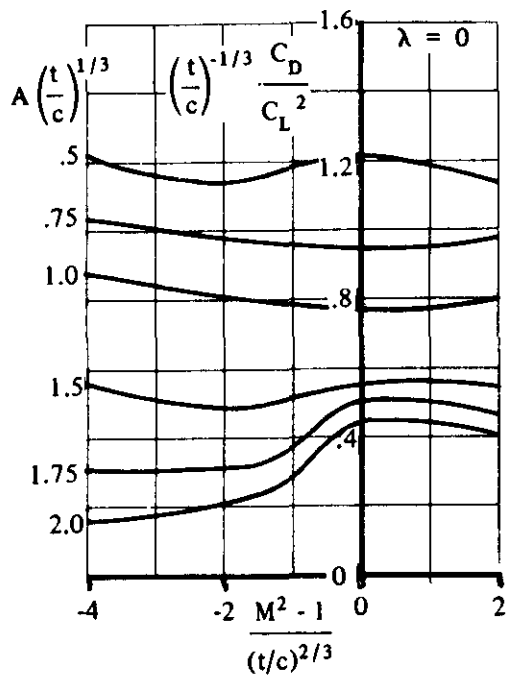FIGURE 4.1.5.2-55 (CONTD)

(b) A TAN Λ_{LE} = 3
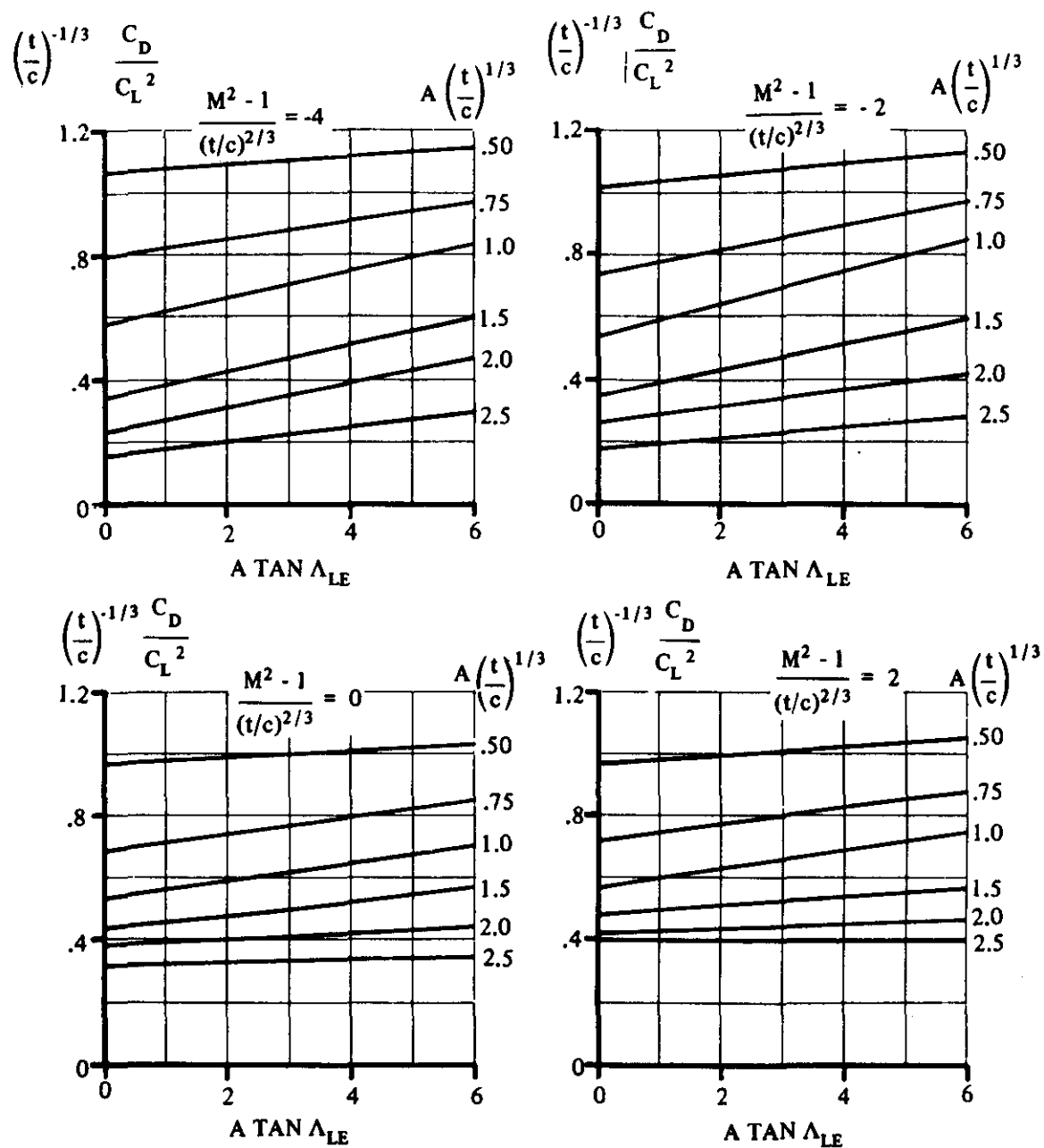
FIGURE 4.1.5.2-55 (CONTD)

(c)   TAPER RATIO, λ = 0.50

SUPERSONIC SPEEDS

$$\pi A \; \frac{C_{D_L}}{C_L{}^2} \; \frac{p}{1+p}$$

ROUND LEADING EDGES

SHARP LEADING EDGES

$\beta b_W/(2\ell)$
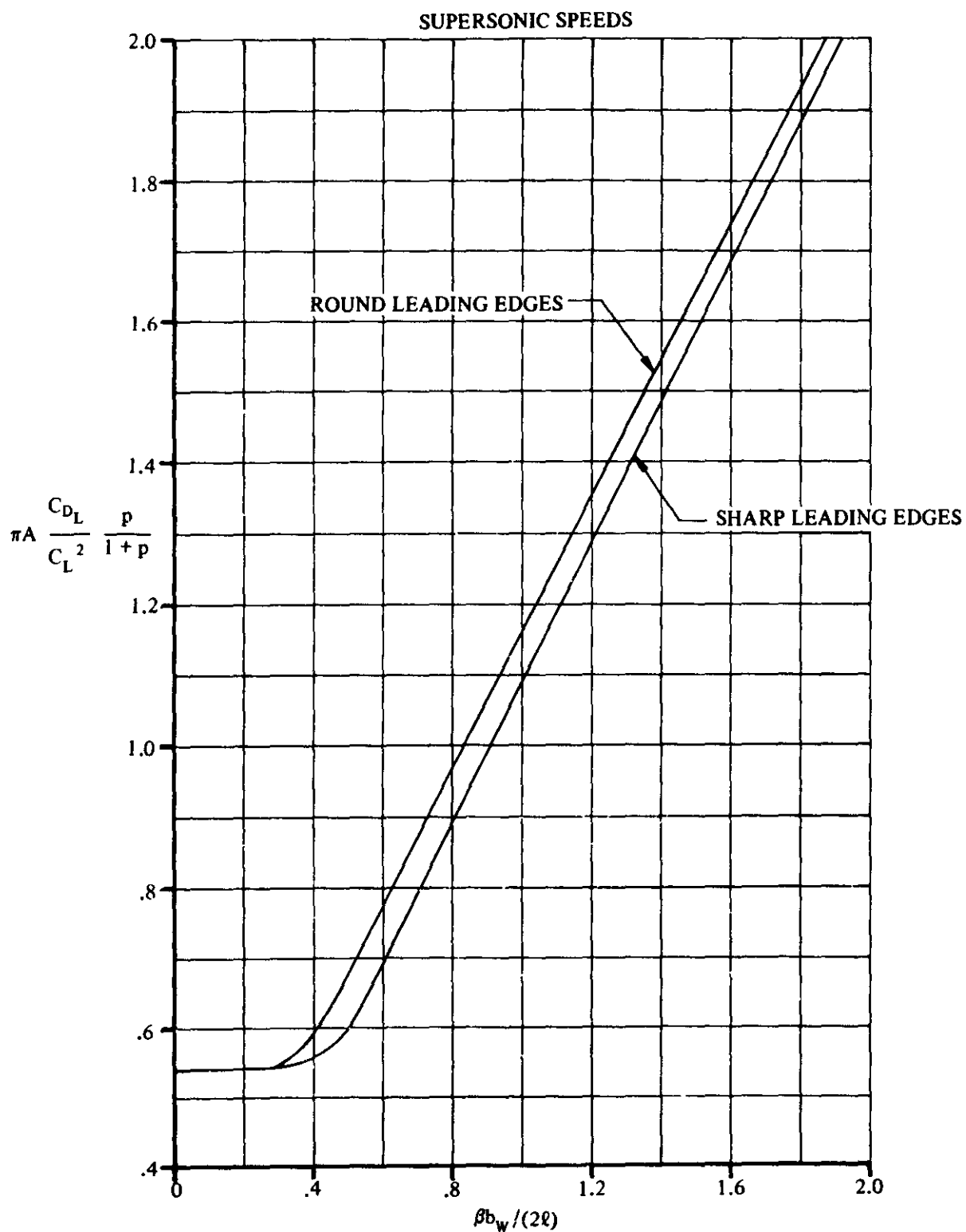
FIGURE 4.1.5.2-58 CORRELATION OF DRAG DUE TO LIFT OF STRAIGHT-TAPERED WINGS

SUPERSONIC SPEEDS

$\pi A \dfrac{C_{D_L}}{C_L^2} \dfrac{p}{1+p}$

$\beta b_w / (2\ell)$
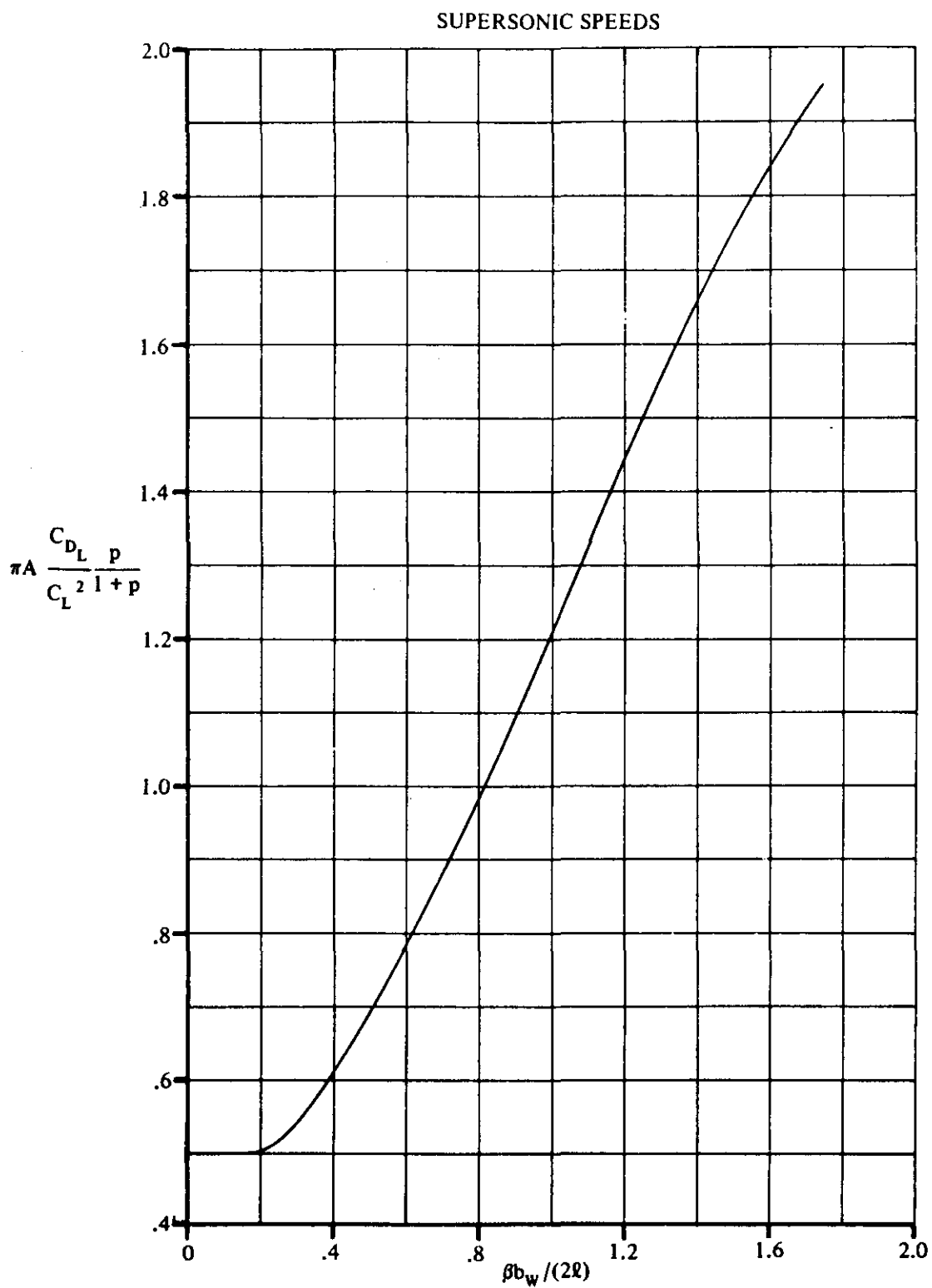
FIGURE 4.1.5.2-59 CORRELATION OF DRAG DUE TO LIFT OF COMPOSITE PLANFORMS

4.2 BODIES AT ANGLE OF ATTACK

4.2.1 BODY LIFT

4.2.1.1 BODY LIFT-CURVE SLOPE

A. SUBSONIC

One of the first attempts to use potential theory for the estimation of lift for bodies of revolution was made by Munk (reference 1). Several similar methods have since been developed that give essentially the same results (references 2 and 3). Potential theory is limited to angles of attack near zero, where viscous cross-flow forces are small. At higher angles of attack the viscous forces become increasingly important (see Section 4.2.1.2).

DATCOM METHOD

The method presented for estimating the lift-curve slope of bodies of revolution at subsonic speeds uses the potential flow term of the expression for body lift from reference 4. The lift-curve slope, based on $V_B^{2/3}$, is

$$C_{L_\alpha} = \frac{2(k_2 - k_1) S_o}{V_B^{2/3}} \quad \text{(per radian)} \qquad \text{4.2.1.1-a}$$

where

V_B is the total body volume.

$(k_2 - k_1)$ is the apparent mass factor developed by Munk and presented in figure 4.2.1.1-20a as a function of body fineness ratio.

S_o is the body cross-sectional area at x_o.

x_o is the body station where the flow ceases to be potential. This is a function of x_1, the body station where the parameter, dS_x/dx first reaches its maximum negative value. x_o and x_1 are correlated in figure 4.2.1.1-20b.

S_x is the body cross-sectional area at any body station.

In many cases it will be possible to determine the location of x_1 by inspection. For cases that are doubtful, the area distribution should be plotted and examined to determine the location where dS_x/dx first reaches its maximum negative value.

The lift-curve slopes of several bodies of revolution, calculated by this method, have been compared with test data in reference 4. In general, the accuracy of the method at angles of attack near zero is good.

For a rapid but approximate estimation, slender-body theory can be used. This gives $C_{L_\alpha} = 2$ per radian, where C_{L_α} is based on the body cross-sectional area at x_o.

No method is available for estimating the lift-curve slope of a body of noncircular cross section. Consequently, test data must be relied upon as the basis for predicting the lift-curve slope of such configurations. A summary of available test data on bodies of noncircular cross section at subsonic speeds is presented as table 4.2.1.1-A.

Sample Problem

Given: An ogive-cylinder-boattailed body of revolution of reference 18.

$$d = 0.417 \text{ ft} \qquad \ell_N = 2.19 \text{ ft} \qquad \ell_C = 1.98 \text{ ft} \qquad \ell_A = 1.12 \text{ ft}$$
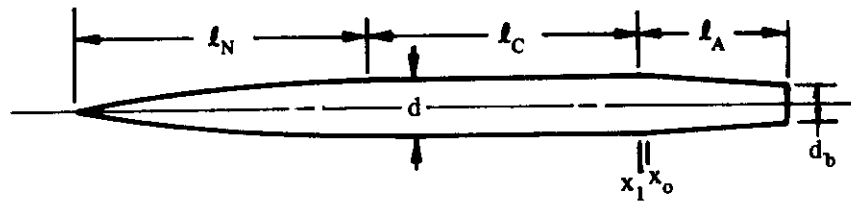
$$\ell_B = 5.29 \text{ ft} \qquad f = \frac{\ell_B}{d} = 12.7 \qquad V_B = 0.537 \text{ cu ft}$$

$$x_1 = 4.17 \text{ ft (determined by inspection)} \qquad d_b = 0.275 \text{ ft}$$

Compute:

$$x_1/\ell_B = 4.17/5.29 = 0.788$$

$$x_0/\ell_B = 0.793 \quad \text{(figure 4.2.1.1-20b)}$$

$$x_0 = (0.793)(5.29) = 4.195 \text{ ft}$$

$$(k_2 - k_1) = 0.96 \quad \text{(figure 4.2.1.1-20a)}$$

$$S_0 = 0.134 \text{ sq ft}$$

$$V_B^{2/3} = 0.537^{2/3} = 0.660$$

Solution:

$$C_{L_\alpha} = \frac{2(k_2 - k_1) S_0}{V_B^{2/3}} \quad \text{(equation 4.2.1.1-a)}$$

$$= \frac{2(0.96)(0.134)}{0.660}$$

$$= 0.390 \text{ per rad (based on } V_B^{2/3})$$

This compares with a test value of 0.378 per radian, based on $V_B^{2/3}$, from reference 18. The slender-body-theory approximation gives $C_{L_\alpha} = 0.406$ per radian, based on $V_B^{2/3}$.

B. TRANSONIC

Slender-body theory states that body force characteristics are not functions of Mach number. Experimental data substantially verify this result (references 5, 6, and 7). Any differences in the subsonic value of C_{L_α} obtained from paragraph A and the supersonic value of C_{L_α} obtained from paragraph C should be faired out smoothly in the transonic range.

Transonic test data on bodies of noncircular cross section are available in references 25, 26, and 5 (see table 4.2.1.1-A).

C. SUPERSONIC

Several theoretical methods that have been developed for estimating the lift-curve slope of bodies of revolution are best applied by machine methods. Three of the methods that can be used to estimate characteristics of simple nose-cylinder bodies of revolution at small angles of attack throughout the supersonic range are briefly discussed. They are the slender-body, hybrid, and second-order shock-expansion theories.

Slender-body theory is based on the assumption that the body surface slope (relative to the free stream) is everywhere so small that the boundary conditions may be applied on the axis. This condition is met if β/f_N is small, i.e., if the nose has a large fineness ratio or if the flow is close to sonic speed. Slender-body theory is applicable in the range of values of the parameter β/f_N from 0 to approximately 0.05. Hybrid theory (reference 8), a combination of a second-order axial solution with a first-order cross-flow solution, is applicable for values of β/f_N from approximately 0.05 to 0.40. The second-order shock-expansion method (reference 9), an extension of the general shock-expansion method at small angles of attack, is applicable for values of β/f_N from approximately 0.40 to ∞.

The flow around bodies with boattails can be calculated by Van Dyke's hybrid theory (reference 8). Reference 10 presents a generalized curve for estimating the normal-force-curve slope of boattails, based on the method of reference 8. Lavender and Deep (reference 11) give methods, based on the work of reference 9, for determining the normal-force-curve slope of cone-cylinder-frustums, cone-cylinder-frustum-boosters, and cone-frustum-boosters.

DATCOM METHOD

Empirical design charts are presented for estimating the normal-force-curve slope of bodies of revolution composed of ogival or conical noses and cylindrical afterbodies. In addition, theoretical results are presented for determining the increment in normal-force-curve slope due to the addition of either a boattailed or a flared body of revolution at the end of semi-infinite cylindrical bodies.

Figures 4.2.1.1-21a and 4.2.1.1-21b present C_{N_α}, based on maximum frontal area, for bodies with ogival and conical noses, respectively, and cylindrical afterbodies of varying fineness ratio. The normal-force-curve slopes of two other common nose shapes, the 3/4-power nose and the parabolic nose (1/2-power nose), are not presented directly. However, experimental data indicate that the force characteristics of cones and 3/4-power noses are similar, as are those of ogives and parabolic noses (reference 12). Tests also indicate that the addition of a cylindrical afterbody results in approximately the same increase in lift, irrespective of nose profile shape (reference 13). Therefore figure 4.2.1.1-21a can be used for parabolic-nose-cylinders and

figure 4.2.1.1-21b for 3/4-power-nose-cylinders with sufficient accuracy for most purposes.

The increments in normal-force-curve slope due to the addition of a boattailed or a flared body of revolution at the end of a semi-infinite cylindrical body are presented in figures 4.2.1.1-22a and 4.2.1.1-22b, respectively. Both of these increments are based on the cross-sectional area of the cylindrical body preceding the boattail or the flare. Figure 4.2.1.1-22a is taken from reference 10 and is based on the results of reference 8. Figure 4.2.1.1-22b is based on impact theory.

A comparison of test data with C_{N_α} of ogive-cylinder and cone-cylinder bodies calculated by this method is presented as table 4.2.1.1-B. The ranges of body geometry and Mach number of the test data are:

Cone-Cylinder					Ogive-Cylinder				
0	$\leqslant$	f_A	$\leqslant$	10.00	0	$\leqslant$	f_A	$\leqslant$	11.00
2.50	$\leqslant$	f_N	$\leqslant$	7.00	1.50	$\leqslant$	f_N	$\leqslant$	7.00
0	$\leqslant$	f_A/f_N	$\leqslant$	3.17	0	$\leqslant$	f_A/f_N	$\leqslant$	3.87
1.36	$\leqslant$	M	$\leqslant$	5.04	1.28	$\leqslant$	M	$\leqslant$	5.04

No method is available for estimating the lift-curve slope of a body of noncircular cross section. Consequently, test data must be relied upon as the basis for predicting the lift-curve slope of such configurations. A summary of available test data on bodies of noncircular cross section at supersonic speeds is presented as table 4.2.1.1-C.

Sample Problem

Given: The cone-cylinder-flare body of reference 27.
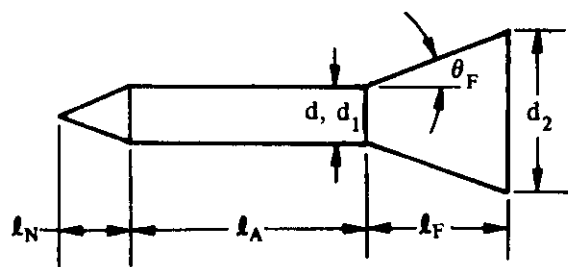
ℓ_N = 1.21 in. ℓ_A = 4.00 in. ℓ_F = 2.40 in.

d = d_1 = 1.0 in. d_2 = 2.75 in.

θ_F = 20°

M = 5.05; β = 4.95

Compute:

Cone-cylinder:

f_N = ℓ_N/d = 1.21

f_A = ℓ_A/d = 4.00

4.2.1.1-4

$$f_A/f_N \quad = 4.0/1.21 \quad = 3.31$$

$$f_N/\beta \quad = 1.21/4.95 \quad = 0.244$$

$C_{N_\alpha} = 3.52$ per rad (linear extrapolation, figure 4.2.1.1-21b)
(based on cone-cylinder maximum frontal area)

Flare:

$$d_2/d_1 \quad = 2.75$$

$$\frac{\left(\Delta C_{N_\alpha}\right)_F}{\cos^2 \theta_F} = 13.30 \quad \text{(figure 4.2.1.1-22b)}$$

$$\left(\Delta C_{N_\alpha}\right)_F = 13.30 \quad (\cos 20^\circ)^2$$

$$= 11.73 \quad \text{per rad} \left(\text{based on } \frac{\pi d_1^2}{4} = \text{cone-cylinder maximum frontal area}\right)$$

Solution:

$$C_{N_\alpha} \quad = C_{N_{\alpha_{\text{cone-cylinder}}}} + \left(\Delta C_{N_\alpha}\right)_F$$

$$= 3.52 + 11.73$$

$$= 15.25 \text{ per rad (based on cone-cylinder maximum frontal area)}$$

This compares with a test value of 17.70 per radian from reference 27.

D. HYPERSONIC

Newtonian impact theory is used for estimating the normal-force-curve slope of bodies of revolution at hypersonic Mach numbers. Newtonian theory assumes that the component of momentum normal to the surface is canceled on impact, thus giving rise to a normal force. The stagnation pressure predicted by Newtonian theory is about ten percent higher than the theoretical adiabatic pressure rise for an infinite Mach number. To correct this overestimation, a modified Newtonian method has been developed in which the assumptions of Newtonian flow are used, but the theoretical stagnation-pressure coefficient for the Mach number being considered is substituted for the Newtonian stagnation-pressure coefficient. Another modification of Newtonian theory considers the centrifugal forces in the flow around bodies of revolution (reference 14). This effect is small for conventional slender noses such as cones and ogives at moderate angles of attack, and the pressure forces on such slender noses are satisfactorily approximated by simple impact theory. For cylindrical afterbodies, inclusion of the effect of the centrifugal forces reduces the estimated normal-force-curve slope approximately ten percent.

Newtonian theory and its modifications are discussed in detail in reference 14. In this work Newtonian analysis is presented for an arbitrary body of revolution and the resulting forces on a cone and cylinder are given. In reference 15 a method of application of Newtonian concepts similar to that of reference 14 is presented. Reference 15 presents design charts which allow the aerodynamic characteristics of arbitrary

bodies of revolution to be obtained without the computation or radial integration of pressure distributions. In reference 16 the modified Newtonian approximation for the pressure distribution on bodies of revolution has been used to derive expressions for the aerodynamic characteristics at zero angle of attack for blunted cones, truncated cones, spherical segments, and rounded-shoulder cylinders. Approximate equations are also presented which may be used in conjunction with the design charts to obtain the zero angle-of-attack characteristics of composite missile components. The Datcom method uses the results of Newtonian impact theory presented in reference 17. This work presents design charts and equations for determining the aerodynamic characteristics of missile shapes composed of one or more cone frustums with or without a spherical nose. In addition, design charts are presented for the special cases of spherically blunted cones and ogives which can be used in conjunction with the results of reference 17.

DATCOM METHOD

The normal-force-curve slope of a body composed of one or more cone frustums with or without a spherical nose, a blunted conical nose, or a blunted ogival nose, based on the body base area, is given by

$$C_{N_\alpha} = \sum_{n=1}^{m} \left(C_{N_\alpha}\right)_n \left(\frac{d_n}{d_b}\right)^2 \qquad \text{4.2.1.1-b}$$

To apply equation 4.2.1.1-b the body is divided into m segments, the first segment being either a spherical nose, a blunted conical nose, a blunted ogival nose, or a cone frustum, and each succeeding segment a cone frustum. The normal-force-curve slope of a spherical nose, based on its base area, is obtained from figure 4.2.1.1-23. The normal-force-curve slope of a blunted conical or blunted ogival nose, based on their respective base areas, is obtained from figures 4.2.1.1-24 and 4.2.1.1-25, respectively. The normal-force-curve slope of a cone frustum, based on the base area of the specific segment, is obtained from figure 4.2.1.1-26. (Note that a cylinder is considered a cone frustum with $\theta = 0$ and $a/d = 1.0$, and that $C_{N_\alpha} = 0$ by Newtonian impact theory.) The ratio $(d_n/d_b)^2$ refers the normal-force-curve slope to the base area of the configuration.

It should be noted that the design charts used in this method are based on Newtonian theory with no modifications of the stagnation-pressure coefficient or the centrifugal forces.

Sample Problem

Given: Configuration 5115 of reference 45, consisting of a cone-cylinder-frustum body with a spherical nose.
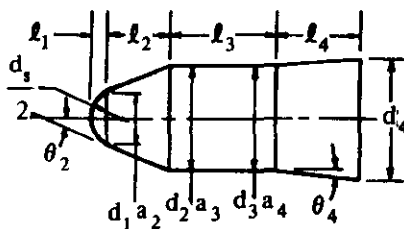
All dimensions in feet

Spherical Segment

$$\ell_1 = 0.18 \qquad \frac{d_s}{2} = 0.36 \qquad d_1 = 0.62$$

Forward Cone Frustum

$$a_2 = 0.62 \qquad d_2 = 1.20$$

$$\ell_2 = 0.72 \qquad \theta_2 = 22.5^\circ$$

Cylinder	Rear Cone Frustum
$a_3 = 1.20$	$a_4 = 1.20$
$\ell_3 = 1.20$	$\ell_4 = 0.96$
$d_3 = 1.20$	$d_4 = d_b = 1.368$
$\theta = 0$	$\theta_4 = 5°$

Compute:

Spherical Segment

$$2\ell_1/d_s = 0.18/0.36 = 0.50$$

$$\left(C_{N_\alpha}\right)_1 = 0.75 \text{ per rad (figure 4.2.1.1-23)} \left(\text{based on } \frac{\pi d_1^2}{4}\right)$$

Foreward Cone Frustum

$$a_2/d_2 = 0.62/1.20 = 0.517$$

$$\left(C_{N_\alpha}\right)_2 = 1.250 \text{ per rad (figure 4.2.1.1-26)} \left(\text{based on } \frac{\pi d_2^2}{4}\right)$$

Cylinder

$$a_3/d_3 = 1.20/1.20 = 1.00$$

$$\left(C_{N_\alpha}\right)_3 = 0 \quad \text{(figure 4.2.1.1-26)}$$

Rear Cone Frustum

$$a_4/d_4 = 1.20/1.368 = 0.877$$

$$\left(C_{N_\alpha}\right)_4 = 0.450 \text{ per rad (figure 4.2.1.1-26)} \left(\text{based on } \frac{\pi d_b^2}{4}\right)$$

Solution:

$$C_{N_\alpha} = \sum_{n=1}^{m} \left(C_{N_\alpha}\right)_n \left(\frac{d_n}{d_b}\right)^2 \quad \text{(equation 4.2.1.1-b)}$$

$$= \left(C_{N_\alpha}\right)_1 \left(\frac{d_1}{d_b}\right)^2 + \left(C_{N_\alpha}\right)_2 \left(\frac{d_2}{d_b}\right)^2 + \left(C_{N_\alpha}\right)_3 \left(\frac{d_3}{d_b}\right)^2 + \left(C_{N_\alpha}\right)_4 \left(\frac{d_4}{d_b}\right)^2$$

$$= (0.75)\left(\frac{0.62}{1.368}\right)^2 + (1.250)\left(\frac{1.20}{1.368}\right)^2 + (0)\left(\frac{d_3}{d_b}\right)^2 + (0.450)\left(\frac{1.368}{1.368}\right)^2$$

$$= 0.1540 + 0.9618 + 0 + 0.450$$

$$= 1.566 \text{ per rad } \left(\text{based on configuration base area } \frac{\pi d_b^2}{4}\right)$$

This compares with a test value of 1.719 per radian from reference 45 at a Mach number of 4.04.

REFERENCES

1. Munk, M. M.: The Aerodynamic Forces on Airship Hulls. NACA TR 184, 1924. (U)

2. Upson, R. H., and Klikoff, W. A.: Application of Practical Hydrodynamics to Airship Design. NACA TR 405, 1931. (U)

3. Laitone, E. V.: The Linearized Subsonic and Supersonic Flow About Inclined Bodies of Revolution. Jour. Aero. Sci., Vol. 14, No. 11, 1947. (U)

4. Hopkins, E. J.: A Semiempirical Method for Calculating the Pitching Moment of Bodies of Revolution at Low Mach Numbers. NACA RM A51C14, 1951. (U)

5. McDevitt, J. B., and Taylor, R. A.: Force and Pressure Measurements at Transonic Speeds for Several Bodies Having Elliptical Cross Sections. NACA TN 4362, 1958. (U)

6. McDevitt, J. B., and Taylor, R. A.: Pressure Distributions at Transonic Speeds for Slender Bodies Having Various Axial Locations of Maximum Diameter. NACA TN 4280, 1958. (U)

7. Taylor, R. A., and McDevitt, J. B.: Pressure Distributions at Transonic Speeds for Parabolic-Arc Bodies of Revolution Having Fineness Ratios of 10, 12, and 14. NACA TN 4234, 1958. (U)

8. Van Dyke, M.: First- and Second-order Theory of Supersonic Flow Past Bodies of Revolution. Jour. Aero. Sci., Vol. 18, No. 3, 1951. (U)

9. Syvertson, C. A., and Dennis, D. H.: A Second-Order Shock-Expansion Method Applicable to Bodies of Revolution Near Zero Lift. NACA TR 1328, 1957. (U)

10. Anon: Royal Aeronautical Society Data Sheets — Aerodynamics, Vol. IV (Bodies S.01.03.03), 1958. (U)

11. Lavender, R., and Deep, R.: Application of Second-Order Shock Expansion Theory to Several Types of Bodies of Revolution. Jour. Aero. Sci., Vol. 23, No. 11, 1956. (U)

12. Dennis, D. H., and Cunningham, B. E.: Forces and Moments on Pointed and Blunt-Nosed Bodies of Revolution at Mach Numbers From 2.75 to 5.00. NACA RM A52E22, 1952. (U)

13. Dennis, D. H., and Cunningham, B. E.: Forces and Moments on Inclined Bodies at Mach Numbers From 3.0 to 6.3. NACA RM A54E03, 1954. (U)

14. Grimminger, G., Williams, E. P., and Young, G. B. W.: Lift on Inclined Bodies of Revolution in Hypersonic Flow. Jour. Aero. Sci., Vol. 17, No. 11, 1950. (U)

15. Rainey, R. W.: Working Charts for Rapid Prediction of Force and Pressure Coefficients on Arbitrary Bodies of Revolution by Use of Newtonian Concepts. NASA TN D-176, 1959. (U)

16. Gray, J. D.: Drag and Stability Derivatives of Missile Components According to the Modified Newtonian Theory. AEDC-TN-60-191, 1960. (U)

17. Fisher, L. R.: Equations and Charts for Determining the Hypersonic Stability Derivatives of Combinations of Cone Frustums Computed by Newtonian Impact Theory. NASA TN D-149, 1959. (U)

18. Goodson, K. W.: Effect of Nose Length, Fuselage Length, and Nose Fineness Ratio on the Longitudinal Aerodynamic Characteristics of Two Complete Models at High Subsonic Speeds. NASA Memo 10-10-58L, 1958. (U)

19. Spencer, B., Jr., and Phillips, W. P.: Effects of Cross-Section Shape on the Low-Speed Aerodynamic Characteristics of a Low-Wave-Drag Hypersonic Body. NASA TN D-1963, 1963. (U)

20. Letko, W., and Williams, J. L.: Experimental Investigation at Low Speed of Effects of Fuselage Cross Section on Static Longitudinal and Lateral Stability Characteristics of Models Having 0° and 45° Swept-back Surfaces. NACA TN 3551, 1955. (U)

21. Jacobs, E. N., and Ward, K. E.: Interference of Wing and Fuselage From Tests of 209 Combinations in the NACA Variable-Density Tunnel. NACA TR 540, 1935. (U)

22. House, R. O., and Wallace, A. R.: Wind-Tunnel Investigation of Effect of Interference on Lateral-stability Characteristics of Four NACA 23012 Wings, an Elliptical and a Circular Fuselage and Vertical Fins. NACA TR 705, 1941. (U)

23. King, T. J., Jr.: Wind-Tunnel Investigation at High Subsonic Speeds of Some Effects of Fuselage Cross-Section Shape and Wing Height on the Static Longitudinal and Lateral Stability Characteristics of a Model Having a 45° Swept Wing. NACA RM L55J25, 1956. (U)

24. Sherman, A.: Interference of Wing and Fuselage From Tests of 30 Combinations With Triangular and Elliptical Fuselages in the NACA Variable-Density Tunnel. NACA TN 1272, 1947. (U)

25. Taylor, R. A.: Transonic Aerodynamic Characteristics of Several Bodies Having Elliptical Cross Sections and Various Plan Forms. NASA TN D-14, 1959. (U)

26. Spencer, B., Jr., and Phillips, W. P.: Transonic Aerodynamic Characteristics of a Series of Bodies Having Variations in Fineness Ratio and Cross-Sectional Ellipticity. NASA TN D-2622, 1965. (U)

27. Dennis, D. H., and Syvertson, C. A.: Effects of Boundary-Layer Separation on Normal Force and Center of Pressure of a Cone-Cylinder Model With a Large Base Flare at Mach Numbers From 3.0 to 6.28. NACA RM A55H09, 1955. (U)

28. Buford, W. E., and Shatunoff, S.: The Effects of Fineness Ratio and Mach Number on the Normal Force and Center of Pressure of Conical and Ogival Head Bodies. BRL MR 760, 1954. (U)

29. Delancey, L. M., Jaeger, B. F., and Schroedter, G. M.: The Aerodynamic Characteristics at Mach Number 4.24 of Bodies of Revolution With Varying Lengths and Head Shapes. NOTS TM 358, 1951. (U)

30. Ferri, A.: Supersonic-Tunnel Tests of Projectiles in Germany and Italy. NACA WR L-152, 1945. (U)

31. Walchner, O.: Systematic Wind-Tunnel Measurement on Missiles. NACA TM 1122, 1947. (U)

32. Delameter: Preliminary Analysis of Wind-Tunnel Test Data — First Daingerfield Wind-Tunnel Test Period Preliminary Report. Douglas SM 13256, 1948. (U)

33. Spencer, B., Jr., Phillips, W. P., and Fournier, R. H.: Supersonic Aerodynamic Characteristics of a Series of Bodies Having Variations in Fineness Ratio and Cross-Section Ellipticity. NASA TN D-2389, 1964. (U)

34. Jack, J. R., and Moskowitz, B.: Aerodynamic Characteristics of Two Flat-Bottomed Bodies at a Mach Number of 3.12. NACA RM E53L11b, 1954. (U)

35. Fuller, D. E., Shaw, D. S., and Wassum, D. L.: Effect of Cross-Section Shape on the Aerodynamic Characteristics of Bodies at Mach Numbers From 2.50 to 4.63. NASA TN D-1620, 1963. (U)

36. Lange, R. H., and Wittliff, C. E.: Force and Pressure-Distribution Measurements at a Mach Number of 3.12 of Slender Bodies Having Circular, Elliptical, and Triangular Cross Sections and the Same Longitudinal Distribution of Cross-Sectional Area. NACA RM L56D17, 1956. (U)

37. Jorgensen, L. H.: Inclined Bodies of Various Cross Sections at Supersonic Speeds. NASA Memo 10-3-58A, 1958. (U)

38. Rainey, R. W.: Investigation at Supersonic Speeds of the Effects of Bomb-Bay Configuration Upon the Aerodynamic Characteristics of Fuselages With Noncircular Cross Sections. NACA RM L56H20, 1956. (U)

39. Fuller, D. E., and Campbell, J. F.: Supersonic Lateral-Directional Stability Characteristics of 45° Swept Wing-Body-Tail Model With Various Cross-Sectional Shapes. NASA TN D-2376, 1964. (U)

40. Carlson, H. W., and Gapcynski, J. P.: An Experimental Investigation at a Mach Number of 2.01 of the Effects of Body Cross-Section Shape on the Aerodynamic Characteristics of Bodies and Wing-Body Combinations. NACA RM L55E23, 1955. (U)

41. Jorgensen, L. H.: Elliptic Cones Alone and With Wings at Supersonic Speeds. NACA TR 1376, 1958. (U)

42. Morris, O. A.: Aerodynamic Characteristics in Pitch at a Mach Number of 2.01 of Several Wing-Body Combinations With Wedge Shaped Bodies Located Above and Below at 54.5° Swept Delta Wing. NASA TN D-1823, 1963. (U)

43. Dryer, M., and Luidens, R. W.: Aerodynamic Characteristics of Several Flat-Bottom Configurations at Mach 3.0 and 3.5. NASA Memo 1-2-59E, 1959. (U)

44. Ridyard, H. W.: The Aerodynamic Characteristics of Two Series of Lifting Bodies at Mach Number 6.86. NACA RM L54C15, 1954. (U)

45. Henderson, J. H.: Effect of Nose Bluntness on Normal Force, Pitching Moment, and Center of Pressure on Cone-Cylinder and Cone-Cylinder-Frustum Bodies of Revolution at Mach Numbers of 1.50, 2.18, 2.81, and 4.04. Ordnance Missile Laboratories Redstone Arsenal Rpt. No. GR11F, 1958. (C) Title Unclassified

TABLE 4.2.1.1-A

SUMMARY OF EXPERIMENTAL DATA ON BODIES OF NONCIRCULAR CROSS SECTION

SUBSONIC SPEEDS

Ref.	Nose Shape	Body Cross Section	Afterbody Cross Section	S_b (sq in.)	ℓ_B (in.)	$x_{c.g.}$	w (in.)	h (in.)	p (in.)	c (in.)	ℓ_N (in.)	$f_{N_{equiv}}$	M
19	Ogival Ellipsoid	Horizontal Ellipse	None	18.06	48.0	0.667	5.37	4.29	15.27	2.15	48.0	10.0	0.40
				18.10			5.88	3.92	15.71	1.96			
				18.08			6.79	3.39	16.84	1.70			
				18.12			7.59	3.04	18.16	1.52			
		Vertical Ellipse		18.12			3.04	7.59	18.16	3.79			
				18.08			3.39	6.79	16.84	3.39			
				18.10			3.92	5.88	15.71	2.94			
				18.06			4.29	5.37	15.27	2.68			
20	Ogival Ellipsoid	Square	Square	28.27	45.0	0.533	5.40	5.40	19.88	2.70	18.0	8.33	0.13
						0.565							
		Deep Rectangle	Deep Rectangle			0.533	4.00	7.28	20.84	3.64		8.34	
						0.565							
	Ogival	Shallow Rectangle	Shallow Rectangle			0.533	7.28	4.00		2.00			
						0.565							
21	Rounded	Deep Rectangle	Deep Rectangle	9.29	20.16	see ref.	2.70	3.44	12.28	1.72	8.0	5.86	Low Speed
22	Round	Ellipse	Ellipse	37.17	40.31	0.322	5.20	9.10	23.29	4.55	16.3	5.86	0.107
23	Ogival	Semicircle +Rectangle	Semicircle +Rectangle	22.20	54.72	0.571	5.00	5.00	17.65	2.27	17.8	10.1	0.80– 0.92
		Square	Square	24.90					19.60	2.50		9.8	
24	Rounded	Triangle	Triangle	9.29	20.16	see ref.	3.85	3.60	13.23	1.28	8.0	5.24	Low Speed
		Inverted Triangle	Inverted Triangle							2.56			
		Vertical Ellipse	Vertical Ellipse				2.60	4.55	11.62	2.275		5.86	
		Horizontal Ellipse	Horizontal Ellipse				4.55	2.60		1.30			

TABLE 4.2.1.1-A (CONTD)

Ref.	Nose Shape	Body Cross Section	Afterbody Cross Section	S_b (sq in.)	ℓ_B (in.)	$x_{c.g.}$	w (in.)	h (in.)	p (in.)	c (in.)	N (in.)	$f_{N_{equiv}}$	M
25	Ogival Ellipsoid	Ellipse	Ellipse	28.2	61.45	0.50	10.39	3.46	24.30	1.73	36.0	10.24	0.40–1.2
					41.60	0.65						6.93	
				28.3	61.45	0.50	12.00	3.00	27.46	1.50		10.24	
					51.60	0.60						8.60	
					41.60	0.65						6.93	
	Ogival	Circular Segment	Circular Segment	25.1	61.45	0.50	12.00	3.00	25.90	1.50	36.0	10.0	
					51.60	0.60						8.6	
					41.60	0.65						6.9	
26	Ogival Ellipsoid	Horizontal Ellipse	None	12.56	12.00	0.667	4.99	3.27	18.49	1.63	12.0	3.0	0.4–1.4
							5.66	2.83	18.87	1.41			
		Vertical Ellipse					2.83	5.66	18.87	2.83			
		Horizontal Ellipse			20.00		4.99	3.27	18.49	1.63	20.0	5.0	
							5.66	2.83	18.87	1.41			
		Vertical Ellipse					2.83	5.66	18.87	2.83			
		Horizontal Ellipse			28.00		4.99	3.27	18.49	1.63	36.0	10.24	
							5.66	2.83	18.87	1.41			
		Vertical Ellipse					2.83	5.66	18.87	2.83			
5	Ogival Ellipsoid	Vertical Ellipse	Vertical Ellipse	28.3	61.45	—	4.90	7.35	18.62	3.68	36.0	10.24	0.8–1.2
						—	4.24	8.48	21.06	4.24			
						—	3.46	10.38	24.30	5.19			

S_b	maximum cross-section area	p	body cross-section perimeter
ℓ_B	body length	c	distance from body cross-section (max) centroid to bottom of section
$x_{c.g.}$	location of moment reference center from body nose (body lengths)	ℓ_N	nose length
w	body cross-section breadth		
h	body cross-section height	$f_{N_{equiv}}$	equivalent fineness ratio $= \dfrac{\ell_B}{d_{equiv}}$

$$\text{where } d_{equiv} = \sqrt{\frac{\text{cross-section area}}{0.7854}}$$

TABLE 4.2.1.1-B

SUPERSONIC NORMAL-FORCE-CURVE SLOPE OF CONE-CYLINDER
AND OGIVE-CYLINDER BODIES
DATA SUMMARY AND SUBSTANTIATION

Ref.	Nose Shape	M	f_N	f_N	C_{N_α} Calc. (per rad)	C_{N_α} Test (per Rad)	e Percent Error
28	Conical	1.36	2.84	0	1.98	1.79	10.6
				0.24	2.10	1.95	7.7
				0.50	2.22	2.17	2.3
				0.75	2.38	2.34	1.7
				1.66	2.66	2.58	3.1
				2.00	2.70	2.60	3.8
				3.00	2.75	2.58	6.6
				4.00	2.78	2.45	13.5
		1.72		0	1.92	1.78	7.9
				0.50	2.18	2.22	− 1.8
				0.75	2.34	2.38	− 1.7
				1.66	2.68	2.61	2.7
				3.00	2.83	2.60	8.8
				5.00	2.94	2.58	14.0
		3.02		0	1.85	1.83	1.1
				1.66	2.56	2.75	− 6.9
				5.00	3.20	3.27	− 2.1
				7.00	3.28	3.27	0.3
				9.00	3.33	3.20	4.1
		3.55		0	1.85	1.91	− 3.1
				0.24	1.95	1.99	− 2.0
				1.66	2.54	2.76	− 8.0
				4.00	3.10	3.19	− 2.8
				5.00	3.20	3.28	− 2.4
				7.00	3.32	3.43	− 3.2
				9.00	3.37	3.50	− 3.7
		4.00		0	1.85	1.83	1.1
				0.75	2.16	2.23	− 3.1
				2.00	2.64	2.69	− 1.9
				3.00	2.94	2.98	− 1.3
				7.00	3.34	3.32	0.6
13	Conical	3.01	3.00	2.00	2.67	2.82	− 5.3
				4.00	3.10	2.89	7.3
				7.00	3.28	3.10	5.8
			5.00	0	1.89	1.89	0
				2.00	2.55	2.42	5.4
				5.00	2.86	2.48	15.3
			7.00	0	1.95	1.89	3.2
				3.00	2.61	2.65	− 1.5
	3/4 Power	3.01	5.00	2.00	2.55	2.42	5.4
				5.00	2.86	2.56	11.7
	Conical	3.49	3.00	7.00	3.28	3.32	− 1.2
			5.00	5.00	2.89	2.93	− 1.4
			7.00	3.00	2.60	2.73	− 4.8
		4.24	3.00	4.00	3.08	2.80	10.0
				7.00	3.32	3.27	1.5
			5.00	2.00	2.46	2.40	2.5
				5.00	2.93	2.58	9.8
			7.00	0	1.88	1.95	− 3.6
				3.00	2.57	2.29	12.2
		5.04	3.00	2.00	2.61	2.70	− 3.3
				4.00	3.05	2.65	15.1
				7.00	3.35	3.28	2.1

TABLE 4.2.1.1-8 (CONTD)

Ref.	Nose Shape	M	f_N	f_A	C_{N_α} Calc. (per rad)	C_{N_α} Test (per Rad)	e Percent Error
13	Conical	5.04	5.00	0	1.85	2.09	−11.5
				2.00	2.38	2.70	−11.9
				5.00	2.93	2.93	0
			7.00	0	1.85	1.94	− 4.6
				3.00	2.53	2.26	11.9
	3/4 Power	5.04	5.00	2.00	2.38	2.38	0
				5.00	2.93	2.76	6.2
12	Conical	3.49	3.00	0	1.85	1.72	7.6
			5.00	0	1.85	1.79	3.4
		4.01	3.00	0	1.85	1.78	3.9
			4.00	0	1.85	2.07	−10.6
			5.00	0	1.85	1.67	10.8
			7.00	0	1.89	1.99	− 5.0
		5.00	3.00	0	1.85	2.15	−14.0
			4.00	0	1.85	1.84	0.5
			5.00	0	1.85	1.63	13.5
			7.00	0	1.85	2.22	−16.7
29	Conical	4.00	4.00	10.00	3.28	3.37	− 2.7
30	Conical	1.72	2.50	2.50	2.67	3.25	−17.8
		1.99			2.66	3.32	−19.9
		2.64			3.58	3.48	2.9
		3.06			3.53	3.49	1.1
28	Ogival	1.36	2.84	0	2.51	2.41	4.1
				0.24	2.56	2.41	6.2
				0.50	2.60	2.58	0.8
				0.75	2.65	2.61	1.5
				1.00	2.70	2.58	4.7
				1.66	2.72	2.61	4.2
				4.00	2.73	2.58	5.8
		1.72		0	2.47	2.46	0.4
				0.24	2.53	2.52	0.4
				0.50	2.58	2.69	− 4.1
				1.00	2.72	2.75	− 1.1
				1.66	2.79	2.81	− 0.7
				2.00	2.80	2.81	− 0.4
				3.00	2.82	2.81	0.4
				5.00	2.88	2.81	2.5
		3.02		0	2.23	2.46	− 9.3
				0.50	2.42	2.51	− 3.6
				1.66	2.81	3.01	− 6.6
				3.00	3.03	3.38	−10.4
				5.00	3.20	3.38	− 5.3
				7.00	3.30	3.39	− 2.7
				9.00	3.36 extrap	3.21	4.7
				11.00	−	3.38	−
		3.55		0	2.12	2.21	− 4.1
				0.24	2.22	2.26	− 1.8
				0.50	2.32	2.28	1.8
				1.66	2.75	2.70	1.9
				3.00	2.99	3.20	− 6.6
				5.00	3.20	3.27	− 2.1
				7.00	3.31	3.29	0.6
				9.00	3.37	3.32	1.5
		4.00		0	2.04	2.17	− 6.0
				0.75	2.36	2.52	− 6.3
				1.66	2.67	2.81	− 5.0
				2.00	2.76	2.87	− 3.8

TABLE 4.2.1.1-B (CONTD)

Ref.	Nose Shape	M	f_N	f_A	C_{N_α} Calc. (per rad)	C_{N_α} Test (per Rad)	e Percent Error
28	Ogival	4.00	2.84	3.00	2.93	3.04	− 3.6
				4.00	3.07	3.15	− 2.5
				5.00	3.20	3.21	− 0.3
				7.00	3.26	3.44	− 5.2
				9.00	3.30	3.59	− 8.1
13	Ogive	3.01	5.00	2.00	2.76	2.72	1.5
				5.00	2.87	2.89	− 0.7
	Parabola			2.00	2.76	2.62	5.3
				5.00	2.87	2.60	10.4
	Ogive	5.04		2.00	2.70	2.63	2.7
				5.00	3.02	3.00	0.7
	Parabola			2.00	2.70	2.28	18.4
	Ogive	4.01	3.00	0	2.08	2.04	2.0
			5.00	0	2.35	2.25	4.4
			7.00	0	2.44	2.61	− 6.5
			5.00	3.00	0	1.94	1.93	0.5
			5.00	0	2.24	2.11	6.2
			7.00	0	2.39	2.13	12.2
29	Ogival	4.24	2.50	7.50	3.11	3.15	− 1.3
			3.50	6.50	3.22	3.12	3.2
				10.50	3.38	3.56	− 5.1
			4.00	10.00	3.30	3.40	− 2.9
30	Ogival	1.72	2.50	2.50	2.86	3.02	− 5.3
			1.50		3.16	3.11	1.6
			3.00		2.80	2.89	− 3.1
		1.28	1.50		2.92	2.93	− 0.3
		1.99	2.50		2.93	3.32	−11.7
			1.50		3.20	3.19	0.3
			3.00		2.85	3.07	− 7.2
			3.50		2.79	2.41	15.8
		2.64	2.50		3.02	3.44	−12.2
			3.00		2.93	3.27	−20.2
			3.50		2.86	3.41	−16.1
		3.06	2.50		3.00	3.52	−14.8
			3.00		2.96	3.24	− 8.6
			3.50		2.88	3.52	−18.2
31	Ogival	1.28	3.50	1.50	2.72	2.76	− 1.4
			2.50	2.50	2.70	2.90	− 6.9
		1.72	3.50	1.50	2.76	2.93	− 5.8
			2.50	2.50	2.87	3.15	− 8.9
		1.99	1.50	3.50	3.30	3.45	− 4.3
			3.50	1.50	2.76	3.00	− 8.0
			2.50	1.50	2.76	3.04	− 9.2
			2.50	2.50	2.94	3.24	− 9.3
			3.50	1.50	2.77	3.00	− 7.7
		3.06	3.50	1.50	2.75	2.95	− 6.8
			2.50	2.50	3.00	3.15	− 4.8
32	Ogival	1.73	6.25	9.45	2.62	2.49	5.2
		2.00			2.68	2.57	4.3

Average Error $= \dfrac{\Sigma \,|e|}{n} = 5.55\%$

Cone-Cylinder 5.9%

Ogive-Cylinder 5.3%

TABLE 4.2.1.1-C

SUMMARY OF EXPERIMENTAL DATA ON BODIES OF NONCIRCULAR CROSS SECTION
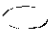
SUPERSONIC SPEEDS
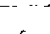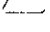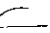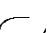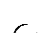
Ref.	Nose Shape	Body Cross Section	Afterbody Cross Section	S_b (sq in.)	l_B (in.)	$x_{c.g.}$	w (in.)	h (in.)	p (in.)	c (in.)	l_N (in.)	$f_{N_{equiv}}$	M
33	Ogival Ellipsoid	Horizontal Ellipse	None	12.56	12.00	0.667	4.90	3.27	18.49	1.63	12.00	3.0	1.5–2.86
							5.66	2.83	18.87	1.41			
		Vertical Ellipse					2.83	5.66	18.87	2.83			
		Horizontal Ellipse			20.00		4.90	3.27	18.49	1.63	20.00	5.0	
							5.66	2.83	18.87	1.41			
		Vertical Ellipse					2.83	5.66	18.87	2.83			
		Horizontal Ellipse			28.00		4.90	3.27	18.49	1.63	28.00	7.0	
							5.66	2.83	18.87	1.41			
		Vertical Ellipse					2.83	5.66	18.87	2.83			
34	Semicirc. Cone	Semicircle	Semicircle	1.20	21.00	see rpt.	1.75	0.875	4.50	0.371	11.50	17.0	3.12
	Semiellip. Cone	Semiellipse	Semiellipse	2.40			3.50		7.50			12.0	
35	Cone	Triangle	Triangle	12.44	40.00	0.500	4.48	4.08	13.62	1.36	13.33	10.0	2.5–4.63
		Inverted Triangle	Inverted Triangle							2.72			
		Horizontal Ellipse	Horizontal Ellipse	12.57			4.90	3.27	13.08	1.63			
							5.66	3.83	14.05	1.41			
		Vertical Ellipse	Vertical Ellipse				2.83	5.66		2.83			
	Semicone	Semiellipse	Semiellipse				6.93	2.31	16.18	0.98			
		Inverted Semiellipse	Inverted Semiellipse							1.33			
36	Ogival	Horizontal Ellipse	Horizontal Ellipse	1.13	14.65	see rpt.	1.70	0.87	4.22	4.25	9.00	12.2	3.12
		Vertical Ellipse	Vertical Ellipse				0.87	1.70		0.85			
		Triangle	Triangle				1.23	1.28	4.00	0.50			
37	Ogival	Horizontal Ellipse	Horizontal Ellipse	1.54	14.00	see rpt.	1.71	1.14	4.57	0.571	4.20	10.0	1.98, 3.88
		Vertical Ellipse	Vertical Ellipse				1.14	1.71		0.857			
		Horizontal Ellipse	Horizontal Ellipse				1.98	0.99	4.92	0.495			

TABLE 4.2.1.1-C (CONTD)
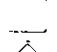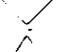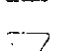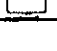
Ref.	Nose Shape	Body Cross Section		Afterbody Cross Section	S_b (sq in.)	l_B (in.)	$x_{c.g.}$	w (in.)	h (in.)	p (in.)	c (in.)	l_N (in.)	$t_{N_{equiv}}$	M
37	Ogival		Vertical Ellipse	Vertical Ellipse	1.54	14.00	see rpt.	0.99	1.98	4.92	0.990	4.20	10.0	1.98, 3.88
			Square	Square				1.24	1.24	4.93	0.620			
			Diamond	Diamond				1.75	1.75		0.875			
			Triangle	Triangle				1.89	1.63	5.60	0.544			
			Inverted Triangle	Inverted Triangle							1.090			
			Horizontal Ellipse	Horizontal Ellipse		8.40		1.98	0.99	4.92	0.495		6.0	
			Vertical Ellipse	Vertical Ellipse				0.99	1.98		0.990			
38	Cone		Horizontal Ellipse	Horizontal Ellipse	0.503	8.00	0.500	1.13	0.57	2.81	0.283	1.701	10.0	1.62– 2.40
			Vertical Ellipse	Vertical Ellipse				0.57	1.13		0.566			
			Triangle	Triangle										
			Teardrop	Teardrop				0.71	0.95	2.45	0.446			
39	Ogival Cone		Circle	Circle	9.62	39.10	0.454	3.50	3.50	11.00	1.75	12.25	11.17	1.41, 2.20
	Ogival Ellipsoid		Ellipse	Ellipse	14.43				5.26	13.98	2.63		9.09	
	Ogival		Flat-Bottom Teardrop	Flat-Bottom Teardrop	13.02				4.38	13.56	1.98		9.61	
			Triangle	Triangle	14.50			4.90	4.42	12.40	1.47		9.09	
			Inverted Triangle	Inverted Triangle							2.95			
40	Ogival		Horizontal Ellipse	Horizontal Ellipse	12.60	42.00	0.697	4.90	3.27	12.94	1.64	14.00	10.50	2.01
			Diamond	Diamond				4.46	4.46	13.12	2.23			
			Triangle	Triangle				4.50	4.10	13.74	1.64			
			Inverted Triangle	Inverted Triangle							2.47			
			Tent	Tent				3.60	4.17	13.14	1.85			
			Inverted Tent	Inverted Tent							2.32			
			Square	Square				3.62	3.62	13.12	1.81			

TABLE 4.2.1.1-C (CONTD)
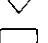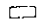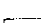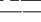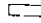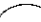
Ref.	Nose Shape	Body Cross Section		Afterbody Cross Section	S_b (sq in.)	ℓ_B (in.)	$x_{c.g.}$	w (in.)	h (in.)	p (in.)	c (in.)	ℓ_N (in.)	$f_{N_{equiv}}$	M
40	Ogival		90° Teardrop	90° Teardrop	12.60	42.00	0.697	3.89	4.37	12.73	2.02	14.00	10.50	2.01
			Inverted 90° Teardrop	Inverted 90°Teardrop				↓	↓	↓	2.36			
			45° Teardrop	45° Teardrop				3.49	5.02	13.60	2.16			
			Inverted 45° Teardrop	Inverted 45° Teardrop				↓	↓	↓	2.86			
			Vertical Ellipse	Vertical Ellipse				3.27	4.90	12.94	2.45			
			Horizontal Ellipse	Horizontal Ellipse				4.90	3.27	↓	1.64			
			Diamond	Diamond				4.46	4.46	13.12	2.23			
			Triangle	Triangle				4.50	4.10	13.74	1.64			
			Inverted Triangle	Inverted Triangle				↓	↓	↓	2.47			
			Tent	Tent				3.60	4.17	13.14	1.85			
			Inverted Tent	Inverted Tent				3.16	↓	↓	2.32			
			Square	Square				3.62	3.62	13.12	1.81			
			90° Teardrop	90° Teardrop				3.90	4.37	12.73	2.02			
			Inverted 90° Teardrop	Inverted 90° Teardrop				↓	↓	↓	2.36			
			45° Teardrop	45° Teardrop				3.50	5.02	13.60	2.16			
			Inverted 45° Teardrop	Inverted 45° Teardrop				↓	↓	↓	2.86			
			Vertical Ellipse	Vertical Ellipse	↓	↓	↓	3.27	4.90	12.94	2.45	↓	↓	↓
41	Pointed Ellipsoid		Vertical Ellipse	None	5.73	9.90	see rpt.	2.20	3.29	8.80	1.65	9.90	3.67	1.97, 2.94
								1.57	4.70	11.00	2.35			
						↓		1.10	6.59	14.83	3.29	↓	↓	
						13.50		2.20	3.29	8.80	1.65	13.50	5.00	
			Horizontal Ellipse			9.90		3.29	2.20	↓	1.10	9.90	3.67	
								4.70	1.57	11.00	0.78			
								6.59	1.10	14.83	0.55			

TABLE 4.2.1.1-C (CONTD)

Ref.	Nose Shape	Body Cross Section		Afterbody Cross Section	S_b (sq in.)	ℓ_B (in.)	$x_{c.g.}$	w (in.)	h (in.)	ρ (in.)	c (in.)	ℓ_N (in.)	$f_{N_{equiv}}$	M
42	Wedge		Rectangle	None	2.80	18.32	see rpt.	2.24	1.25	6.98	0.63	18.32	10.95	2.01
					4.82				2.15	8.78	1.08		8.35	
					3.39			3.85	0.88	9.46	0.44		9.95	
					4.81				1.25	10.20	0.63		8.35	
					6.35				1.65	11.00	0.83		7.27	
					4.82			5.84	0.88	12.72	0.44		8.34	
					6.85				1.25	13.46	0.63		7.00	
				Rectangle	2.69			2.15		6.80		10.22	11.18	
						22.38							13.65	
						26.34							16.13	
					3.59			2.87		8.25			13.95	
43	Conical Duck Bill		Modified Semiellipse	Modified Semiellipse	1.73	17.25	0.584	2.94	1.00	see rpt.	see rpt.	7.12	23.3	3.0
						16.95	0.576					6.93	22.9	
					2.33								19.7	
					1.73		0.569						22.9	
	Conical				102.0	198.1	0.526	21.48	5.52			64.6	34.75	3.0, 3.5
44	Conical Upper Surf		Semicircle on Rectangle	Semicircle on Rectangle	0.50	8.80	see rpt.	0.75	0.75	2.68	0.361	4.3	11.7	6.86
	Cylindrical Upper Surf				1.06			1.50		4.18			8.3	

S_b	maximum cross-section area	p	body cross-section perimeter
ℓ_B	body length	c	distance from body cross-section (max) centroid to bottom of section
$x_{c.g.}$	location of moment reference center from body nose (body lengths)	ℓ_N	nose length
w	body cross-section breadth		
h	body cross-section height	$f_{N_{equiv}}$	equivalent fineness ratio $= \dfrac{\ell_B}{d_{equiv}}$

$$\text{where } d_{equiv} = \sqrt{\frac{\text{cross-section area}}{0.7854}}$$

SUBSONIC SPEEDS
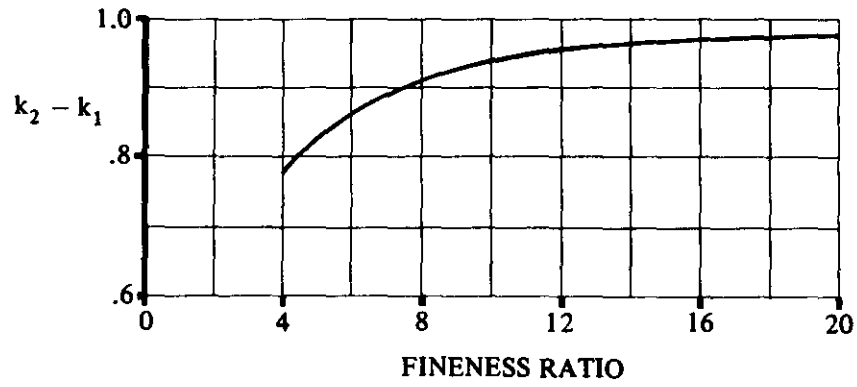
FIGURE 4.2.1.1-20a APPARENT MASS FACTOR
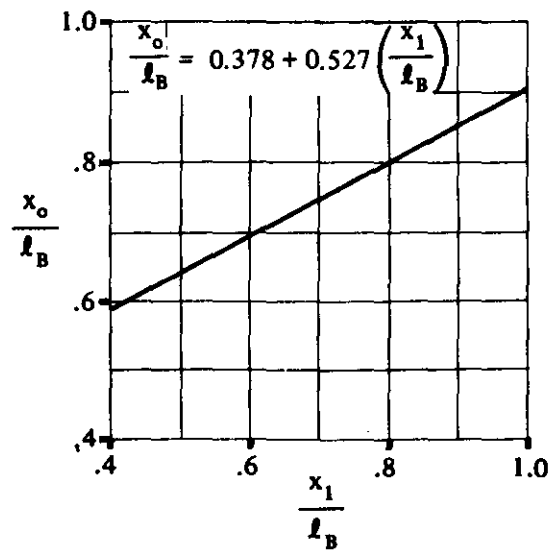
FIGURE 4.2.1.1-20b BODY STATION WHERE FLOW BECOMES VISCOUS

SUPERSONIC SPEEDS
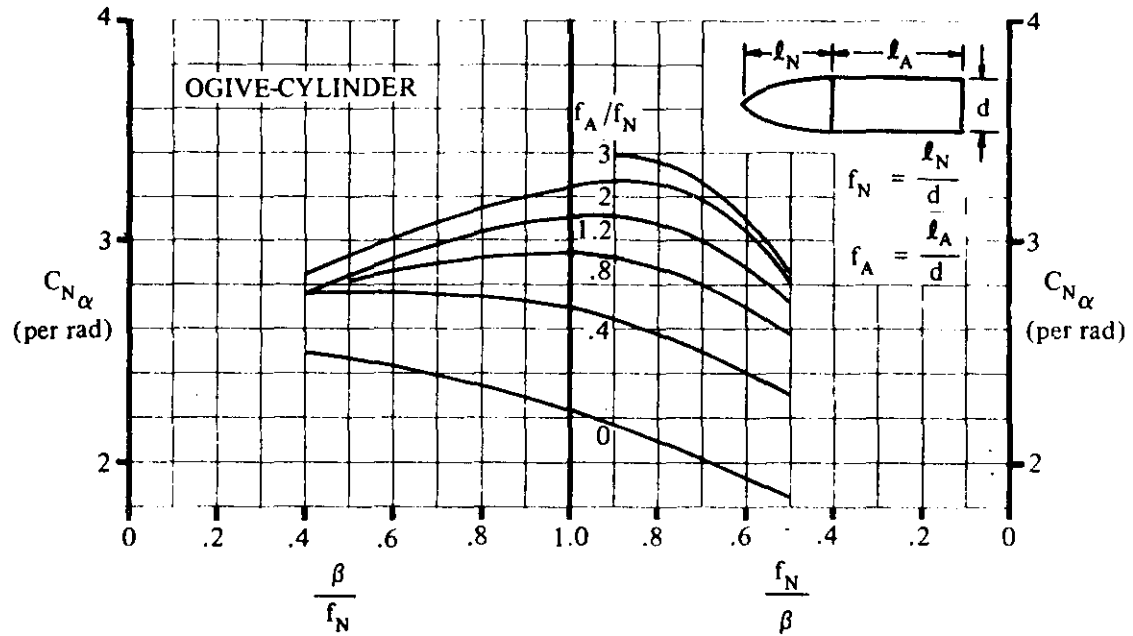
FIGURE 4.2.1.1-21a SUPERSONIC NORMAL-FORCE-CURVE SLOPE FOR OGIVE-CYLINDERS
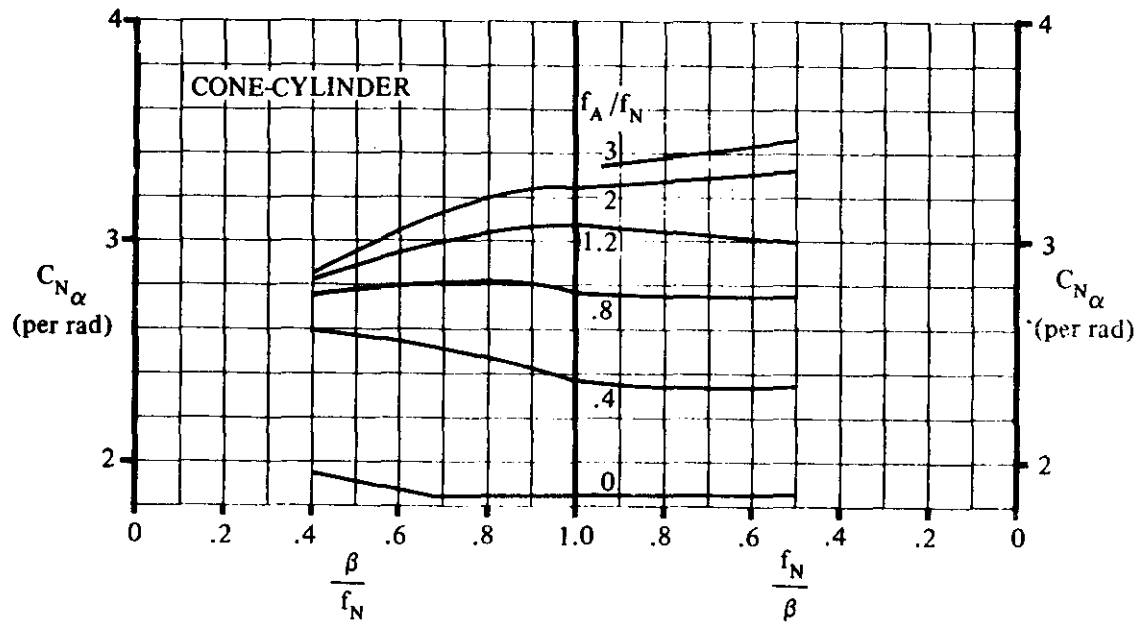
FIGURE 4.2.1.1-21b SUPERSONIC NORMAL-FORCE-CURVE SLOPE FOR CONE-CYLINDERS
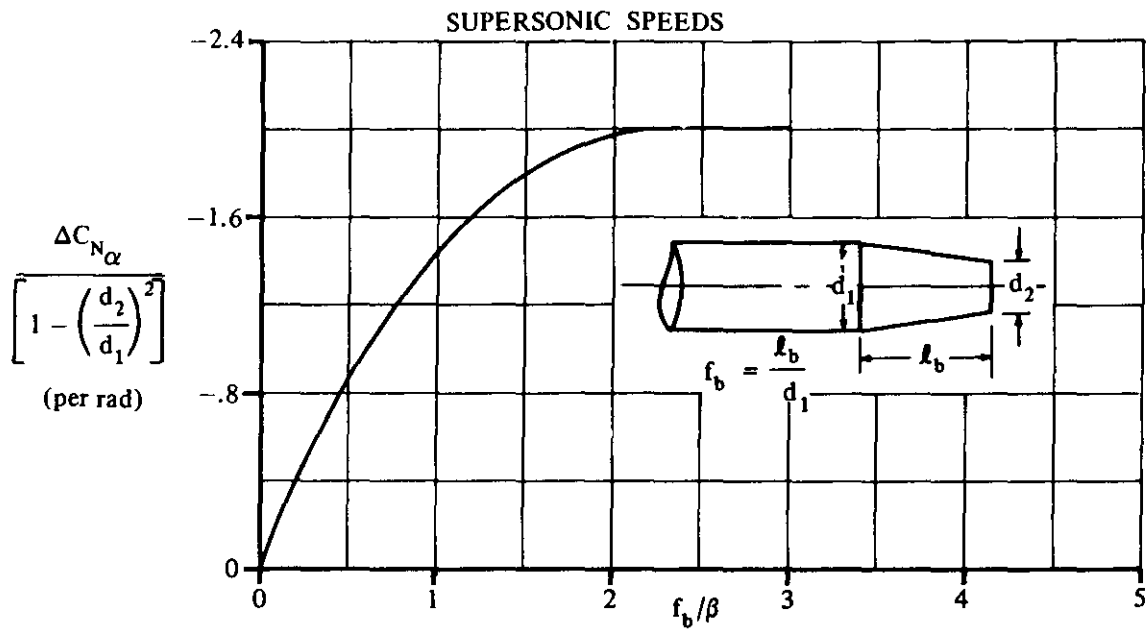
FIGURE 4.2.1.1-22a   NORMAL-FORCE-CURVE-SLOPE INCREMENT OF A BOATTAILED
BODY OF REVOLUTION FOLLOWING A SEMI-INFINITE CYLINDER
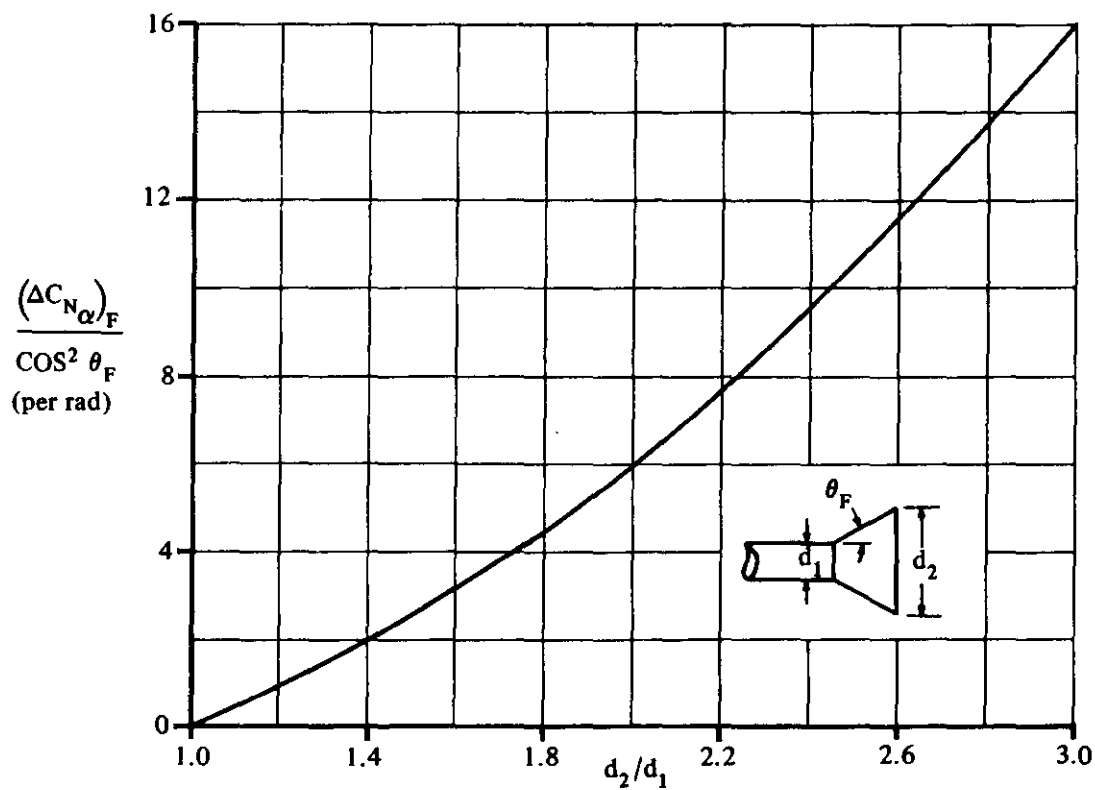
FIGURE 4.2.1.1-22b   NORMAL-FORCE-CURVE-SLOPE INCREMENT OF A FLARED BODY OF
REVOLUTION FOLLOWING A SEMI-INFINITE CYLINDER — IMPACT
THEORY
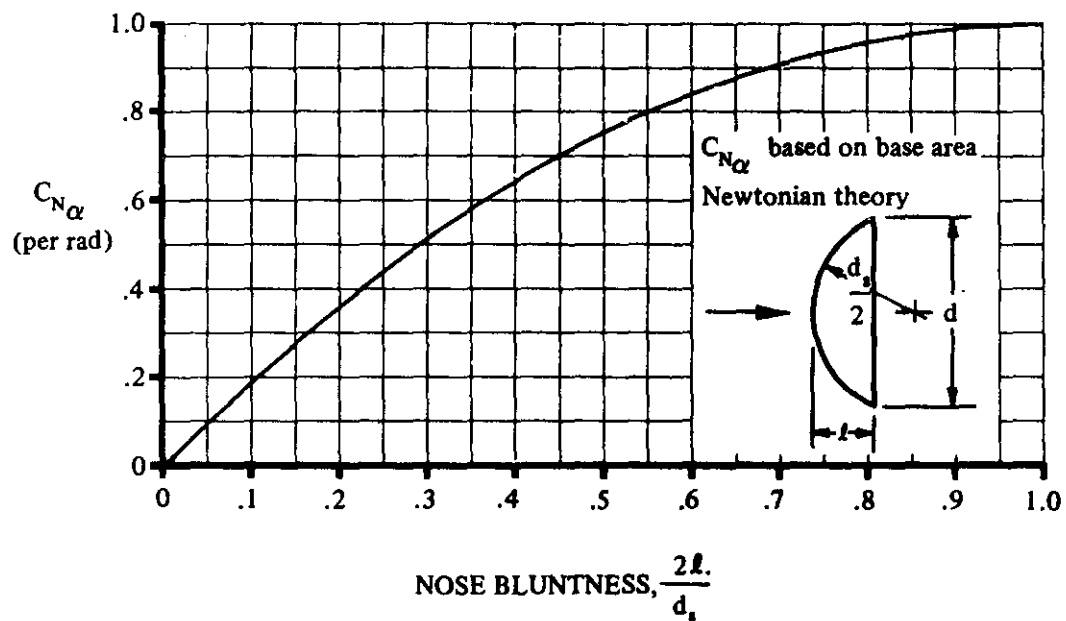
4.2.1.1-22

FIGURE 4.2.1.1-23 NORMAL-FORCE-CURVE SLOPE FOR SPHERICAL SEGMENTS
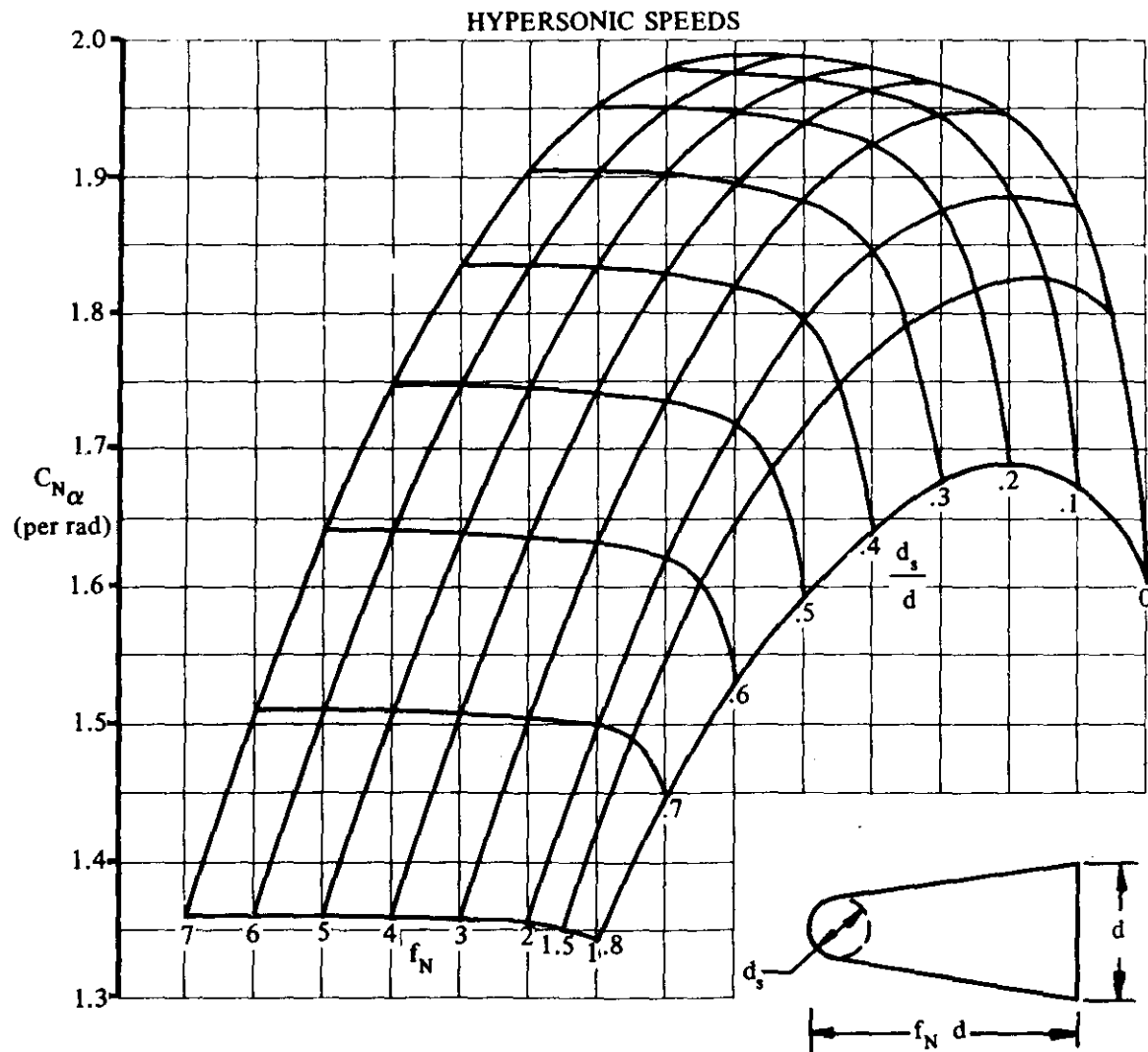
FIGURE 4.2.1.1-24 NORMAL-FORCE-CURVE SLOPE FOR SPHERICALLY BLUNTED CONES
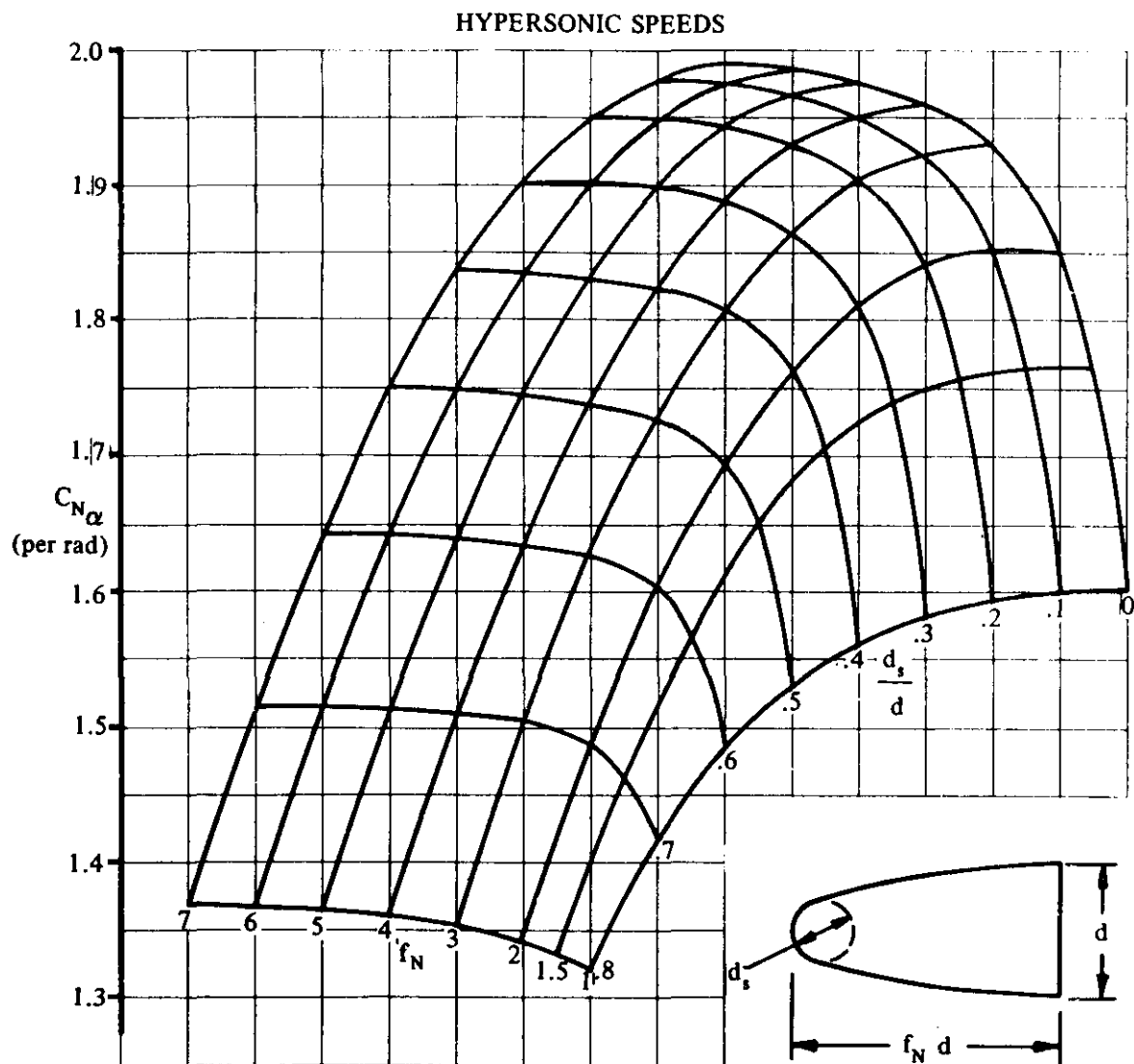
(IMPACT THEORY)

FIGURE 4.2.1.1-25 NORMAL-FORCE-CURVE SLOPE FOR SPHERICALLY BLUNTED OGIVES

(IMPACT THEORY)
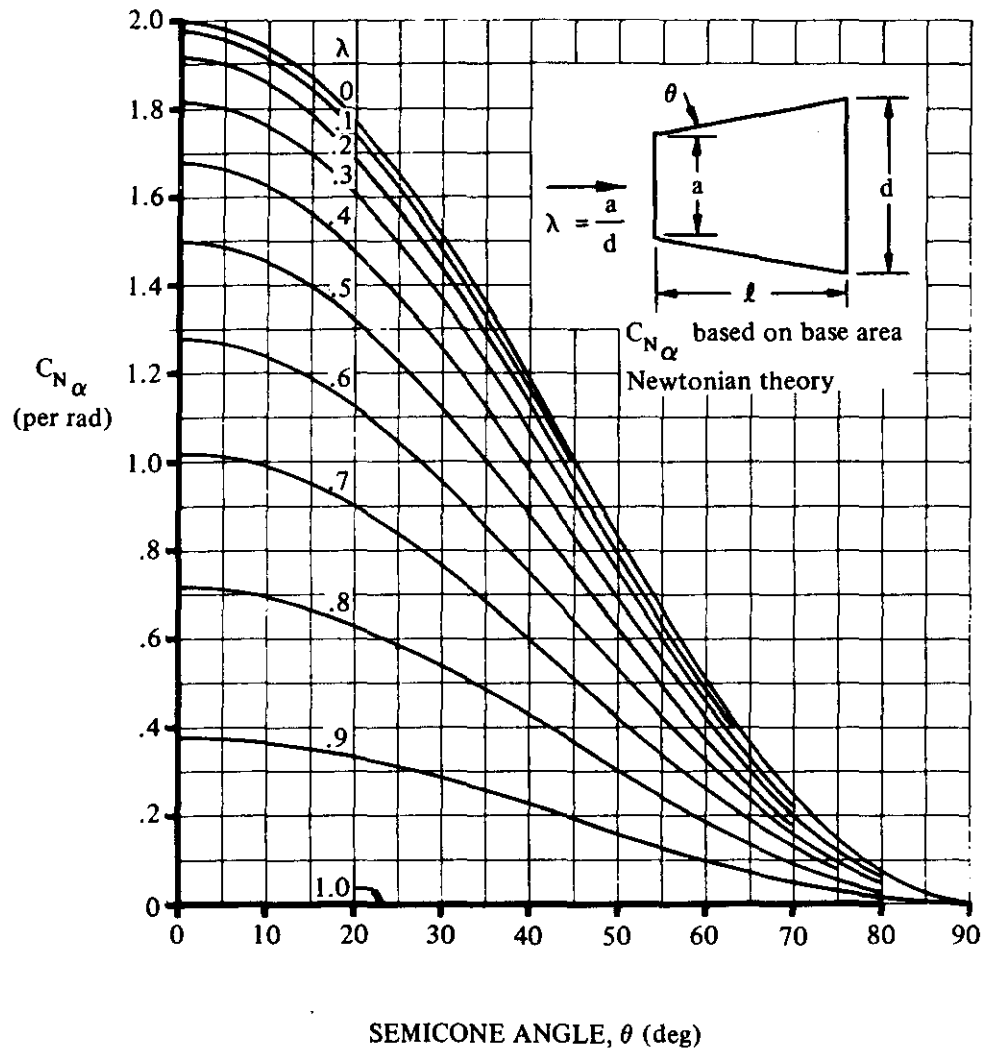
FIGURE 4.2.1.1-26 NORMAL-FORCE-CURVE SLOPE FOR CONE FRUSTUMS

Potential-flow theory shows that the lift on a body is a linear function of angle of attack and is proportional to the body base area. In particular, the lift on a closed body is zero. Slender-body theory also shows that the lift of an inclined body is independent of Mach number from low subsonic to supersonic Mach numbers.

The prediction of body-lift characteristics using potential-flow theory is necessarily limited to those cases where negligible viscous flow separation occurs, i.e., low angles of attack. Divergence between test data and potential-flow predictions can occur at very low angles of attack. Thus, to eliminate the potential-flow-theory angle-of-attack limitation requires consideration of the viscous flow separation effects.

Experimentally, the flow separates over the leeward side of the body, and the normal force increases nonlinearly with angle of attack. A pair of standing body vortices originate near the nose and increase in strength along the length of the body. A cross section of the flow is very similar to the two-dimensional flow about an infinite cylinder with laminar separation. That is, the flow separates in the region of the lateral meridians of the body rather than at points closer to the top meridian, as in turbulent separation. This effect is further accentuated by shocklets that appear (at subsonic speeds) near the maximum half-breadth at about $M \approx 0.4$ and fix the boundary-layer separation. For these reasons a cross-flow drag coefficient for laminar-boundary-layer conditions is used to evaluate viscous cross-flow forces for body lift even though the actual boundary layer is usually turbulent.

Several methods have been developed that assume that the normal forces acting on bodies of revolution at angles of attack can be represented by the linear combination of potential-flow and viscous cross-flow contributions. The lift-curve slope at zero angle of attack is used for the potential-flow term. Some form of cylinder cross-flow drag is used to evaluate viscous cross-flow lift. The methods differ mainly in their treatment of the nonlinear cross-flow term. Some of the better known methods for subsonic and supersonic analyses are discussed below.

In Reference 1 Allen and Perkins assume that the viscous contribution at each station along the body is equal to the steady-state drag of a section of an infinite cylinder placed normal to the flow with velocity $V \sin \alpha$. This method is accurate to within ±10 percent for high fineness-ratio bodies (fineness ratios of approximately 20 or greater). However, the accuracy of the method deteriorates as fineness ratio is decreased.

Kelly, in Reference 2, presents a method that is a refinement of that presented in Reference 1. Kelly uses the hybrid theory of Van Dyke (Reference 3), with a correction for boundary-layer displacement thickness for the potential-flow contribution. For the viscous term, the unsteady cross-flow drag of a cylinder started impulsively from rest is used instead of the steady-state value. This method is limited to cross-flow Mach numbers less than 0.4 and to values of the parameter $2f \tan \alpha \leqslant 9$.

The method of Reference 4 assumes that viscous cross-flow effects occur only on the cylindrical afterbody.

These methods are approximate, however, and each gives accurate answers over a limited range of test conditions. None of them is valid for all conditions.

A. SUBSONIC

Three methods are presented for predicting body lift. The first method, taken from Reference 5, applies only to bodies of revolution and is rather general in its application. It is based on the assumption that the flow is potential over the forward part of the body and has no viscous contribution in this region. On the aft part of the body, the flow is assumed to be entirely viscous, with lift arising solely from cross-flow drag.

The second method applies to bodies of elliptical cross section and bodies of revolution. This method is based on the concept of vortex lift for sharp delta wings as presented in Reference 6. The method as presented herein has been extended to include a set of empirical curves designed to estimate the angle of attack where the onset of vortex lift begins. This modification to the theory is necessary, since the onset of vortex lift for thick bodies does not correspond to that for flat-plate wings, i.e., zero angle of attack. The experimental data used in the correlation are presented in References 7 through 11.

The third method is, in principle, the most general in application, but can be substantiated the least by test data. This method, presented in Reference 12 by Jorgensen, applies to bodies of arbitrary cross section and angles of attack from 0 to 180° in the Mach-number range from 0 to 7. The method is based on the original proposal of Allen (Reference 1), that the cross flow or lift distribution over a body can be expressed as the sum of a slender-body potential term and an empirical viscous cross-flow term. Although the method has been extended in the literature to include bodies with nonconstant cross sections of various types with and without lifting surfaces and afterbodies (References 12 and 13), the lack of substantiating test data has restricted the Datcom method to bodies with constant circular and elliptical cross sections. References are cited to assist in analyzing other configurations. Normal-force coefficient is calculated by this method. See Section 4.2.3.2 for calculation of axial-force coefficient using the method of Jorgensen. The experimental data used in the correlation are presented in References 12, 14, 15, and 16.

As noted above, all methods are applicable to bodies of revolution. It is suggested that Method 1 be used for bodies of revolution at low angles of attack because of its general application and sensitivity to the many possible body profile shapes. It should be noted that for those cases where the predictions from Method 1 diverge from test data (approximately 12° angle of attack or higher), they generally tend to underpredict the lift coefficient. Conversely, the results from Method 2 generally tend to yield estimates that exceed the test data in the high-angle-of-attack range. Therefore, it is recommended that Method 3 be used in the high-angle-of-attack range.

DATCOM METHODS

Method 1

The expression for the lift coefficient of a body of revolution, based on $V_B^{2/3}$, taken from Reference 5, is

$$C_L = \frac{(k_2 - k_1) 2 \alpha S_o}{V_B^{2/3}} + \frac{2 \alpha^2}{V_B^{2/3}} \int_{x_o}^{\ell_B} \eta \, r \, c_{d_c} \, dx \qquad \text{4.2.1.2-a}$$

where

$$\frac{(k_2 - k_1) \, 2 \, \alpha \, S_o}{V_B^{2/3}}$$ is the potential-flow contribution from Paragraph A of Section 4.2.1.1.

α is the angle of attack in radians.

η is the ratio of the drag on a finite cylinder to the drag on an infinite cylinder, obtained from Figure 4.2.1.2-35a.

r is the body radius at any longitudinal station.

c_{d_c} is the steady-state cross-flow drag coefficient of a circular cylinder of infinite length, obtained from Figure 4.2.1.2-35b.

ℓ_B is the body length.

The remaining terms are defined in Paragraph A of Section 4.2.1.1.

The lift coefficients of several bodies of revolution, calculated by the Datcom method, have been compared with test data in Reference 5. In general, the accuracy of the method is satisfactory up to angles of attack of approximately 12°.

Method 2

The expression for the lift coefficient of bodies of revolution and elliptical cross-section bodies, based on the projected body planform area, is given by

$$C_L = K_p \sin \alpha \cos^2 \alpha + K_v \sin^2 (\alpha - \alpha_v) \cos (\alpha - \alpha_v) \qquad \qquad 4.2.1.2\text{-b}$$

where

K_p is the potential-flow lift parameter, obtained from Figure 4.2.1.2-36a as a function of body aspect ratio.

K_v is the viscous-flow lift parameter, obtained from Figure 4.2.1.2-36b as a function of body aspect ratio.

α is the body angle of attack.

α_v is the angle of attack where the onset of vortex lift begins, obtained from Figure 4.2.1.2-37 as a function of body fineness ratio and thickness ratio.

When $\alpha_v > \alpha$ the viscous-lift contribution (second term) of Equation 4.2.1.2-b is not considered; i.e., it is zero. Thus the second term is considered only for those cases where $\alpha - \alpha_v$ yields a positive value.

The test data used to generate Figure 4.2.1.2-37 were limited to Mach numbers less than 0.6. Therefore it is advisable that Equation 4.2.1.2-b be applied to Mach numbers less than 0.6. For higher Mach numbers the user is referred to the parametric test data contained in References 8 through 11.

A comparison of test data with results calculated by this method is presented in Table 4.2.1.2-A. It should be noted that these test data and all other available test data were used in the development of the empirical curves, which estimate the angle of attack where the onset of vortex lift begins.

In general, the accuracy of the method was found to be satisfactory up to angles of attack of approximately 20°.

For those noncircular cross-section bodies that cannot be analyzed by this method, the user is referred to the summary of available test data on bodies of noncircular cross section at subsonic speeds presented in Table 4.2.1.1-A.

Method 3

The normal-force coefficient* for bodies with circular and elliptical cross sections, based on cross-sectional reference area S, is given by

$$C_N = \left(\frac{C_N}{C_{N_{cir}}}\right)_{SB} \left(\frac{S_b}{S} \sin 2\alpha' \cos \frac{\alpha'}{2}\right) + \left(\frac{C_N}{C_{N_{cir}}}\right)_{NT} \left(\eta c_{d_c} \frac{S_p}{S} \sin^2 \alpha'\right) \qquad 4.2.1.2\text{-c}$$

where

$\left(\dfrac{C_N}{C_{N_{cir}}}\right)_{SB}$ is the ratio of the normal-force coefficient for the body of noncircular cross section to that for the equivalent body of circular cross section (same cross-sectional area) as determined by slender-body theory. For circular cross sections this ratio is one. For elliptical cross sections this ratio is given by

$$\left(\frac{C_N}{C_{N_{cir}}}\right)_{SB} = \frac{a}{b} \cos^2 \phi + \frac{b}{a} \sin^2 \phi \qquad 4.2.1.2\text{-d}$$

where

a   is the major axis of the elliptical cross section.

b   is the minor axis of the elliptical cross section.

ϕ is the angle of bank of the body about its longitudinal axis; $\phi = 0$ with the major axis horizontal, and $\phi = 90^{\circ}$ with the minor axis horizontal.

---

*The body lift can be determined by $C_L = C_N \cos \alpha + C_X \sin \alpha$ where C_X is obtained from Section 4.2.3.2.

S_b is the body base area.

S is the cross-sectional reference area of the cylindrical portion of the body (can be arbitrarily selected).

α' is an incidence angle defined as $\alpha' = \alpha$ for $0 \leqslant \alpha \leqslant 90^{\circ}$ and $\alpha' = 180^{\circ} - \alpha$ for $90^{\circ} \leqslant \alpha \leqslant 180^{\circ}$.

$\left(\dfrac{C_N}{C_{N_{cir}}}\right)_{NT}$ is the ratio of the normal-force coefficient for the body of noncircular cross section to that for the equivalent body of circular cross section (same cross-sectional area) as determined by Newtonian impact theory. For circular cross sections this ratio is one. For elliptical cross sections this ratio is described below.

When the major axis (a) is perpendicular to the cross-flow velocity,

$$\left(\frac{C_N}{C_{N_{cir}}}\right)_{NT} = \frac{3}{2}\sqrt{\frac{a}{b}}\left\{\frac{-b^2/a^2}{\left(1-\dfrac{b^2}{a^2}\right)^{3/2}}\log_e\left[\frac{a}{b}\left(1+\sqrt{1-\frac{b^2}{a^2}}\right)\right] + \frac{1}{1-\dfrac{b^2}{a^2}}\right\}$$

4.2.1.2-e

When the minor axis (b) is perpendicular to the cross-flow velocity,

$$\left(\frac{C_N}{C_{N_{cir}}}\right)_{NT} = \frac{3}{2}\sqrt{\frac{b}{a}}\left[\frac{a^2/b^2}{\left(\dfrac{a^2}{b^2}-1\right)^{3/2}}\tan^{-1}\left(\sqrt{\frac{a^2}{b^2}-1}\right) - \frac{1}{\dfrac{a^2}{b^2}-1}\right]$$

4.2.1.2-f

where a and b are as defined above.

η is the cross-flow drag proportionality factor, obtained from Figure 4.2.1.2-35a as a function of body fineness ratio.

c_{d_c} is the cross-flow drag coefficient of the cylindrical section, obtained from Figure 4.2.1.2-35b as a function of cross-flow Mach number M_c, where $M_c = M\sin\alpha$.

S_p is the body planform area. In applying the method to bodies with elliptical cross section, the term S_p in Equation 4.2.1.2-c is based on an equivalent body of revolution with the same cross-sectional area.

Reference 12 discusses methods of computing C_N for bodies with noncircular and nonelliptical cross sections. Reference 13 treats the general case of axially varying cross-sectional shape and bodies with lifting surfaces. However, since substantiating data for these methods are lacking, they have been omitted from the Datcom.

It is noted in Reference 12 that the cross-flow drag coefficient c_{d_c} may be reduced dramatically under the simultaneous conditions of $M_c \leqslant 0.4$ and $R_\varrho \sin \alpha > 10^5$ (R_ϱ is Reynolds number based on diameter). These conditions have only recently been analyzed in detail and have not been included in the Datcom method because of considerable uncertainty in the magnitude and trend of the effects. For more detailed information regarding these effects, the user should refer to Reference 12.

Although the method is applicable up to $\alpha = 180^\circ$, no test verification has been obtained for $\alpha > 60^\circ$ at subsonic speeds. Table 4.2.1.2-B presents substantiation data taken at two Mach numbers. The calculated values for C_N tend to underestimate the test values at high α's. The method is probably less accurate as transonic speeds are approached ($M > 0.9$). It is further recommended that Methods 1 and 2 be used at the low angles of attack whenever possible, since the accuracies of these methods are better substantiated at low α's.

Sample Problems

Method 1

Given: An ogive-cylinder-boattail body of revolution of Reference 20. This is the body of the sample problem of Paragraph A of Section 4.2.1.1.

Body Characteristics:

d = 5.0 in. ℓ_N = 26.25 in. ℓ_C = 23.77 in. ℓ_A = 13.45 in.

d_b = 3.30 in. ℓ_B = 63.47 in. f = ℓ_B/d = 12.7

$(k_2 - k_1)$ = 0.960

$V_B{}^{2/3}$ = 0.660 sq ft

x_o = 50.34 in.   (Sample Problem, Paragraph A, Section 4.2.1.1)

S_o = 0.134 sq ft

Additional Characteristics:

M = 0.80 $\alpha = 4^\circ, 8^\circ, 12^\circ, 16^\circ, 20^\circ$

Compute:

$$\frac{(k_2 - k_1) \, 2 \, \alpha \, S_o}{V_B{}^{2/3}} = \frac{(0.960) \, (2) \, \alpha \, (0.134)}{0.660} = 0.390 \, \alpha$$

4.2.1.2-6

$$c_{d_c} = f(M_c); \quad M_c = M \sin \alpha$$

M_c varies from $0.80 \sin 4^O$ to $0.80 \sin 20^O$; $0.056 \leqslant M_c \leqslant 0.274$

$$c_{d_c} = 1.20 \text{ (constant)} \qquad \text{(Figure 4.2.1.2-35b)}$$

$$\eta = 0.710 \qquad \text{(Figure 4.2.1.2-35a)}$$

$$\int_{x_o}^{\ell_B} \eta\, r\, c_{d_c}\, dx = \int_{50.34}^{63.47} (0.710)\,(r)\,(1.20)\, dx$$

$$= (0.710)\left(\frac{2.48 + 1.65}{2}\right)(1.20)\,(63.47 - 50.34)$$

$$= 23.10 \text{ sq in.} = 0.160 \text{ sq ft}$$

Solution:

$$C_L = \frac{(k_2 - k_1)\,2\alpha S_o}{V_B^{2/3}} + \frac{2\alpha^2}{V_B^{2/3}} \int_{x_o}^{\ell_B} \eta\, r c_{d_c}\, dx \qquad \text{(Equation 4.2.1.2-a)}$$

$$= 0.390\,\alpha + \frac{2\alpha^2}{0.660}\,(0.160)$$

$$= 0.390\,\alpha + 0.485\,\alpha^2$$

α (deg)	α (rad)	C_L (based on $V_B^{2/3}$) Eq. 4.2.1.2-a
4	0.0698	0.0296
8	0.1396	0.0639
12	0.2094	0.1030
16	0.2792	0.1467
20	0.3490	0.1954

The calculated results are compared with test values in Sketch (a).
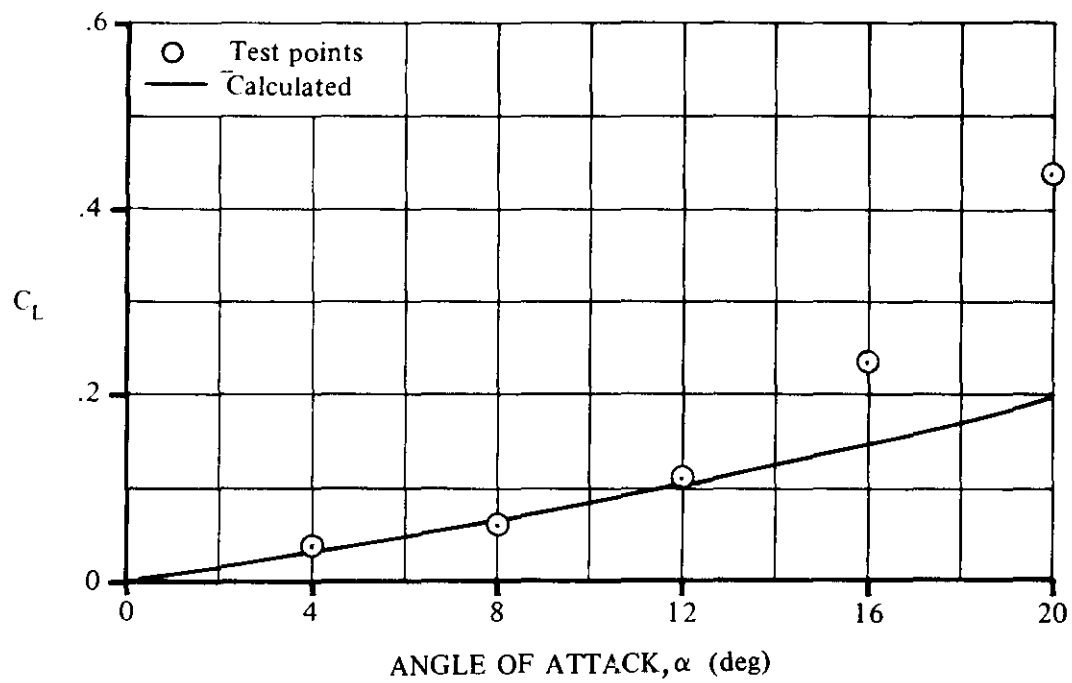
SKETCH (a)

Method 2

Given. The Model A elliptical cross-section body of Reference 11.
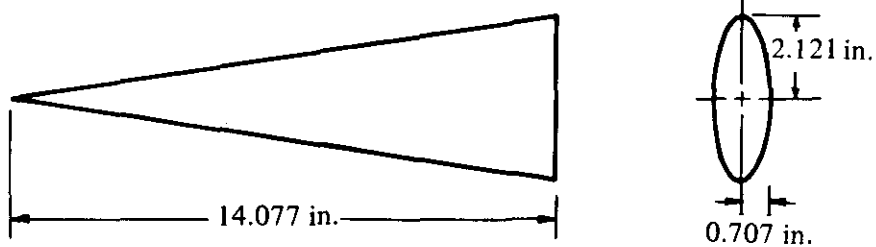
PLANFORM

$S = 29.857$ in.^{2} $A = 0.602$ $S_b = 4.712$ in.^{2}

$M = 0.60$ $R_\ell = 1.4 \times 10^6$

4.2.1.2-8

Compute:

$$d_{equiv} = 2\sqrt{\frac{ab}{4}}$$

$$= 2\sqrt{(0.707)(2.121)}$$

$$= 2.45$$

$$f = \frac{\ell_B}{d_{equiv}} = \frac{14.077}{2.45} = 5.74$$

$$\frac{a}{b} = \frac{2.121}{0.707} = 3.0$$

$K_p = 0.85$ (Figure 4.2.1.2-36a)

$K_v = 3.14$ (Figure 4.2.1.2-36b)

$\alpha_v = 4.3^o$ (Figure 4.2.1.2-37)

Solution:

$$C_L = K_p \sin \alpha \cos^2 \alpha + K_v \sin^2 (\alpha - \alpha_v) \cos (\alpha - \alpha_v) \qquad \text{(Equation 4.2.1.2-b)}$$

① α (deg)	② $K_p \sin \alpha \cos^2 \alpha$ (Potential component)	③ $K_v \sin^2 (\alpha - \alpha_v) \cos (\alpha - \alpha_v)$ (Vortex component)	④ C_L ②+③
0	0	0	0
2	0.0296	0	0.0296
4	0.0590	0	0.0590
6	0.0879	0.0028	0.0907
8	0.1160	0.0131	0.1291
10	0.1432	0.0308	0.1740
12	0.1691	0.0559	0.2250
14	0.1936	0.0879	0.2815
16	0.2165	0.1265	0.3430
18	0.2376	0.1712	0.4088
20	0.2567	0.2215	0.4782

The calculated values are compared with test values from Reference 11 in Sketch (b).

ANGLE OF ATTACK, α (deg)

SKETCH (b)
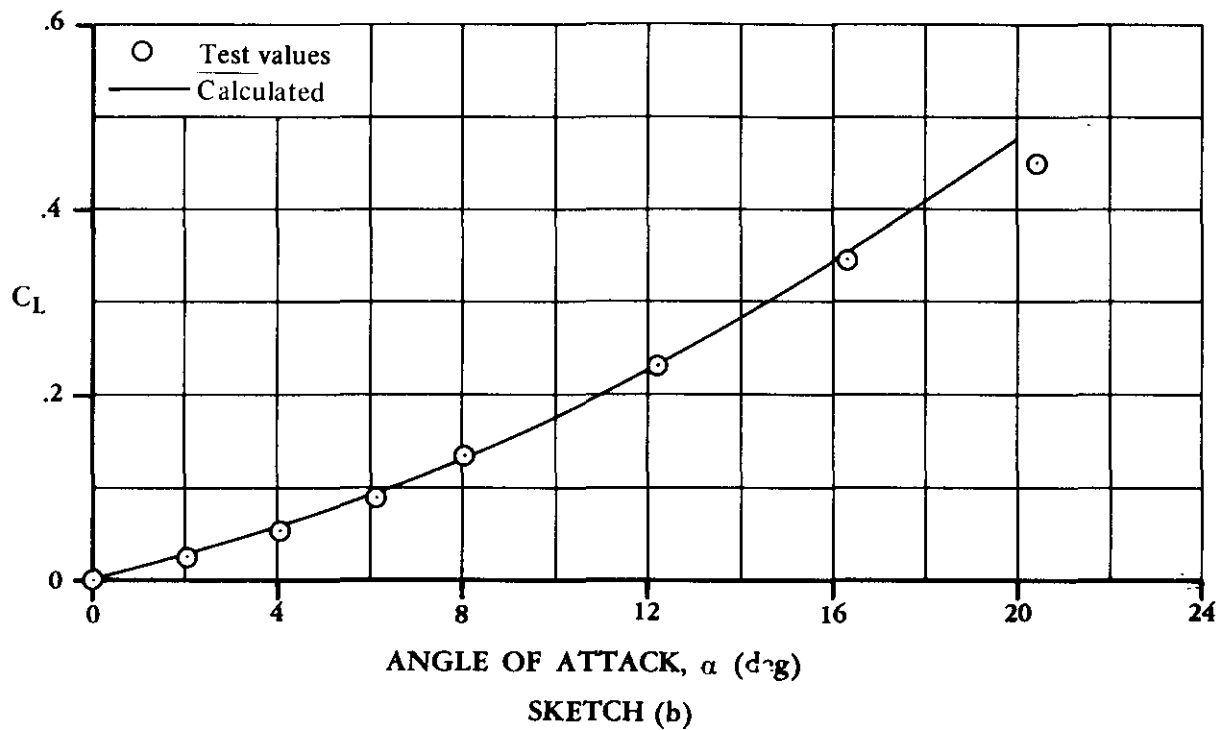
Method 3

Given: Elliptical cross-sectional body with tangent ogive nose of Reference 15.
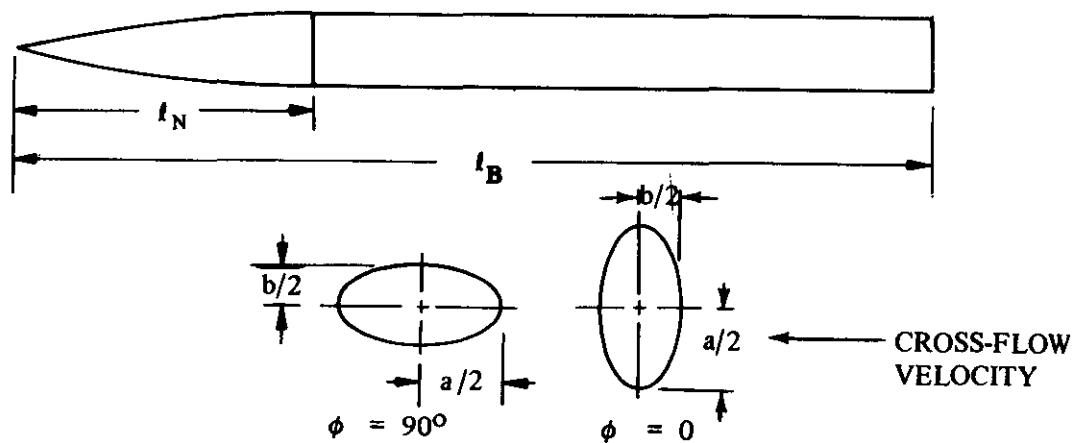
Body Characteristics:

$\dfrac{a}{2} = 4.667 \text{ cm}$ $\quad\quad \ell_B = 66.0 \text{ cm}$ $\quad\quad S_p = 392.466 \text{ cm}^2$

$\dfrac{b}{2} = 2.333 \text{ cm}$ $\quad\quad \ell_N = 19.8 \text{ cm}$

4.2.1.2-10

Additional Characteristics:

$\alpha = 50^{\circ}$ $\phi = 0$ $M = 0.6$ $R_{\varrho} = 6.5 \times 10^5$ (based on diameter)

and the major axis (a) is perpendicular to cross-flow velocity.

Compute:

$\alpha' = \alpha = 50^{\circ}$

$S = \dfrac{\pi ab}{4} = \pi(4.667)(2.333) = 34.206 \text{ cm}^2$

$S_b = S = 34.206 \text{ cm}^2$

$d = d_{equiv} = 2\sqrt{\dfrac{ab}{4}} = 6.6 \text{ cm}$

Slender-body potential-theory term

$\dfrac{S_b}{S} \sin 2\alpha' \cos\dfrac{\alpha'}{2} = \dfrac{34.206}{34.206}(0.9848)(0.9063) = 0.8925$

Viscous cross-flow term

$f = \dfrac{\ell_B}{d} = \dfrac{66.0}{6.6} = 10$

$\eta = 0.685$ (Figure 4.2.1.2-35a)

$M_c = M \sin \alpha = 0.6 (0.7660) = 0.46$

$c_{d_c} = 1.32$ (Figure 4.2.1.2-35b)

$\eta c_{d_c} \dfrac{S_p}{S} \sin^2\alpha = (0.685)(1.32)\dfrac{392.466}{34.206}(0.766)^2 = 6.09$

Ratios for noncircular cross section

$\left(\dfrac{C_N}{C_{N_{cir}}}\right)_{SB} = \dfrac{a}{b}\cos^2\phi + \dfrac{b}{a}\sin^2\phi$ (Equation 4.2.1.2-d)

$= \dfrac{4.667}{2.333}(1) + \dfrac{2.333}{4.667}(0)$

$= 2.0$

$$\left(\frac{C_N}{C_{N_{cir}}}\right)_{NT} = \frac{3}{2}\sqrt{\frac{a}{b}}\left\{\frac{-b^2/a^2}{\left(1-\frac{b^2}{a^2}\right)^{3/2}}\log_e\left[\frac{a}{b}\left(1+\sqrt{1-\frac{b^2}{a^2}}\right)\right]+\frac{1}{1-\frac{b^2}{a^2}}\right\}$$

(Equation 4.2.1.2-e)

$$= \frac{3}{2}\sqrt{\frac{4.667}{2.333}}\left\{\frac{-(2.333)^2/(4.667)^2}{\left(1-\frac{2.333^2}{4.667^2}\right)^{3/2}}\right.$$

$$\left.\log_e\left[\frac{4.667}{2.333}\left(1+\sqrt{1-\frac{2.333^2}{4.667^2}}\right)\right]+\frac{1}{1-\frac{2.333^2}{4.667^2}}\right\}$$

$$= 2.121\left|-0.3849\log_e 3.732+1.333\right|$$

$$= 2.121\left|-0.3849(1.3169)+1.333\right|$$

$$= 1.752$$

Solution:

$$C_N = \left(\frac{C_N}{C_{N_{cir}}}\right)_{SB}\left(\frac{S_b}{S}\sin 2\alpha'\cos\frac{\alpha'}{2}\right)+\left(\frac{C_N}{C_{N_{cir}}}\right)_{NT}\left(\eta c_{d_c}\frac{S_p}{S}\sin^2\alpha'\right) \quad \text{(Equation 4.2.1.2-c)}$$

$$= 2.0(0.8925)+1.752(6.09)$$

$$= 12.45 \quad \text{(based on body cross-sectional reference area, S)}$$

Additional values have been tabulated below:

M	α (deg)	C_N
0.6	10	1.2
0.6	20	3.2
0.6	30	5.9
0.6	40	9.0
0.6	50	12.5
0.6	60	15.8

The calculated results of the sample problem are compared to test values from Reference 15 in Sketch (c).

SKETCH (c)
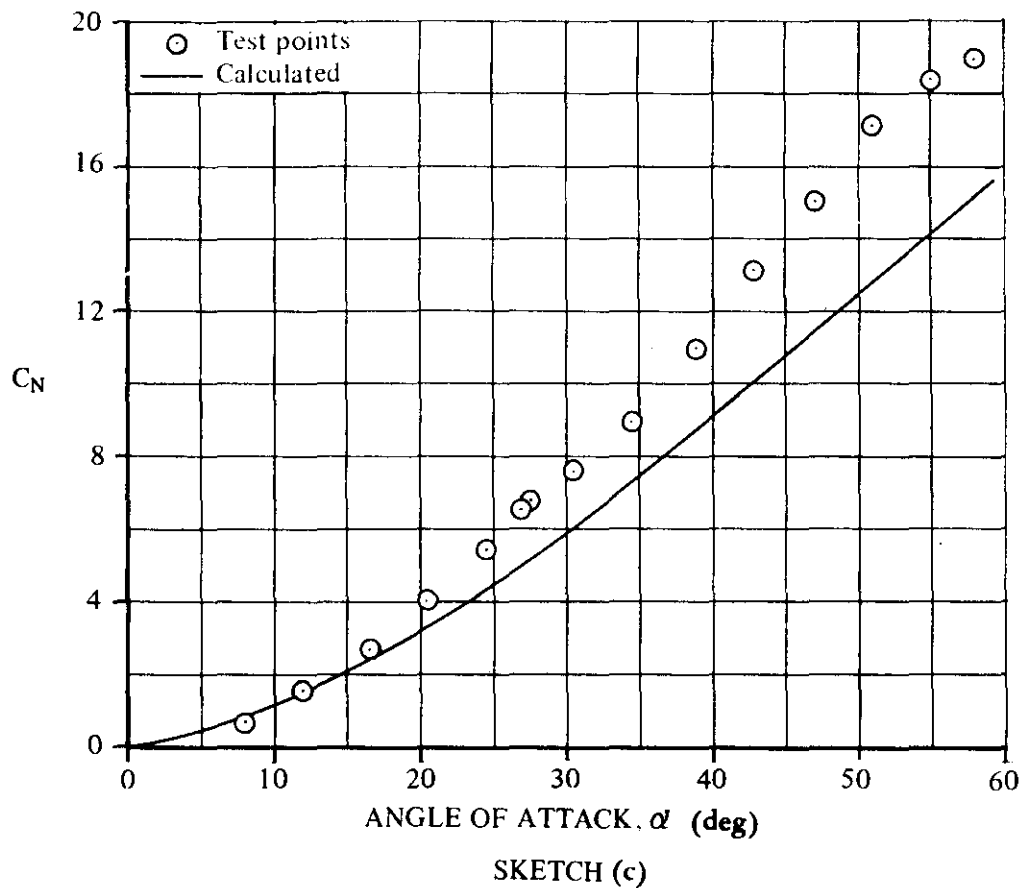
B. TRANSONIC

At transonic Mach numbers, the flow about a body of moderate to large angles of attack is very complex. Analytically, the handling of inviscid mixed subsonic and supersonic flows, which interact at their mutual boundaries, is quite difficult. The presence of the body boundary layer, which may provide an additional mode of interaction between the locally subsonic and supersonic flows, presents an additional complication.

DATCOM METHOD

Because of the analytical difficulties of the problem, no method is given for estimating the transonic lift of a body at angle of attack. It is suggested that subsonic estimates be faired into supersonic results, with experimental data for similar configurations used as a guide in fairing. For bodies of revolution, the reader is referred to the test data of References 17 through 21.

For elliptical cross-section bodies in the transonic speed regime, the reader is referred to the parametric test data presented in References 8 through 11.

C. SUPERSONIC

Three methods are given for predicting body lift. The first method uses the results of the cross-flow analysis presented in Reference 1 to predict the lift on a body of revolution at angle of attack. This result has been modified by Jorgensen in Reference 22 to include bodies of elliptical cross section, and that modification is also presented under Method 1. The cross-flow method of Reference 1 is discussed at the beginning of this section.

The second approach uses hypersonic-similarity concepts that have been adapted to supersonic speeds. The hypersonic-similarity parameters are extended to supersonic Mach numbers by replacing M by β in the hypersonic parameters (Reference 23). Test data for a wide range of cone cylinders for Mach numbers between 1.57 and 4.24 are used in Reference 24 to derive supersonic design charts based on these modified hypersonic-similarity parameters. These charts are presented in this section. They have been slightly modified at the upper limit of their range to make them consistent with the hypersonic charts presented in Paragraph D. These charts can be used for pointed noses other than cones with only small losses in accuracy.

The third method is an improvement on Method 1 developed by Jorgensen in Reference 12. This method calculates the normal-force coefficient up to angles of attack of 180° on bodies with circular and elliptic cross sections. The method is identical to that presented as Method 3 in Paragraph A of this section. It is recommended that this method be used at high angles of attack whenever the first two methods are not applicable.

DATCOM METHODS

Method 1

The method presented for predicting the lift of a body of revolution at angle of attack is that of Allen and Perkins, in Reference 1. The lift of bodies of elliptical cross section is that of Reference 1 as modified by Jorgensen in Reference 22.

The lift coefficient of a body of revolution, based on body base area, is

$$C_L = 2\alpha + c_{d_c} \frac{S_p}{S_b} \alpha^2 \qquad \text{4.2.1.2-g}$$

where

α is the angle of attack in radians.

c_{d_c} is the cross-flow drag coefficient, obtained from Figure 4.2.1.2-35b.

S_p is the body planform area.

S_b is the body base area.

4.2.1.2-14

The supersonic lift coefficient at angle of attack of a body having an elliptical cross section, based on body base area, is

$$\left(C_L\right)_{a/b} = \left[\frac{a}{b}\cos^2\phi + \frac{b}{a}\sin^2\phi\right]C_L \qquad\qquad 4.2.1.2\text{-h}$$

where

a   is the major axis of the elliptical cross section.

b   is the minor axis of the elliptical cross section.

ϕ is the angle of bank of the body about its longitudinal axis; $\phi = 0$ with the major axis horizontal and $\phi = 90^\circ$ with the minor axis horizontal.

C_L is the lift coefficient of a body of revolution having the same cross-sectional area distribution along its axis as the elliptical-cross-section body of interest. It is given by Equation 4.2.1.2-g.

The Datcom method has been used to calculate the variation of lift coefficient with angle of attack for the bodies of elliptic cross section of Reference 22 and the bodies of revolution of References 1, 22, and 25 through 28. Although the nose shapes of most of the configurations analyzed were tangent ogives, a few bodies of revolution had conical or hemispherical noses. All the afterbodies were straight (no boattail or flare). In general, the calculated results agree well with test data, particularly for angles of attack up to approximately 10°. The comparison of calculated and test values for the sample problems at the conclusion of Paragraph C of this section is indicative of the degree of accuracy of this method.

Method 2

The alternate method uses hypersonic-similarity parameters that have been adapted to supersonic speeds by the method of Reference 23. The variation of normal-force coefficient with angle of attack for pointed or nearly pointed bodies of revolution is estimated by using Figures 4.2.1.2-38a through -38d, where $\beta = \sqrt{M^2 - 1}$. The normal-force coefficient presented in these design charts is referred to the base area of the configurations.

With the exception of bodies with elliptical cross sections there are no methods for predicting the lift on bodies of noncircular cross section at supersonic speeds. A summary of available test data on bodies of noncircular cross section at supersonic speeds is presented as Table 4.2.1.1-C. It is of interest to note that in Reference 22 (Reference 37 of Table 4.2.1.1-C) the effect of cross-sectional shape on body aerodynamics has been assessed for bodies with circular, elliptic, square, and triangular cross sections. The results for bodies with noncircular cross sections have been compared with results for bodies of revolution having the same axial distribution of cross-sectional area. Data taken from Reference 22 are presented in Sketch (d), which shows the experimental ratio of the lift of bodies with square and triangular cross sections to the lift of the body of revolution having the same axial distribution of cross-sectional area as a function of angle of attack and Mach number.

These data show that at certain angles of bank, noncircular bodies develop considerably more lift than their equivalent bodies of revolution at a given angle of attack. The data of Reference 22 also show that the ratio of lift coefficient for a body of elliptic cross section to that for an equivalent body of revolution is practically constant with change in both angle of attack and Mach number, and that the ratio is given closely by slender-body theory. The slender-body-theory result for the ratio of potential-flow lift for an elliptic body to that for an equivalent body of revolution is the bracketed term in Equation 4.2.1.2-h, i.e., $\left[\dfrac{a}{b}\cos^2\phi + \dfrac{b}{a}\sin^2\phi\right]$. No such simple correlation is available for other bodies of noncircular cross section.

M = 1.98

M = 3.88

ANGLE OF ATTACK, α (deg)

SKETCH (d)
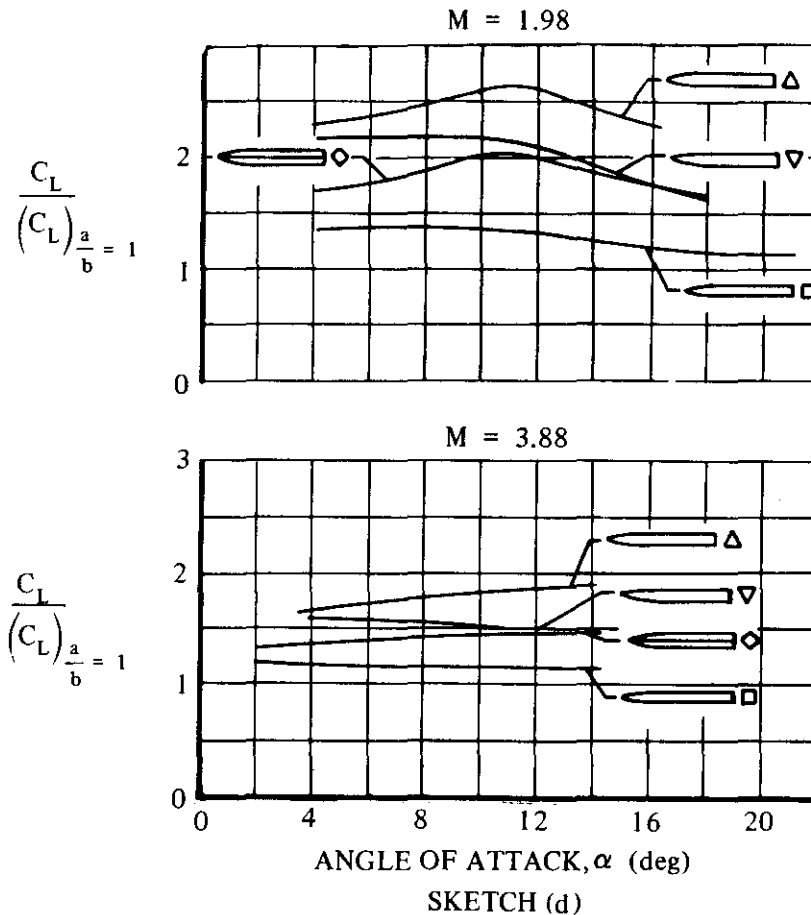
Method 3

The method of Jorgensen for bodies of revolution and bodies with elliptical cross sections, described in Method 3 of Paragraph A of this section, is also applicable throughout the supersonic speed regime up to M = 7. The method is applicable for angles of attack from 0 to 180°.

The cross-flow drag proportionality factor η in Equation 4.2.1.2-c is equal to 1.0 for M $\geqslant$ 1.0.

Comparisons of calculated and test values of C_N are presented in Table 4.2.1.2-C for bodies with circular and elliptical cross sections and various nose shapes. The method is intended primarily for the high-angle-of-attack analysis, and it is recommended that either Datcom Method 1 or 2 be used at low angles of attack.

1. Method 1

Given: An ogive-cylinder body of Reference 22
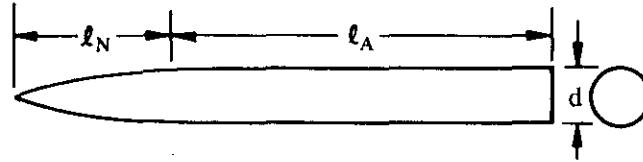
Body Characteristics:

$$f_N = \frac{\ell_N}{d} = 3.0 \qquad f_A = \frac{\ell_A}{d} = 7.0 \qquad f = \frac{\ell_B}{d} = 10.0$$

$$d = 1.40 \text{ in.} \qquad S_p = 17.66 \text{ sq in.} \qquad S_b = 1.539 \text{ sq in.}$$

$$S_p/S_b = 11.47$$

Additional Characteristics:

$$\dot{M} = 1.98 \qquad \alpha = 4^\circ, 8^\circ, 12^\circ, 16^\circ, 20^\circ$$

Compute:

$$c_{d_c} = f(\alpha, M) \qquad \text{(Figure 4.2.1.2-35b)} \quad \text{(See calculation table below.)}$$

Solution:

$$C_L = 2\alpha + c_{d_c} \frac{S_p}{S_b} \alpha^2 \qquad \text{(Equation 4.2.1.2-g) (based on } S_b\text{)}$$

①	②	③	④	⑤	⑥	⑦	⑧
α (deg)	α (rad)	α^2 (rad^2)	M_c M sin α	c_{d_c} Fig. 4.2.1.2-35b	2α 2 ②	$c_{d_c} \frac{S_p}{S_b} \alpha^2$ ⑤ (11.47) ③	C_L Eq. 4.2.1.2-g ⑥ + ⑦
4	0.0698	0.00487	0.138	1.20	0.1396	0.0670	0.2066
8	0.1396	0.01949	0.276	1.208	0.2792	0.2700	0.5492
12	0.2094	0.04385	0.412	1.275	0.4188	0.6410	1.0598
16	0.2792	0.07795	0.546	1.41	0.5584	1.2600	1.8184
20	0.3490	0.12180	0.677	1.62	0.6980	2.2620	2.9600

2. Method 1

Given: A body of Reference 22 having an elliptical cross section and the same axial distribution of cross-sectional area as the body of revolution of Sample Problem 1.
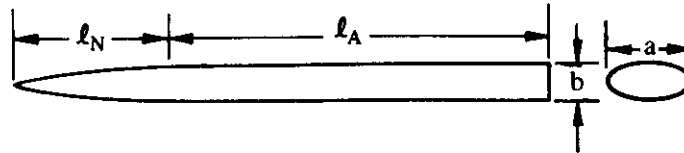
Body Characteristics:

$a = 1.98$ in. $\qquad b = 0.99$ in. $\qquad a/b = 2.0 \qquad \phi = 0$

Additional Characteristics:

$M = 1.98 \qquad \alpha = 4^{\circ}, 8^{\circ}, 12^{\circ}, 16^{\circ}, 20^{\circ}$

Compute:

C_L vs α for a body of revolution having the same cross-sectional area distribution. (from Sample Problem 1)

Solution:

$$\left(C_L \right)_{a/b} = \left[\frac{a}{b} \cos^2 \phi + \frac{b}{a} \sin^2 \phi \right] C_L \qquad \text{(Equation 4.2.1.2-h) (based on } S_b \text{)}$$

$$= [(2.0)(1.0) + 0] \, C_L = 2.0 \, C_L$$

α (deg)	C_L Sample Problem 1	$(C_L)_{a/b}$ Eq. 4.2.1.2-h
4	0.207	0.414
8	0.549	1.098
12	1.060	2.120
16	1.818	3.636
20	2.960	5.920

The calculated results of Sample Problems 1 and 2 are compared with test values from Reference 22 in Sketch (e).
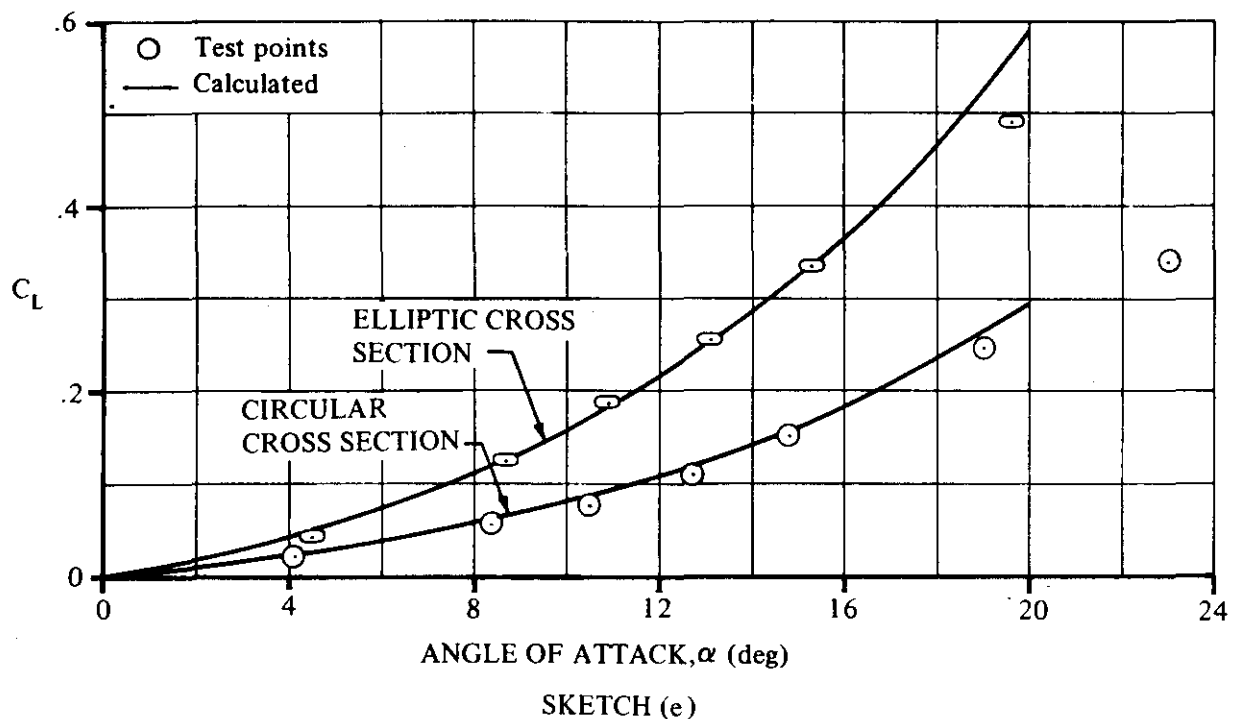
SKETCH (e)

3. Method 3

Refer to Sample Problem 3 in Paragraph A of this section for an example of the application of the method.

D. HYPERSONIC

Three methods are presented for estimating forces on bodies of revolution at hypersonic speeds. One is the hypersonic-similarity method. Another is the Newtonian impact theory and its modifications, discussed in Paragraph D of Section 4.2.1.1. A third method is the method of Jorgensen presented in Paragraphs A and C of this section.

The first method presented in this section is based on hypersonic similarity with Newtonian-theory modifications. Data from References 23 and 29 through 32 have been correlated by means of the hypersonic-similarity parameters and the results extended to high Mach numbers by means of Newtonian theory. These data are limited to pointed, unflared bodies.

The incremental normal-force coefficient due to spherical nose blunting of cones has been calculated by using Newtonian theory. The calculations assume that pressures aft of the intersection of the sphere and the cone are not affected by the blunt nose.

Increments in normal forces due to the addition of flares on cylindrical bodies have also been calculated on the basis of Newtonian flow. Caution should be used in using body flares, however, because they can cause flow separation due to the pressure rise across the shock wave at the beginning of the flare. These separated flows can be unsteady and can cause large losses in lift and moment effectiveness. The conditions that aggravate boundary-layer separation tendencies are large flare angles, lower Mach numbers, high Reynolds number (for a given laminar or turbulent condition), and high wall temperatures. Corner radii or filleting can greatly alleviate this problem. Reference 33 gives some idea of the magnitude of these effects.

The second method is based on Newtonian impact theory. Design charts, taken from Reference 34, are presented for estimating the normal-force characteristics of arbitrary bodies of revolution. These charts are applicable to angles of attack up to 90°.

The third method is the method given by Jorgensen in Reference 12, and presented as Method 3 of Paragraphs A and C of this section. This method calculates the normal-force coefficient up to angles of attack of 180° on bodies with circular and elliptical cross sections. It is recommended that this method be used at high angles of attack whenever the first two methods are not applicable.

DATCOM METHODS

Method 1

The normal-force coefficient for a body composed of a circular cone-cylinder with or without a blunted nose and/or a flared skirt, based on the body base area, is

$$C_N = \left(C_N\right)_{\substack{\text{cone-} \\ \text{cylinder}}} \left(\frac{d_{cyl}}{d_b}\right)^2 + \left(\Delta C_N\right)_N \left(\frac{d}{d_b}\right)^2 + \left(\Delta C_N\right)_F \qquad 4.2.1.2\text{-i}$$

where

$\left(C_N\right)_{\substack{\text{cone} \\ \text{cylinder}}}$ is the normal-force coefficient of a circular cone-cylinder, based on the cylinder base area. This parameter is obtained from Figure 4.2.1.2-40.

$\left(\Delta C_N\right)_N$ is the increment in normal-force coefficient due to blunting the nose of the cone, based on the base area of the spherical nose segment. This parameter is obtained from Figure 4.2.1.2-42a.

$\left(\Delta C_N\right)_F$ is the increment in normal-force coefficient due to the addition of a flared body of revolution at the end of a semi-infinite cylindrical body, based on the base area of the flared body. This parameter is obtained from Figure 4.2.1.2-42b.

d_{cyl} is the diameter of the cylinder.

d is the diameter of the spherical nose segment. (See Figure 4.2.1.2-42a.)

d_b is the body base diameter.

Method 2

The expression for the normal-force coefficient of an arbitrary body of revolution, based on the body base area, taken from Reference 34, is

$$C_N = \frac{K}{\pi} \frac{\ell_B}{R} \int_0^1 K_\theta \frac{r}{R} d\left(\frac{x}{\ell_B}\right) \qquad 4.2.1.2\text{-j}$$

where

K = 2, according to Newtonian theory, which corresponds to $M_\infty = \infty$ and $\gamma = 1.0$. This value does not account for either Mach number or γ variations, but for pointed bodies with attached shocks it gives results of acceptable accuracy. For blunt bodies the actual value of the stagnation-point pressure coefficient may be used for K:

$$K = C_{P_{stag}} = \frac{\gamma + 3}{\gamma + 1} \left[1 - \frac{2}{\gamma + 3} \frac{1}{M_\infty^2} \right]$$

4.2.1.2-k

ℓ_B is the body length.

R   is the reference radius (radius of the base).

r   is the local radius at any body station.

K_θ is a pressure-surface-slope integral factor obtained from Figure 4.2.1.2-43 as a function of angle of attack and the surface slope θ of the body of revolution.

The following steps outline the calculation procedure:

Step 1.   From the equation of the body of revolution obtain the expression for the surface slope using the relation

$$\theta = \tan^{-1}\left(\frac{dr}{dx}\right)$$

where θ, dr, and dx are illustrated in Sketch (f).

ELEMENT OF SURFACE   DETAIL
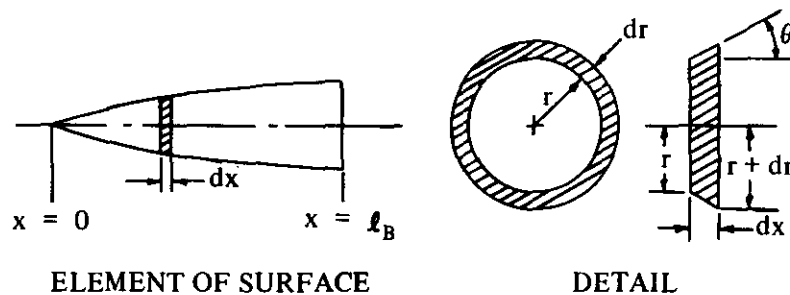
SKETCH (f)

Step 2.   Compute the values of r/R and θ at various longitudinal stations x/ℓ_B.

Step 3. For various x/ℓ_B enter Figure 4.2.1.2-43 with the corresponding θ from Step 2 and obtain K_θ at the desired angle of attack.

Step 4. Plot the product $K_\theta \dfrac{r}{R}$ versus x/ℓ_B.

Step 5. Obtain C_N by integrating the area under the curve described in Step 4 and multiplying that value by $\dfrac{K}{\pi} \dfrac{\ell_B}{R}$.

Method 3

This method is identical to Method 3 presented in Paragraphs A and C of this section. The method is applicable to angles of attack from 0 to 180° and Mach numbers up to 7. The method has been partially substantiated by test data from Reference 16 in Table 4.2.1.2-C.

The method shows reasonable agreement with test data at hypersonic speeds in the low-angle-of-attack range. Because of the scarcity of substantiating test data, caution should be used when applying the method at higher angles of attack ($\alpha > 25^\circ$).

Sample Problems

1. Method 1

Given: Configuration 5115 of Reference 35, consisting of a cone-cylinder-frustum body with a spherical nose. This is the configuration of the sample problem in Paragraph D of Section 4.2.1.1.
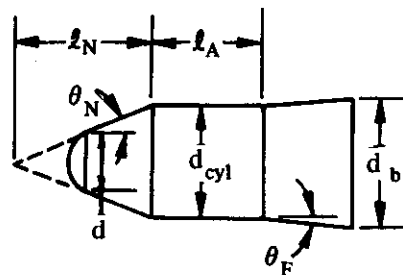
$\ell_N = 1.45$ ft $\ell_A = 1.20$ ft $d = 0.62$ ft $d_{cyl} = 1.20$ ft $d_b = 1.268$ ft

$\theta_N = 22.5^\circ$ $\theta_F = 5^\circ$ $M = 4.04; \beta = 3.91$

Compute:

$$f_A = \frac{\ell_A}{d_{cyl}} = \frac{1.20}{1.20} = 1.00$$

$$f_N = \frac{\ell_N}{d_{cyl}} = \frac{1.45}{1.20} = 1.21$$

$$f_A/f_N = 1.00/1.21 = 0.83$$

$$\beta/f_N = 3.91/1.21 = 3.23$$

$$(d/d_b)^2 = (0.62/1.368)^2 = 0.205$$

$$(d_{cyl}/d_b)^2 = (1.20/1.368)^2 = 0.769$$

$$1 - (d_{cyl}/d_b)^2 = 0.231$$

Solution:

$$C_N = \left(C_N\right)_{\substack{cone-\\cylinder}} \left(\frac{d_{cyl}}{d_b}\right)^2 + \left(\Delta C_N\right)_N \left(\frac{d}{d_b}\right)^2 + \left(\Delta C_N\right)_F \qquad \text{(Equation 4.2.1.2-i)}$$

①	②	③	④	⑤	⑥	⑦	⑧	⑨
α (deg)	$\beta\alpha$ (deg)	$(\beta C_N)_{\substack{cone-\\cylinder}}$ Fig. 4.2.1.2-40 interpolated	$(C_N)_{\substack{cone-\\cylinder}}\left(\frac{d_{cyl}}{d_b}\right)^2$ [③/(3.91)] (0.769)	$(\Delta C_N)_N$ Fig. 4.2.1.2-42a	$(\Delta C_N)_N\left(\frac{d}{d_b}\right)^2$ ⑤(0.205)	$\dfrac{(\Delta C_N)_F}{1-\left(\dfrac{d_{cyl}}{d_b}\right)^2}$ Fig. 4.2.1.2-42b	$(\Delta C_N)_F$ ⑦(0.231)	C_N (based on S_b) ④+⑥+⑧
0	—	—	—	—	—	—	—	0
10	39.1	1.5	0.295	−0.435	−0.0892	0.40	0.092	0.298
20	78.2	3.5	0.688	−0.820	−0.168	0.92	0.212	0.732
30	117.3	5.4	1.062	−1.125	−0.231	1.66	0.383	1.214
40	156.4	7.8	1.534	−1.350	−0.277	2.55	0.589	1.846

2. Method 2

Given: A second-power body of revolution of fineness ratio 1.0.
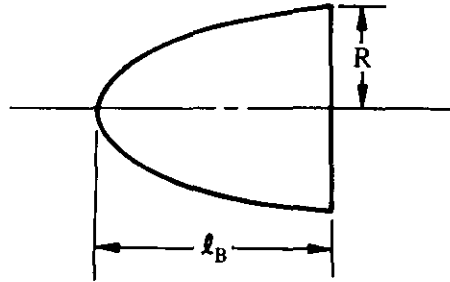
$$x = \left(\frac{4}{\ell_B}\right) r^2 \quad \text{(equation of body)} \qquad \ell_B = 2.0 \text{ ft} \qquad R = 1.0 \text{ ft}$$

$$M_\infty = 3.55 \qquad \alpha = 6^0 \qquad \gamma = 1.40$$

Compute:

Determine K for a blunt-nosed body

$$K = \frac{\gamma + 3}{\gamma + 1} \left[1 - \frac{2}{\gamma + 3} \frac{1}{M_\infty^2} \right] = 1.77 \qquad \text{(Equation 4.2.1.2-k)}$$

$$\theta = \tan^{-1}\left(\frac{dr}{dx}\right) = \tan^{-1}\left(\frac{1}{4\sqrt{x/\ell_B}}\right)$$

Calculate r/R and θ at various longitudinal stations x/ℓ_B and plot (see Sketch (g)).
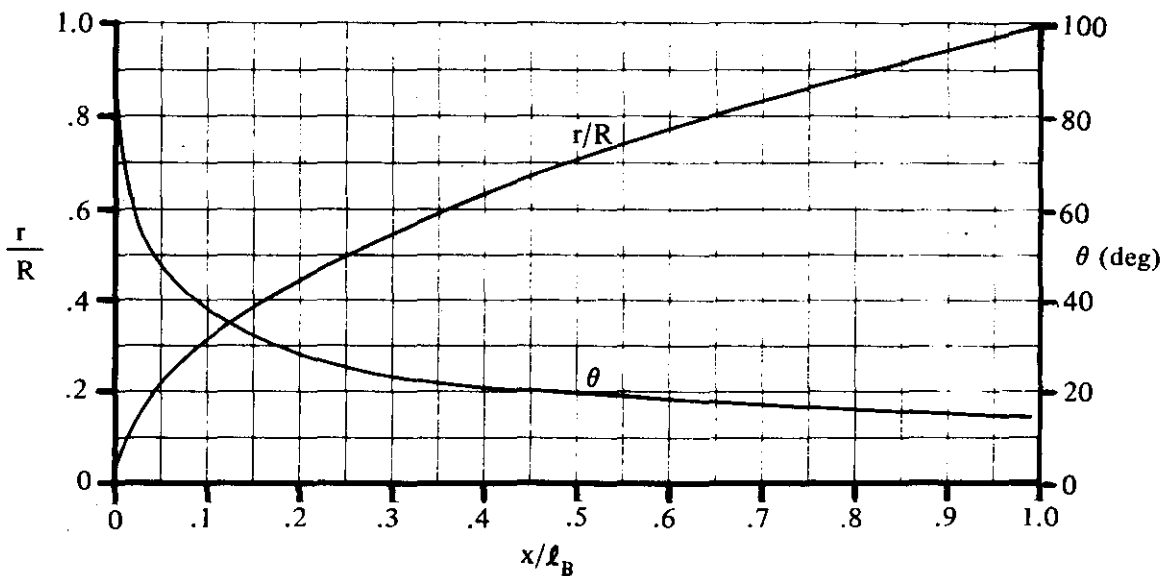
SKETCH (g)

Obtain values for K_θ from Figure 4.2.1.2-43 for various values of θ at $\alpha \doteq 6^\circ$.

Plot the product of $K_\theta \dfrac{r}{R}$ versus x/ℓ_B (see Sketch (h)).

Integrate the area under the curve of Sketch (h).
$$\int_0^1 K_\theta \; \frac{r}{R} \; d\left(\frac{x}{\ell_B}\right) = 0.135$$

SKETCH (h)
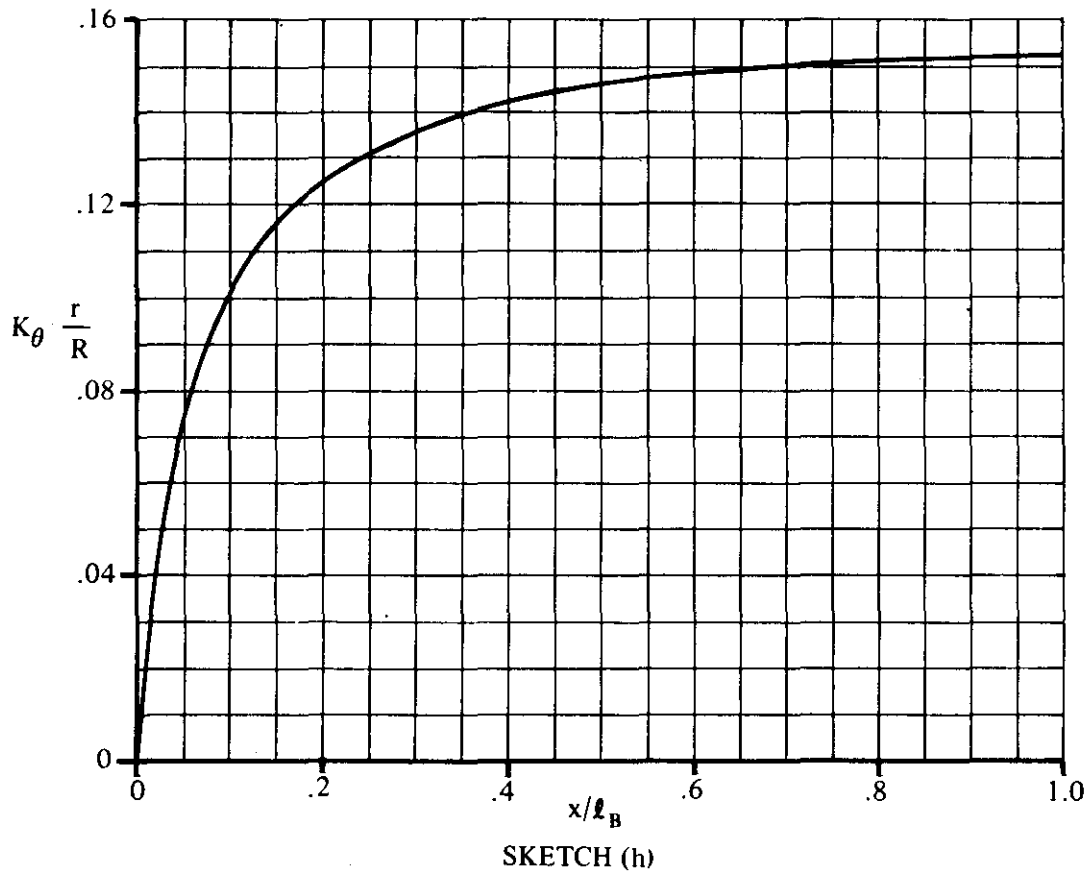
Solution:

$$C_N = \frac{K}{\pi} \frac{\ell_B}{R} \int_0^1 K_\theta \; \frac{r}{R} \; d\left(\frac{x}{\ell_B}\right) \qquad \text{(Equation 4.2.1.2-j)}$$

$$= \frac{(1.77)(2.0)}{\pi \; (1.0)}(0.135)$$

$$= 0.152 \text{ (based on } S_b\text{)}$$

3. Method 3

Refer to Sample Problem 3 in Paragraph A of this section for an example of the application of the method.

REFERENCES

1. Allen, H. J., and Perkins, E. W.: A Study of Effects of Viscosity on Flow Over Slender Inclined Bodies of Revolution. NACA TR 1048, 1951. (U)

2. Kelly, H. R.: The Estimation of Normal-Force, Drag, and Pitching-Moment Coefficients for Blunt-Based Bodies of Revolution at Large Angles of Attack. Jour. Aero. Sci., Vol. 21, No. 8, 1954. (U)

3. Van Dyke, M. D.: First- and Second-Order Theory of Supersonic Flow Past Bodies of Revolution. Jour. Aero. Sci., Vol. 18, No. 3, 1951. (U)

4. Phythian, J. E., and Dommett, R. L.: Semi-Empirical Methods of Estimating Forces on Bodies at Supersonic Speeds. Jour. Roy. Aero. Soc., Vol. 62, No. 571, 1958. (U)

5. Hopkins, E. J.: A Semiempirical Method for Calculating the Pitching Moment of Bodies of Revolution at Low Mach Numbers. NACA RM A51C14, 1951. (U)

6. Polhamus, E. C.: A Concept of the Vortex Lift of Sharp-Edge Delta Wings Based on a Leading-Edge-Suction Analogy. NACA TN D-3767, 1966. (U)

7. Spencer, B., Jr., and Phillips, W. P.: Effects of Cross-Section Shape on the Low-Speed Aerodynamic Characteristics of a Low-Wave-Drag Hypersonic Body. NASA TN D-1963, 1963. (U)

8. Spencer, B., Jr., and Phillips, W. P.: Transonic Aerodynamic Characteristics of a Series of Bodies Having Variations in Fineness Ratio and Cross-Sectional Ellipticity. NASA TN D-2622, 1965. (U)

9. Spencer, B., Jr.: Transonic Aerodynamic Characteristics of a Series of Related Bodies with Cross-Sectional Ellipticity. NASA TN D-3203, 1966. (U)

10. Taylor, R. A.: Transonic Aerodynamic Characteristics of Several Bodies Having Elliptical Cross Sections and Various Plan Forms. NASA TN D-14, 1959. (U)

11. Stivers, L. S, Jr., and Levy, L. L., Jr.: Longitudinal Force and Moment Data at Mach Numbers from 0.60 to 1.40 for a Family of Elliptic Cones with Various Semiapex Angles. NASA TN D-1149, 1961. (U)

12. Jorgensen, L. H.: Prediction of Static Aerodynamic Characteristics for Space-Shuttle-Like and Other Bodies at Angles of Attack from 0° to 180°. NASA TN D-6996, 1973. (U)

13. Jorgensen, L. H.: A Method for Estimating Static Aerodynamic Characteristics for Slender Bodies of Circular and Noncircular Cross Section Alone and with Lifting Surfaces at Angles of Attack from 0° to 90°. NASA TN D-7228, 1973. (U)

14. Jernell, L. S.: Aerodynamic Characteristics of Bodies of Revolution of Mach Numbers from 1.50 to 2.86 and Angles of Attack to 180°. NASA TM X-1658, 1968. (U)

15. Jorgensen, L. H., and Nelson, E. R.: Experimental Aerodynamic Charateristics for Bodies of Elliptic Cross Section at Angles of Attack from 0° to 58° and Mach Numbers from 0.6 to 2.0. NASA TM X-3129, 1975. (U)

16. Dennis, D. H., and Cunningham, B. E.: Forces and Moments on Inclined Bodies at Mach Numbers from 3.0 to 6.3. NACA RM A54E03, 1954. (U)

17. Hayes, W. C., Jr., and Henderson, W. P.: Some Effects of Nose Bluntness and Fineness Ratio on the Static Longitudinal Aerodynamic Characteristics of Bodies of Revolution at Subsonic Speeds. NASA TN D-650, 1961. (U)

18. Reese, D. E., Jr., and Wehrend, W. R., Jr.: An Investigation of the Static and Dynamic Aerodynamic Characteristics of a Series of Blunt-Nosed Cylinder-Flare Models at Mach Numbers from 0.65 to 2.20. NASA TM X-110, 1960. (U)

19. Polhamus, E. C.: Effect of Nose Shape on Subsonic Aerodynamic Characteristics of a Body of Revolution Having a Fineness Ratio of 10.94. NACA RM L57F25, 1957. (U)

20. Goodson, K. W.: Effect of Nose Length, Fuselage Length, and Nose Fineness Ratio on the Longitudinal Aerodynamic Characteristics of Two Complete Models at High Subsonic Speeds. NASA Memo 10-10-58L, 1958. (U)

21. Coe, P. L., Jr., Chambers, J. R., and Letko, W.: Asymmetric Lateral-Directional Characteristics of Pointed Bodies of Revolution at High Angles of Attack. NASA TN D-7095, 1972. (U)

22.　Jorgensen, L. H.: Inclined Bodies of Various Cross Sections at Supersonic Speeds. NASA Memo 10-3-58A, 1958. (U)

23.　Van Dyke, M. D.: The Combined Supersonic-Hypersonic Similarity Rule. Jour. Aero. Sci., Vol. 18, No. 7, 1951. (U)

24.　Dorrance, W. H., and Norrell, R. G.: Correlation of Cone-Cylinder Normal Force and Pitching Moment Data by the Hypersonic Similarity Rule. Jour. Aero. Sci., Vol. 24, No. 5, 1957. (U)

25.　Perkins, E. W., and Jorgensen, L. H.: Comparison of Experimental and Theoretical Normal-Force Distributions (Including Reynolds Number Effects) on an Ogive-Cylinder Body at Mach Number 1.98. NACA TN 3716, 1956. (U)

26.　Jack, J. R.: Aerodynamic Characteristics of a Slender Cone-Cylinder Body of Revolution at Mach Number of 3.85. NACA RM E51H17, 1951. (U)

27.　Ferri, A.: Supersonic-Tunnel Tests of Projectiles in Germany and Italy. NACA WR L-152, 1945. (U)

28.　Delancey, L. M., Jaeger, B. F., and Schroedter, G. M.: The Aerodynamic Characteristics at Mach Number 4.24, of Bodies of Revolution with Varying Lengths and Head Shapes. NOTS TM 358, 1951. (U)

29.　Dennis, D. H., and Cunningham, B. E.: Forces and Moments on Pointed and Blunt-Nosed Bodies of Revolution at Mach Numbers from 2.75 to 5.00. NACA RM A52F22, 1952. (U)

30.　Resnikoff, M. M.: Optimum Lifting Bodies at High Supersonic Airspeeds. NACA RM A54B15, 1954. (U)

31.　Jaeger, B. F., and Morgan, A. J. A.: Review of Experiment and Theory Applicable to Cone-Cylinder and Ogive-Cylinder Bodies of Revolution in Supersonic Flow. NAVORD 5239, 1956. (U)

32.　Buford, W. E., and Shatunoff, S.: The Effects of Fineness Ratio and Mach Number on the Normal Force and Center of Pressure of Conical- and Ogival-Head Bodies. BRL MR 760, 1954. (U)

33.　Dennis, D. H.: The Effects of Boundary-Layer Separation Over Bodies of Revolution With Conical Tail Flares. NACA RM A57I30, 1957. (U)

34.　Rainey, R. W.: Working Charts for Rapid Prediction of Force and Pressure Coefficients on Arbitrary Bodies of Revolution by Newtonian Concepts. NASA TN D-176, 1959. (U)

35.　Henderson, J. H.: Effect of Nose Bluntness on Normal Force, Pitching Moment, and Center of Pressure on Cone-Cylinder and Cone-Cylinder-Frustum Bodies of Revolution at Mach Numbers of 1.50, 2.18, 2.81, and 4.04. Ordnance Missile Laboratories Redstone Arsenal Report No. GR11F, 1958. (U)

Ref	M	A	a/b	d_{equiv}	ℓ_B/d_{equiv}	α_v Fig. 4.2.1.2-37	α (deg)	$C_{L_{calc}}$	$C_{L_{test}}$	Percent Error e
7	0.4	0.245	1.5	4.80	10.0	7.3	4	0.031	0.024	29.2
							8	0.061	0.063	−3.2
							12	0.113	0.115	−1.7
							16	0.199	0.173	15.0
		0.283	2.0	4.80	10.0	5.5	4	0.041	0.033	24.2
							8	0.089	0.087	2.3
							12	0.174	0.170	2.4
							16	0.295	0.256	15.2
							18	0.368	0.303	21.5
		0.316	2.5	4.80	10.0	4.0	4	0.052	0.051	2.0
							8	0.125	0.134	−6.7
							12	0.243	0.245	−0.8
							16	0.399	0.367	8.7
8	0.4	0.408	1.5	4.0	5.0	12.4	4	0.192	0.20	−4.0
							8	0.377	0.355	6.2
							12	0.549	0.58	−5.3
							16	0.761	0.82	−7.2
							20	1.09	1.12	−2.7
		0.286	1.5	4.0	7.0	8.8	4	0.197	0.21	−6.2
							8	0.387	0.43	−10.0
							12	0.629	0.675	−6.8
							16	1.05	0.97	8.2
							20	1.63	1.46	11.6
		0.786	2.0	4.0	3.0	16.3	4	0.240	0.24	0
							8	0.472	0.45	4.9
							12	0.688	0.665	3.5
							16	0.881	0.89	−1.0
							20	1.087	1.133	−4.1
		0.337	2.0	4.0	7.0	6.7	4	0.257	0.285	−9.8
							8	0.518	0.555	−6.7
							12	0.939	0.95	−1.2
							16	1.556	1.475	5.5
							20	2.343	2.145	9.2

TABLE 4.2.1.2-A   (CONTD)

Ref	M	A	a/b	d_{equiv}	ℓ_B/d_{equiv}	α_v Fig. 4.2.1.2-37	α (deg)	$C_{L_{calc}}$	$C_{L_{test}}$	Percent Error e
9	0.5	0.5656	2.0	5.0	5.0	9.1	4	0.055	0.052	5.8
							8	0.108	0.103	4.9
							12	0.165	0.170	−2.9
							16	0.246	0.246	0
							20	0.349	0.343	1.7
		0.3075	3.0	3.535	7.07	3.45	4	0.0315	0.035	−10.0
							8	0.081	0.084	−3.6
							12	0.158	0.159	−0.6
							16	0.259	0.256	1.2
							18	0.318	0.310	2.6
10	0.4	0.350	3.0	6.0	6.93	3.53	4	0.036	0.044	−18.2
							8	0.090	0.090	0
							12	0.171	0.172	−0.6
		0.311	4.0	6.0	8.60	1.93	4	0.036	0.030	20.0
							8	0.098	0.078	25.6
							12	0.186	0.170	9.4
11	0.6	1.674	3.0	2.45	2.07	12.95	4	0.137	0.125	9.6
							8	0.269	0.250	7.6
							12	0.392	0.380	3.2
							16	0.511	0.510	0.2
							20	0.643	0.675	−4.7
		2.41	3.0	2.45	1.436	16.85	4	0.175	0.160	9.4
							8	0.344	0.320	7.5
							12	0.501	0.465	7.7
							16	0.642	0.625	2.7
							20	0.771	0.780	−1.2

Percent Error $= \Sigma \dfrac{|e|}{n} = 6.9\%$

Ref	M	R_{ℓ} (based on d_{equiv})	a/b	$\dfrac{\ell_B}{d_{equiv}}$	Nose Shape	α (deg)	$C_{N_{calc}}$	$C_{N_{test}}$	ΔC_N
15	0.6	6.5×10^5	1.0	10	Ogive	10	0.6	0.5	0.1
						20	1.7	1.4	0.3
						30	3.2	2.7	0.5
						40	5.0	4.6	0.4
						50	6.9	6.4	0.5
						60	8.9	8.9	0
	0.9					10	0.6	0.4	0.2
						20	1.7	1.5	0.2
						30	3.3	3.5	−0.2
						40	5.7	6.4	−0.7
						50	8.4	9.8	−1.4
						60	11.1	13.4	−2.3
	0.6		2.0			10	1.2	1.2	0
						20	3.2	3.9	−0.7
						30	5.9	7.3	−1.4
						40	9.0	11.5	−2.5
						50	12.5	16.7	−4.2
						60	15.9	19.2	−3.3
	0.9					10	1.2	1.2	0
						20	3.3	4.3	−1.0
						30	6.2	8.4	−2.2
						40	10.1	14.8	−4.7
						50	15.1	19.1	−4.0
						60	19.7	22.3	−2.6
	0.6		0.5			10	0.3	0.1	0.2
						20	0.8	0.4	0.4
						30	1.6	0.8	0.8
						40	2.6	1.3	1.3
						50	3.5	1.5	2.0
						60	4.5	1.2	3.3
	0.9					10	0.3	0.1	0.2
						20	0.9	0.5	0.4
						30	1.7	1.1	0.6
						40	2.8	2.3	0.5
						50	4.2	5.2	−1.0
						60	5.5	7.0	−1.5

$$\text{Average Error} = \sum \frac{|\Delta C_N|}{n} = 1.27$$

Ref	M	R_ℓ (based on d_{equiv})	a/b	$\dfrac{\ell_B}{d_{equiv}}$	Nose Shape	α (deg)	$C_{N_{calc}}$	$C_{N_{test}}$	ΔC_N
14	1.50	1.25×10^5	1.0	6	Blunt	35	4.5	5.0	−0.5
						65	10.5	9.0	1.5
						95	11.7	10.0	1.7
				8	Cone	35	4.2	4.5	−0.3
						65	9.7	8.5	1.2
						95	10.7	8.7	2.0
						125	8.6	6.2	2.4
						155	2.6	2.7	−0.1
				9		35	5.4	6.0	−0.6
						65	13.0	10.7	2.3
						95	14.6	11.5	3.1
						125	11.5	8.5	3.0
						155	3.3	7.0	−3.7
				11		35	6.6	7.5	−0.9
						65	16.3	14.0	2.3
						95	18.4	14.6	3.8
						125	14.3	11.5	2.8
						165	1.5	2.0	−0.5
				9	Ogive	35	5.7	6.2	−0.5
						65	13.8	11.5	2.3
						95	15.5	12.0	3.5
						125	12.2	9.5	2.7
						155	3.5	3.8	−0.3
				7		35	4.1	4.7	−0.6
						65	9.4	8.4	1.0
						95	10.4	8.3	2.1
						125	8.4	6.0	2.4
						155	2.6	3.0	−0.4
				11		35	6.5	7.3	−0.8
						65	16.0	13.0	3.0
						95	18.1	14.5	3.6
						125	14.1	10.9	3.2
						155	4.0	4.5	−0.5
	2.86			6	Blunt	35	4.6	4.0	0.6
						65	9.1	8.4	0.7
						95	10.3	10.0	0.3
				8		35	5.8	5.4	0.4
						65	12.0	11.0	1.0
						85	13.6	12.9	0.7

TABLE 4.2.1.2-C (CONTD)

Ref	M	R_ℓ (based on d_{equiv})	a/b	$\frac{\ell_B}{d_{equiv}}$	Nose Shape	α (deg)	$C_{N_{calc}}$	$C_{N_{test}}$	ΔC_N
14	2.86	1.25×10^5	1.0	7	Cone	35	4.3	3.8	0.5
						65	8.4	8.0	0.4
						95	9.4	9.0	0.4
						125	7.3	6.0	1.3
						155	2.8	1.7	1.1
				9		35	5.5	5.2	0.3
						65	11.2	10.5	0.7
						95	12.8	12.0	0.8
						125	9.6	8.1	1.5
						155	3.6	2.4	1.2
				11		35	6.8	6.5	0.3
						65	14.1	13.5	0.6
						95	16.2	15.0	1.2
						125	11.9	10.5	1.4
						155	4.4	3.3	1.1
				9	Ogive	35	5.8	5.5	0.3
						65	12.0	11.0	1.0
						95	13.7	12.6	1.1
						125	10.2	9.0	1.2
						155	3.8	2.6	1.2
				7		35	4.2	4.0	0.2
						65	8.2	7.8	0.4
						95	9.2	8.4	0.8
						125	7.1	5.9	1.2
						155	2.8	1.7	1.1
				9		35	5.4	5.4	0
						65	11.0	10.5	0.5
						95	12.5	11.6	0.9
						125	9.4	8.5	0.9
						155	3.5	2.6	0.9
				11		35	6.7	6.6	0.1
						65	13.8	13.0	0.8
						95	15.9	14.5	1.4
						125	11.8	10.4	1.4
						155	4.3	3.4	0.9
16	4.24	5.4×10^5	1.0	7	Cone	4	0.16	0.22	−0.06
						8	0.49	0.50	−0.01
						12	0.94	0.85	0.09
						16	1.42	1.22	0.20

TABLE 4.2.1.2-C (CONTD)

Ref	M	R_ℓ (based on d_{equiv})	a/b	$\dfrac{\ell_B}{d_{equiv}}$	Nose Shape	α (deg)	$C_{N_{calc}}$	$C_{N_{test}}$	ΔC_N
16	4.24	5.4×10^5	1.0	7	Cone	20	1.90	1.62	0.28
						24	2.39	2.05	0.34
				10		4	0.20	0.26	−0.06
						8	0.59	0.64	−0.05
						12	1.24	1.11	0.13
						16	1.92	1.66	0.26
						20	2.57	2.30	0.27
						24	3.34	3.03	0.31
	5.04	2.6×10^5				4	0.21	0.28	−0.07
						8	0.63	0.65	−0.02
						12	1.23	1.06	0.17
						16	1.81	1.53	0.28
						20	2.45	2.08	0.37
						24	3.23	2.67	0.56
				7	Ogive	4	0.18	0.21	−0.03
						8	0.49	0.46	0.03
						12	0.93	0.78	0.15
						16	1.32	1.14	0.18
	6.28	1.1×10^5			Cone	4	0.19	0.20	−0.01
						8	0.51	0.47	0.04
						12	0.89	0.78	0.11
						16	1.31	1.18	0.13
						20	1.76	1.64	0.12
						24	2.28	2.14	0.14
15	1.2	3.8×10^5	1.0	10	Ogive	10	0.8	0.5	0.3
						20	2.3	2.0	0.3
						30	5.1	4.8	0.3
						40	9.2	8.4	0.8
						50	13.0	11.1	1.9
						60	16.0	14.8	1.2
	1.5					10	0.7	0.5	0.2
						20	2.5	2.6	−0.1
						30	5.8	5.6	0.2
						40	9.4	8.7	0.7
						50	12.4	11.8	0.6
						60	14.7	14.2	0.5
	2.0					10	0.8	0.8	0
						20	2.8	2.8	0
						30	6.0	5.4	0.6

TABLE 4.2.1.2-C (CONTD)

Ref	M	R_ℓ (based on d_{equiv})	a/b	$\dfrac{\ell_B}{d_{equiv}}$	Nose Shape	α (deg)	$C_{N_{calc}}$	$C_{N_{test}}$	ΔC_N
15	2.0	3.8×10^5	1.0	10	Ogive	40	8.6	8.2	0.4
						50	11.0	11.0	0
						60	13.3	13.0	0.3
	1.2		2.0			10	1.4	1.3	0.1
						20	4.3	5.2	−0.9
						30	9.2	9.8	−0.6
						40	16.3	15.0	1.3
						50	23.0	18.8	4.2
						60	28.3	21.9	6.4
	1.5					10	1.4	1.7	−0.3
						20	4.5	5.4	−0.9
						30	10.2	10.0	0.2
						40	16.8	14.7	2.1
						50	22.2	19.0	3.2
						60	25.9	21.2	4.7
	2.0					10	1.4	1.6	−0.2
						20	5.1	5.1	0
						30	10.7	9.3	1.4
						40	15.4	13.4	2.0
						50	19.5	17.3	2.2
						60	23.4	20.4	3.0
	1.2		0.5			10	0.3	0.2	0.1
						20	1.2	0.7	0.5
						30	2.6	2.2	0.4
						40	4.6	4.6	0
						50	6.5	6.4	0.1
						60	8.0	7.5	0.5
	1.5					10	0.4	0.3	0.1
						20	1.2	0.9	0.3
						30	2.9	2.8	0.1
						40	4.7	5.1	−0.4
						50	6.2	6.9	−0.7
						60	7.4	8.5	−1.1
	2.0					10	0.4	0.4	0
						20	1.4	1.3	0.1
						30	3.0	3.0	0
						40	4.4	4.7	−0.3
						50	5.6	7.4	−1.8
						60	6.6	7.5	−0.9

$$\text{Average Error} = \sum \frac{|\Delta C_N|}{n} = 0.94$$
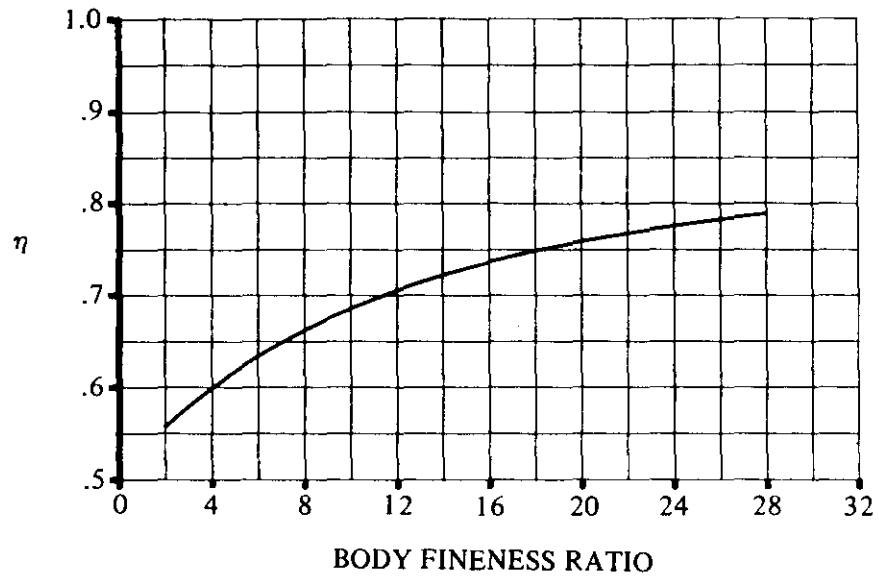
FIGURE 4.2.1.2-35a RATIO OF THE DRAG COEFFICIENT OF A CIRCULAR CYLINDER OF
FINITE LENGTH TO THAT OF A CYLINDER OF INFINITE LENGTH
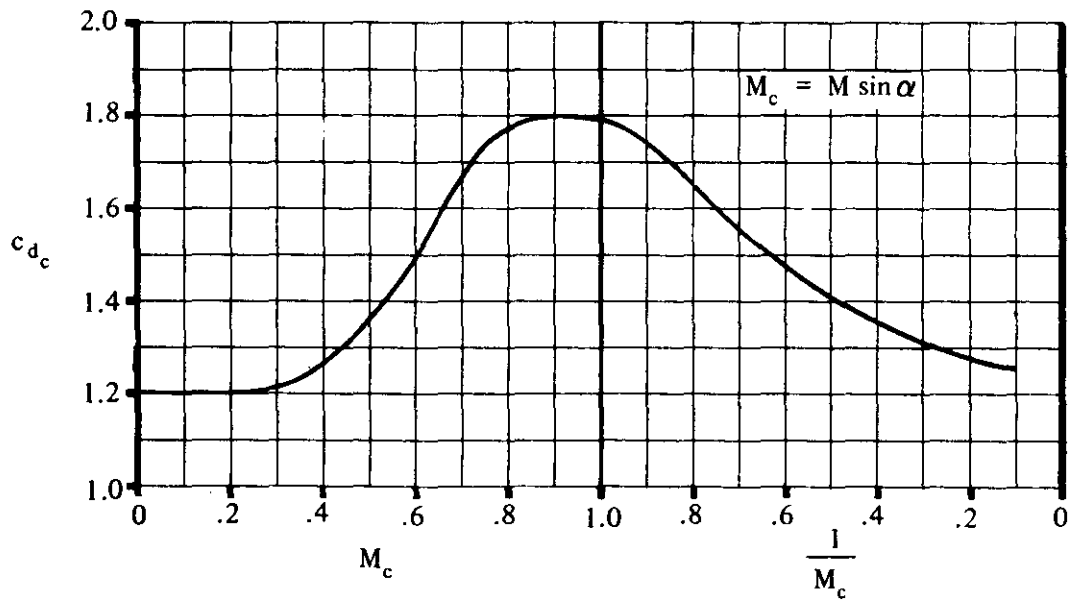
FIGURE 4.2.1.2-35b STEADY-STATE CROSS-FLOW DRAG COEFFICIENT FOR CIRCULAR
CYLINDERS (TWO DIMENSIONAL)
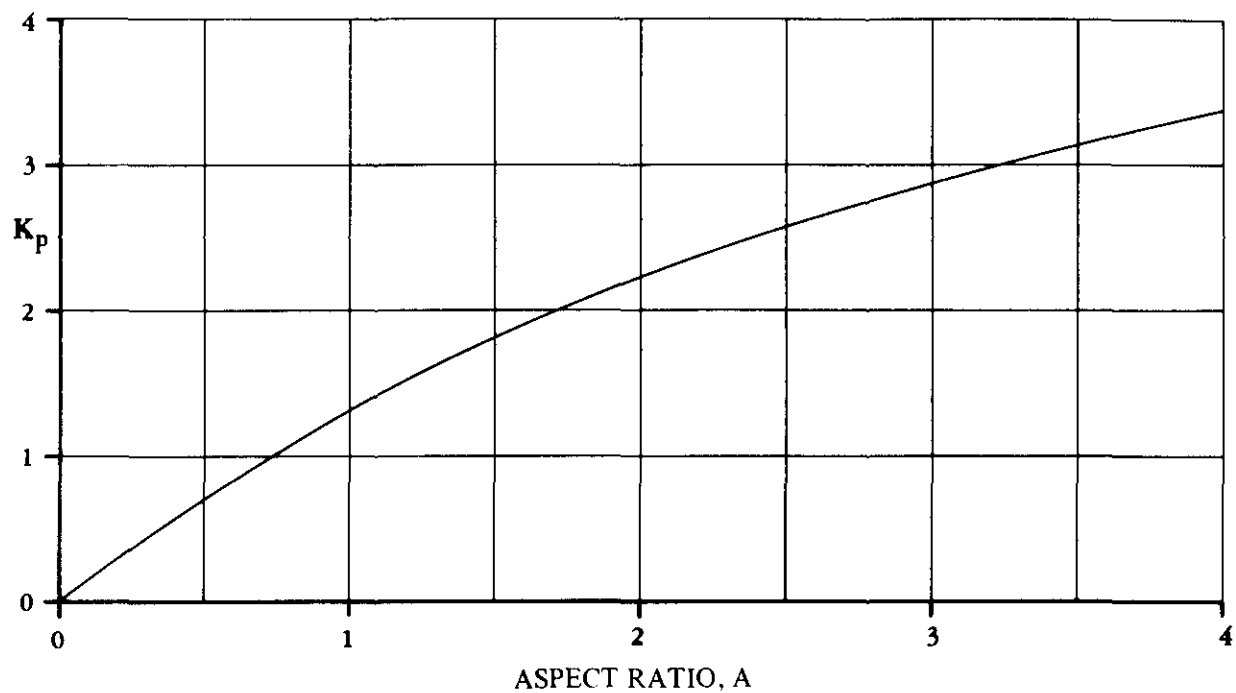
FIGURE 4.2.1.2-36a VARIATION OF POTENTIAL-FLOW LIFT PARAMETER WITH ASPECT
RATIO FOR ELLIPTICAL CROSS-SECTION BODIES
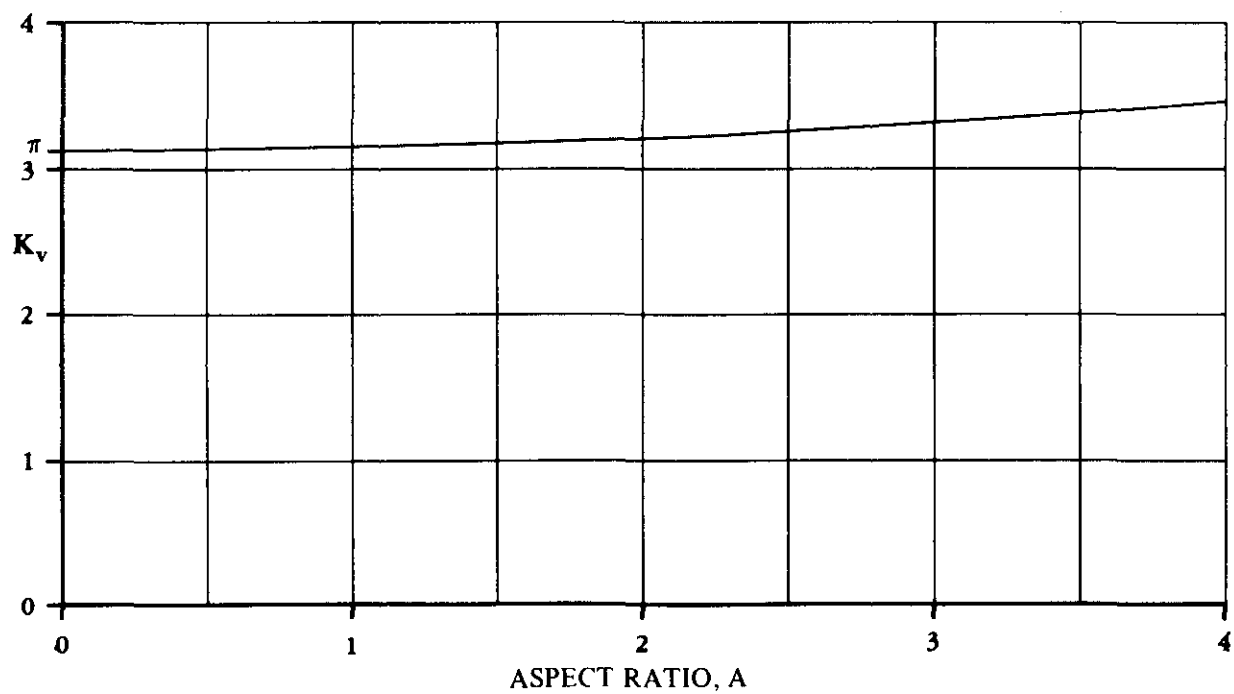
FIGURE 4.2.1.2-36b VARIATION OF VORTEX LIFT PARAMETER WITH ASPECT RATIO
FOR ELLIPTICAL CROSS-SECTION BODIES

4.2.1.2-36

BODY PLANFORM

$$d_{equiv} = 2 \sqrt{\frac{a\,b}{4}}$$
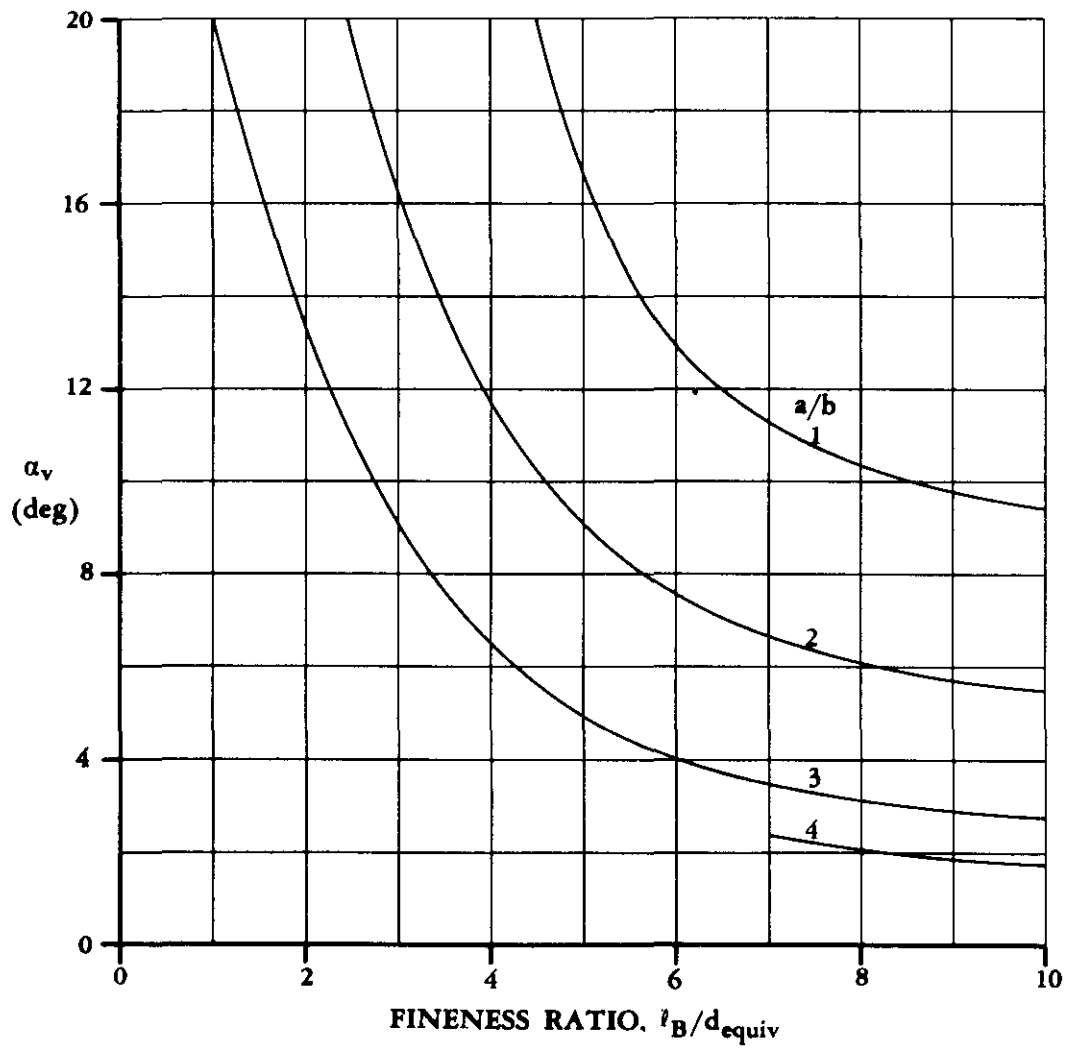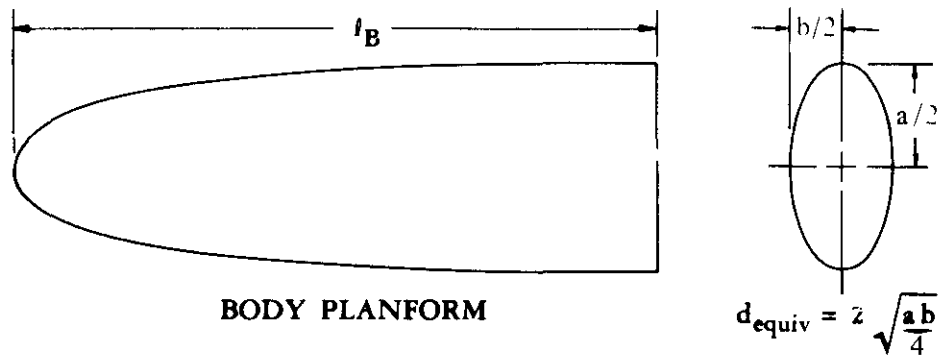
FIGURE 4.2.1.2-37 VARIATION OF ANGLE OF ATTACK FOR ONSET OF VORTEX
LIFT WITH FINENESS RATIO AND THICKNESS RATIO FOR
ELLIPTICAL BODIES
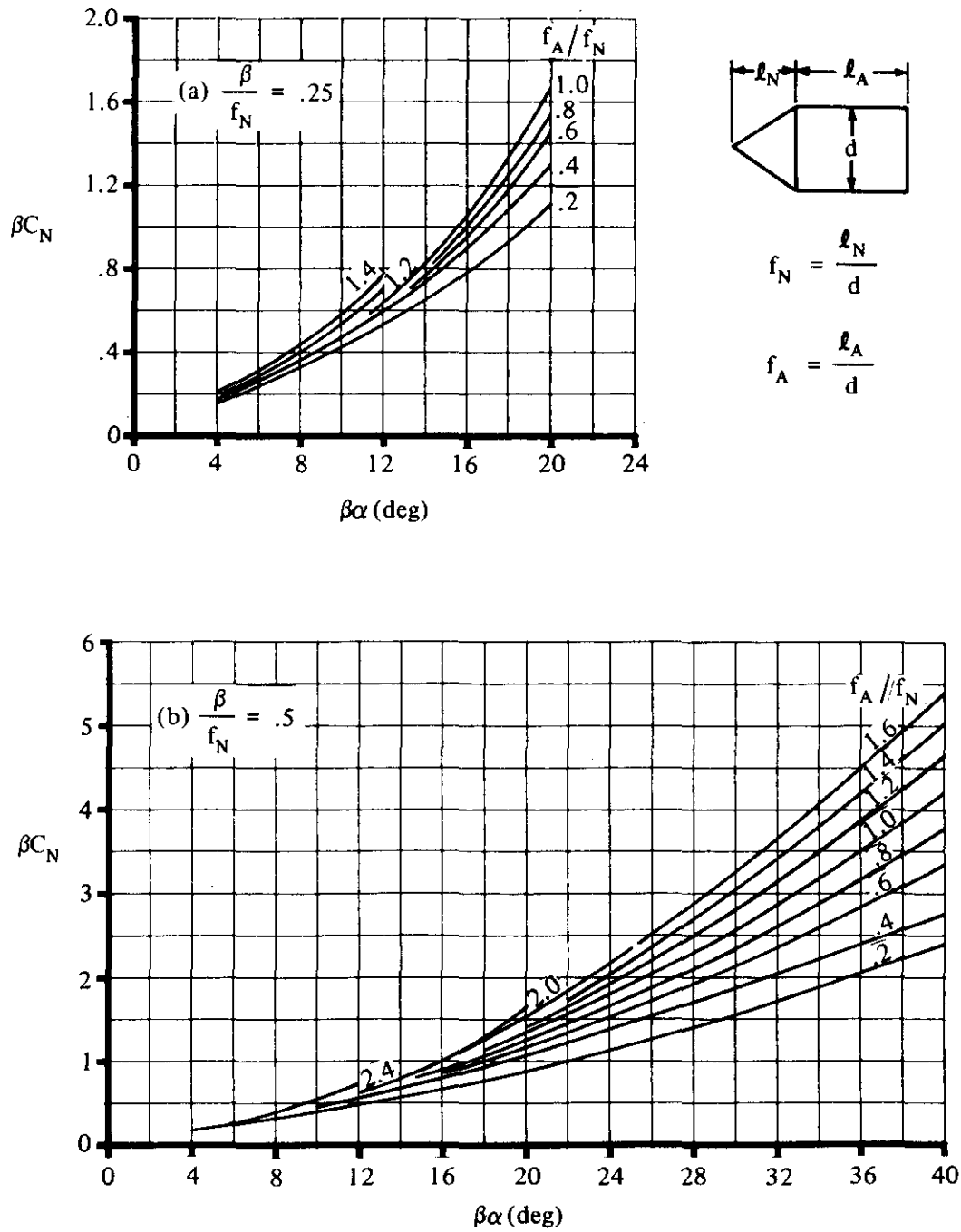
FIGURE 4.2.1.2-38 NORMAL-FORCE COEFFICIENT FOR CONE-CYLINDERS AT
SUPERSONIC SPEEDS
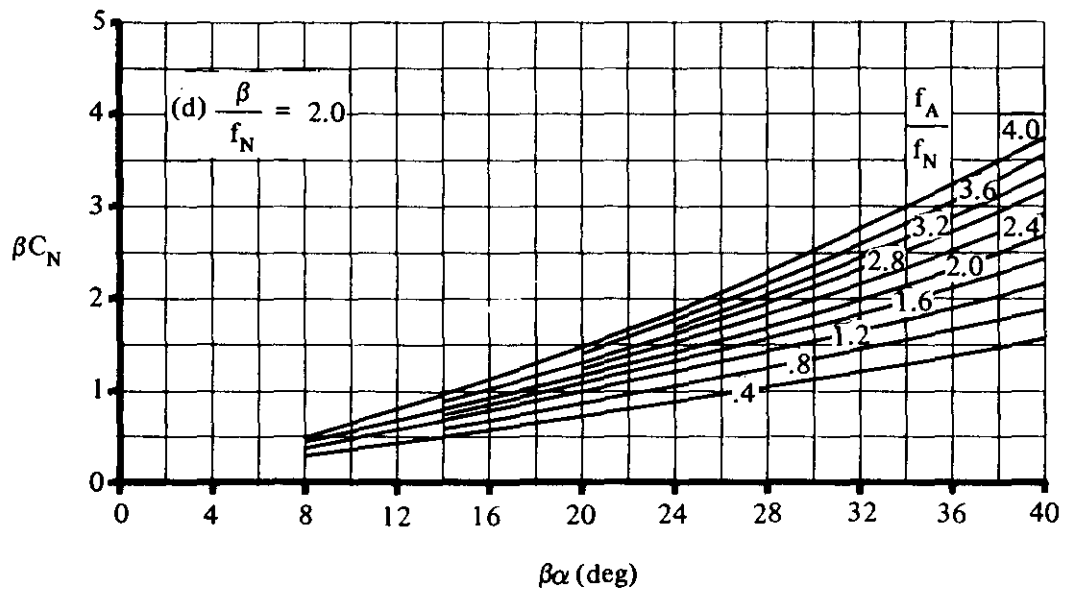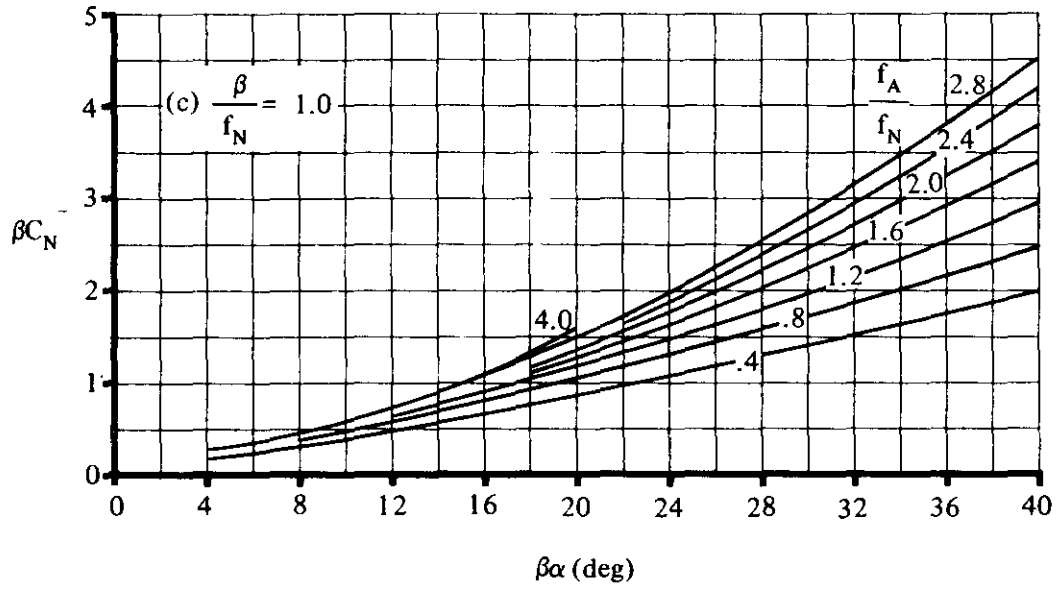
FIGURE 4.2.1.2-38 (CONTD)
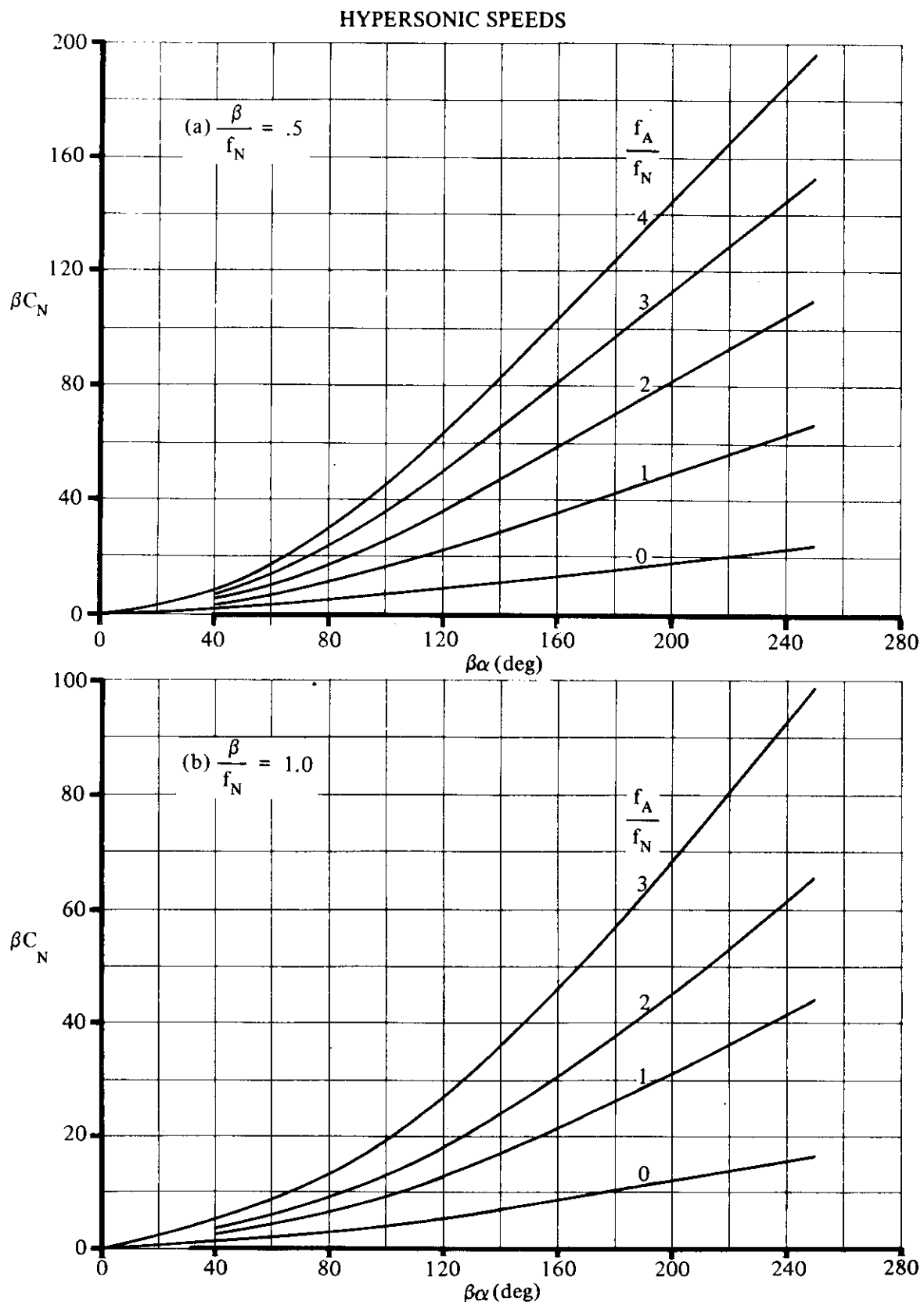
FIGURE 4.2.1.2-40 NORMAL-FORCE COEFFICIENT FOR CIRCULAR CONE-CYLINDERS
AT HYPERSONIC SPEEDS

4.2.1.2-40
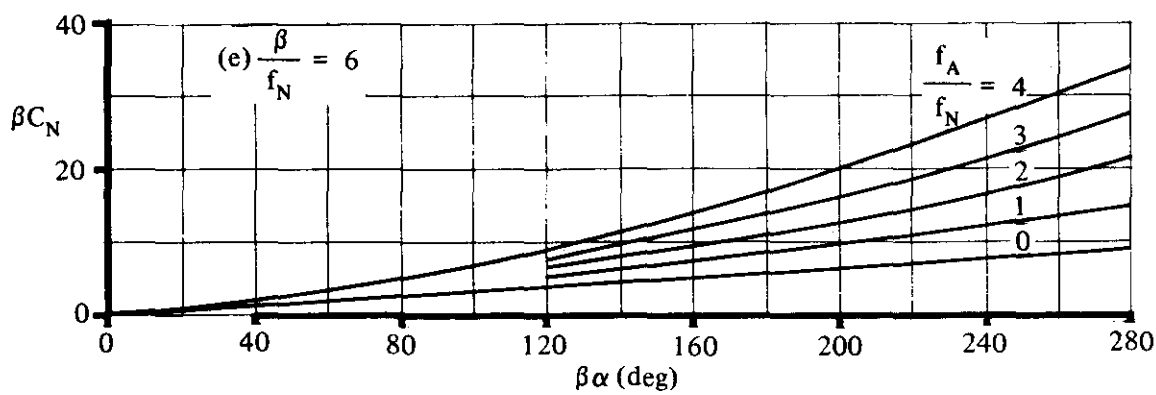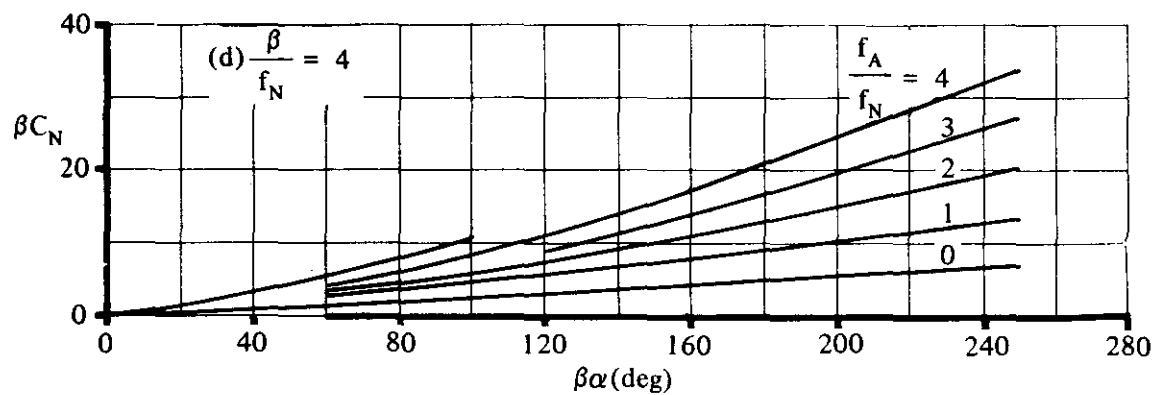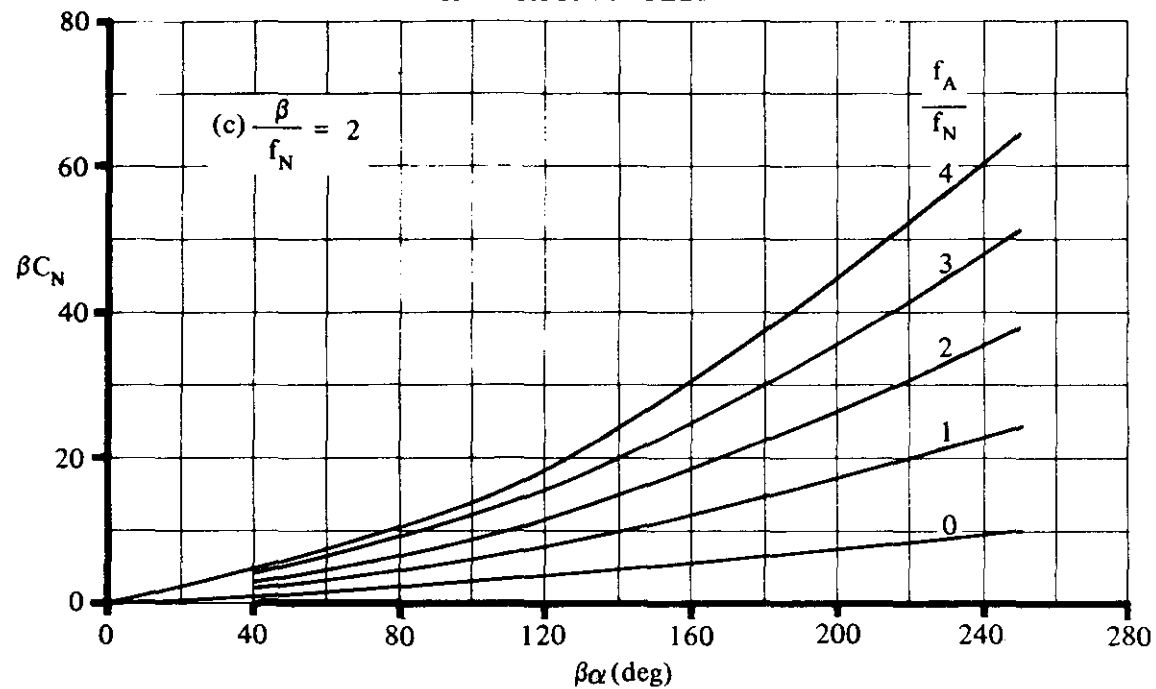
HYPERSONIC SPEEDS

FIGURE 4.2.1.2-40 (CONTD)

HYPERSONIC SPEEDS
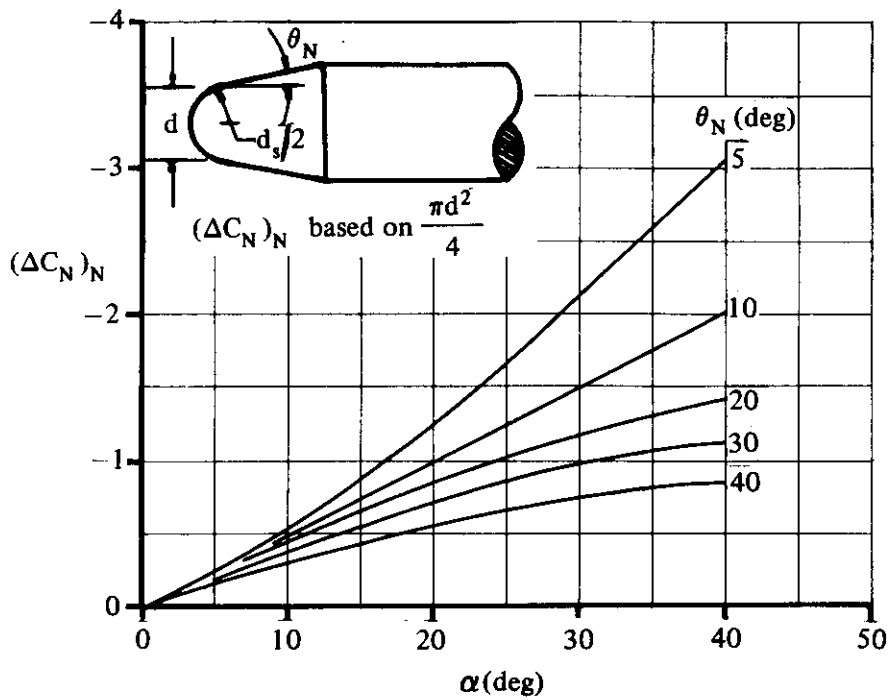
FIGURE 4.2.1.2-42a INCREMENT IN NORMAL FORCE DUE TO NOSE BLUNTING OF A CONE
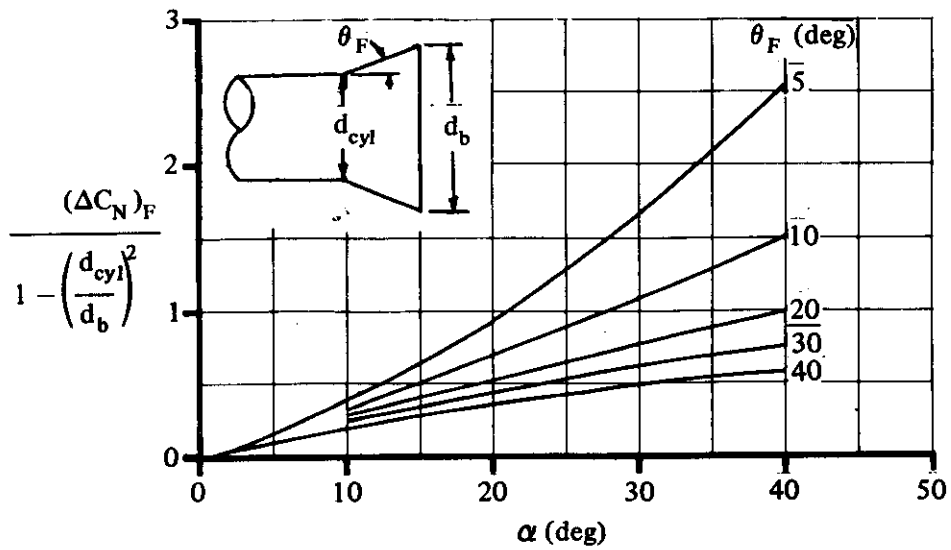
FIGURE 4.2.1.2-42b INCREMENT IN NORMAL FORCE DUE TO BODY FLARE

4.2.1.2-42

(a) $0 \leqslant \theta \leqslant 90^{\circ}$; $0 \leqslant \alpha \leqslant 40^{\circ}$
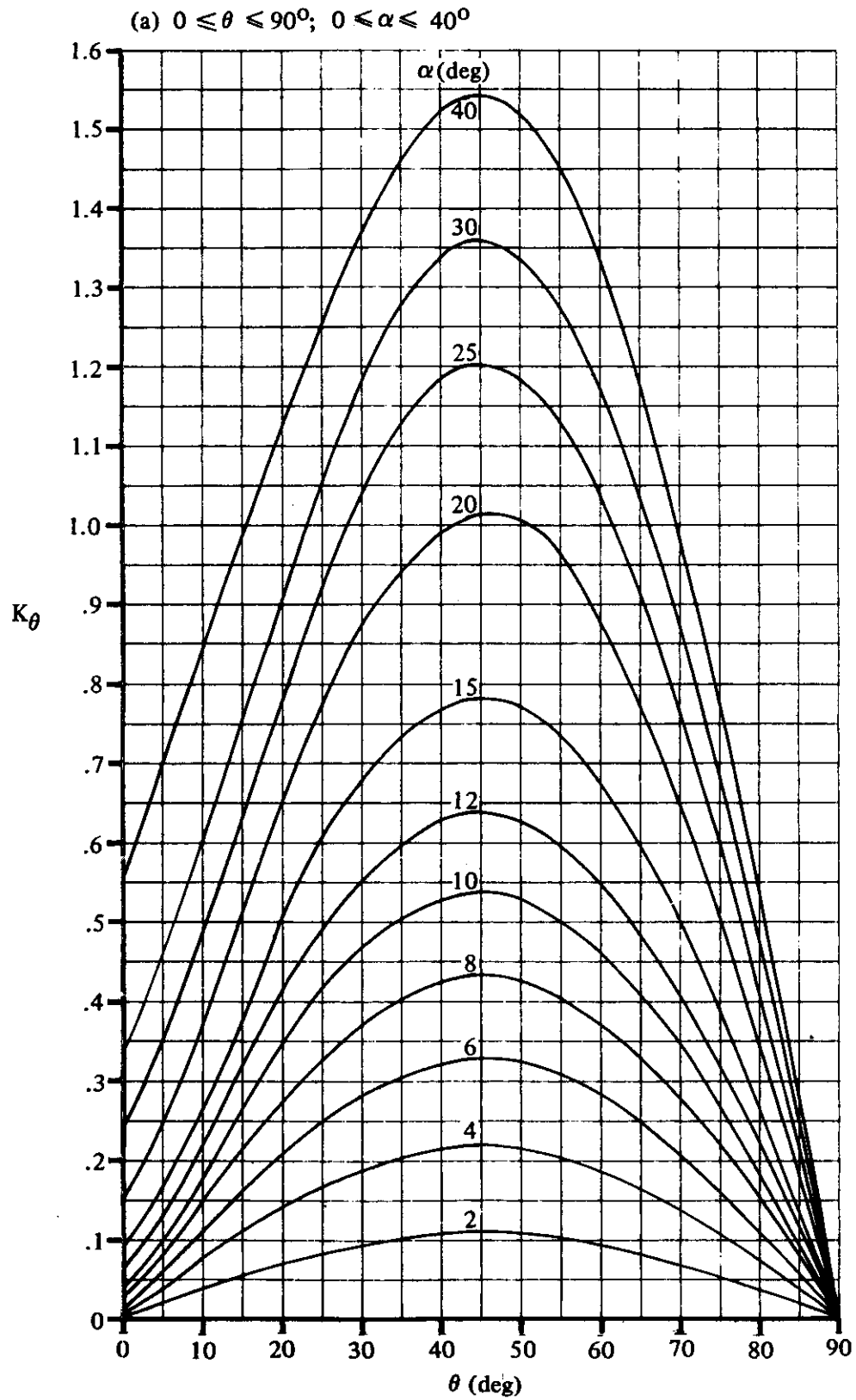
FIGURE 4.2.1.2-43 PRESSURE-SURFACE-SLOPE INTEGRAL FACTOR

4.2.1.2-43

(b) $0 \leqslant \theta \leqslant 90^{\circ}$; $50^{\circ} \leqslant \alpha \leqslant 90^{\circ}$
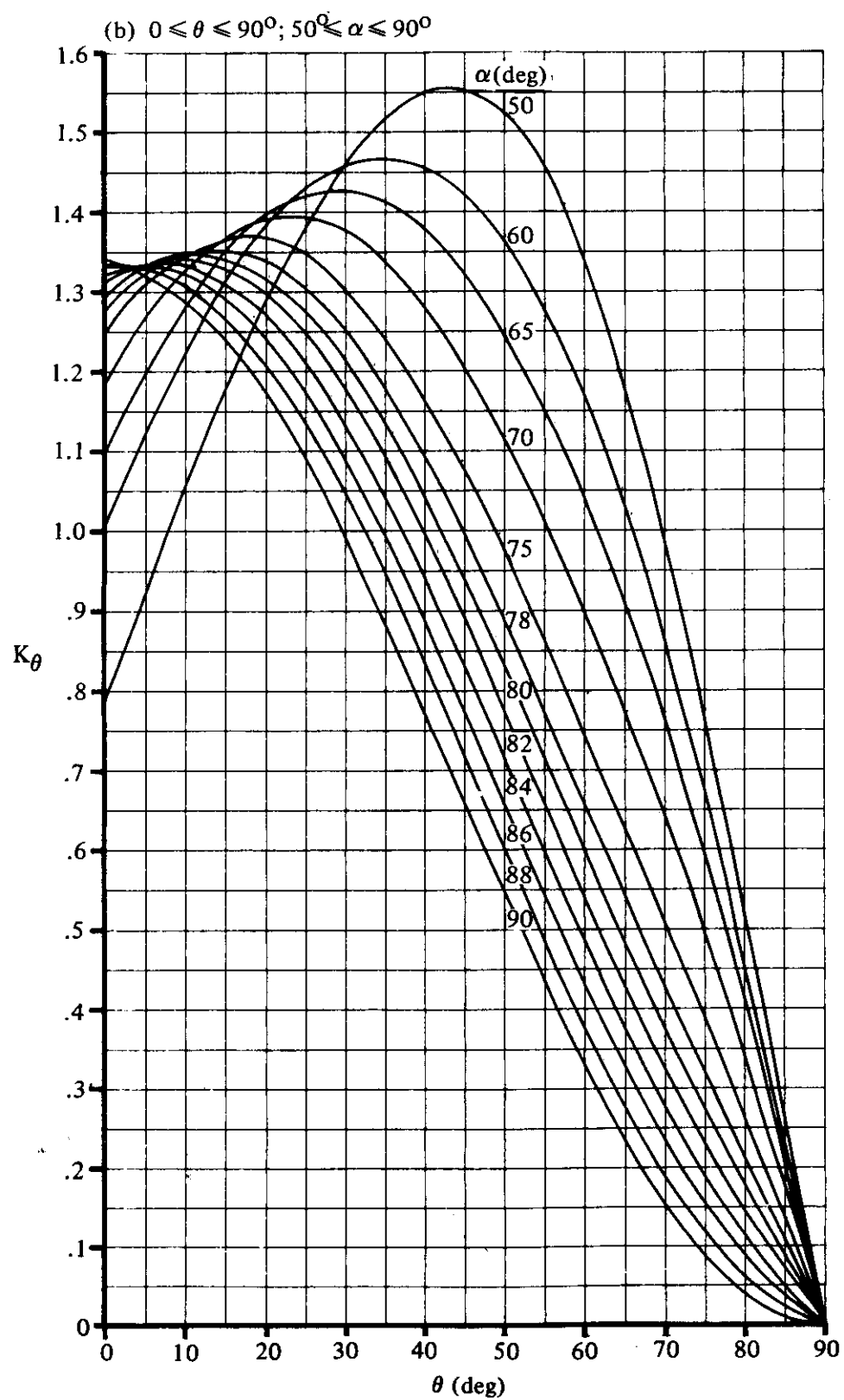
FIGURE 4.2.1.2-43 (CONTD)

4.2.1.2-44

4.2.2 BODY PITCHING MOMENT

4.2.2.1 BODY PITCHING-MOMENT-CURVE SLOPE

A. SUBSONIC

Two methods are presented in this section for estimating the body pitching-moment-curve slope at angles of attack near zero. Several additional methods are presented in References 1 through 4 of Section 4.2.1.1. As in the case with lift, moments acting on bodies are frequently considered in the literature to be divisible into two contributions — one due to potential flow over the forward part of the body and the other due to viscous cross flow over the aft part of the body. The general discussion of Section 4.2.1.2 on these flow conditions is directly applicable to this section.

DATCOM METHODS

The two methods presented for calculating the body pitching-moment-curve slope are distinguished from one another in that Method 1 is applicable only to bodies in the presence of a wing flow field; whereas Method 2 is valid only when applied to a body in undisturbed flow.

It is not feasible to present generalized design charts; however, both Equations 4.2.2.1-a and -b can be integrated for any arbitrary body of revolution.

Method 1

Multhopp's method, taken from Reference 1, estimates the body pitching-moment-curve slope in the presence of a wing flow field. This method is valid for bodies of revolution in the low subsonic speed regime. Application of this method is practical only when test data are available for the wing pitching-moment-curve slope of the wing-body combination. This method then allows a separate analysis of the body effects to be made, enabling a build-up of the wing-body pitching-moment-curve slope based on test data for the wing contribution and on this method for the body contribution. If no wing pitching-moment-curve-slope test data are available, the method of Section 4.3.2.2 is recommended for estimating the wing-body pitching-moment-curve slope. The body pitching-moment-curve slope in the presence of a wing flow field, based on the product of wing area and wing MAC $S_W \bar{c}_W$, is given by

$$C_{m_\alpha} = \frac{1}{36.5 \, S_W \bar{c}_W} \int_0^{\ell_B} w_f^2 \left(\frac{\partial \epsilon_u}{\partial \alpha} + 1 \right) dx \quad \text{(per degree)} \qquad 4.2.2.1\text{-a}$$

where

S_W is the wing reference area.

$\bar{c}_W$ is the wing mean aerodynamic chord.

ℓ_B is the length of the body

w_f is the average width of a given body segment (see Sketch (a)).

$\dfrac{\partial \epsilon_u}{\partial \alpha}$ is the rate of change of upwash with respect to angle of attack. The estimation of $\dfrac{\partial \epsilon_u}{\partial \alpha}$ varies for various fuselage segments. These definitions of $\dfrac{\partial \epsilon_u}{\partial \alpha}$ with their respective body segments are presented in Sketch (a). The values of $\dfrac{\partial \epsilon_u}{\partial \alpha}$ for the body increments forward of the wing are estimated by the curves presented in Figures 4.2.2.1-22a and -22b. The separate curve for the body increment immediately forward of the wing is necessary because of the rapid increase of upwash in this vicinity. Both curves of $\dfrac{\partial \epsilon_u}{\partial \alpha}$ presented in Figures 4.2.2.1-22a and -22b are based on a wing-body lift-curve slope of 0.0785 per degree. To correct for other values of $\left(C_{L_\alpha}\right)_{WB}$, multiply the values of $\dfrac{\partial \epsilon_u}{\partial \alpha}$ obtained from these figures by the ratio $\left(C_{L_\alpha}\right)_{WB}/0.0785$. (The values of $\left(C_{L_\alpha}\right)_{WB}$ should be obtained from test data or Section 4.3.1.2 and expressed in units of per degree.) The estimation of $\dfrac{\partial \epsilon_u}{\partial \alpha}$ for that portion of the body aft of the wing is based on the assumption of a linear variation of downwash from the trailing edge of the exposed wing root chord to the horizontal tail. If the methods of Section 4.4.1 are to be used for estimating $\dfrac{\partial \bar{\epsilon}}{\partial \alpha}$, the downwash should be calculated for the trailing-edge point of the body; i.e., assume the horizontal-tail MAC quarter-chord point coincides with the trailing edge of the fuselage.

Segments 1-5 $\partial \epsilon_u / \partial \alpha$ from figure 4.2.2.1-22b

Segment 6 $\partial \epsilon_u / \partial \alpha$ from figure 4.2.2.1-22a

Segments 7-14 $1 + \dfrac{\partial \epsilon_u}{\partial \alpha} = \dfrac{x_1}{\ell_h}\left(1 - \dfrac{\partial \bar{\epsilon}}{\partial \alpha}\right)$
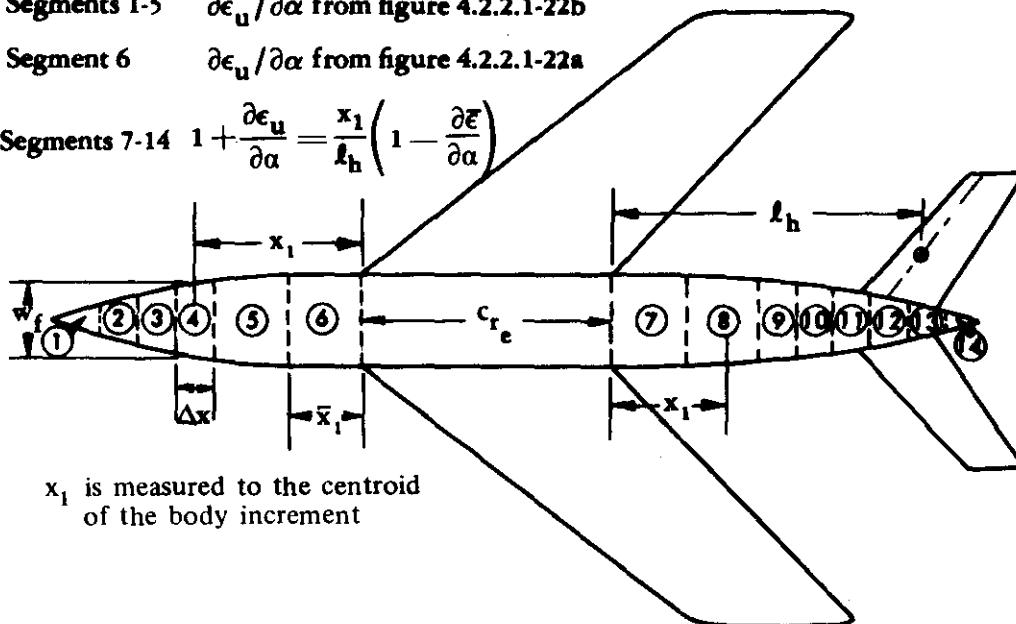
x_1 is measured to the centroid of the body increment

SKETCH (a)

4.2.2.1-2

Method 2

The method of Reference 2 is presented for estimating the body pitching-moment-curve slope. Only the potential-flow portion of the method of Reference 2 is applied, limiting the application of the method to angles of attack near zero. The body pitching-moment-curve slope, based on the total body volume V_B, is given by

$$C_{m_\alpha} = \frac{2(k_2 - k_1)}{V_B} \int_0^{x_0} \frac{dS_x}{dx}(x_m - x) \, dx \quad \text{(per radian)} \qquad 4.2.2.1\text{-b}$$

where

$(k_2 - k_1)$ is the apparent mass factor developed by Munk and given in Figure 4.2.1.1-20a.

V_B is the volume of the body.

x_0 is the body station where the flow ceases to be potential. It is a function of x_1, the body station where the parameter dS_x/dx first reaches its maximum negative value. The parameters x_0 and x_1 are correlated in Figure 4.2.1.1-20b.

S_x is the body cross-sectional area at any body station.

x_m is the longitudinal distance from the nose to the chosen moment center.

x is the location of the center of pressure of a given body segment, measured from the nose.

In many cases it will be possible to determine the location of x_1 by inspection. For cases that are doubtful, the area distribution should be plotted and examined to determine the location where dS_x/dx first reaches its maximum negative value.

The pitching-moment-curve slopes of several bodies of revolution have been calculated by this method and compared with test data in Reference 2. In general, the method has a fair degree of accuracy at angles of attack near zero.

For a rapid but approximate estimation, slender-body theory can be used, which gives

$$C_{m_\alpha} = 2\left(\frac{x_m}{\ell_B} + \frac{V_B}{S_b \ell_B} - 1\right) \quad \text{(per radian)} \qquad 4.2.2.1\text{-c}$$

where C_{m_α} is based on $S_b \ell_B$, S_b being the base area of the body of revolution and ℓ_B the total length of the body of revolution.

No method is available for estimating the pitching-moment-curve slope of a body of noncircular

cross section. Consequently, test data must be relied upon as the basis for predicting the pitching-moment-curve slope of such configurations. A summary of available test data on bodies of noncircular cross section at subsonic speeds is presented as Table 4.2.1.1-A.

Sample Problems

1. Body in the wing flow field

Given: The wing-body configuration of Reference 3
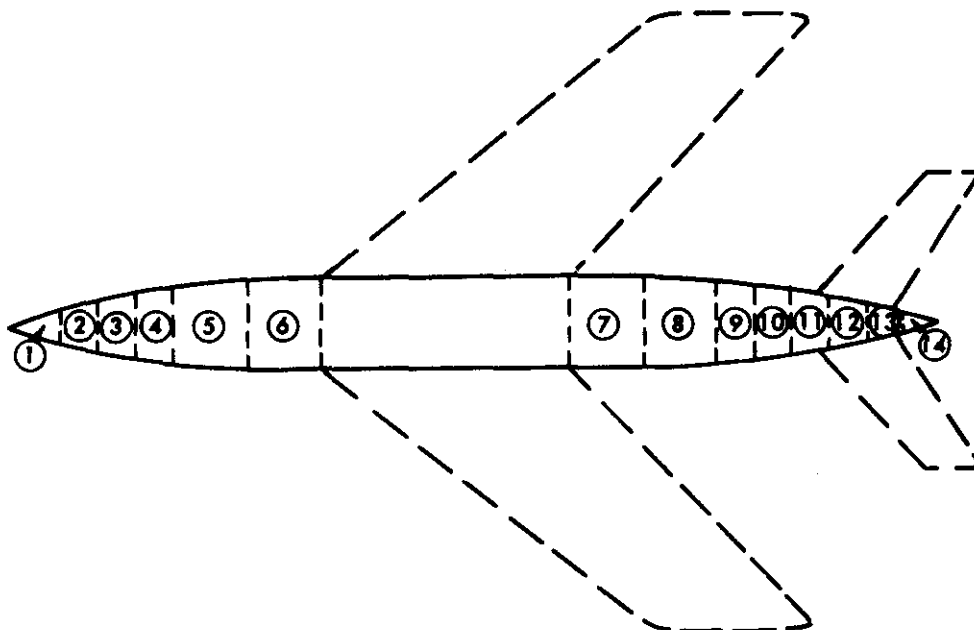
Body Increment	Δx (in.)	w_f (in.)	x_1 (in.)
1	8.07	2.7	53.0
2	7	6.9	45.5
3	7	10.3	38.5
4	7	13.4	31.5
5	14	16.1	21.0
6	14	16.8	14.0
7	14	16.8	7.0
8	14	16.1	21.0
9	7	14.1	31.5
10	7	12.7	38.5
11	7	11.1	45.5
12	7	8.2	52.5
13	7	5.1	59.5
14	5.21	1.7	65.6

$$S_W = 4429 \text{ sq in.} \qquad \bar{c}_W = 39.97 \text{ in.} \qquad \frac{\partial \bar{\epsilon}}{\partial \alpha} = 0.50 \text{ (test data)}$$

$$\ell_B = 170.95 \text{ in.} \qquad \ell_h = 56.26 \text{ in.} \qquad \left(C_{L_\alpha}\right)_{WB} = 0.047 \text{ per degree (test data)}$$

$$c_{r_e} = 45.67 \text{ in.}$$

Compute:

Determine $\dfrac{\partial \epsilon_u}{\partial \alpha}$ at each body increment

①	②	③	④
Body Increment	$\dfrac{x_1}{c_{r_e}}$ and $\dfrac{\bar{x}_1}{c_{r_e}}$	$\partial \epsilon_u / \partial \alpha$ Figures 4.2.2.1-22a, -22b	$(\partial \epsilon_u / \partial \alpha)_{corrected}$ ③ (0.047)/0.0785
1	1.16	0.14	0.084
2	1.00	0.18	0.108
3	0.84	0.22	0.132
4	0.69	0.27	0.162
5	0.46	0.37	0.222
6	0.31	1.95	1.168

①	②	③	④
Body Increment	$\dfrac{x_1}{\ell_h}$	$\dfrac{x_1}{\ell_h}\left(1 - \dfrac{\partial \bar{\epsilon}}{\partial \alpha}\right)$	$\partial \epsilon_u / \partial \alpha$ ③ − 1.0
7	0.124	0.062	−0.928
8	0.373	0.187	−0.813
9	0.560	0.280	−0.720
10	0.684	0.342	−0.658
11	0.809	0.404	−0.596
12	0.933	0.467	−0.533
13	1.058	0.529	−0.471
14	1.166	0.583	−0.417

Evaluate $\displaystyle\int_0^{\ell_B} w_f^2 \left(\frac{\partial \epsilon_u}{\partial \alpha} + 1\right) dx$

	①	②	③	④
Body Increment	w_f^2 (in.^{2})	$\dfrac{\partial \epsilon_u}{\partial \alpha} + 1$	Δx (in.)	$w_f^2 \left(\dfrac{\partial \epsilon_u}{\partial \alpha} + 1\right) \Delta x$ ②③④
1	7.29	1.084	8.07	63.77
2	47.6	1.108	7.0	369.19
3	106.1	1.132	7.0	840.74
4	179.6	1.162	7.0	1460.87
5	259.2	1.222	14.0	4434.39
6	282.2	2.168	14.0	8565.33
7	282.2	0.062	14.0	244.96
8	259.2	0.187	14.0	678.59
9	198.8	0.280	7.0	389.66
10	161.3	0.342	7.0	386.15
11	123.2	0.404	7.0	348.41
12	67.2	0.467	7.0	219.68
13	26.0	0.529	7.0	96.28
14	2.89	0.583	5.21	8.78

$$\sum_{x=0}^{\ell_B} w_f^2 \left(\frac{\partial \epsilon_u}{\partial \alpha} + 1\right) \Delta x = 18{,}106.78 \text{ cu. in.}$$

Solution:

$$C_{m_\alpha} = \frac{1}{36.5 \, S_w \bar{c}_w} \int_0^{\ell_B} w_f^2 \left(\frac{\partial \epsilon_u}{\partial \alpha} + 1\right) dx \quad \text{(Equation 4.2.2.1-a)}$$

$$= \frac{18{,}106.78}{(36.5)(4429)(39.97)} = 0.00280 \text{ per degree}$$

No test data are available for the body in the presence of the wing flow field.

2. Potential Flow

Given: The 3/4-power body of revolution of Reference 12.
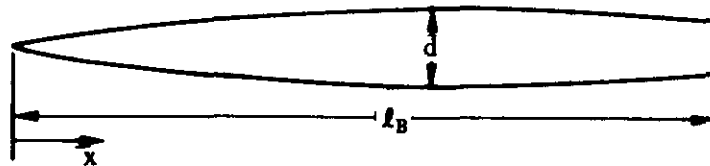
$$r = 0.255 \left[1 - \left(1 - \frac{2x}{6.375} \right)^2 \right]^{3/4} \qquad \ell_B = 5.036 \text{ ft} \qquad d = 0.510 \text{ ft}$$

$$V_B = 0.687 \text{ cu ft} \qquad f = \ell_B/d = 9.87 \qquad x_m = 3.54 \text{ ft} \qquad M = 0.40$$

Compute:

Determine x_1

The body station where dS_x/dx first reaches a maximum negative value can be determined by inspection; however, the area distribution is plotted to illustrate the determination of x_1.
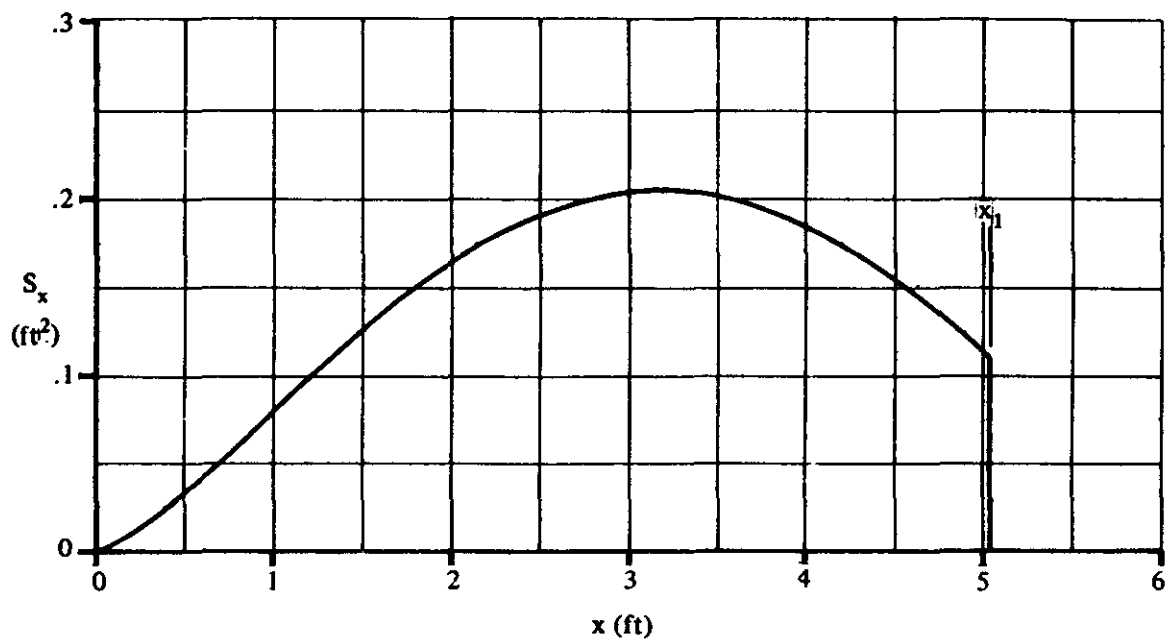
Cross-Sectional Area Distribution

$x_1 = 5.036 \text{ ft}$

$x_1/\ell_B = 5.036/5.036 = 1.0$

$x_0/\ell_B = 0.905 \quad \text{(figure 4.2.1.1-20b)}$

$x_0 = (0.905)(5.036) = 4.558 \text{ ft}$

$(k_2 - k_1) = 0.937 \quad \text{(figure 4.2.1.1-20a)}$

$$\frac{2(k_2 - k_1)}{V_B} = \frac{2(0.937)}{0.687} = 2.728$$

Evaluate $\displaystyle\int_0^{x_0} \frac{dS_x}{dx} (x_m - x)\, dx$

Station (ft)	r (ft)	S_x (ft²)	$\frac{dS_x}{dx} \Delta x = \Delta S_x$ (ft²)	x* (ft)	$(x_m - x)$ (ft)	$\frac{dS_x}{dx}(x_m - x)\Delta x$ (ft³)
0	0	0				
			0.0317	0.333	3.21	0.102
0.5	0.1005	0.0317				
			0.0468	0.769	2.77	0.130
1.0	0.1581	0.0785				
			0.0376	1.260	2.28	0.086
1.5	0.1922	0.1161				
			0.0472	1.756	1.78	0.084
2.0	0.2280	0.1633				
			0.0270	2.263	1.29	0.0348
2.5	0.2461	0.1903				
			0.0127	2.751	0.79	0.0100
3.0	0.2542	0.2030				
			−0.0016	3.250	0.29	−0.00046
3.5	0.2532	0.2014				
			−0.0166	3.748	−0.21	0.0035
4.0	0.2425	0.1848				
			−0.0327	4.275	−0.74	0.0242
$x_0 = 4.56$	0.2200	0.1521				

$$\sum_{x=0}^{x_0} \frac{dS_x}{dx}(x_m - x)\Delta x = 0.474 \text{ cu ft}$$

Solution:

$$C_{m_\alpha} = \frac{2(k_2 - k_1)}{V_B}\int_0^{x_0} \frac{dS_x}{dx}(x_m - x)\, dx \quad \text{(equation 4.2.2.1-b)}$$

$$= (2.728)(0.474)$$

$$= 1.293 \text{ per rad (based on } V_B)$$

This compares with a test value of 1.369 per radian from reference 12.

*x is taken at the center of volume of each body segment.

4.2.2.1-8

3. Slender-Body Theory

Given: The same configuration as sample problem 2.

$$x_m = 3.54 \text{ ft} \qquad \ell_B = 5.036 \text{ ft} \qquad V_B = 0.687 \text{ cu ft} \qquad S_b = 0.1103 \text{ sq ft}$$

Compute:

$$x_m/\ell_B = 3.54/5.036 = 0.7029$$

$$\frac{V_B}{S_b \ell_B} = \frac{0.687}{(0.1103)(5.036)} = 1.237$$

Solution:

$$C_{m_\alpha} = 2\left(\frac{x_m}{\ell_B} + \frac{V_B}{S_b \ell_B} - 1\right) \qquad \text{(equation 4.2.2.1-c)}$$

$$= 2(0.7029 + 1.237 - 1)$$

$$= 1.880 \text{ per rad (based on } S_b \ell_B)$$

$$= 1.52 \text{ per rad (based on } V_B)$$

B. TRANSONIC

Slender-body theory states that body force and moment characteristics are not functions of Mach number. Experimental data verify this result (references 4, 5, and 6). Any differences in the subsonic value of C_{m_α} obtained from paragraph A and the supersonic value of C_{m_α} obtained from paragraph C should be faired out smoothly in the transonic range. Experimental data should be used, when available, as a guide in fairing in the transonic range.

Transonic test data on bodies of noncircular cross section are available in references 25, 26, and 5 of table 4.2.1.1-A.

C. SUPERSONIC

Several theoretical methods have been developed that can be used for estimating the moment characteristics of bodies of revolution at supersonic speeds. However, these are best applied by machine methods. Some of these methods are discussed in paragraph C of Section 4.2.1.1.

DATCOM METHOD

An empirical method is presented, based on the data from reference 7, for ogive-cylinder and cone-cylinder bodies at supersonic speeds. Figure 4.2.2.1-23a gives the center-of-pressure location for ogive-cylinders, and figure 4.2.2.1-23b gives the center-of-pressure location for cone-cylinders. The moment slope, based on the product of the maximum frontal area and body length $S_B \ell_B$, is

$$C_{m_\alpha} = \left(\frac{x_m}{\ell_B} - \frac{x_{c.p.}}{\ell_B}\right) C_{N_\alpha} \qquad \text{(per radian)} \qquad \text{4.2.2.1-d}$$

where

$\dfrac{x_m}{\ell_B}$ is the desired moment-center location in fraction of body length.

4.2.2.1-9

$\dfrac{X_{c.p}}{\ell_B}$ is the center-of-pressure location in fraction of body length, obtained from figure 4.2.2.1-23a or figure 4.2.2.1-23b, depending upon the given configuration.

C_{N_α} is the normal-force-curve slope, based on maximum frontal area of the ogive-cylinder or cone-cylinder body, obtained from paragraph C of Section 4.2.1.1 (figures 4.2.1.1-21a and 4.2.1.1-21b, respectively).

Experimental data from reference 6 indicate that the center-of-pressure location of 1/2-power bodies is closely approximated by corresponding (same fineness ratio) ogive values. This reference also indicates that the center-of-pressure location for 3/4-power bodies is approximately 5 percent of the body length ahead of the corresponding cone location. Figure 4.2.2.1-23a is recommended for 1/2-power bodies. For 3/4-power bodies it is recommended that figure 4.2.2.1-23b be used with the center-of-pressure location moved forward approximately 5 percent from the chart value.

The center-of-pressure location of a boattail at the end of a semi-infinite cylindrical body is presented in figure 4.2.2.1-24. This chart is taken from reference 9 and is based on the results of reference 10.

The moment slope of an ogive-cylinder or cone-cylinder body with a boattail afterbody, based on the product of the maximum frontal area and the length of the ogive-cylinder or cone-cylinder body $S_B \ell_B$, is (see sketch (b))

$$ C_{m_\alpha} = \left(C_{m_\alpha}\right)_{\substack{\text{ogive/cone-}\\\text{cylinder}}} + \left\{ \frac{x_m}{\ell_B} - \left[\frac{(x_{c.p.})_b}{\ell_b} \frac{\ell_b}{\ell_B} + \left(1 - \frac{x_m}{\ell_B}\right) \right] \right\} \Delta C_{N_\alpha} \quad \text{(per radian)} \quad 4.2.2.1\text{-e} $$

where $\left(C_{m_\alpha}\right)_{\substack{\text{ogive/cone-}\\\text{cylinder}}}$ is obtained from equation 4.2.2.1-d, x_m/ℓ_B is defined above, and

$\dfrac{(x_{c.p.})_b}{\ell_b}$ is the center-of-pressure location of the boattail in fraction of boattail length, measured aft of the forward face of the boattail. This parameter is obtained from figure 4.2.2.1-24.

$\dfrac{\ell_b}{\ell_B}$ is the ratio of the boattail length to the length of the ogive-cylinder or cone-cylinder body.

ΔC_{N_α} is the increment in normal-force-curve slope, based on S_B, due to the addition of a boattail to a semi-infinite cylindrical body. This parameter is obtained from paragraph C of Section 4.2.1.1 (figure 4.2.1.1-22a).
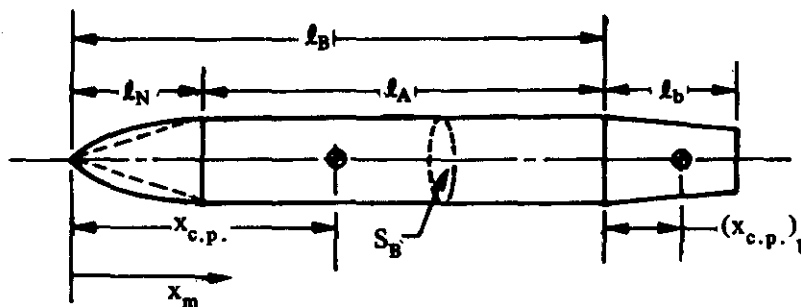
SKETCH (b)

The moment coefficient of a flared body of revolution is taken to be that predicted by impact theory.

The moment slope of an ogive-cylinder or cone-cylinder body with a flared afterbody, based on the product of the maximum frontal area and length of the ogive-cylinder or cone-cylinder body $S_B \ell_B$, is (see sketch (c))

$$C_{m_\alpha} = \left(C_{m_\alpha}\right)_{\substack{\text{ogive/cone-} \\ \text{cylinder}}} + C'_{m_\alpha}\,\frac{d^3}{a^2 \ell_B} + \frac{n}{\ell_B}\left(\Delta C_{N_\alpha}\right)_F \quad \text{(per radian)} \qquad 4.2.2.1\text{-f}$$

where

$\left(C_{m_\alpha}\right)_{\substack{\text{ogive/cone-} \\ \text{cylinder}}}$ is obtained from equation 4.2.2.1-d, and

C_{m_α} is the pitching-moment-curve slope of the flared afterbody about its own front face, based on the product of its base area and base diameter. This parameter is obtained from figure 4.2.2.1-25a.

d is the diameter of the base of the flared body.

a is the diameter of the front face of the flared body.

ℓ_B is the length of the ogive-cylinder or cone-cylinder body.

n is the distance from the face of the flared afterbody to the desired moment reference axis of the configuration, positive aft.

$\left(\Delta C_{N_\alpha}\right)_F$ is the normal-force-curve-slope increment, based on S_B, due to the addition of a flared afterbody behind a semi-infinite cylinder. This parameter is obtained from paragraph C of Section 4.2.1.1 (figure 4.2.1.1-22b).
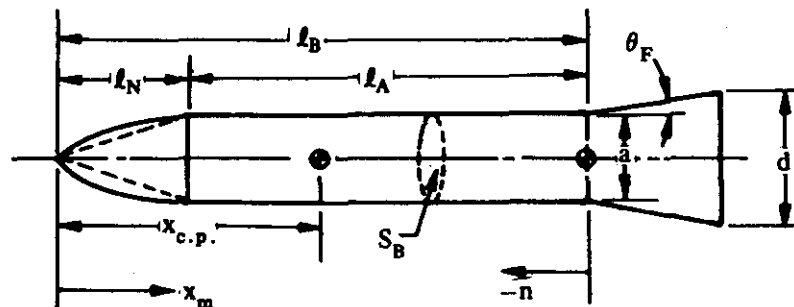
SKETCH (c.)

A comparison of test data with C_{m_α} of ogive-cylinder and cone-cylinder bodies calculated by this method is presented as table 4.2.2.1-A. The ranges of body geometry and Mach number of the test data are:

Cone-Cylinder	Ogive-Cylinder
$0 < f_A < 12$	$0 < f_A < 10$
$2.112 < f_N < 12$	$1.5 < f_N < 7$
$0 < f_A/f_N < 2.5$	$0 < f_A/f_N < 2.5$
$1.5 < M < 5.0$	$1.20 < M < 4.24$

No method is available for estimating the pitching-moment-curve slope of a body of noncircular cross section at supersonic speeds. Consequently, test data must be relied upon as the basis for predicting the pitching-moment-curve slope of such configurations. A summary of available test data on bodies of noncircular cross section at supersonic speeds is presented as table 4.2.1.1-C.

Sample Problem

Given: The cone-cylinder-flare body of reference 13. This is the same configuration as the sample problem of paragraph C of Section 4.2.1.1.
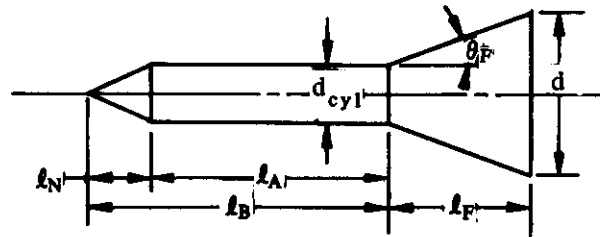
ℓ_N = 1.21 in. ℓ_A = 4.00 in. ℓ_B = 5.21 in.

ℓ_F = 2.40 in. d_{cyl} = a_{flare} = 1.0 in.

d_{flare} = d = 2.75 in. θ_F = 20°

n = −5.21 in. x_m = 0   M = 5.05; β = 4.95

Compute:

Cone-cylinder

f_N = ℓ_N/d_{cyl} = 1.21

f_A = ℓ_A/d_{cyl} = 4.00

$$f_A/f_N \quad = 4.00/1.21 = 3.31$$

$$f_N/\beta \quad = 1.21/4.95 = 0.244$$

$$x_{c.p.}/\ell_B = 0.36 \text{ (linear extrapolation)} \qquad \text{(figure 4.2.2.1-23b)}$$

$$C_{N_\alpha} = 3.52 \text{ per rad (based on } S_B) \text{ (sample problem, paragraph C, Section 4.2.1.1)}$$

$$\left(C_{m_\alpha}\right)_{\substack{\text{cone-}\\\text{cylinder}}} = \left(\frac{x_m}{\ell_B} - \frac{x_{c.p.}}{\ell_B}\right) C_{N_\alpha} \qquad \text{(equation 4.2.2.1-d)}$$

$$= (0 - 0.36)(3.52)$$

$$= -1.267 \text{ per rad (based on } S_B \ell_B)$$

Flare:

$$\left(\Delta C_{N_\alpha}\right)_F = 11.73 \text{ per rad (based on } S_B) \text{ (sample problem, paragraph C, Section 4.2.1.1)}$$

$$n/\ell_B \quad = -5.21/5.21 = -1.0$$

$$a/d \quad = 1.0/2.75 = 0.364$$

$$C'_{m_\alpha} \quad = -1.0 \text{ per rad}\left(\text{based on } \frac{\pi d^3}{4}\right) \qquad \text{(figure 4.2.2.1-25a)}$$

Solution:

$$C_{m_\alpha} \quad = \left(C_{m_\alpha}\right)_{\substack{\text{cone-}\\\text{cylinder}}} + C'_{m_\alpha} \frac{d^3}{a^2 \ell_B} + \frac{n}{\ell_B}\left(\Delta C_{N_\alpha}\right)_F \quad \text{(equation 4.2.2.1-f)}$$

$$= -1.267 + (-1.0) \frac{(2.75)^3}{(1.0)^2 (5.21)} + (-1.0)(11.73)$$

$$= -1.267 - 3.992 - 11.73$$

$$= -16.99 \text{ per rad (based on } S_B \ell_B)$$

This compares with a test value of -14.51 per radian from reference 13.

D. HYPERSONIC

Newtonian theory is used in this section to estimate the pitching-moment-curve slope of cone frustums with or without a spherical nose, a blunted conical nose, or a blunted ogival nose. Newtonian impact theory and its modifications are discussed in paragraph D of Section 4.2.1.1.

DATCOM METHOD

Charts that give the pitching-moment-curve slope of cone-frustum bodies and spherical noses are presented in figures 4.2.2.1-25a and 4.2.2.1-25b, respectively. These charts are taken from reference 11 and are based on Newtonian impact theory. By properly combining values from these charts, the total C_{m_α} may be determined for bodies composed of multiple cone frustums with or without spherically blunted noses.

The center-of-pressure locations of spherically blunted cones and ogives are presented in figures 4.2.2.1-26 and 4.2.2.1-27, respectively. These charts are also based on impact theory, and represent a specific application of the method described below for configurations consisting of cone frustums with spherical noses.

The procedure for computing the total pitching-moment-curve slope for a complex body is given in the following steps. The moment values for each individual segment of a multiple cone-frustum body with or without a spherical nose are referred to a moment axis at the front face of that particular segment, and are based on the product of the base area and base diameter of that particular segment.

Step 1. Compute C'_{m_α} for each body segment about its own front face, using figures 4.2.2.1-25a and 4.2.2.1-25b.

Step 2. Transfer the individual moment slopes to a common reference axis by applying the following moment transfer equation to each body segment.

$$C_{m_\alpha} = C'_{m_\alpha} + \frac{n}{d} C_{N_\alpha} \quad \text{(per radian)} \qquad 4.2.2.1\text{-g}$$

where

C_{N_α} is the normal-force-curve slope of the individual cone-frustum or spherical nose segment, based on its own base area, from figures 4.2.1.1-26 and 4.2.1.1-23, respectively.

d is the base diameter of the individual cone-frustum or spherical nose segment.

n is the distance from the front face of a given segment to the desired moment reference axis of the configuration, positive aft.

C'_{m_α} is the pitching-moment-curve slope of an individual segment from figure 4.2.2.1-25a for cone frustums and from figure 4.2.2.1-25b for spherical nose segments. C'_{m_α} is based on the product of the base area and the base diameter of the individual segment.

C_{m_α} is the pitching-moment-curve slope of an individual segment based on the product of the base area and base diameter of the individual segment and referred to a common reference axis.

Step 3. The transferred pitching-moment-curve slopes of the individual body segments are then converted to a common basis by

$$C_{m_\alpha} = \sum_{n=1}^{m} \left(C_{m_\alpha}\right)_n \left(\frac{d_n}{d_b}\right)^3 \quad \text{(per radian)} \qquad\qquad 4.2.2.1\text{-h}$$

where the subscript n refers to an individual segment of m segments, and C_{m_α} is referred to a common reference axis and is based on the product of the area and diameter of the base of the configuration $S_b d_b$.

In using figures 4.2.2.1-26 and 4.2.2.1-27 to obtain the pitching-moment-curve slope of spherically blunted cones and ogives, respectively, use is made of equation 4.2.2.1-d, i.e.,

$$C_{m_\alpha} = \left(\frac{x_m}{\ell_B} - \frac{x_{c.p.}}{\ell_B}\right) C_{N_\alpha} \quad \text{(per radian)}$$

where

$\dfrac{x_{c.p.}}{\ell_B}$ is obtained from figure 4.2.2.1-26 for spherically blunted cones and from figure 4.2.2.1-27 for spherically blunted ogives.

$\dfrac{x_m}{\ell_B}$ is the desired moment-center location in fraction of body length.

C_{N_α} is the normal-force-curve slope of spherically blunted cones and spherically blunted ogives from figures 4.2.1.1-24 and 4.2.1.1-25, respectively.

C_{m_α} is the pitching-moment-curve slope, referred to a desired moment axis and based on the product of the maximum frontal area and body length $S_B \ell_B$.

Values of C_{m_α} computed by the above method for spherically blunted cones and ogives may be used in conjunction with the results presented for conical-frustum bodies in figure 4.2.2.1-25a, provided the individual results are transferred to a common reference axis and converted to a common basis.

Sample Problem

Given: Configuration 5115 of reference 14, consisting of a cone-cylinder-frustum body with a spherical nose. This is the same configuration as the sample problem in paragraph D of Section 4.2.1.1.
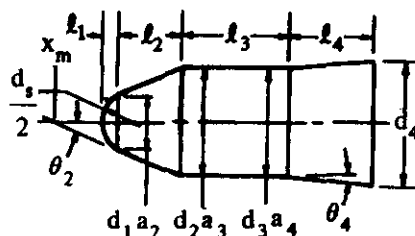
(All dimensions are in feet. x_m located 0.55 ft forward of nose.)

Spherical Segment

$\ell_1 = 0.18$ $\dfrac{d_s}{2} = 0.36$ $d_1 = 0.62$

Forward Cone Frustum

$a_2 = 0.62$ $d_2 = 1.20$ $\ell_2 = 0.72$

$\theta_2 = 22.5^\circ$

Cylinder

$$a_3 = 1.20 \qquad d_3 = 1.20 \qquad \ell_3 = 1.20 \qquad \theta = 0$$

Rear Cone Frustum

$$a_4 = 1.20 \qquad d_4 = d_b = 1.368 \qquad \ell_4 = 0.96 \qquad \theta_4 = 5^\circ$$

Compute:

Spherical segment

$$2\ell_1/d_s \quad = 0.18/0.36 = 0.50$$

$$C'_{m_{\alpha_1}} \quad = -0.430 \text{ per rad (figure 4.2.2.1-25b) (based on } \left(\frac{\pi d_1^2}{4}\right) d_1, \text{ and taken about its front face)}$$

$$n_1 \quad = -0.55$$

$$C_{N_{\alpha_1}} \quad = 0.75 \text{ per rad } \left(\text{based on } \frac{\pi d_1^2}{4}\right) \text{ (sample problem, paragraph D, Section 4.2.1.1)}$$

$$C_{m_{\alpha_1}} \quad = C'_{m_{\alpha_1}} + \frac{n_1}{d_1} C_{N_{\alpha_1}} \qquad \text{(equation 4.2.2.1-g)}$$

$$= -0.430 + \left(\frac{-0.55}{0.62}\right) 0.75$$

$$= -1.095 \text{ per rad (based on } \left(\frac{\pi d_1^2}{4}\right) d_1, \text{ and taken about } x_m)$$

Forward Cone Frustum

$$a_2/d_2 \quad = 0.62/1.20 = 0.517$$

$$C'_{m_{\alpha_2}} \quad = -0.590 \text{ per rad (figure 4.2.2.1-25a) (based on } \left(\frac{\pi d_2^2}{4}\right) d_2, \text{ and taken about its front face)}$$

$$n_2 \quad = -(0.55 + \ell_1) = -0.73$$

$$C_{N_{\alpha_2}} \quad = 1.250 \text{ per rad } \left(\text{based on } \frac{\pi d_2^2}{4}\right) \text{(sample problem, paragraph D, Section 4.2.1.1)}$$

$$C_{m_{\alpha_2}} = C'_{m_{\alpha_2}} + \frac{n_2}{d_2} C_{N_{\alpha_2}} \quad \text{(equation 4.2.2.1-g)}$$

$$= -0.590 + \left(\frac{-0.73}{1.20}\right) 1.250$$

$$= -1.350 \text{ per rad (based on } \left(\frac{\pi d_2{}^2}{2}\right) d_2, \text{ and taken about } x_m)$$

Cylinder

$$a_3/d_3 = 1.20/1.20 = 1.00$$

$$C'_{m_{\alpha_3}} = 0 \quad \text{(figure 4.2.2.1-25a)}$$

$$n_3 = -(0.55 + \ell_1 + \ell_2) = -1.45$$

$$C_{N_{\alpha_2}} = 0 \quad \text{(sample problem, paragraph D, Section 4.2.1.1)}$$

$$C_{m_{\alpha_3}} = C'_{m_{\alpha_3}} + \frac{n_3}{d_3} C_{N_{\alpha_3}} = 0 \quad \text{(equation 4.2.2.1-g)}$$

Rear Cone Frustum

$$a_4/d_4 = 1.20/1.368 = 0.877$$

$$C'_{m_{\alpha_4}} = -0.325 \text{ per rad (figure 4.2.2.1-23a) (based on } \left(\frac{\pi d_b{}^2}{4}\right) d_b, \text{ and taken about its front face)}$$

$$n_4 = -(0.55 + \ell_1 + \ell_2 + \ell_3) = -2.65$$

$$C_{N_{\alpha_4}} = 0.450 \text{ per rad } \left(\text{based on } \frac{\pi d_b{}^2}{4}\right) \quad \text{(sample problem, paragraph D, Section 4.2.1.1)}$$

$$C_{m_{\alpha_4}} = C'_{m_{\alpha_4}} + \frac{n_4}{d_4} C_{N_{\alpha_4}} \quad \text{(equation 4.2.2.1-g)}$$

$$= -0.325 + \left(\frac{-2.65}{1.368}\right) 0.450$$

$$= -1.196 \text{ per rad (based on } \left(\frac{\pi d_b{}^2}{4}\right) d_b, \text{ and taken about } x_m)$$

Solution:

$$= \sum_{n=1}^{m} \left(C_{m_\alpha}\right)_n \left(\frac{d_n}{d_b}\right)^3 \quad \text{(equation 4.2.2.1-h)}$$

$$C_{m_\alpha} = \left(C_{m_\alpha}\right)_1 \left(\frac{d_1}{d_b}\right)^3 + \left(C_{m_\alpha}\right)_2 \left(\frac{d_2}{d_b}\right)^3 + \left(C_{m_\alpha}\right)_3 \left(\frac{d_3}{d_b}\right)^3 + \left(C_{m_\alpha}\right)_4 \left(\frac{d_4}{d_b}\right)^3$$

$$= (-1.095) \left(\frac{0.62}{1.368}\right)^3 + (-1.350) \left(\frac{1.20}{1.368}\right)^3 + 0 \left(\frac{d_3}{d_b}\right)^3 + (-1.196) \left(\frac{1.368}{1.368}\right)^3$$

$$= -0.1019 - 0.9112 + 0 - 1.196$$

$$= -2.209 \text{ per rad} \quad \left(\text{based on} \left(\frac{\pi d_b{}^2}{4}\right) d_b, \text{ and referred to a moment axis at } x_m\right)$$

REFERENCES

1. Multhopp, H.: Aerodynamics of the Fuselage. NACA TM 1036, 1942. (U)

2. Hopkins, E. J.: A Semiempirical Method for Calculating the Pitching Moment of Bodies of Revolution at Low Mach Numbers. NACA RM A51C14, 1951. (U)

3. Foster, G., and Fitzpatrick, J.: Longitudinal-Stability Investigation of High-Lift and Stall-Control Devices on a 52° Sweptback Wing with and Without Fuselage and Horizontal Tail at a Reynolds Number of 6.8 x 10⁶. NACA RM L8I08, 1948. (U)

4. McDevitt, J. B., and Taylor, R. A.: Force and Pressure Measurements at Transonic Speeds for Several Bodies Having Elliptical Cross Sections. NACA TN 4362, 1958. (U)

5. McDevitt, J. B., and Taylor, R. A.: Pressure Distributions at Transonic Speeds for Slender Bodies Having Various Axial Locations of Maximum Diameter. NACA TN 4280, 1958. (U)

6. Taylor, R. A., and McDevitt, J. B.: Pressure Distributions at Transonic Speeds for Parabolic-Arc Bodies of Revolution Having Fineness Ratios of 10, 12, and 14. NACA TN 4234, 1958. (U)

7. Syvertson, C. A., and Dennis, D. H.: A Second-Order Shock-Expansion Method Applicable to Bodies of Revolution Near Zero Lift. NACA TR 1328, 1957. (U)

8. Dennis, D. H., and Cunningham, B. E.: Forces and Moments on Pointed and Blunt-Nosed Bodies of Revolution at Mach Numbers From 2.75 to 5.00. NACA RM A52E22, 1952. (U)

9. Anon: Royal Aeronautical Society Data Sheets — Aerodynamics, Vol. IV (Bodies S.08.03.03), 1958. (U)

10. Van Dyke, M.: First- and Second-Order Theory of Supersonic Flow Past Bodies of Revolution. Jour. Aero. Sci., Vol. 18, No. 3, 1951. (U)

11. Fisher, L. R.: Equations and Charts for Determining the Hypersonic Stability Derivatives of Combinations of Cone Frustums Computed by Newtonian Impact Theory. NASA TN D-149, 1959. (U)

12. Jones, J. L., and Demele, F. A.: Aerodynamic Study of a Wing-Fuselage Combination Employing a Wing Swept Back 63°. — Characteristics Throughout the Subsonic Speed Range with the Wing Cambered and Twisted for a Uniform Load at a Lift Coefficient of 0.25. NACA RM A9D25, 1949. (U)

13. Dennis, D. H., and Syvertson, C. A.: Effects of Boundary-Layer Separation on Normal Force and Center of Pressure of a Cone-Cylinder Model With a Large Base Flare at Mach Numbers From 3.00 to 6.28. NACA RM A55H09, 1955. (U)

14. Henderson, J. H.: Effect of Nose Bluntness on Normal Force, Pitching Moment, and Center of Pressure on Cone-Cylinder and Cone-Cylinder-Frustum Bodies of Revolution at Mach Numbers of 1.50, 2.18, 2.81 and 4.04. Ordnance Missile Laboratories Redstone Arsenal Rpt. No. GR11F, 1958. (C) Title Unclassified

15. Owens, R. V.: Aerodynamic Characteristics of Spherically Blunted Cones at Mach Numbers From 0.5 to 5.0. NASA TN D-3088, 1965. (U)

16. Ferri, A.: Supersonic-Tunnel Tests of Projectiles in Germany and Italy. NACA WR L-152, 1945. (U)

17. Walchner, O.: Systematic Wind-Tunnel Measurements on Missiles. NACA TM 1122, 1947. (U)

18. Delancey, L. M., Jaeger, B. F., and Schroedter, G. M.: The Aerodynamic Characteristics at Mach No. 4.24 of Bodies of Revolution With Varying Lengths and Head Shapes. NOTS TM 358, 1951. (U)

19. Perkins, E. W., and Jorgensen, L. H.: Comparison of Experimental and Theoretical Normal-Force Distributions (Including Reynolds Number Effects) on an Ogive-Cylinder Body at Mach Number 1.98. NACA TN 3716, 1956. (U)

20. Jack, J. R.: Aerodynamic Characteristics of a Slender Cone-Cylinder Body of Revolution at a Mach Number of 3.85. NACA RM E51H17, 1951. (U)

TABLE 4.2.2.1-A

SUPERSONIC PITCHING-MOMENT-CURVE SLOPE OF CONE-CYLINDER
AND OGIVE-CYLINDER BODIES
DATA SUMMARY AND SUBSTANTIATION

Ref.	Nose Shape	M	f_N	f_A	$\dfrac{x_m}{l_B}$	c_{m_α} Calc. (per rad)	c_{m_α} Test (per rad)	Percent Error
13	Cone	1.5	2.836	(	1.0	0.653	0.592	10.3
		1.6				0.650	0.601	8.2
		1.92				0.630	0.592	6.4
		2.0				0.626	0.613	2.1
		2.44				0.620	0.600	3.3
		2.73					0.592	4.7
		3.0					0.597	3.9
		3.0					0.584	6.2
		3.25					0.583	6.3
		3.49					0.579	7.1
		3.6					0.586	5.8
		3.89					0.560	10.7
		4.4					0.571	8.6
		4.45					0.566	9.5
		4.93					0.592	4.7
		1.5	2.112	0	1.0	0.633	0.536	18.1
		1.6				0.626	0.524	19.5
		1.92				0.620	0.549	12.9
		2.0					0.559	10.9
		2.44					0.553	12.1
		2.74					0.553	12.1
		3.0					0.559	10.9
		3.25					0.546	13.6
		3.5					0.560	10.7
		3.6					0.544	14.0
		3.89					0.566	9.5
		4.0					0.552	12.3
		4.4					0.563	10.1
		4.45					0.549	12.9
		4.93					0.572	8.4

TABLE 4.2.2.1-A (CONTD)

Ref.	Nose Shape	M	f_N	f_A	$\dfrac{x_m}{\ell_B}$	c_{m_α} Calc. (per rad)	c_{m_α} Test (per rad)	e Percent Error
14	Ogive	2.10	3.5	2.5	1.0	1.76	1.80	− 2.2
		2.29				1.75	1.85	− 5.4
		2.57				1.74	2.07	−15.9
		2.60				1.75	1.95	−10.3
		2.84				1.74	2.04	−14.7
		3.06				1.73	2.04	−15.2
		1.63	2.5	2.5	1.0	1.89	2.03	− 6.9
		2.03				1.91	2.12	− 9.9
		2.23				1.90	2.29	−17.0
		2.54				1.90	2.18	−12.8
		2.77				1.88	2.26	−16.8
		3.15				1.83	2.07	−11.6
		1.61	2.5	2.5	1.0	1.89	1.64	15.2
		2.02				1.91	1.83	4.4
		2.23				1.90	2.09	− 9.1
		2.59				1.89	2.03	− 6.9
		2.78				1.88	2.11	−10.9
		3.15				1.83	1.96	− 6.6
		1.63	2.5	2.5	1.0	1.89	1.80	5.0
		1.97				1.97	1.89	4.2
		2.25				1.90	1.76	8.0
		2.54				1.90	1.81	5.0
		2.75				1.88	2.05	− 8.3
		3.17				1.82	1.89	− 3.7
	Cone	1.60	2.5	2.5	1.0	1.64	1.57	4.5
		2.03				1.60	1.68	− 4.8
		2.24				1.58	1.66	− 4.8
		2.56				1.56	1.81	−13.8
		2.80				1.54	1.71	− 9.9
		3.15				1.53	1.91	−19.9
	Ogive	1.35	1.5	2.5	1.0	2.16	2.11	2.4
		1.67				2.19	1.86	17.7
		2.08				2.11	1.96	7.7
		2.27				2.05	2.03	1.0
		2.57				1.93	2.21	−12.7
		2.74				1.86	2.12	−12.3
		3.10				1.73	2.09	−17.2
		1.67	3.0	2.5	1.0	1.81	1.91	− 5.2
		2.07				1.81	1.93	− 6.2
		2.28				1.81	1.95	− 7.2
		2.58				1.81	1.93	− 6.2
		2.83				1.79	2.07	−13.5
		3.15				1.77	2.07	−14.5
15	Ogive	1.20	2.5	2.5	1.0	1.83	1.85	− 1.1
		1.45				1.87	1.97	− 5.1
		1.99				1.91	2.05	− 6.8
		2.64				1.89	2.01	− 6.0
		3.20				1.81	1.82	− 0.5
		1.20	1.5	3.5	1.0	2.26	2.02	11.9
		1.45				2.31	2.14	7.9
		1.99				2.29	2.42	− 5.4
		2.64				2.03	2.26	−10.2
		3.20				1.80	2.12	−16.1

4.2.2.1 -20

TABLE 4.2.2.1-A (CONTD)

Ref.	Nose Shape	M	f_N	f_A	$\frac{x_m}{\ell_B}$	C_{m_α} Calc. (per rad)	C_{m_α} Test (per rad)	e Percent Error
15	Ogive	1.20	3.5	1.5	1.0	1.62	1.54	5.2
		1.45				1.62	1.65	− 1.8
		1.99				1.61	1.68	− 4.2
		2.64				1.57	1.68	− 6.5
		3.20				1.53	1.57	− 2.5
		2.64	2.5	1.5	1.0	1.63	1.75	− 6.9
		1.99				1.68	1.67	0.6
		2.64	2.5	3.5	1.0	2.08	2.07	0.5
		2.64	2.5	4.5	1.0	2.24	2.26	− 0.9
6	Cone	2.75	3	0	0	−1.23	−1.19	3.4
		3.49					−1.19	3.4
		4.01					−1.22	0.8
		4.48					−1.11	10.8
		2.75	4	0	0	−1.24	−1.26	− 1.6
		4.01				−1.23	−1.39	−11.5
		4.48					−1.48	−16.9
		5.00					−1.23	0
		2.75	5	0	0	−1.27	−1.31	∼ 3.1
		3.49				−1.23	−1.22	0.8
		4.01					−1.32	− 6.8
		4.48					−1.32	− 6.8
		5.00					−1.17	5.1
		2.75	7	0	0	−1.30	−1.18	10.2
		4.01				−1.26	−1.32	− 4.5
		5.00				−1.23	−1.20	2.5
	Ogive	2.75	3	0	0	−1.23	−1.21	1.7
		4.01				−1.07	−1.15	− 7.0
		2.75	5			−1.33	−1.15	15.7
		4.01				−1.26	−1.25	0.8
		2.75	7			−1.35	−1.35	0
		4.01				−1.32	−1.35	− 2.2
16	Ogive	4.24	3.5	6.5	1.0	2.22	2.12	4.7
			4.0	10.0		2.44	2.43	0.4
	Cone		4.0	10.0		2.31	2.14	7.9
17	Ogive	1.98	3.0	7.0	0	−0.69	−0.63	9.5
18	Cone	3.85	12.0	12.0	1.0	1.68	2.18	−22.9

$$\text{Average Error} = \frac{\Sigma\,|e|}{n} = 8.0\%$$

(a)

(b)
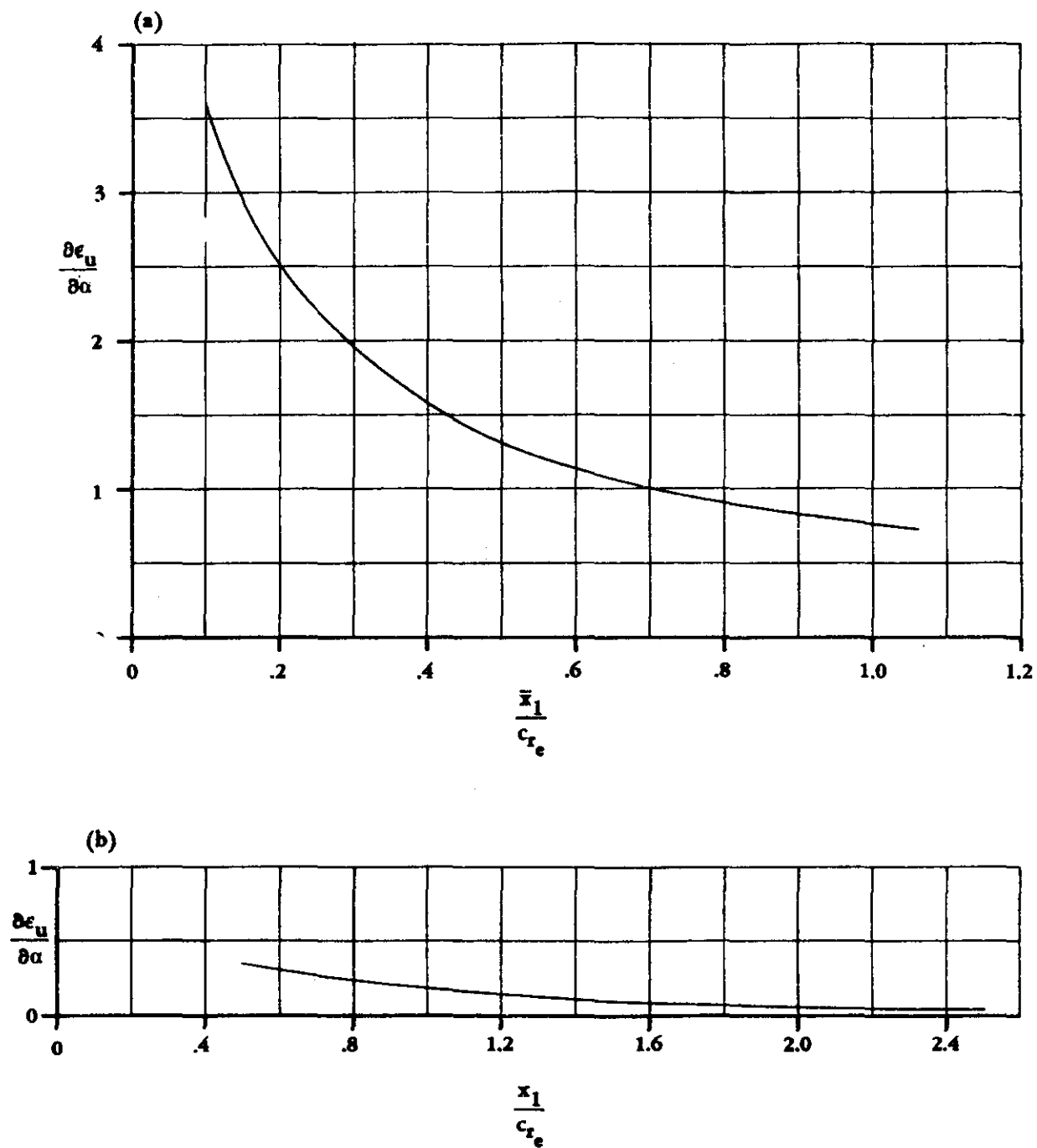
FIGURE 4.2.2.1-22 VARIATION OF UPWASH WITH DISTANCE FROM WING
LEADING EDGE
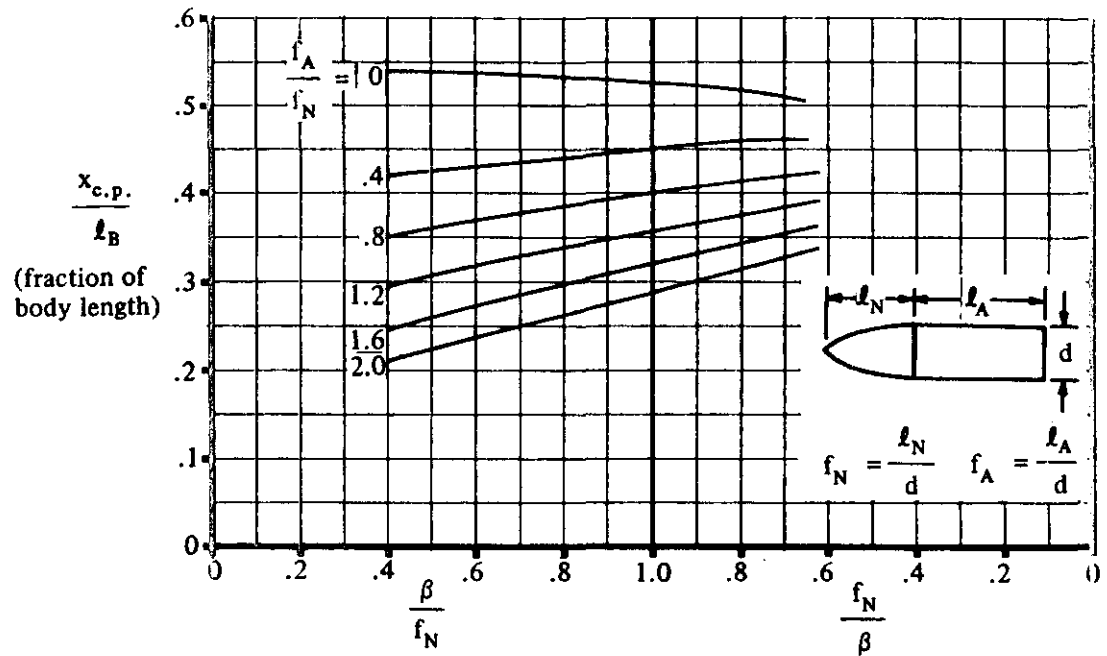
FIGURE 4.2.2.1-23a SUPERSONIC CENTER OF PRESSURE OF OGIVE WITH CYLINDRICAL AFTERBODY
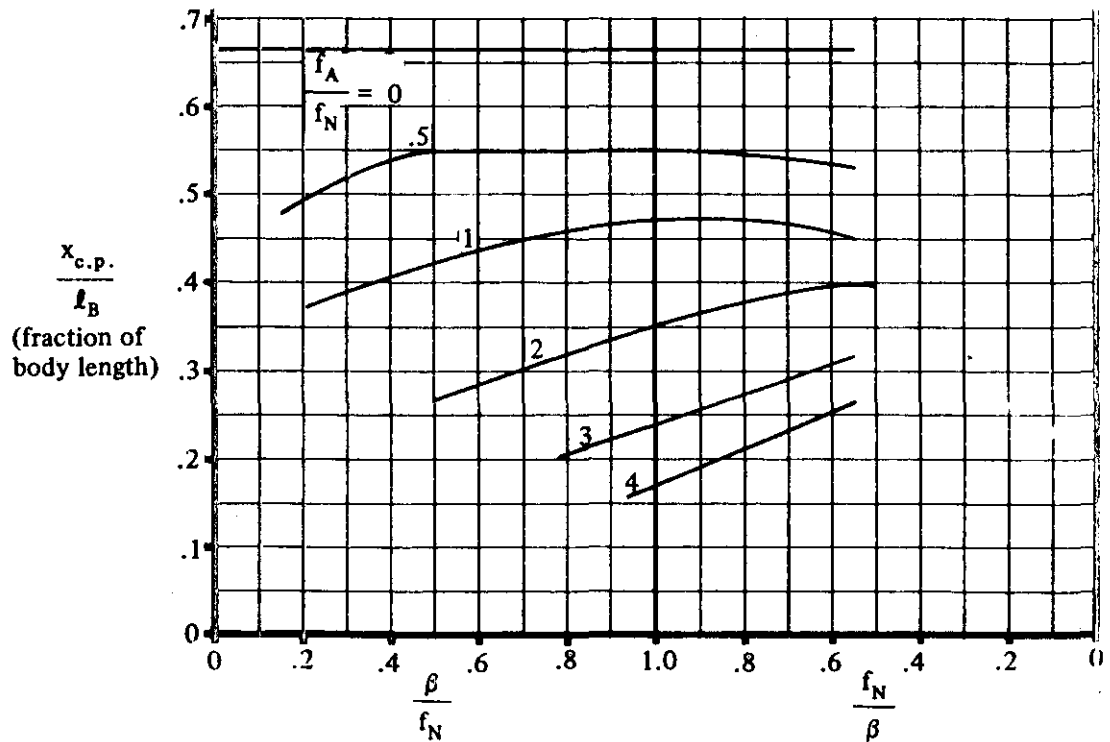
FIGURE 4.2.2.1-23b SUPERSONIC CENTER OF PRESSURE OF CONE WITH CYLINDRICAL AFTERBODY
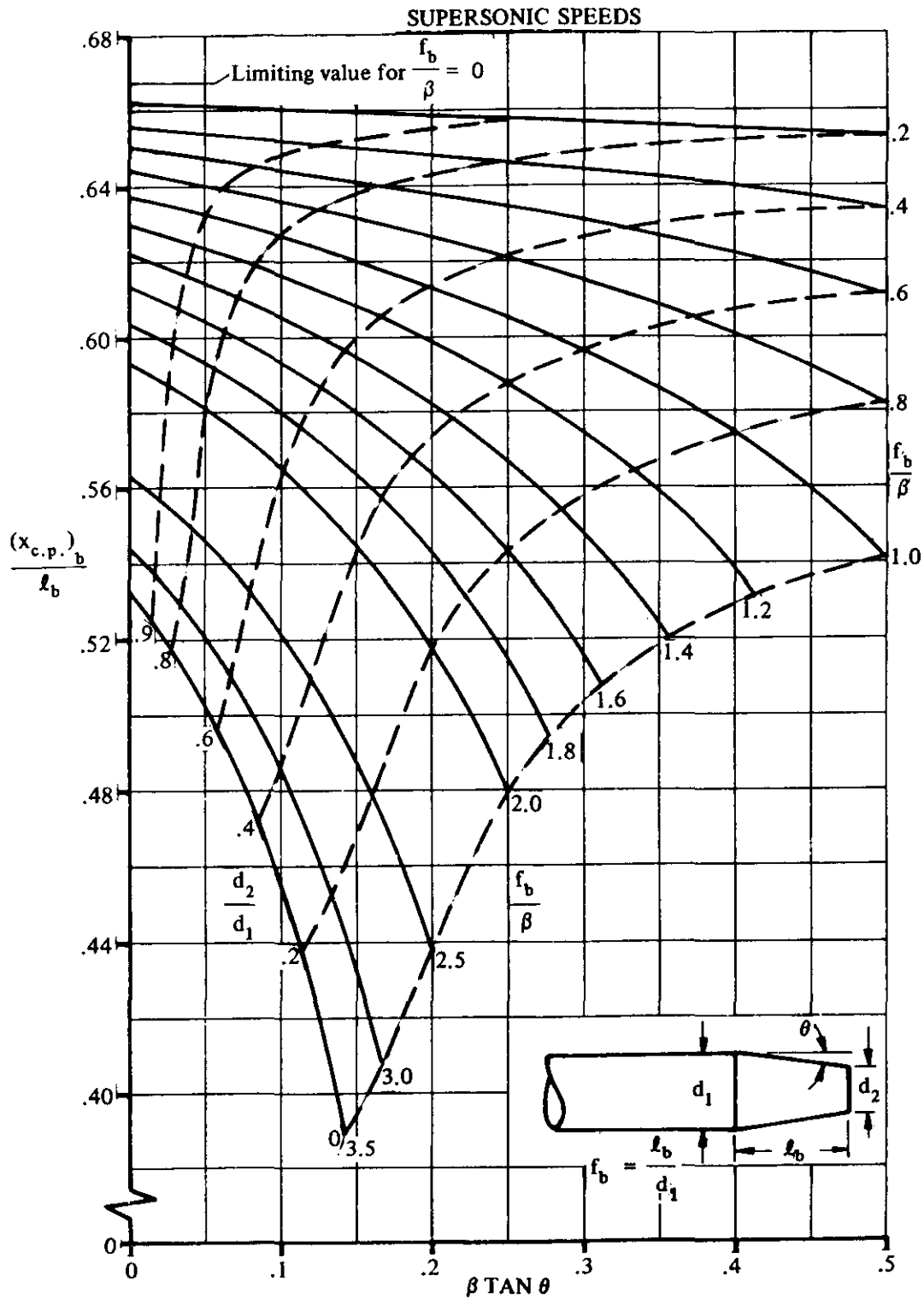
FIGURE 4.2.2.1-24 SUPERSONIC CENTER OF PRESSURE OF BOATTAILED BODY OF
REVOLUTION MOUNTED BEHIND A SEMI-INFINITE CYLINDER
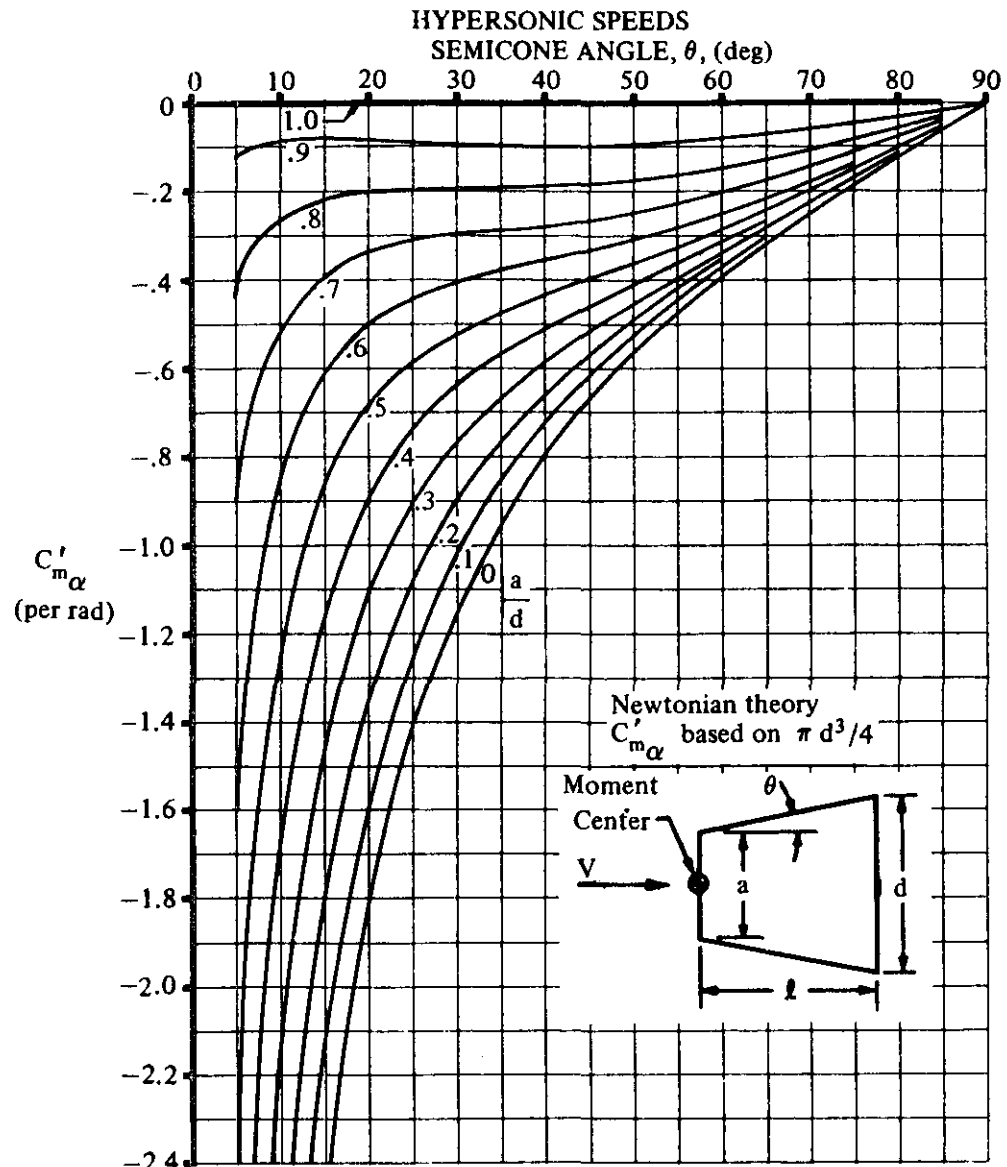
HYPERSONIC SPEEDS
SEMICONE ANGLE, θ, (deg)

FIGURE 4.2.2.1-25a C'_{m_α} FOR CONE FRUSTUMS

NOSE BLUNTNESS, $2\ell/d_s$

FIGURE 4.2.2.1-25b C'_{m_α} FOR SPHERICAL SEGMENTS

$x_{c.p.}/\ell_N$

FRACTION OF
NOSE LENGTH

For sharp nose cones: $\dfrac{x_{c.p.}}{\ell_N} = \dfrac{2}{3\cos^2\theta_c}$

where θ_c is the cone angle and ℓ_N the cone length
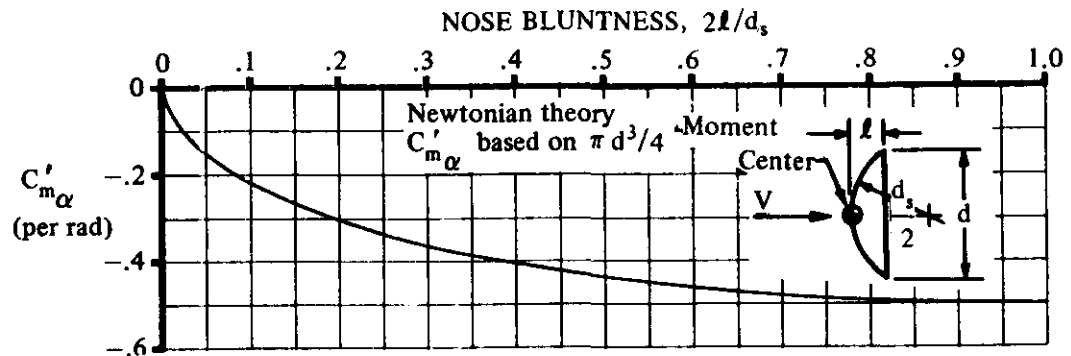
FIGURE 4.2.2.1-26 CENTER OF PRESSURE OF SPHERICALLY
BLUNTED CONES (IMPACT THEORY)
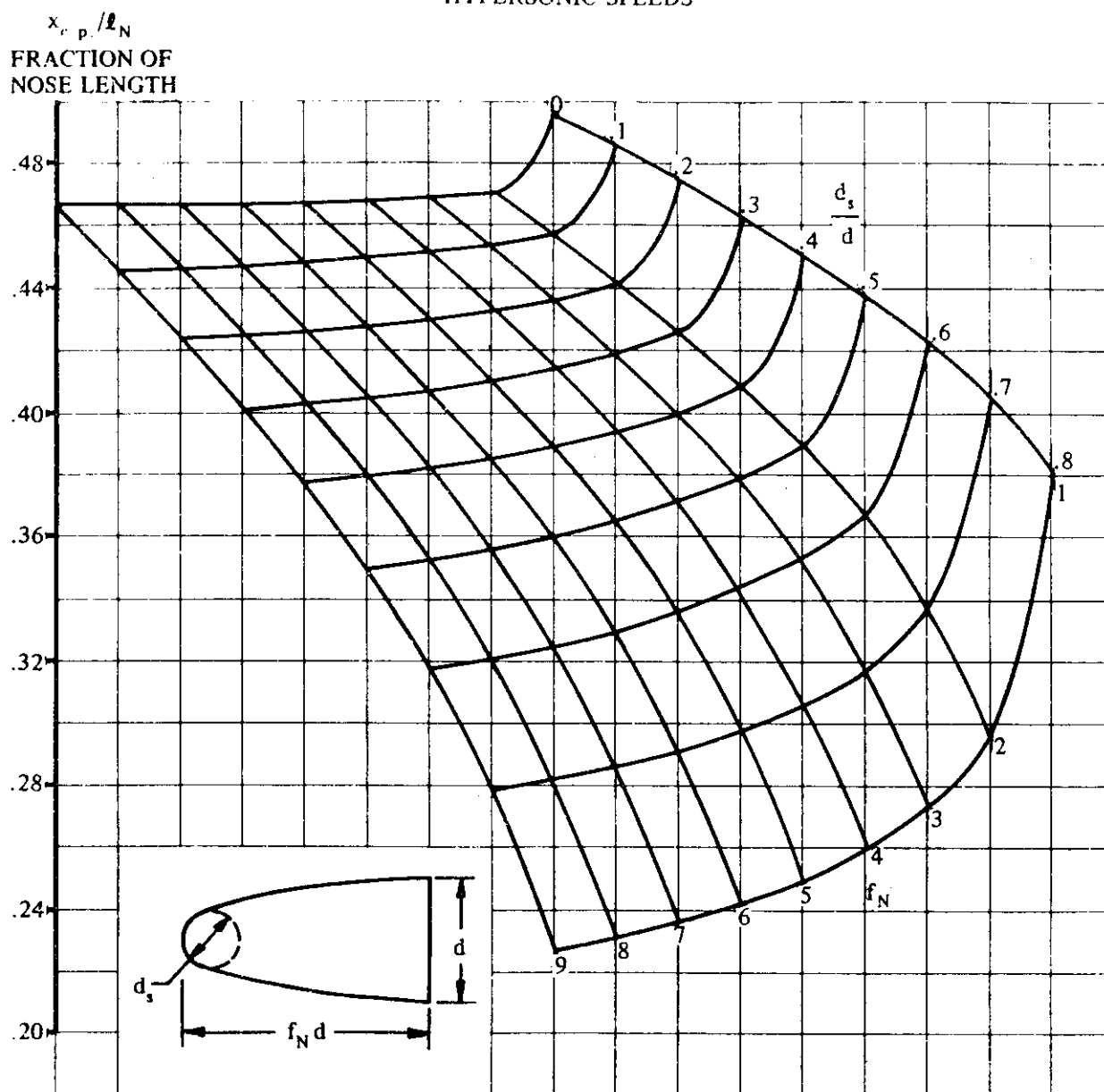
FIGURE 4.2.2.1-27 CENTER OF PRESSURE OF SPHERICALLY BLUNTED OGIVES
(IMPACT THEORY)

4.2.2.2 BODY PITCHING MOMENT IN THE NONLINEAR ANGLE-OF-ATTACK RANGE

A. SUBSONIC

Two methods are presented for calculating subsonic pitching-moment coefficient. The first method is applicable to bodies with circular cross sections and angles of attack up to about 12°. This method allows for a variation of the cross-sectional diameter along the length of the body. The second method is applicable to bodies with circular or elliptical cross sections for angles of attack from 0 to 180°. This method has been substantiated only for bodies with a constant cross-sectional size and shape.

DATCOM METHODS

Method 1

As discussed in Section 4.2.1.2, the viscous cross flow over a body at moderate to large angles of attack makes a substantial contribution to both lift and pitching moment. This method for predicting body pitching moment therefore differs chiefly from the method of Section 4.2.2.1 in that the viscous cross forces are considered.

The method of Reference 1 is presented for estimating the pitching moment of a body of revolution at angle of attack, based on the total body volume and referred to an arbitrary moment axis.

$$C_m = \frac{(k_2 - k_1)}{V_B} 2\alpha \int_0^{x_o} \frac{dS_x}{dx}(x_m - x)dx + \frac{2\alpha^2}{V_B} \int_{x_o}^{\ell_B} \eta r c_{d_c}(x_m - x)dx \qquad 4.2.2.2\text{-}a$$

where the terms in the above expression are defined in Paragraph A of either Section 4.2.1.2 or Section 4.2.2.1.

The pitching-moment coefficients of several bodies of revolution, calculated by the Datcom method, have been compared with test data in Reference 1. The method appears to give the best results at the lower angles of attack, but in general the method is satisfactory up to angles of attack of approximately 12°.

Method 2

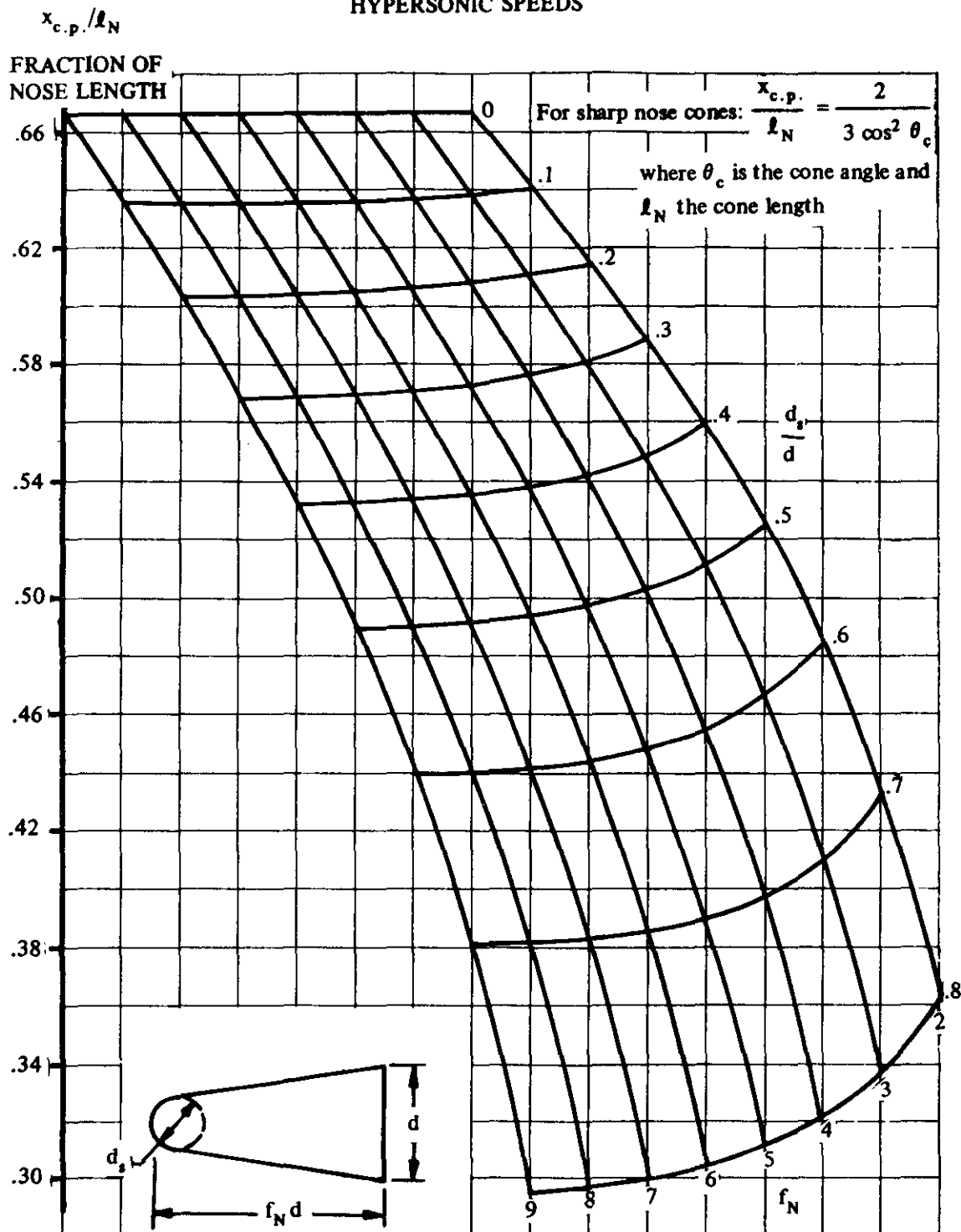This method is based on the method of Jorgensen (Reference 2) and consists of the sum of a slender-body potential term and an empirical viscous cross-flow term. The method is applicable to bodies of circular and elliptical cross sections for angles of attack from 0 to 180°. However, it is recommended that Method 1 be used for $\alpha \leqslant 12^\circ$. Bodies with other types of cross sections and those with variable cross sections have been investigated by this method (References 2 and 3), but very little substantiating test data are available. A summary of available test data on bodies of noncircular cross section at subsonic speeds is presented as Table 4.2.1.1-A.

The pitching-moment coefficient for bodies of revolution and bodies with elliptical cross sections, based on body cross-sectional reference area and diameter, is determined from the following equations.

4.2.2.2-1

For $0 \leqslant \alpha \leqslant 90^{\circ}$

$$C_m = \left(\frac{C_N}{C_{N_{cir}}}\right)_{SB} \left[\frac{V_B - S_b(\ell_B - x_m)}{Sd}\right] \sin 2\alpha' \cos \frac{\alpha'}{2}$$
$$+ \left(\frac{C_N}{C_{N_{cir}}}\right)_{NT} \eta c_{d_c} \frac{S_p}{S} \left(\frac{x_m - x_c}{d}\right) \sin^2 \alpha' \qquad \text{4.2.2.2-b}$$

For $90^{\circ} \leqslant \alpha \leqslant 180^{\circ}$

$$C_m = -\left(\frac{C_N}{C_{N_{cir}}}\right)_{SB} \left(\frac{V_B - S_b x_m}{Sd}\right) \sin 2\alpha' \cos \frac{\alpha'}{2}$$
$$+ \left(\frac{C_N}{C_{N_{cir}}}\right)_{NT} \eta c_{d_c} \frac{S_p}{S} \left(\frac{x_m - x_c}{d}\right) \sin^2 \alpha' \qquad \text{4.2.2.2-c}$$

where

$\left(\dfrac{C_N}{C_{N_{cir}}}\right)_{SB}$ is the ratio of the normal-force coefficient for the body of noncircular cross section to that for the equivalent body of circular cross section (same cross-sectional area) as determined by slender-body theory. For circular cross sections this ratio is one. For elliptical cross sections this ratio is given by Equation 4.2.1.2-d.

V_B is the total body volume.

S_b is the body base area.

ℓ_B is the body length.

x_m is the distance from the nose to the moment reference center of the body.

S is the cross-sectional reference area of the body (can be arbitrarily selected).

d is the body diameter (or the diameter of an equivalent body of revolution for an elliptic cross section).

α' is an incidence angle defined as $\alpha' = \alpha$ for $0 \leqslant \alpha \leqslant 90^{\circ}$ and $\alpha' = 180^{\circ} - \alpha$ for $90^{\circ} \leqslant \alpha \leqslant 180^{\circ}$.

$\left(\dfrac{C_N}{C_{N_{cir}}}\right)_{NT}$ is the ratio of the normal-force coefficient for the body of noncircular cross section to that for the equivalent body of circular cross section (same cross-sectional area) as determined by Newtonian impact theory. For circular cross sections this ratio is one. For elliptical cross sections this ratio is given by Equations 4.2.1.2-e and 4.2.1.2-f.

η is the cross-flow drag proportionality factor, obtained from Figure 4.2.1.2-35a, as a function of body fineness ratio.

c_{d_c} is the cross-flow drag coefficient of the cylindrical section, obtained from Figure 4.2.1.2-35b, as a function of cross-flow Mach number M_c, where $M_c = M \sin \alpha$.

S_p is the body planform area. In applying the method to bodies with elliptical cross section, the term S_p in Equations 4.2.2.2-b and 4.2.2.2-c is based on an equivalent body of revolution with the same cross-sectional area.

x_c is the distance from the nose to the centroid of the body planform area.

This method is applied to bodies of noncircular cross sections in the same manner as Method 3 of Section 4.2.1.2, Paragraph A. Refer to this paragraph for a more detailed explanation of bodies with elliptical cross sections. Bodies with other cross sections are discussed in Reference 3.

It is noted in Reference 2 that the cross-flow drag coefficient may be reduced dramatically under the simultaneous conditions of $M_c \leqslant 0.4$ and $R_\varrho \sin \alpha > 10^5$ (R_ϱ is Reynolds number based on diameter). These conditions have only recently been analyzed in detail and have not been included in the Datcom method because of considerable uncertainty in the magnitude and trend of the effects. For more detailed information regarding these effects, the user should refer to Reference 2.

Calculated results using this method have been compared with test data from Reference 6 in Table 4.2.2.2-A. The method shows fairly good agreement at angles of attack up to 20°, but significantly underestimates the data at higher angles of attack. Caution should be exercised when using this method at subsonic Mach numbers because of the shortage of substantiating test data. It is recommended that Method 1 be used for $0 \leqslant \alpha \leqslant 12^o$.

Sample Problems

1.   Method 1

Given: The 3/4-power body of revolution of Reference 10. This is the same configuration as that in Paragraph A of Section 4.2.2.1.

$$r = 0.255 \left[1 - \left(1 - \frac{2x}{6.375} \right)^2 \right]^{3/4} \qquad \varrho_B = 5.036 \text{ ft} \qquad d = 0.510 \text{ ft}$$

$f = \varrho_B/d = 9.87$ $V_B = 0.687$ cu ft $x_m = 3.54$ ft

$M = 0.40$ $\alpha = 0$ to 18°

Compute:

$x_o = 4.558$ ft

$$\frac{2(k_2 - k_1)}{V_B} \int_0^{x_o} \frac{dS_x}{dx} (x_m - x)\, dx = 1.293 \text{ per rad}$$

(Sample Problem 2, Paragraph A, Section 4.2.2.1)

$\eta = 0.685$ (Figure 4.2.1.2-35a)

$c_{d_c} = f(M_c); \quad M_c = M \sin \alpha$

M_c varies from 0 to 0.40 sin 18°; $0 \leqslant M_c \leqslant 0.1236$

$c_{d_c} = 1.20$ (constant) (Figure 4.2.1.2-35b)

Evaluate $\displaystyle\int_{x_o}^{l_B} r(x_m - x)\, dx$

Station (ft)	r* (ft)	Δx (ft)	x* (ft)	$(x_m - x)$ ft	$r(x_m - x)\Delta x$ (ft³)
$x_o = 4.56$ $l_B = 5.036$	0.2037	0.476	4.79	−1.25	−0.121

$$\sum_{x_o}^{l_B} r(x_m - x)\, \Delta x = -0.121 \text{ cu ft}$$

Solution:

$$C_m = \frac{(k_2 - k_1)}{V_B} 2\alpha \int_0^{x_o} \frac{dS_x}{dx} (x_m - x)\, dx + \frac{2\alpha^2}{V_B} \int_{x_o}^{l_B} \eta r c_{d_c} (x_m - x)\, dx$$

(Equation 4.2.2.2-a)

$$= 1.293\alpha + \frac{2\alpha^2}{0.687} (0.685)(1.20) \int_{x_o}^{l_B} r(x_m - x)\, dx$$

$$= 1.293\alpha - 0.290\alpha^2$$

---

*x and r are taken at the center of volume of the body segment.

α (deg)	α (rad)	α^2 (rad^2)	C_m (Eq. 4.2.2.2-a)
0	0	0	0
2	0.0349	0.00122	0.0448
4	0.0698	0.00487	0.0888
6	0.1047	0.01096	0.1322
8	0.1396	0.01947	0.1749
10	0.1745	0.03045	0.2168
12	0.2094	0.04385	0.2580
14	0.2443	0.05968	0.2986
16	0.2792	0.07795	0.3384
18	0.3141	0.09866	0.3775

The calculated results are compared with test values from Reference 15 in Sketch (a).
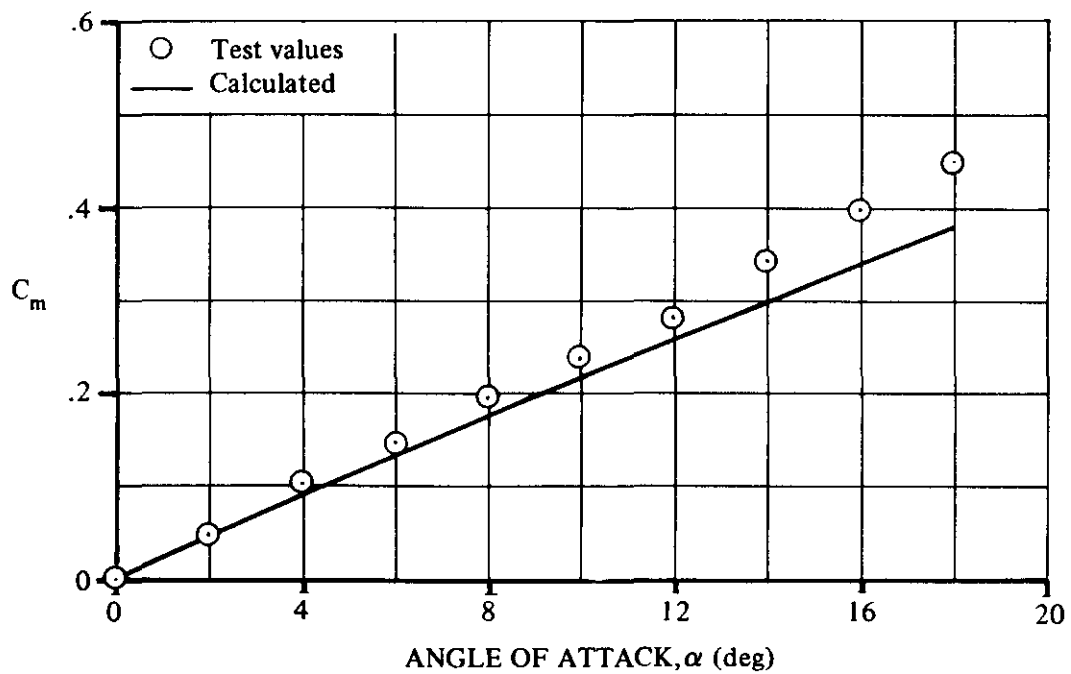
SKETCH (a)

2. Method 2

Given: The elliptical cross-section body with tangent ogive nose of Reference 6. This is the same configuration as given in the sample problem for Method 3 of Paragraph A of Section 4.2.1.2.

Body Characteristics:

V_B = 1944.64 cm^3 x_c = 36.08 cm

ℓ_B = 66.0 cm x_m = 39.58 cm S_p = 392.466 cm^2

$\left. \begin{array}{l} d = 6.6 \text{ cm} \\[10pt] S = 34.206 \text{ cm}^2 \\[10pt] S_b = 34.206 \text{ cm}^2 \\[10pt] \left(\dfrac{C_N}{C_{N_{cir}}} \right)_{SB} = 2.0 \\[20pt] \left(\dfrac{C_N}{C_{N_{cir}}} \right)_{NT} = 1.752 \end{array} \right\}$ Sample Problem 3, Paragraph A, Section 4.2.1.2

Additional Characteristics:

$\alpha' = \alpha = 50^o$ M = 0.6 R_ϱ = 6.5 x 10^5 (based on diameter)

$\phi = 0$

Compute:

Slender-body Potential Term

$\left. \begin{array}{l} \eta = 0.685 \\[10pt] c_{d_c} = 1.32 \end{array} \right\}$ Sample Problem 3, Paragraph A, Section 4.2.1.2

$$\left(\frac{C_N}{C_{N_{cir}}} \right)_{SB} \left[\frac{V_B - S_b(\ell_B - x_m)}{Sd} \right] \sin 2\alpha' \cos \frac{\alpha'}{2}$$

$$= (2.0) \left[\frac{1944.64 - 34.206(66.0 - 39.58)}{(34.206)(6.6)} \right] (0.9848)(0.9063) = 8.23$$

Viscous Cross-Flow Term

$$\left(\frac{C_N}{C_{N_{cir}}}\right)_{NT} \eta c_{d_c} \frac{S_p}{S}\left(\frac{x_m - x_c}{d}\right) \sin^2\alpha'$$

$$= (1.752)(0.685)(1.32)\left(\frac{392.466}{34.206}\right)\left(\frac{39.58 - 36.08}{6.6}\right)(0.5868) = 5.66$$

Solution:

C_m = slender-body potential term + viscous cross-flow term

= 8.23 + 5.66

= 13.89 (based on Sd)

Additional values have been tabulated below:

M	α (deg)	C_m
0.6	10	3.41
0.6	20	6.87
0.6	30	9.94
0.6	40	12.34
0.6	50	13.89
0.6	60	14.51

The calculated results of the sample problem are compared to test values from Reference 6 in Sketch (b).
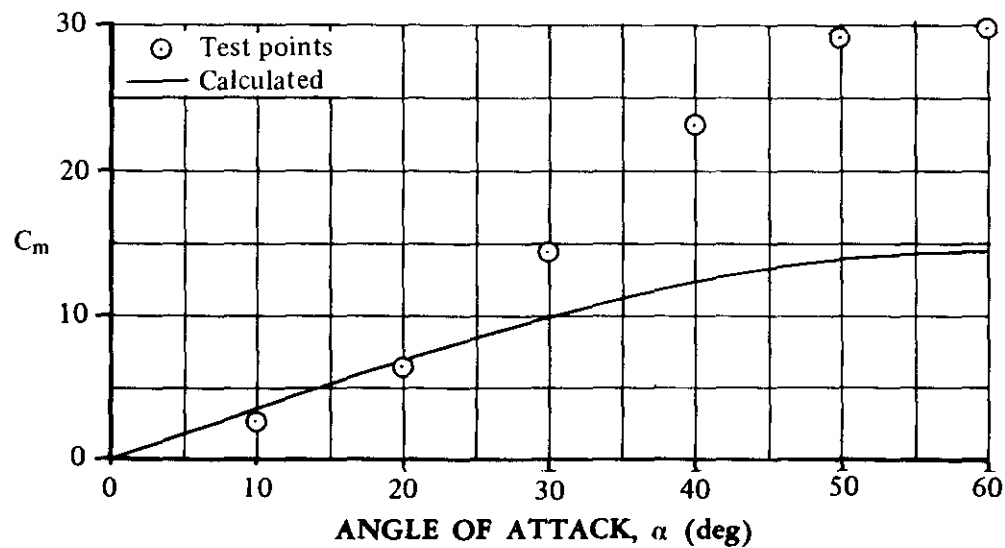
SKETCH (b)

B. TRANSONIC

Transonic flow, which consists by definition of a combination of locally subsonic and supersonic flow regions, is particularly difficult for either theoretical or empirical analysis. The two types of flow interact directly on their mutual boundaries and indirectly through the boundary layer. The resulting flow pattern is highly sensitive to seemingly small changes in geometry. Prediction of transonic body lift is at best an approximation; prediction of transonic body lift distribution is considerably more difficult.

DATCOM METHOD

Because of the difficulty of predicting transonic-flow phenomena to the accuracy required for lift distribution, no Datcom method is given for predicting body pitching moment at transonic speeds. It is suggested that the transonic region be faired smoothly from the subsonic region to the supersonic region.

C. SUPERSONIC

Several theoretical methods have been developed that can be used to estimate the moment characteristics of bodies of revolution at supersonic speeds. Some of these methods are discussed in Paragraph C of Section 4.2.1.2.

Three methods are presented for estimating body pitching moment at supersonic speeds. The first method is based on the method of Allen and Perkins (Reference 7) and includes a modification by Jorgensen (Reference 8) to accommodate bodies with elliptical cross sections. The second approach uses hypersonic-similarity concepts that have been adapted to supersonic speeds (Reference 9). These two methods are discussed in Paragraph C of Section 4.2.1.2. The third method is an improvement on Method 1 developed by Jorgensen in Reference 2. This method extends the capability for calculating pitching moments to 180°. The method is identical to that presented as Method 2 in Paragraph A of this section.

DATCOM METHODS

Method 1

The method presented for predicting the pitching moment of a body of revolution at angle of attack is that of Allen and Perkins, in Reference 7. The method for estimating the pitching moment of bodies of elliptical cross section is that of Reference 7 as modified by Jorgensen in Reference 8.

The pitching-moment coefficient of a body of revolution, based on body base area and body length $S_b \ell_B$ and referred to an arbitrary moment center, is

$$C_m = 2\alpha \left[\frac{V_B}{S_b \ell_B} - \left(1 - \frac{x_m}{\ell_B} \right) \right] + c_{d_c} \frac{S_p}{S_b} \left(\frac{x_m - x_c}{\ell_B} \right) \alpha^2 \qquad \text{4.2.2.2-d}$$

where x_c is the axial distance from the vertex of the nose to the centroid of the planform area, and the remaining terms are defined in Paragraph C of either Section 4.2.1.2 or Section 4.2.2.1.

4.2.2.2-8

The supersonic pitching-moment coefficient at angle of attack of a body having an elliptical cross section, based on body base area and body length $S_b \ell_B$ and referred to an arbitrary moment center, is

$$(C_m)_{a/b} = \left[\frac{a}{b} \cos^2\phi + \frac{b}{a} \sin^2\phi \right] C_m$$

4.2.2.2-e

where C_m is the pitching-moment coefficient of a body of revolution having the same cross-sectional area distribution along its axis as the elliptical-cross-section body of interest. It is given by Equation 4.2.2.2-d. The parameters a, b, and ϕ are defined in Paragraph C of Section 4.2.1.2.

The Datcom method has been used to calculate the variation of pitching-moment coefficient with angle of attack for the bodies of elliptic cross section of Reference 8 and for the bodies of revolution of References 7, 8, and 10 through 13. Although the nose shapes of most of the configurations analyzed were tangent ogives, a few bodies of revolution had conical or hemispherical noses. All the afterbodies were straight (no boattail or flare). In general, the calculated results agree well with the test data. The comparison of calculated and test values for the sample problems at the conclusion of this paragraph is indicative of the degree of accuracy of this method.

Method 2

This method uses hypersonic-similarity parameters that have been adapted to supersonic speeds by the method of Reference 9. This method is based on experimental data for a wide range of models for Mach numbers between 1.57 and 2.87. The variation of pitching-moment coefficient with angle of attack for pointed or nearly pointed bodies of revolution is estimated by using Figure 4.2.2.2-26 where $\beta = \sqrt{M^2 - 1}$. The body pitching moment obtained from this chart is referred to the nose apex and is based on the product of body frontal area and the body length $S_B \ell_B$.

A comparison of test data with the pitching-moment coefficient calculated by this method is presented as Table 4.2.2.2-B.

Method 3

This method is the same as Method 2 presented in Paragraph A of this section. The only exception is that the term η in Equations 4.2.2.2-b and 4.2.2.2-c is set equal to 1.0 for $M \geqslant 1.0$.

The method is applicable to angles of attack from 0 to 180° and Mach numbers up to 7. The method is substantiated by test data from References 4, 5, and 6 in Table 4.2.2.2-C.

The method shows reasonable agreement with most test data, but Methods 1 and 2 are recommended in the low-angle-of-attack range.

With the exception of bodies with elliptical cross sections, there are no Datcom methods for predicting the pitching moment on bodies of noncircular cross section at supersonic speeds. A summary of available test data on bodies of noncircular cross section at supersonic speeds is presented as Table 4.2.1.1-C. In

Reference 8 (Reference 37 of Table 4.2.1.1-C) the effect of cross-sectional shape on body aerodynamics has been assessed for bodies with circular, elliptic, square, and triangular cross sections. These data show that at certain angles of bank, noncircular bodies develop considerably more pitching moment than their equivalent bodies of revolution at a given angle of attack. The data of Reference 8 also show that the ratio of pitching-moment coefficient for a body with elliptic cross section to that for an equivalent body of revolution is practically constant with change in both angle of attack and Mach number. However, no such simple correlation is available for other bodies of noncircular cross section. Method 3 has been applied to other bodies with noncircular and axially varying cross sections by Jorgensen in References 2 and 3. The lack of sufficient substantiating data has precluded inclusion of this application in the Datcom.

Sample Problems

1. Method 1

Given: An ogive-cylinder body of Reference 8. This is the same configuration as that of Sample Problem 1 of Paragraph C of Section 4.2.1.2.

Body Characteristics:

$$d = 1.40 \text{ in.} \quad \ell_B = 14.0 \text{ in.} \quad \ell_N = 4.20 \text{ in.} \quad \ell_A = 9.80 \text{ in.}$$

$$V_B = 18.56 \text{ cu in.} \quad S_b = 1.539 \text{ sq in.} \quad S_p = 17.66 \text{ sq in.}$$

$$S_p/S_b = 11.47 \quad x_c = 7.69 \text{ in.} \quad x_m/\ell_B = 1.0 \text{ (moments referred to body base)}$$

Additional Characteristics:

$$M = 1.98 \quad \alpha = 4^o, 8^o, 12^o, 16^o, 20^o$$

Compute:

$$c_{d_c} = f(M_c) = f(M \sin\alpha)$$

α	4°	8°	12°	16°	20°	(Sample Problem 1, Paragraph C,
c_{d_c}	1.20	1.208	1.275	1.41	1.62	Section 4.2.1.2)

$$\left[\frac{V_B}{S_b \ell_B} - \left(1 - \frac{x_m}{\ell_B}\right)\right] = \left[\frac{18.56}{(1.539)(14.0)} - (1 - 1.0)\right] = 0.8614$$

$$c_{d_c} \frac{S_p}{S_b}\left(\frac{x_m - x_c}{\ell_B}\right) = c_{d_c} (11.47)\left(\frac{14.0 - 7.69}{14.0}\right) = 5.170 \, c_{d_c}$$

Solution:

$$C_m = 2\alpha \left[\frac{V_B}{S_b \ell_B} - \left(1 - \frac{x_m}{\ell_B} \right) \right] + c_{d_c} \frac{S_p}{S_b} \left(\frac{x_m - x_c}{\ell_B} \right) \alpha^2 \quad \text{(Equation 4.2.2.2-d)}$$

$$= 2\alpha(0.8614) + 5.170 \, c_{d_c} \, \alpha^2$$

$$= 1.723\alpha + 5.170 \, c_{d_c} \, \alpha^2$$

α (deg)	α (rad)	α^2 (rad^2)	c_{d_c}	1.723α	$5.170 \, c_{d_c} \, \alpha^2$	C_m Eq. 4.2.2.2-d (based on $S_b \ell_B$)
4	0.0698	0.00487	1.20	0.1203	0.0302	0.151
8	0.1396	0.01950	1.208	0.2405	0.1218	0.362
12	0.2094	0.04386	1.275	0.3608	0.2891	0.650
16	0.2793	0.07798	1.41	0.4812	0.5685	1.050
20	0.3491	0.12185	1.62	0.6015	1.0205	1.622

2. Method 1

Given: A body of Reference 8 having an elliptical cross section and the same axial distribution of cross-sectional area as the body of revolution of Sample Problem 1.

Body Characteristics:

a = 1.98 in.   b = 0.99 in.   a/b = 2.0 $\phi = 0$

x_m/ℓ_B = 1.0 (moments referred to body base)

Additional Characteristics:

M = 1.98 α = 4°, 8°, 12°, 16°, 20°

Compute:

C_m vs α for a body of revolution having the same cross sectional area distribution and with the moment axis located at the base of the body. (from Sample Problem 1)

Solution:

$$C_m = \left[\frac{a}{b} \cos^2\phi \; + \; \frac{b}{a} \sin^2\phi \right] \; C_m \qquad \text{(Equation 4.2.2.2-e)}$$

$$= \; [(2.0) \; (1.0) \; + \; 0] \; C_m \; = \; 2.0 \; C_m$$

α (deg)	C_m Sample Problem 1	$(C_m)_{a/b}$ Eq. 4.2.2.2-e (based on $S_b \ell_B$)
4	0.151	0.302
8	0.362	0.724
12	0.650	1.300
16	1.050	2.100
20	1.622	3.244

The calculated results of Sample Problems 1 and 2 are compared with test values from Reference 8 in Sketch (c)

SKETCH (c)
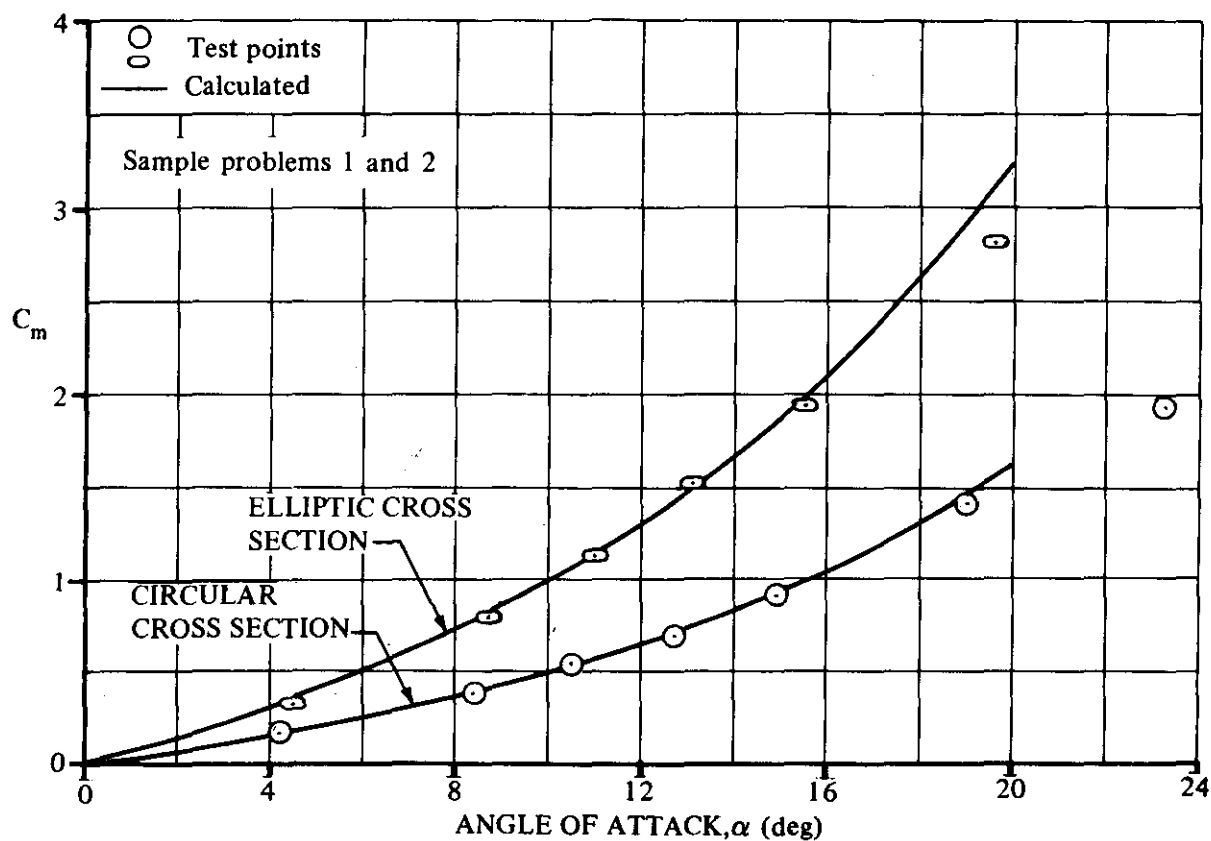
3. Method 2

Given: The ogive-cylinder body of Sample Problem 1.

Body Characteristics:

$d = 1.40$ in. $\ell_N = 4.20$ in. $\ell_A = 9.80$ in.

Additional Characteristics:

$M = 1.98$; $\beta = 1.71$ $\alpha = 4^o, 8^o, 12^o$

Compute:

$f_N = \ell_N/d = 4.2/1.4 = 3.0$ $f_A = \ell_A/d = 9.8/1.4 = 7.0$

$f_A/f_N = 7.0/3.0 = 2.33$

$\beta/f_N = 1.71/3.0 = 0.570$

Solution:

α (deg)	$\beta\alpha$ (deg)	βC_m Fig. 4.2.2.2-26	C_m (based on $S_B\ell_B$) (referred to nose apex)
4	6.84	−0.073	−0.043
8	13.68	−0.275	−0.161
12	20.52	−0.930	−0.544

The calculated results are compared with test values from Reference 8 in Sketch (d). (The test results have been transferred to a moment axis at the nose apex).

SKETCH (d)
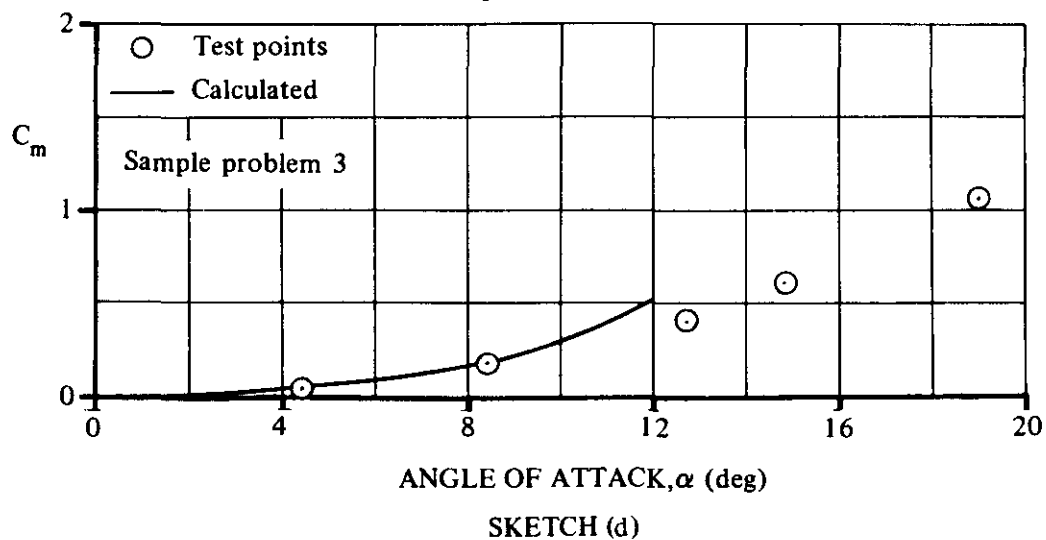
4. Method 3

Refer to Sample Problem 2 in Paragraph A of this section for an example of the application of the method.

D. HYPERSONIC

Three methods are available for estimating the pitching moment of bodies of revolution at hypersonic speeds. The first method, based on Newtonian impact theory and its modifications, is discussed in Paragraph D of Section 4.2.1.1. The second method is the hypersonic-similarity method. The third method is the method of Jorgensen previously presented as Method 3 of Paragraph C of this section.

DATCOM METHODS

Method 1

The expression for the pitching moment of an arbitrary body of revolution, from the modified Newtonian theory of Reference 14, referred to an arbitrary moment center and based on the product of the body base area and body length $S_b \ell_B$, is

$$C_m = \frac{K}{\pi} \frac{\ell_B}{R} \int_0^1 K_\theta \frac{r}{R} \frac{\ell_x}{\ell_B} d\left(\frac{x}{\ell_B}\right) \qquad 4.2.2.2\text{-f}$$

where ℓ_x is the distance from the moment center to a transverse element, positive where the element is forward of the moment center. The remaining parameters are defined under Method 2 in Paragraph D of Section 4.2.1.2.

The following steps outline the calculation procedure (Steps 1 through 3 are identical to Steps 1 through 3 of Method 2 of Paragraph D of Section 4.2.1.2):

Step 1. From the equation of the body of revolution obtain the expression for the surface slope using the relation

$$\theta = \tan^{-1}\left(\frac{dr}{dx}\right)$$

where θ, dr, and dx are defined in Sketch (f) of Section 4.2.1.2.

Step 2. Compute the values of r/R and θ at various longitudinanal stations x/ℓ_B.

Step 3. For various x/ℓ_B enter Figure 4.2.1.2-43 with the corresponding θ from Step 2 and obtain K_θ at the desired angle of attack.

Step 4. Plot the product $K_\theta \dfrac{r}{R} \dfrac{\ell_x}{\ell_B}$ against x/ℓ_B.

Step 5. Obtain the required value of C_m by integrating the area under the curve described in Step 4 and multiplying by $\dfrac{K}{\pi} \dfrac{\ell_B}{R}$.

4.2.2.2-14

Method 2

The second method of estimating body pitching moments applies only to ogive-cylinder bodies. This method is based on experimental data for a wide range of models at a Mach number of 4.24. These data have been used to derive a hypersonic design chart (Figure 4.2.2.2-27) based on hypersonic-similarity parameters. The body pitching moment obtained from Figure 4.2.2.2-27, where $\beta = \sqrt{M^2 - 1}$, is referred to the nose apex and is based on the product of the body frontal area and body length $S_B \ell_B$.

Pitching moments calculated by this method are compared with test data in Table 4.2.2.2-D.

Method 3

This method is identical to Method 3 presented in Paragraph C of this section. The method is applicable to angles of attack from 0 to 180° and Mach numbers up to 7. The method has been partially substantiated by the test data from Reference 5 in Table 4.2.2.2-C.

The method shows reasonable agreement with test data at hypersonic speeds in the low-angle-of-attack range. Because of the scarcity of substantiating test data, caution should be used when applying the method at higher angles of attack ($\alpha > 25^O$).

Sample Problems

1. Method 1

Given: A second-power body of revolution of fineness ratio 1.0. This is the same configuration as Sample Problem 2 of Paragraph D of Section 4.2.1.2.

$$x = \left(\frac{4}{\ell_B}\right) r^2 \quad \text{(equation of body)} \qquad \ell_B = 2.0 \text{ ft} \qquad R = 1.0 \text{ ft}$$

$$\ell_x/\ell_B = 0.50 - (x/\ell_B) \quad \text{(moment center at } 0.50 \ell_B)$$

$$M_\infty = 3.55 \qquad \alpha = 6^O \qquad \gamma = 1.40$$

$$K = 1.77 \quad \text{(Sample Problem 2, Paragraph D, Section 4.2.1.2)}$$

Compute:

Calculate r/R and θ at various longitudinal stations x/ℓ_B and plot. (See Sketch (g), Sample Problem 2, Paragraph D, Section 4.2.1.2.)

Obtain values of K_θ from Figure 4.2.1.2-43 for various values of θ at $\alpha = 6^O$.

Plot the product $K_\theta \dfrac{r}{R} \dfrac{\ell_x}{\ell_B}$ versus x/ℓ_B (Sketch (e)).
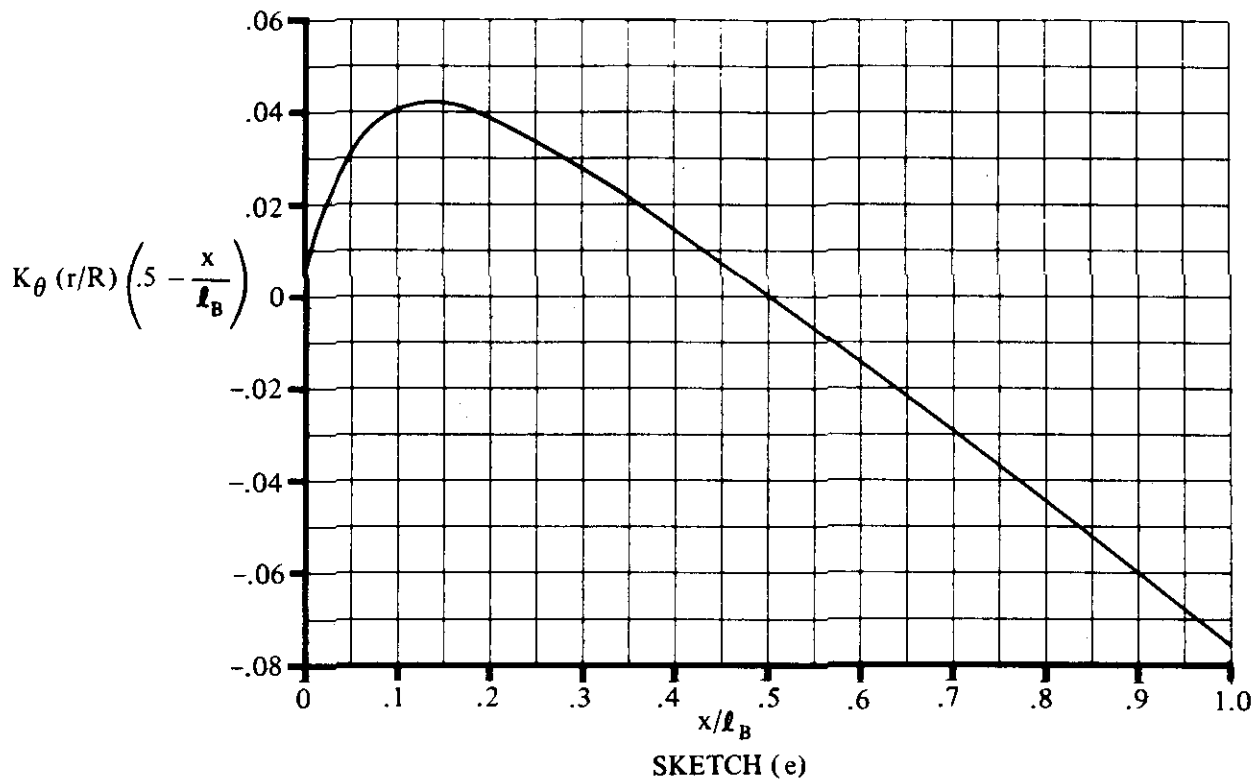
SKETCH (e)

Integrate the area under the curve of Sketch (e).

$$\int_0^1 K_\theta \, \frac{r}{R} \left(0.50 - \frac{x}{\ell_B} \right) d \left(\frac{x}{\ell_B} \right) = -0.00615$$

Solution:

$$C_m = \frac{K}{\pi} \frac{\ell_B}{R} \int_0^1 K_\theta \, \frac{r}{R} \frac{\ell_x}{\ell_B} \, d \left(\frac{x}{\ell_B} \right) \quad \text{(Equation 4.2.2.2-f)}$$

$$= \frac{1.77}{\pi} \frac{2}{1} \, (-0.00615)$$

$$= -0.0069 \quad \text{(referred to a moment center at } 0.50\,\ell_B \text{ and based on } S_b\ell_B)$$

2. Method 2

Given: An ogive-cylinder body of Reference 16.
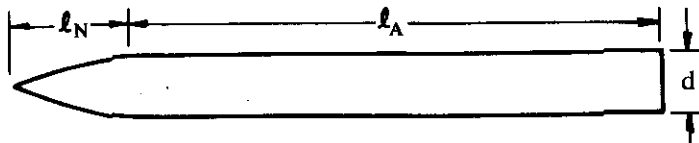
Body Characteristics:

ℓ_N = 2.50 ft ℓ_A = 11.50 ft   d = 1.0 ft

Additional Characteristics:

M = 4.24; β = 4.12 α = 2°, 4°, 6°

Compute:

f_N = ℓ_N/d = 2.50 f_A = ℓ_A/d = 11.50

f_A/f_N = 11.50/2.50 = 4.60 β/f_N = 4.12/2.50 = 1.648

Solution:

α (deg)	$\beta\alpha$ (deg)	βC_m Fig. 4.2.2.2-27	C_m (based on $S_B\ell_B$) (referred to nose apex)
2	8.24	−0.15	−0.0364
4	16.48	−0.38	−0.0922
6	24.72	−0.79 (extrapolated)	−0.1917
8	32.96	−1.29 (extrapolated)	−0.3131

The calculated results are compared with test values from Reference 15 in Sketch (f).
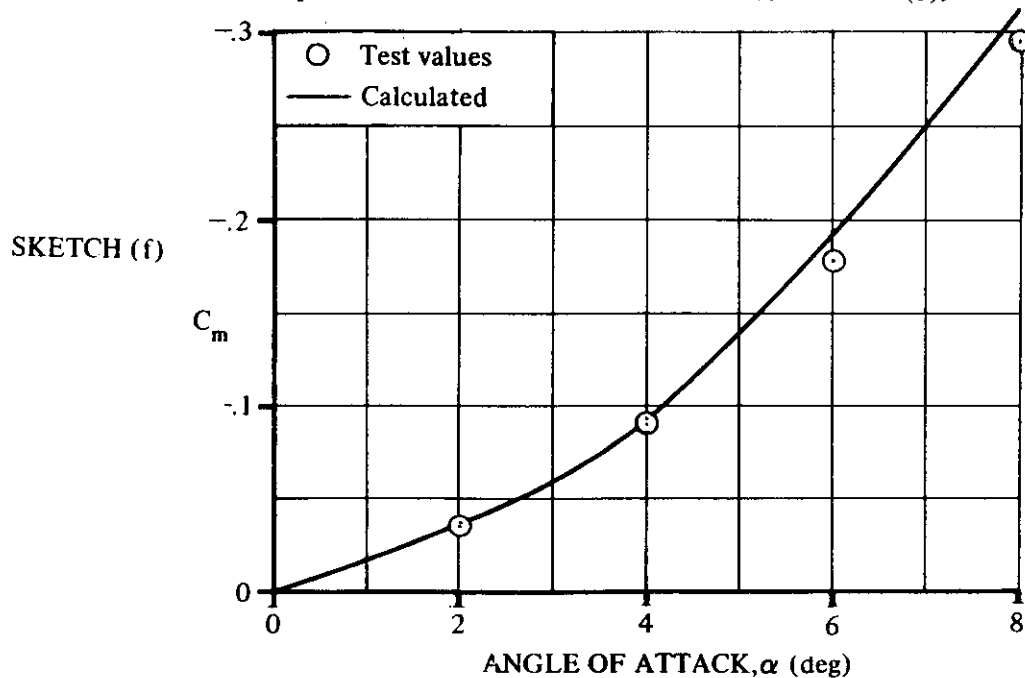
SKETCH (f)

3. Method 3

Refer to Sample Problem 2 in Paragraph A of this section for an example of the application of the method.

REFERENCES

1. Hopkins, E. J.: A Semiempirical Method for Calculating the Pitching Moment of Bodies at Low Mach Numbers. NACA RM A51C14, 1951. (U)

2. Jorgensen, L. H.: Prediction of Static Aerodynamic Characteristics for Space-Shuttle-Like and Other Bodies at Angles of Attack from 0° to 180°. NASA TN D-6996, 1973. (U)

3. Jorgensen, L. H.: A Method for Estimating Static Aerodynamic Characteristics for Slender Bodies of Circular and Noncircular Cross Section Alone and with Lifting Surfaces at Angles of Attack from 0° to 90°. NASA TN D-7228, 1973. (U)

4. Jernell, L. S.: Aerodynamic Characteristics of Bodies of Revolution at Mach Numbers from 1.50 to 2.86 and Angles of Attack to 180°. NASA TM X-1658, 1968. (U)

5. Dennis, D. H., and Cunningham, B. E.: Forces and Moments on Inclined Bodies at Mach Numbers from 3.0 to 6.3. NACA RM A54E03, 1954. (U)

6. Jorgensen, L. H., and Nelson, E. R.: Experimental Aerodynamic Characteristics for Bodies of Elliptic Cross Section at Angles of Attack from 0° to 58° and Mach Numbers from 0.6 to 2.0. NASA TM X-3129, 1975. (U)

7. Allen, H. J., and Perkins, E. W.: A Study of Effects of Viscosity on Flow Over Slender Inclined Bodies of Revolution. NACA TR 1048, 1951. (U)

8. Jorgensen, L. H.: Inclined Bodies of Various Cross Section at Supersonic Speeds. NASA Memo 10-3-58A, 1958. (U)

9. Van Dyke, M. D.: The Combined Supersonic-Hypersonic Similarity Rule. Jour. Aero. Sci., Vol. 18, No. 7, 1951. (U)

10. Perkins, E. W., and Jorgensen, L. H.: Comparison of Experimental and Theoretical Normal-Force Distributions (Including Reynolds Number Effects) on an Ogive-Cylinder Body at Mach Number 1.98. NACA TN 3716, 1956. (U)

11. Jack, J. R.: Aerodynamic Characteristics of a Slender Cone-Cylinder Body of Revolution at Mach Number of 3.85. NACA RM E51H17, 1951. (U)

12. Ferri, A.: Supersonic-Tunnel Tests of Projectiles in Germany and Italy. NACA WR L-152, 1945. (U)

13. Delancey, L. M., Jaeger, B. F., and Schroedter, G. M.: The Aerodynamic Characteristics at Mach No. 4.24 of Bodies of Revolution With Varying Lengths and Head Shapes. NOTS TM 358, 1951. (U)

14. Rainey, R. W.: Working Charts for Rapid Prediction of Force and Pressure Coefficients on Arbitrary Bodies of Revolution by Use of Newtonian Concepts. NASA TN D-176, 1959. (U)

15. Jones, J. R., and Demele, F. A.: Aerodynamic Study of a Wing-Fuselage Combination Employing a Wing Swept Back 63° — Characteristics Throughout the Subsonic Speed Range with the Wing Cambered and Twisted for a Uniform Load at a Lift Coefficient of 0.25. NACA RM A9D25, 1949. (U)

16. Jaeger, B. F., and Morgan, A. J. A.: Review of Experiment and Theory Applicable to Cone-Cylinder and Ogive-Cylinder Bodies of Revolution in Supersonic Flow. NAVORD 5239, 1956. (U)

Ref	M	R_ℓ (based on d_{equiv})	a/b	$\dfrac{\ell_B}{d_{equiv}}$	Nose Shape	α (deg)	$C_{m_{calc}}$	$C_{m_{test}}$	ΔC_m
6	0.6	6.5×10^5	1.0	10	Ogive	10	1.7	1.2	0.5
						20	3.4	2.8	0.6
						30	5.2	4.9	0.3
						40	6.4	8.2	−1.8
						50	7.3	10.9	−3.6
						60	7.8	9.7	−1.9
	0.9					10	1.7	1.3	0.4
						20	3.5	3.2	0.3
						30	5.3	7.0	−1.7
						40	6.8	12.5	−5.7
						50	8.1	15.7	−7.6
						60	8.8	14.4	−5.6
	0.6		2.0			10	3.4	2.6	0.8
						20	6.9	6.3	0.6
						30	9.9	14.5	−4.6
						40	12.3	23.1	−11.0
						50	13.9	29.1	−15.3
						60	14.5	29.8	−15.2
	0.9		1.0			10	3.5	2.7	0.8
						20	6.7	8.3	−1.6
						30	10.0	16.7	−6.7
						40	12.9	24.8	−11.9
						50	15.2	29.5	−14.3
						60	16.5	29.0	−12.5
	0.6		0.5			10	0.9	0.4	0.5
						20	1.8	1.3	0.5
						30	2.5	1.7	0.8
						40	3.2	2.5	0.7
						50	3.6	3.5	0.1
						60	3.9	3.3	0.6
	0.9					10	1.0	0.5	0.5
						20	1.7	1.5	0.2
						30	2.6	2.6	0
						40	3.5	5.0	−1.5
						50	4.1	7.5	−3.4

$$\text{Average Error} = \sum \frac{|\Delta C_m|}{n} = 3.8$$

TABLE 4.2.2.2-B

SUPERSONIC PITCHING-MOMENT COEFFICIENT OF
OGIVE-CYLINDER BODIES

METHOD 2

DATA SUMMARY AND SUBSTANTIATION

Ref.	M	f_N	f_A	α (deg)	C_m Calc.	C_m Test	e Percent Error
10	1.57	1.12	12.90	4	−.037	−.046	−19.6
				8	−.149	−.116	28.4
	1.86			4	−.035	−.045	−22.2
				8	−.204	−.134	52.2
	2.49			4	−.035	−.032	9.4
				8	−.263	−.246	6.9
	2.87			4	−.043	−.0375	14.7
				8	−.264	−.229	15.3
	1.57	1.50	8.50	4	−.037	−.0311	19.0
				8	−.110	−.0782	40.7
	1.86			4	−.030	−.0385	−22.1
				8	−.140	−.105	33.3
	2.49			4	−.030	−.0225	33.3
				8	−.230	−.193	19.2
	2.87			4	−.040	−.055	−27.3
				8	−.250	−.248	0.8
	1.57	2.50	11.50	4	−.040	−.047	−14.9
				8	−.130	−.126	3.2
	1.86			4	−.045	−.047	− 4.3
				8	−.170	−.143	18.9
	2.49			4	−.050	−.032	56.3
				8	−.270	−.230	17.4
	2.87			4	−.050	−.039	28.2
				8	−.310	−.290	6.9
	1.57	3.00	15.00	4	−.048	−.063	−23.7
				8	−.145	−.147	− 1.4
	2.49			4	−.054	−.0513	5.3
				8	−.325	−.276	17.8
	2.87			4	−.059	−.0647	− 8.8
				8	−.435	−.375	16.0
	1.57	4.00	10.00	4	−.045	−.054	−16.6
				8	−.136	−.140	− 2.9
	1.86			4	−.045	−.0555	−18.9
				8	−.166	−.150	10.7
	2.49			4	−.050	−.0496	0.8
				8	−.259	−.250	3.6
	2.87			4	−.056	−.051	9.8
				8	−.379	−.277	36.8
	1.57	1.12	16.90	4	−.037	−.0517	−28.4
				8	−.190	−.183	3.8
	2.49			4	−.050	−.0692	−15.5
				8	−.340	−.277	22.7
	2.87			4	−.045	−.0554	−18.8
				8	−.349	−.362	− 3.6

$$\text{Average Error} = \frac{\Sigma |e|}{n} = 17.7\%$$

TABLE 4.2.2.2-C

SUPERSONIC PITCHING-MOMENT COEFFICIENT

METHOD 3

DATA SUMMARY AND SUBSTANTIATION

Ref	M	R_ℓ (based on d_{equiv})	a/b	$\dfrac{\ell_B}{d_{equiv}}$	Nose Shape	α (deg)	$C_{m_{calc}}$	$C_{m_{test}}$	ΔC_m
4	1.5	1.25×10^5	1.0	6	Blunt	35	2.7	1.8	0.9
						65	1.9	1.8	0.1
						95	−0.4	−0.6	0.2
				8	Cone	35	−0.9	−2.0	1.1
						65	−5.2	−4.0	−1.2
						95	−7.4	−7.0	−0.4
						125	−6.6	−8.3	1.7
						155	−2.4	−4.0	1.6
				9		35	−0.9	−2.0	1.1
						65	−7.0	−4.0	−3.0
						95	−10.4	−9.6	−0.8
						125	−9.5	−12.0	2.5
						155	−3.7	−6.2	2.5
				11		35	−0.9	−1.5	0.6
						65	−8.8	−5.0	−3.8
						95	−13.4	−14.0	0.6
						125	−12.5	−16.0	3.5
						165	−2.5	−5.0	2.5
				9	Ogive	35	0.6	0.5	0.1
						65	−4.1	−1.8	−2.3
						95	−7.5	−7.8	0.3
						125	−7.9	−10.5	2.6
						155	−3.6	−5.5	1.9
				7		35	−1.2	−2.0	0.8
						65	−5.4	−4.0	−1.4
						95	−7.3	−7.0	−0.3
						125	−6.3	−7.8	1.5
						155	−2.2	−4.1	1.9
				11		35	−1.4	−1.0	−0.4
						65	−9.5	−5.0	−4.5
						95	−14.0	−15.0	1.0
						125	−12.7	−16.7	4.0
						155	−4.8	−8.7	3.9
	2.86			6	Blunt	35	2.7	0.2	2.5
						65	1.9	0.1	1.8
						95	−0.4	−0.3	−0.1
				8		35	3.6	0.7	2.9
						65	2.6	0.6	2.0
						85	0.5	0.4	0.1

TABLE 4.2.2.2-C (CONTD)

Ref	M	R_ℓ (based on d_{equiv})	a/b	$\dfrac{\ell_B}{d_{equiv}}$	Nose Shape	α (deg)	$C_{m_{calc}}$	$C_{m_{test}}$	ΔC_m
4	2.86	1.25×10^5	1.0	7	Cone	35	−1.0	−1.8	0.8
						65	−4.3	−4.5	0.2
						95	−6.5	−6.2	−0.3
						125	−5.7	−6.3	0.6
						155	−2.6	−2.2	−0.4
				9		35	−1.0	−1.8	0.8
						65	−5.8	−6.0	0.2
						95	−9.2	−9.0	−0.2
						125	−8.2	−9.3	1.1
						155	−3.9	−3.6	−0.3
				11		35	−1.0	−1.8	0.8
						65	−7.3	−7.5	0.2
						95	−11.9	−11.7	−0.2
						125	−10.8	−12.3	1.5
						155	−5.2	−5.0	−0.2
				9	Ogive	35	0.5	−0.9	1.4
						65	−3.2	−3.9	0.7
						95	−6.7	−6.6	−0.1
						125	−6.9	−7.4	0.5
						155	−3.7	−2.8	−0.9
				7		35	−1.3	−1.4	0.1
						65	−4.5	−4.7	0.2
						95	−6.5	−6.5	0
						125	−5.4	−6.3	0.9
						155	−2.3	−2.5	0.2
				9		35	−1.4	−1.9	0.5
						65	−6.2	−6.4	0.2
						95	−9.4	−9.9	0.5
						125	−8.1	−9.0	0.9
						155	−3.7	−3.5	−0.2
				11		35	−1.5	−2.4	0.9
						65	−7.9	−8.0	0.1
						95	−12.3	−13.6	1.3
						125	−10.9	−12.6	1.7
						155	−5.1	−4.7	−0.4
5	4.24	5.4×10^5	1.0	7	Cone	4	−0.4	−0.8	0.4
						8	−1.4	−1.8	0.4
						12	−3.0	−3.2	0.2
						16	−4.8	−4.8	0
						20	−6.5	−6.1	−0.4

TABLE 4.2.2.2-C (CONTD)

Ref	M	R_ℓ (based on d_{equiv})	a/b	$\dfrac{\ell_B}{d_{equiv}}$	Nose Shape	α (deg)	$C_{m_{calc}}$	$C_{m_{test}}$	$\angle C_m$
5	4.24	5.4×10^5	1.0	7	Cone	24	−8.5	−7.9	−0.6
	5.04	2.6×10^5		10		4	−0.8	−1.0	0.2
						8	−2.8	−3.1	0.3
						12	−6.0	−4.5	−1.5
						16	−9.0	−7.3	−1.7
						20	−12.4	−9.6	−2.8
						24	−16.5	−12.9	−3.6
					Ogive	4	−0.5	−0.7	0.2
						8	−1.6	−1.7	0.1
						12	−3.1	−2.8	−0.3
						16	−4.6	−4.1	−0.5
	6.28	1.1×10^5			Cone	4	−0.4	−0.6	0.2
						8	−1.5	−1.6	0.1
						12	−2.8	−2.7	−0.1
						16	−4.3	−4.3	0
						20	−6.0	−6.2	0.2
						24	−8.0	−8.5	0.5
6	1.2	3.8×10^5			Ogive	10	1.7	1.6	0.1
						20	3.7	4.2	−0.5
						30	6.1	8.2	−2.1
						40	8.6	10.1	−1.5
						50	10.5	12.0	−1.5
						60	11.5	14.1	−2.6
	1.5					10	1.6	1.8	−0.2
						20	3.9	5.8	−1.9
						30	6.3	7.0	−0.7
						40	8.8	8.3	0.5
						50	10.2	8.9	1.3
						60	10.8	10.8	0
	2.0					10	1.8	2.0	−0.2
						20	4.0	4.1	−0.1
						30	6.5	5.9	0.6
						40	8.3	7.1	1.2
						50	9.5	8.2	1.3
						60	10.1	9.5	0.6
	1.2		2.0			10	3.5	3.4	0.1
						20	7.4	8.3	−0.9
						30	11.6	14.1	−2.5
						40	16.1	17.5	−1.4
						50	19.5	21.6	−2.1

TABLE 4.2.2.2-C (CONTD)

Ref	M	R_ℓ (based on d_{equiv})	a/b	$\dfrac{\ell_B}{d_{equiv}}$	Nose Shape	α (deg)	$C_{m_{calc}}$	$C_{m_{test}}$	ΔC_m
6	1.2	3.8×10^5	2.0	10	Ogive	60	21.2	23.5	−2.3
	1.5					10	3.5	3.5	0
						20	7.6	8.3	−0.7
						30	12.2	11.4	0.8
						40	16.4	14.5	1.9
						50	18.9	16.1	2.8
						60	19.8	17.5	2.3
	2.0					10	3.5	3.2	0.3
						20	7.6	7.1	0.5
						30	12.5	10.3	2.2
						40	15.6	11.8	3.8
						50	17.6	13.1	4.5
						60	18.6	15.4	3.2
	1.2		0.5			10	0.9	0.9	0
						20	2.0	2.1	−0.1
						30	3.0	4.0	−1.0
						40	4.4	4.5	−0.1
						50	5.2	6.5	−1.3
						60	5.8	8.4	−2.6
	1.5					10	1.0	1.1	−0.1
						20	1.9	2.3	−0.4
						30	3.1	3.7	−0.6
						40	4.4	4.4	0
						50	5.1	5.1	0
						60	5.4	5.4	0
						10	0.8	1.1	−0.3
						20	2.0	2.2	−0.2
						30	3.2	3.2	0
						40	4.1	4.0	0.1
						50	4.8	4.8	0
						60	5.1	4.9	0.2

$$\text{Average Error} = \sum \frac{|\Delta C_m|}{n} = 1.0$$

TABLE 4.2.2.2-D

HYPERSONIC PITCHING-MOMENT COEFFICIENT OF
OGIVE-CYLINDER BODIES
METHOD 2
DATA SUMMARY AND SUBSTANTIATION

Ref.	M	f_N	f_A	α (deg)	C_m Calc.	C_m Test	e Percent Error
10	4.24	1.12	8.88	2	−.024	−.021	14.3
				4	−.063	−.060	5.0
				6	−.129	−.130	− 0.8
				8	−.216	−.222	− 2.7
		1.12	12.90	2	−.027	−.026	3.8
				4	−.073	−.071	2.8
				6	−.155	−.146	6.2
				8	−.250	−.255	− 2.0
		1.50	8.50	2	−.029	−.027	7.4
				4	−.070	−.066	6.1
				6	−.146	−.154	− 5.2
				8	−.245	−.239	2.5
		2.50	11.50	2	−.036	−.034	5.9
				4	−.092	−.092	0
				6	−.194	−.175	10.9
				8	−.313	−.296	5.7
		3.00	15.00	2	−.041	−.035	17.1
				4	−.106	−.102	3.9
				6	−.215	−.222	− 3.2
				8	−.332	−.369	−10.0
		3.50	6.50	2	−.034	−.037	−10.8
				4	−.091	−.087	4.6
				6	−.181	−.165	9.7
				8	−.291	−.267	9.0
		4.00	10.00	2	−.039	−.037	5.4
				4	−.102	−.100	2.0
				6	−.201	−.195	3.1
				8	−.335	−.316	6.0
		5.00	5.00	2	− 039	−.041	− 4.9
				4	−.096	−.098	− 2.0
				6	−.187	−.164	14.0
				8	−.311	−.271	14.8
		1.12	16.90	2	−.032	−.036	−11.1
				4	−.092	−.093	− 1.1
				6	−.189	−.170	11.2
				8	−.299	−.262	14.1
		1.50	16.50	2	−.035	−.039	−10.3
				4	−.097	−.101	− 4.0
				6	−.201	−.170	18.2
				8	−.316	−.311	1.6

$$\text{Average Error} = \frac{\sum |e|}{n} = 6.8\%$$
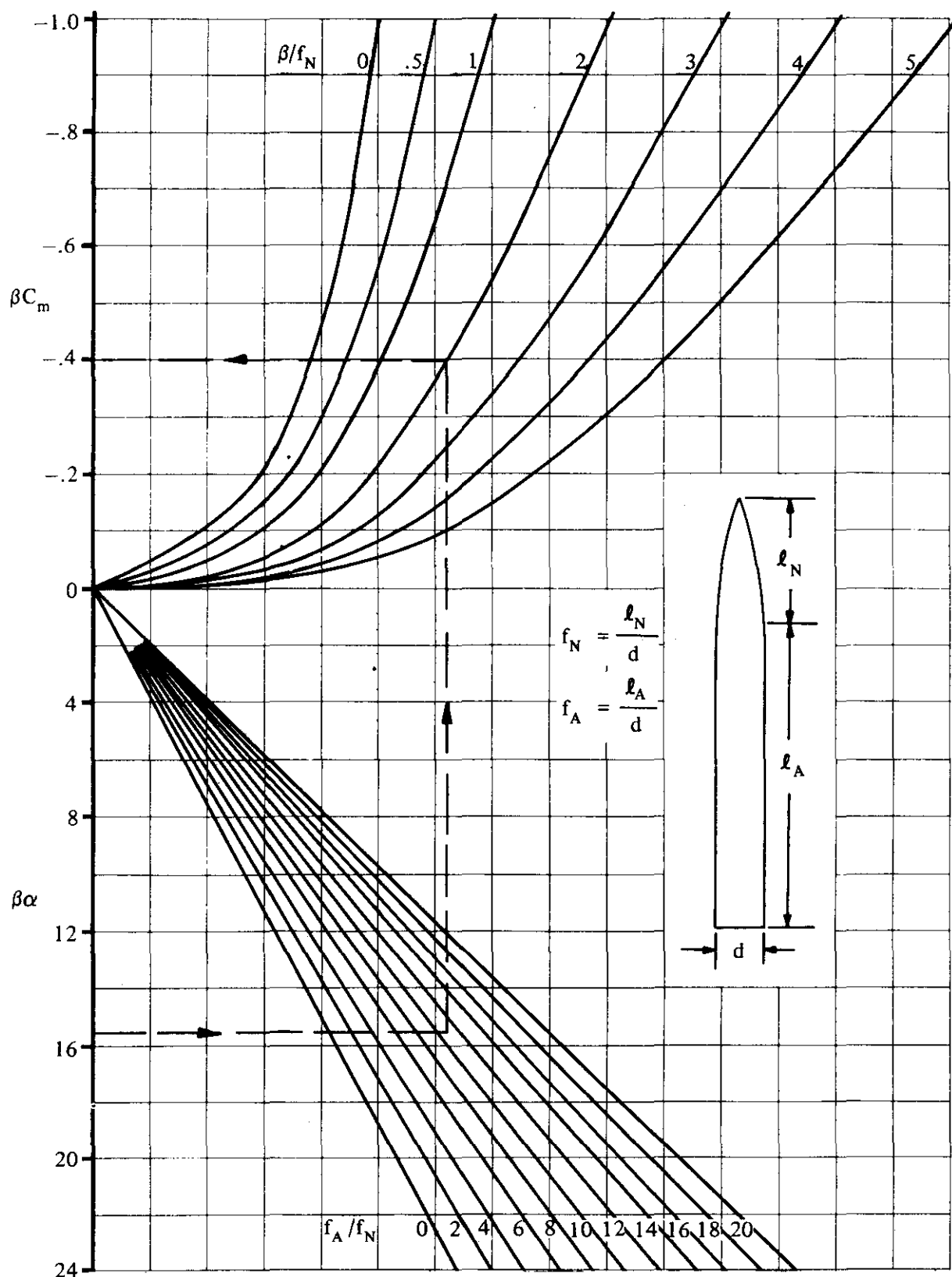
FIGURE 4.2.2.2-26 PITCHING-MOMENT COEFFICIENT FOR OGIVE-CYLINDERS AT
SUPERSONIC SPEEDS 1.6 < M < 3.0
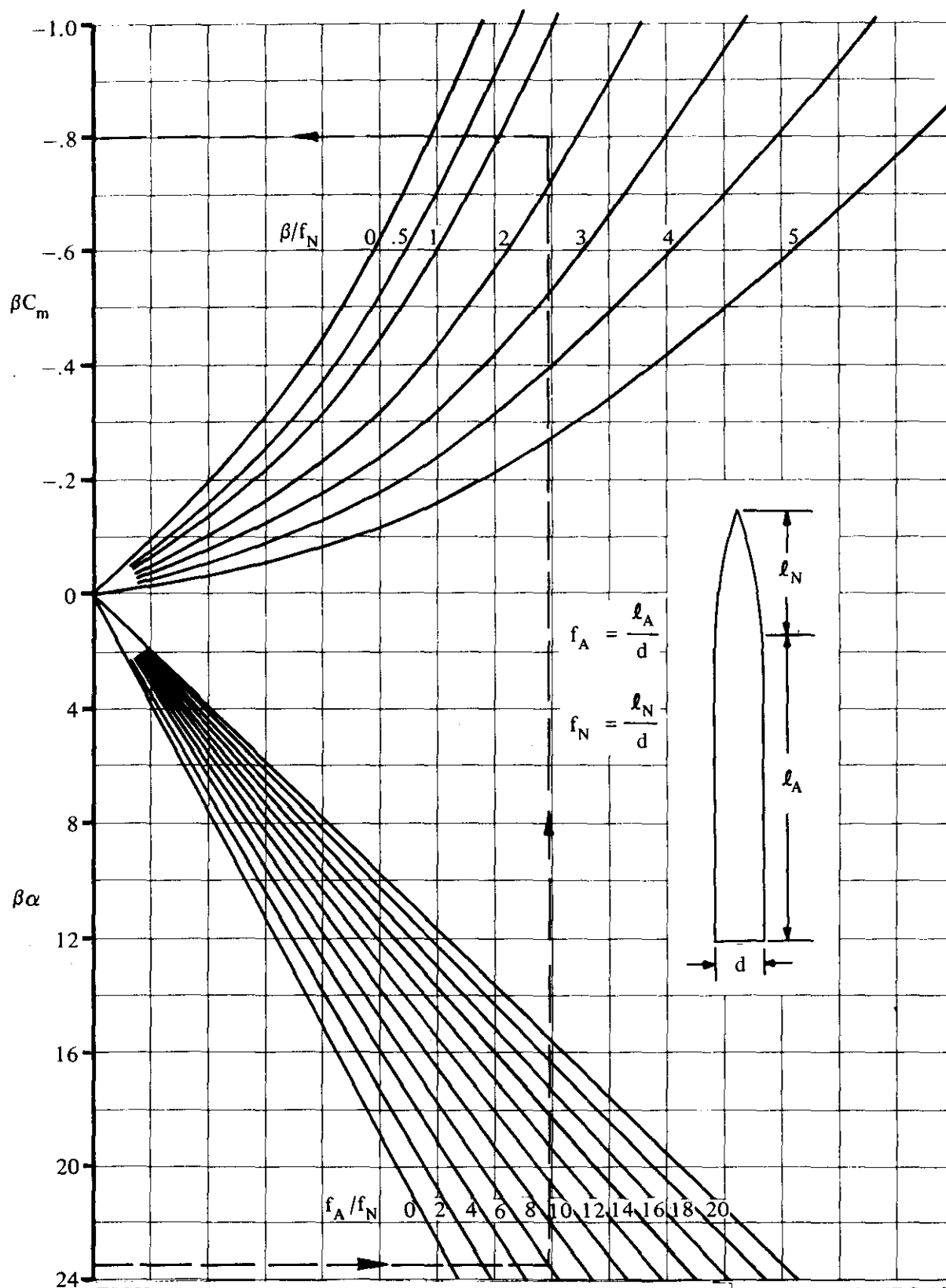
FIGURE 4.2.2.2-27 PITCHING-MOMENT COEFFICIENT FOR OGIVE-CYLINDERS AT
HYPERSONIC SPEEDS 3.0 < M < 5.0

4.2.2.2-27

4.2.3 BODY DRAG

4.2.3.1 BODY ZERO-LIFT DRAG

The composition of body zero-lift drag in the various speed regimes is very similar to that for wings (see Section 4.1.5.1). At subsonic speeds the pressure drag of the forebody is generally small and the total drag is composed mostly of skin friction and base drag. For the higher speed regimes the total drag is split significantly between friction and pressure drag.

The methods presented in this section are valid for bodies of revolution. However, excellent approximations can be made for non-body-of-revolution configurations by treating the equivalent body of revolution; that is, the body of revolution that has the same axial area distribution as the actual body.

A. SUBSONIC

At subsonic speeds the total zero-lift drag of smooth slender bodies is primarily skin friction. The Reynolds number based on body length, boundary-layer condition (laminar or turbulent), and surface roughness are important in the determination of the friction drag (see chapter VI of reference 1). For the Datcom these effects are handled the same as for wings (Section 4.1.5.1). A turbulent boundary-layer condition is assumed over the entire body surface.

The pressure drag of a closed body is zero for an inviscid fluid. Actually the displacement of the boundary layer causes an incomplete pressure recovery at the end of the body and a finite pressure drag results. This drag is small for fineness ratios above approximately four but becomes significant for blunt bodies.

The base drag is also generally small, usually less than 10 percent of the total body drag. The most popular approach to the estimation of base drag is to correlate it with the skin-friction drag of the remainder of the body. This approach is discussed in detail in reference 2 and in chapter VI of reference 1. Reference 3 shows that the presence of a wing increases the base pressure (less drag). Tail fins and·wind-tunnel stings have the same effect (reference 4). Base pressures are also increased at low Reynolds numbers (reference 5).

DATCOM METHOD

The subsonic zero-lift drag of an isolated body based on the maximum body frontal area is given in reference 6 as

$$C_{D_0} = C_f \left[1 + \frac{60}{(\ell_B/d)^3} + 0.0025 \left(\frac{\ell_B}{d} \right) \right] \frac{S_S}{S_B} + C_{D_b} \qquad 4.2.3.1\text{-a}$$

where the first term on the right-hand side of the equation is the zero-lift drag of the body exclusive of the base drag, and

C_f is the turbulent flat-plate skin-friction coefficient, including roughness effects, as a function of Mach number and the Reynolds number based on the reference length ℓ. This value is obtained from figure 4.1.5.1-26 and is determined as discussed in paragraph A of Section 4.1.5.1. The reference length ℓ is the actual length of the body ℓ_B.

$\dfrac{\ell_B}{d}$ is the body fineness ratio defined for different types of bodies of revolution as follows:
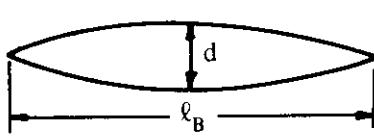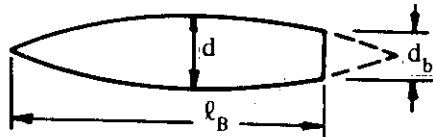
CLOSED BODY   BODY HAVING A BLUNT BASE   FOREBODY
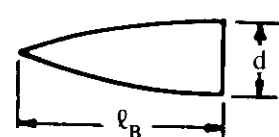
For non-body-of-revolution configurations the equivalent diameter should be used,

$$d_{equiv} = \sqrt{\frac{\text{cross-sectional area}}{0.7854}}$$

C_{D_b} is the base-drag coefficient, based on the maximum body frontal area, given in reference 1 as

$$C_{D_b} = 0.029 \left(\frac{d_b}{d}\right)^3 \Big/ \sqrt{\left(C_{D_f}\right)_b}$$

                4.2.3.1-b

where

$\dfrac{d_b}{d}$ is the ratio of base diameter to maximum diameter (equivalent diameters for non-body-of-revolution configurations).

$\left(C_{D_f}\right)_b$ is the zero-lift drag of the body exclusive of the base as determined by the first term in equation 4.2.3.1-a.

It should be noted that wings or fins (or wind-tunnel stings) can have a sizable effect on base drag.

S_B is the body maximum frontal area.

S_S is the wetted area or surface area of the body excluding the base area. This is normally determined by graphical integration of $\displaystyle\int_0^{\ell_B} p\, dx$, where p is the cross-section perimeter.

The ratio S_S/S_B for a given body can be approximated by using figures 2.3-2 and 2.3-3, which give this ratio for a number of specific body shapes.

The term $0.0025 \dfrac{\ell_B}{d}$ in equation 4.2.3.1-a represents the pressure-drag contribution.

Sample Problem

Given: The body of reference 54 having an elliptical cross section with a cutoff afterbody.
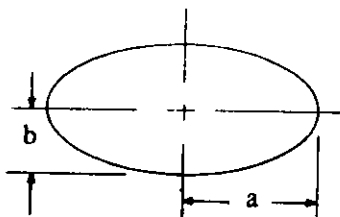
$\ell_B = 61.45$ in. $a_{max} = 5.19$ in. $b_{max} = 1.73$ in.

$S_b = 0.25\, S_B$

$M = 0.8$ $R_\ell = 0.325 \times 10^6$ per in.

BODY CROSS SECTION
$a/b = 3$

Polished metal surface; assume $k = 0.08 \times 10^{-3}$ in.

Compute:

$$S_B = \pi ab = \pi(5.19)(1.73) = 28.2 \text{ sq in.}$$

$$d_{equiv} = \sqrt{\frac{S_B}{0.7854}} = \sqrt{\frac{28.2}{0.7854}} = 6.0 \text{ in.}$$

$$\frac{\ell_B}{d} = \frac{61.45}{6.0} = 10.24$$

$$\frac{S_S}{S_B} = 31.6 \text{ (extrapolated from figure 2.3-2, ellipsoid with cutoff afterbody)}$$

$$R_\ell = (0.325 \times 10^6)(\ell_B) = (0.325 \times 10^6)(61.45) = 1.997 \times 10^7$$

$$\ell/k = 61.45/(0.08 \times 10^{-3}) = 7.68 \times 10^5; \text{ cutoff } R_\ell \simeq 6.8 \times 10^7 \quad \text{(figure 4.1.5.1-27)}$$

Since cutoff R_ℓ > calculated R_ℓ, read C_f at calculated R_ℓ.

$$C_f = 0.00256 \quad \text{(figure 4.1.5.1-26)}$$

Determine the zero-lift drag of the body exclusive of base drag.

$$\left(C_{D_f}\right)_b = C_f\left[1 + \frac{60}{(\ell_B/d)^3} + 0.0025\left(\frac{\ell_B}{d}\right)\right]\frac{S_S}{S_B} = 0.00256\left[1 + \frac{60}{(10.24)^3} + 0.0025(10.24)\right]31.6$$

$$= 0.0875 \text{ (based on } S_B)$$

$$S_b = 0.25\,S_B = (0.25)(28.2) = 7.05 \text{ sq in.}$$

$$(d_b)_{equiv} = \sqrt{\frac{S_b}{0.7854}} = \sqrt{\frac{7.05}{0.7854}} = 3.0 \text{ in.}$$

$$\frac{d_b}{d} = \frac{3.0}{6.0} = 0.5$$

Determine the base drag

$$C_{D_b} = 0.029\left(\frac{d_b}{d}\right)^3 \Big/ \sqrt{\left(C_{D_f}\right)_b} \quad \text{(equation 4.2.3.1-b)}$$

$$= 0.029\,(0.5)^3 \Big/ \sqrt{0.0875}$$

$$= 0.0122 \text{ (based on } S_B)$$

Solution:

$$C_{D_0} = C_f \left[1 + \frac{60}{(\ell_B/d)^3} + 0.0025 \left(\frac{\ell_B}{d} \right) \right] \frac{S_S}{S_B} + C_{D_b} \quad \text{(equation 4.2.3.1-a)}$$

$$= 0.0875 + 0.0122$$

$$= 0.0997 \text{ (based on } S_B)$$

This compares with a test value of 0.0920 from reference 54.

B. TRANSONIC

A fundamental discussion of the transonic aerodynamic characteristics of bodies is given in reference 7 and chapter XVI of reference 1. An extensive bibliography on finned bodies is given in reference 8.

For the Datcom, the general approach consists of predicting the skin friction, the drag-divergence Mach number, and the variation of base drag with Mach number, and the variation of pressure drag for Mach numbers above 1.0. The total drag characteristic as a function of Mach number is then constructed from these estimated characteristics. For the purpose of the Datcom the skin-friction drag is assumed to be constant and equal to the subsonic value at $M = 0.6$ throughout the transonic range.

DATCOM METHOD

The transonic zero-lift drag coefficient of a body is determined by the following procedure.

Step 1.   Calculate the skin-friction drag coefficient at $M = 0.6$, based on maximum frontal area, by

$$C_{D_f} = C_f \frac{S_S}{S_B} \qquad \qquad 4.2.3.1\text{-c}$$

where

C_f is the turbulent flat-plate skin-friction coefficient at $M = 0.6$, including rough-
ness effects, as a function of the Reynolds number based on the reference
length ℓ. This value is obtained from figure 4.1.5.1-26 as discussed in paragraph
A of Section 4.1.5.1. The reference length ℓ is the actual length of the body
ℓ_B. This value is assumed to be constant throughout the transonic region.

$\dfrac{S_S}{S_B}$ is the ratio of body wetted area to maximum body frontal area, determined as
explained in paragraph A of this section.

Step 2.   Calculate the subsonic pressure drag at $M = 0.6$ by

$$C_{D_P} = (C_f)_{M=0.6} \left[\frac{60}{(\ell_B/d)^3} + 0.0025 \left(\frac{\ell_B}{d} \right) \right] \frac{S_S}{S_B} \qquad \qquad 4.2.3.1\text{-d}$$

where the individual terms are the same as in equation 4.2.3.1-a. This component of drag is assumed to be constant for $0 < M < 1.0$ and to decrease linearly to zero at $M = 1.2$. (See sketch (a).)

Step 3. Calculate the base-drag coefficient C_{D_b} as a function of Mach number. First calculate the subsonic base drag (at a Mach number of 0.6) as outlined in paragraph A. Figure 4.2.3.1-24 is then used as a guide to determine the base-drag variation with Mach number through the transonic speed range. The chart is based upon the data of references 4 and 9 through 12.

Step 4. The drag-divergence Mach number M_D is obtained from figure 4.2.3.1-25 as a function of body fineness ratio (reference 13). The drag-divergence Mach number is that Mach number at which $\partial C_D / \partial M = 0.10$, and it defines the break in the drag coefficient versus Mach number curve.

Step 5. The wave-drag coefficient C_{D_w} (for parabolic bodies of revolution) is obtained from figure 4.2.3.1-26 as a function of body fineness ratio for Mach numbers between 1.0 and 1.2 (reference 13). Unfortunately, data on other body shapes are extremely limited, and the construction of general charts is not possible at this time. However, for body profiles not too different from parabolic, figure 4.2.3.1-26 can be used as an approximation.

Step 6. The total zero-lift drag is constructed by combining the information of the above steps as illustrated in sketch (a).

$$C_{D_0} = C_{D_f} + C_{D_p} + C_{D_b} + C_{D_w} \qquad\qquad 4.2.3.1\text{-e}$$

SKETCH (a)

Sample Problem
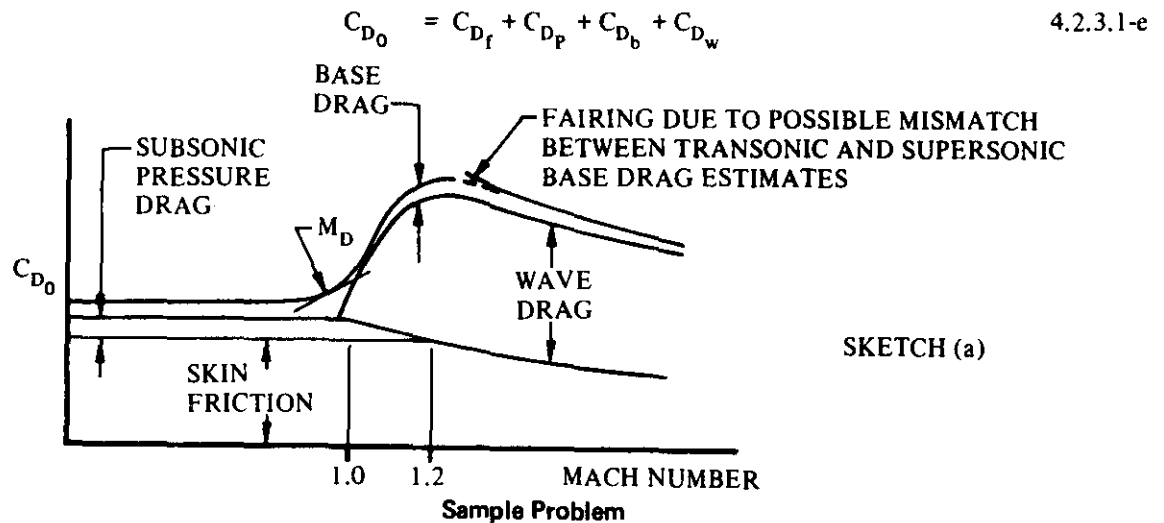
Given: The parabolic-arc body of revolution with a cutoff afterbody (reference 54).

ℓ_B = 61.45 in.   d = 6.0 in. ℓ_B/d = 10.24 S_B = 28.2 sq in.

S_S/S_B = 30.5 d_b/d = 0.50

$R_{\ell_{M=0.6}}$ = 1.997 x 10^7 (based on ℓ_B)

Polished metal surface; assume k = 0.08 x 10^{-3} in.

Compute:

The final calculations are presented in table form on page 4.2.3.1-7. Many of the quantities listed below appear as columns in the table.

Skin-friction drag coefficient C_{D_f}

$\ell/k = 61.45/(0.08 \times 10^{-3}) = 7.68 \times 10^5$; cutoff $R_{\ell_{M=0.6}} \simeq 6.2 \times 10^7$ (figure 4.1.5.1-27)

Since cutoff $R_\ell >$ given R_ℓ, read C_f at given R_ℓ.

$C_f = 0.0026$ (figure 4.1.5.1-26 @ M = 0.6)

$C_{D_f} = C_f \dfrac{S_S}{S_B}$ (equation 4.2.3.1-c)

$= 0.0026 \,(30.5) = 0.0793$

Pressure-drag coefficient C_{D_P}

$$C_{D_P} = (C_f)_{M=0.6} \left[\frac{60}{(\ell_B/d)^3} + 0.0025 \left(\frac{\ell_B}{d}\right) \right] \frac{S_S}{S_B} \quad \text{(equation 4.2.3.1-d)}$$

$$= 0.0026 \left[\frac{60}{(10.24)^3} + 0.0025\,(10.24) \right] 30.5$$

$$= 0.00642$$

This value of C_{D_P} is taken to be constant for $0 < M < 1.0$, then reduced linearly to zero at M = 1.2 (see column ④ of calculation table, page 4.2.3.1-7).

Base-drag coefficient C_{D_b}

$$\left(C_{D_b}\right)_{M=0.8} = 0.029 \left(\frac{d_b}{d}\right)^3 \Big/ \sqrt{\left(C_{D_f}\right)_b} \quad \text{(equation 4.2.3.1-b)}$$

$$\left(C_{D_f}\right)_b = (C_f)_{M=0.6} \left[1 + \frac{60}{(\ell_B/d)^3} + 0.0025\left(\frac{\ell_B}{d}\right) \right] \frac{S_S}{S_B} \quad \text{(first term, eq. 4.2.3.1-a)}$$

$$= (C_f)_{M=0.6} \frac{S_S}{S_B} + C_{D_P}$$

$$= (0.0026)(30.5) + 0.00642 = 0.0857$$

$$C_{D_b} = (0.029)(0.5)^3 \big/ \sqrt{0.0857} = 0.0124$$

$$\left[\frac{C_{D_b}}{\left(\frac{d_b}{d}\right)^2} \right] = \frac{0.0124}{(0.5)^2} = 0.0496$$

With this value and by using the curves of figure 4.2.3.1-24 as guide lines, obtain values of $\dfrac{C_{D_b}}{(d_b/d)^2}$ for $0.8 < M < 1.2$. Then $C_{D_b} = \left[\dfrac{C_{D_b}}{(d_b/d)^2}\right] (d_b/d)^2$ (See columns ⑤ and ⑥ of calculation table, page 4.2.3.1-7.)

Drag-Divergence Mach number M_D

$$M_D = 0.982 \text{ (figure 4.2.3.1-25)}$$

Wave-drag coefficient C_{D_w}

The wave-drag coefficient as a $f(M)$ is obtained from figure 4.2.3.1-26) (See column ⑦ of calculation table, page 4.2.3.1-7.)

Solution:

$$C_{D_0} = C_{D_f} + C_{D_p} + C_{D_b} + C_{D_w} \qquad \text{(equation 4.2.3.1-e)}$$

① ② ③ ④ ⑤ ⑥ ⑦ ⑧

M	c_f	C_{D_f} eq. 4.2.3.1-c ② S_S/S_B	C_{D_p}	$\dfrac{C_{D_b}}{(d_b/d)^2}$ fig. 4.2.3.1-24	C_{D_b} ⑤ $(d_b/d)^2$	C_{D_w} fig. 4.2.3.1-26	C_{D_0} eq. 4.2.3.1-e ③+④+⑥+⑦
0.8	0.0026	0.0793	0.00642	0.0496	0.0124	–	0.0981
0.9			0.00642	0.06	0.0150	–	0.1007
0.95			0.00642	0.075	0.0188	–	0.1045
1.00			0.00642	0.115	0.0288	0.0395	0.1540
1.025			0.00562	0.088	0.0220	0.0580	0.1649
1.05			0.00480	0.065	0.0162	0.0650	0.1653
1.10			0.00320	0.038	0.0095	0.0730	0.1650
1.20			0	0.035	0.0088	0.0770	0.1651

The sample problem results are plotted in sketch (b) along with test values from reference 54.

MACH NUMBER

SKETCH (b)
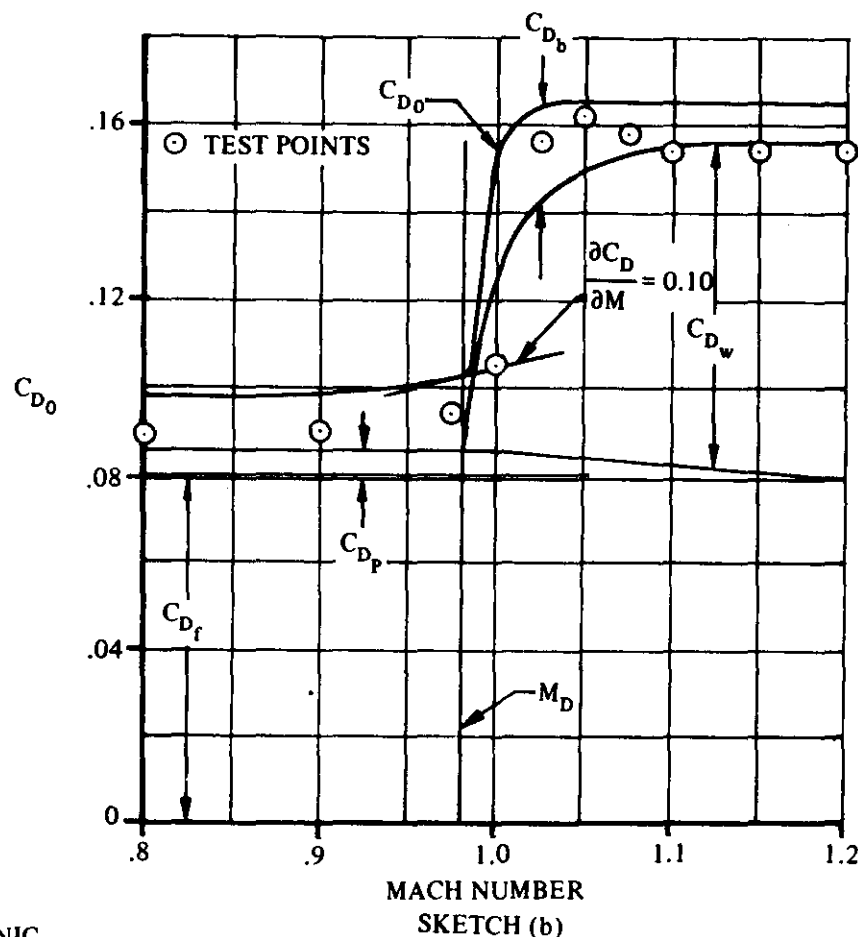
C. SUPERSONIC

The characteristics of compressible skin-friction drag for bodies are similar to those for wings (see paragraph C of Section 4.1.5.1). The skin-friction coefficient decreases with Mach number at constant Reynolds number, and is a function of the ratio of the wall temperature to the free-stream temperature. For the Datcom, zero heat-transfer conditions are assumed; i.e., stabilized flight conditions are assumed. The friction drag for transient flight lies between the incompressible value and the zero heat-transfer value. Another important consideration for estimating the skin-friction drag at supersonic speeds is the Reynolds-number variation throughout the flight regime. The design chart used in the Datcom method is that of Section 4.1.5.1, which presents the turbulent skin-friction coefficient on an insulated flat plate as a function of Mach number and Reynolds number.

Many theoretical solutions are available for estimating the wave drag of the forebody and afterbody. Reference 14 contains an excellent summary of various theories compared to test data. Ten theories are discussed in this reference. It is seen that second-order shock-expansion theory gives the best over-all agreement with data. Many of the theories are seen to give gross errors over certain ranges of the similarity parameters.

Two methods of estimating the forebody and afterbody wave drag are presented in detail in this section. The first is developed in reference 15 and is based on slender-body theory. The second method is based on similarity parameters and is taken from reference 14. For both methods the wave drag is separated into the

lorebody drag, the isolated afterbody drag (afterbody preceded by an infinite cylinder), and the interference drag of the forebody and center (cylindrical) section on the afterbody. Charts are presented for forebody and afterbody drag coefficients of straight-element profiles (cones) and parabolic profiles, and for predicting interference-drag coefficients for conical profiles, pointed parabolic profiles, ducted conical profiles, and truncated afterbodies behind pointed parabolic forebodies. Comprehensive charts based on test data giving the effects of nose bluntness are also presented for the first method.

The first method is applicable to both open-nosed and closed-nosed bodies of revolution. The design charts of the second method for predicting the wave-drag coefficient of the nose are restricted to closed-nosed bodies of revolution. Therefore, the second method is restricted accordingly.

A sizable quantity of data on supersonic base drag exists. Charts derived from test data and theory are presented for a wide range of geometric parameters. For the higher supersonic Mach numbers, theory has been used, and at the lower Mach numbers, empirical results have been used. It should be pointed out that the estimation of the afterbody drag of a body cannot necessarily be accomplished independent of the base. The lambda shock which exists near the end of the body separates the boundary layer over the rear portion of the boattail and thus changes both the base pressure and the pressure loading of the boattail. These effects are included in the base-drag charts presented but are not included in the afterbody charts.

DATCOM METHODS

Method 1.   Slender-Body Theory

The zero-lift drag coefficient of open-nosed or closed-nosed bodies of revolution, based on the maximum frontal area, is given by

$$C_{D_0} = C_f \frac{S_S}{S_B} + C_{D_{N_2}} + C_{D_A} + C_{D_{A(NC)}} + C_{D_{N_1}} + C_{D_b} \qquad 4.2.3.1\text{-}f$$

where

C_f is the turbulent flat-plate skin-friction coefficient, including roughness effects, as a function of Mach number and the Reynolds number based on the reference length ℓ. This value is obtained from figure 4.1.5.1-26 as discussed in paragraph A of Section 4.1.5.1. The reference length ℓ is the total length of the body ℓ_B.

$\dfrac{S_S}{S_B}$ is the ratio of body wetted area to maximum body frontal area, determined as outlined in paragraph A of this section.

$C_{D_{N_2}}$ and C_{D_A} are the wave-drag coefficients (reference 15) based on maximum frontal area of the nose and afterbody, respectively. Figure 4.2.3.1-27 is for parabolic profile shapes of circular cross section. Figure 4.2.3.1-28 is for conical profile shapes of circular cross section. A drag value obtained from these charts is the drag acting on the oblique surface and does not include the forces acting on the front or rear faces. The external drag of open-nosed bodies can thus be determined.

The wave-drag coefficients of the nose and afterbody of parabolic and conical profile shapes with noncircular cross sections may be approximated by using a forebody or afterbody of circular cross section and of the same area distribution (equivalent body of revolution). In this case values of a and d to be used in figures 4.2.3.1-27 and 4.2.3.1-28 are the equivalent diameters defined as $\sqrt{\dfrac{\text{cross-sectional area}}{0.7854}}$.

A more exact estimation of $C_{D_{N_2}}$ and C_{D_A} may be made for parabolic and conical profile shapes with elliptic cross sections by using figure 4.2.3.1-29. This figure presents the decrease in wave-drag coefficient, based on maximum frontal area, from the value for the equivalent body of circular cross section to that for a body of elliptic cross section. The wave-drag coefficient of the equivalent body of circular cross section is first obtained from either figure 4.2.3.1-27 or figure 4.2.3.1-28 by using the equivalent diameters. This value is then reduced by the appropriate value of $\Delta C_{D_{N_2}}$ or ΔC_{D_A} obtained from figure 4.2.3.1-29.

$C_{D_{N_1}}$ is the wave-drag coefficient of spherically blunted noses. The extended fineness ratio of the nose is first determined from figures 4.2.3.1-30 and 4.2.3.1-31 for parabolic and conical noses, respectively. This value is then used to determine the wave drag of the spherical nose segment. Figures 4.2.3.1-32a through 4.2.3.1-32f are for combinations of spherical and parabolic noses. Figures 4.2.3.1-38a through 4.2.3.1-38f are for combinations of spherical and conical noses. These latter charts are based on experimental data of references 17 through 27. When interpolation is necessary, several values should be plotted to provide the correct nonlinear variation. Figures 4.2.3.1-30, -31, -32, and -38 are for noses of circular cross section. For noses with noncircular cross sections $C_{D_{N_1}}$ may be approximated by

using a nose of circular cross section and of the same area distribution. In this case the values of the equivalent diameters and the fineness ratios based on the equivalent diameters are used in the design charts.

$C_{D_{A\,(NC)}}$ is the interference-drag coefficient acting on the afterbody due to the centerbody (cylindrical section) and the nose. This coefficient is obtained from figure 4.2.3.1-44 for parabolic profiles, from figure 4.2.3.1-46 for conical profiles, and from figure 4.2.3.1-48 for ducted conical profiles (reference 15). For bodies of noncircular cross section the interference drag coefficient may be approximated by using a body of circular cross section and of the same area distribution. In this case the equivalent diameters are used in the design charts.

C_{D_b} is the base-drag coefficient given by

$$C_{D_b} = -C_{p_b} \left(\frac{d_b}{d}\right)^2 \qquad\qquad 4.2.3.1\text{-g}$$

where

C_{p_b} is the base-pressure coefficient from figures 4.2.3.1-50 and 4.2.3.1-55 for ogival and conical boattails of circular cross section, respectively. (Although figure 4.2.3.1-50 is derived for ogive boattails, references 28 through 31, it can be applied to parabolic afterbodies if the ratio d_b/d is not small. Actually, if the ratio is small, the magnitude of the base drag would be such as to minimize the importance of large percentage errors.)

$\dfrac{d_b}{d}$ is the ratio of the base diameter to the maximum body diameter.

For bodies of noncircular cross section the equivalent diameters should be used in the design charts and in equation 4.2.3.1-g.

For bodies of revolution with no boattail the base-drag coefficient is read directly from figure 4.2.3.1-60.

Method 2. Similarity Parameters

An alternate method based on the correlation of test data by using similarity parameters is presented below. The zero-lift drag coefficient of closed-nosed bodies of revolution, based on the maximum frontal area, is given by

$$C_{D_0} = C_f \frac{S_S}{S_B} + C_{D_{N_2}} + C_{D_A} + C_{D_A (NC)} + C_{D_{N_1}} + C_{D_b} \qquad 4.2.3.1\text{-h}$$

where C_f, S_S/S_B, $C_{D_A (NC)}$, $C_{D_{N_1}}$, and C_{D_b} are determined as in method 1, and

$C_{D_{N_2}}$ is the zero-lift wave-drag coefficient of the nose obtained from figure 4.2.3.1-61 or 4.2.3.1-62, which are for ogival- and conical-profile noses of circular cross section, respectively. The K_N factor used in figure 4.2.3.1-61 is given in figure 4.2.3.1-63. The chart for cones is based on references 32 through 37 and the chart for ogive noses is based on references 18, 35, and 38 through 40. Slender-body theory and Newtonian theory have also been used. These charts are discussed and substantiated in reference 14.

C_{D_A} is the zero-lift wave-drag coefficient of the afterbody from figure 4.2.3.1-64 or 4.2.3.1-65, which are for ogival and conical afterbodies with circular cross sections, respectively. These charts are based on Van Dyke's second-order theory and the data of reference 41 and are discussed and substantiated in reference 14.

For bodies with noncircular cross sections the component contributions should be based on the equivalent body of circular cross section.

It should be noted that the design charts presented for $C_{D_{N_2}}$ in method 2 are restricted to closed-nosed bodies of revolution.

Sample Problems

1. Method 1. Slender-Body Theory

Given: A cone-cylinder body with the following characteristics (reference 41):

$\ell_B = 129.1$ in.	$\ell_1 = \ell_N = 53.8$ in.
$\ell_2 = \ell_C = 45.0$ in.	$\ell_3 = \ell_A = 30.3$ in.
$d = 7.50$ in.	$d_b = 3.28$ in.
$S_S/S_B = 50.0$	$\theta_N = 4^\circ$
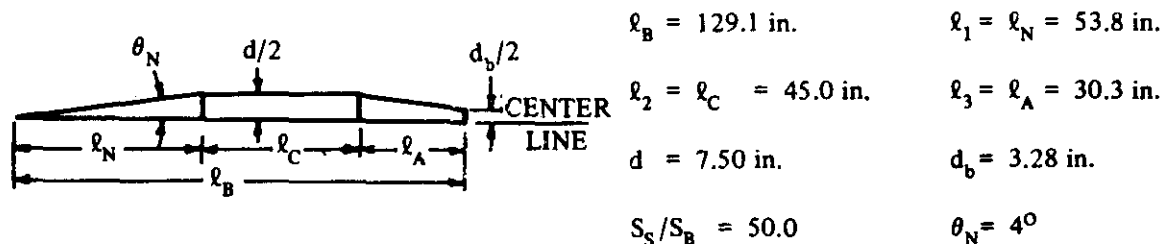
Additional characteristics:

M = 1.4; β = 0.980 R_ℓ = 7.6 x 10^7 (based on ℓ_B)

Polished metal surface; assume k = 0.08 x 10^{-3} in.

Compute:

$$\ell/k = \frac{129.1}{0.08 \times 10^{-3}} = 1.61 \times 10^6 ; \text{cutoff } R_\ell = 2 \times 10^8 \qquad \text{(figure 4.1.5.1-27)}$$

Since cutoff $R_\ell > 7.6 \times 10^7$, read C_f at $R_\ell = 7.6 \times 10^7$

$C_f = 0.00192$ (figure 4.1.5.1-26)

Forebody

$$\left(\frac{a_1}{d_1}\right)^2 = 0; \quad \frac{2\ell_1}{\beta d_1} = \frac{2(53.8)}{(0.98)(7.50)} = 14.6$$

$$\left(\frac{2\ell_1}{d_1}\right)^2 = \left[\frac{2(53.8)}{7.50}\right]^2 = 205.8$$

$$C_{D_{N_2}} \left(\frac{2\ell_1}{d_1}\right)^2 = 5.5 \qquad \text{(figure 4.2.3.1-28, extrapolated)}$$

$$C_{D_{N_2}} = (5.5)/(205.8) = 0.0267$$

$$C_{D_{N_1}} = 0 \qquad \text{(no bluntness)}$$

Afterbody

$$\left(\frac{a_3}{d_3}\right)^2 = \left(\frac{3.28}{7.50}\right)^2 = 0.191; \quad \frac{2\ell_3}{\beta d_3} = \frac{2(30.3)}{(0.98)(7.50)} = 8.24$$

$$\left(\frac{2\ell_3}{d_3}\right)^2 = \left[\frac{2(30.3)}{7.50}\right]^2 = 65.29$$

$$C_{D_A} \left(\frac{2\ell_3}{d_3}\right)^2 = 2.10 \qquad \text{(figure 4.2.3.1-28)}$$

$$C_{D_A} = (2.10)/(65.29) = 0.0322$$

$$\ell_C/\ell_A = \ell_2/\ell_3 = (45)/(30.3) = 1.48$$

$$\ell_N/\ell_A = \ell_1/\ell_3 = (53.8)/(30.3) = 1.78$$

$$C_{D_{A(NC)}} \left(\frac{2\ell_3}{d_3}\right)^2 = 0.27 \quad \text{(figures 4.2.3.1-46b and -46c, interpolated)}$$

$$C_{D_{A(NC)}} = (0.27)/(65.29) = 0.0041$$

$$d_b/d = (3.28)/(7.50) = 0.437; \quad f_A = \ell_A/d = 30.3/7.50 = 4.04$$

$$C_{P_b} = -0.055 \quad \text{(figure 4.2.3.1-55c)}$$

$$C_{D_b} = -C_{P_b}\left(\frac{d_b}{d}\right)^2 \quad \text{(equation 4.2.3.1-g)}$$

$$= -(-0.055)(0.437)^2 = 0.0105$$

Solution:

$$C_{D_0} = C_f \frac{S_S}{S_B} + C_{D_{N_2}} + C_{D_A} + C_{D_{A(NC)}} + C_{D_{N_1}} + C_{D_b} \quad \text{(equation 4.2.3.1-f)}$$

$$= (0.00192)(50.0) + (0.0267) + (0.0322) + (0.0041) + 0 + 0.0105$$

$$= 0.1695 \quad \text{(based on } S_B\text{)}$$

This corresponds to an experimental value of 0.153 from reference 41.

2. Method 1. Slender-Body Theory

Given: The same cone-cylinder body as sample problem 1, except that the nose is spherically blunted.
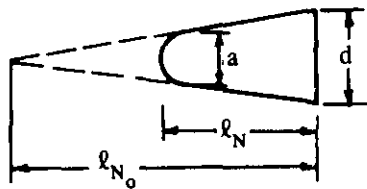
$$\frac{a}{d} = \frac{d_s}{d_o} = 0.60 \qquad \ell_{N_o} = 53.8 \text{ in.}$$

$$d = d_o = 7.50 \text{ in.} \qquad \ell_N = 24.0 \text{ in.}$$

$$\frac{S_S}{S_B} = 45.8 \qquad \ell_B = 99.3 \text{ in.}$$

$$M = 1.40; \quad \beta = 0.98 \qquad R_\ell = 5.85 \times 10^7 \quad \text{(based on } \ell_B\text{)}$$

Polished metal surface; assume $k = 0.08 \times 10^{-3}$ in.

$$\left.\begin{array}{l} C_{D_A} = 0.0322 \\[2ex] C_{D_{A(NC)}} = 0.0041 \\[2ex] C_{D_b} = 0.0105 \end{array}\right\}$$ Afterbody drag components from sample problem 1

Compute:

$$\ell/k = \frac{99.3}{0.08 \times 10^{-3}} = 1.24 \times 10^6; \text{ cutoff } R_\ell = 1.60 \times 10^8 \quad \text{(figure 4.1.5.1-27)}$$

Since cutoff $R_\ell > 5.85 \times 10^7$, read C_f at $R_\ell = 5.85 \times 10^7$

$C_f = 0.0020$ (figure 4.1.5.1-26)

Forebody .

$$\left(\frac{a}{d}\right)^2 = 0.36; \frac{2\ell_N}{\beta d} = \frac{2(24)}{(0.98)(7.50)} = 6.53$$

$$\left(\frac{2\ell_N}{d}\right)^2 = \left[\frac{2(24)}{7.50}\right]^2 = 40.96$$

$$C_{D_{N_2}}\left(\frac{2\ell_N}{d}\right)^2 = 1.16 \quad \text{(figure 4.2.3.1-28)}$$

$$C_{D_{N_2}} = (1.16)/(40.96) = 0.0283$$

$$f_{N_o} = \ell_{N_o}/d_o = (53.8)/(7.50) = 7.17$$

$$C_{D_{N_1}} = 0.200 \quad \text{(figures 4.2.3.1-38a, -38b, -38c; interpolated)}$$

Solution:

$$C_{D_0} = C_f \frac{S_S}{S_B} + C_{D_{N_2}} + C_{D_A} + C_{D_{A(NC)}} + C_{D_{N_1}} + C_{D_b} \quad \text{(equation 4.2.3.1-f)}$$

$$= (0.0020)(45.8) + 0.0283 + 0.0322 + 0.0041 + 0.200 + 0.0105$$

$$= 0.3667 \quad \text{(based on } S_B\text{)}$$

3. Method 2. Similarity Parameters

Given: The same cone-cylinder body as sample problem 1.

$f_N = 7.17$ $\qquad f_A = 4.04$ $\qquad d_b/d = 0.437$ $\qquad \theta_N = 4^\circ$ $\qquad M = 1.4; \beta = 0.98$

$R_\ell = 7.6 \times 10^7$ (based on ℓ_B)

Drag components from sample problem 1:

$$C_f \frac{S_S}{S_B} = 0.0960 \qquad C_{D_{A(NC)}} = 0.0041 \qquad C_{D_{N_1}} = 0 \qquad C_{D_b} = 0.0105$$

Compute:

Forebody

$$\beta/f_N = (0.98)/(7.17) = 0.137$$

$$f_N{}^2 + \frac{1}{4} = (7.17)^2 + \frac{1}{4} = 51.66$$

$$C_{D_{N_2}}\left[(f_N)^2 + \frac{1}{4}\right] = 1.45 \quad \text{(figure 4.2.3.1-62)}$$

$$C_{D_{N_2}} = (1.45)/(51.66) = 0.0280$$

Afterbody

$$f_A{}^2 = (4.04)^2 = 16.32; \quad \beta/f_A = (0.98)/(4.04) = 0.243$$

$$C_{D_A} (f_A)^2 = 0.53 \quad \text{(figure 4.2.3.1-65)}$$

$$C_{D_A} = (0.53)/(16.32) = 0.0325$$

Solution:

$$C_{D_0} = C_f \frac{S_S}{S_B} + C_{D_{N_2}} + C_{D_A} + C_{D_{A(NC)}} + C_{D_{N_1}} + C_{D_b} \quad \text{(equation 4.2.3.1-h)}$$

$$= 0.0960 + 0.0280 + 0.0325 + 0.0041 + 0 + 0.0105$$

$$= 0.1711 \quad \text{(based on } S_B\text{)}$$

This corresponds to a calculated value of 0.1695 obtained using method 1, and to an experimental value of 0.153 from reference 41.

D. HYPERSONIC

At hypersonic speeds the zero-lift drag of a body is caused primarily by the pressure and friction drag of the nose. The base drag decreases and becomes insignificant at the higher Mach numbers (see figures 4.2.3.1-50, 4.2.3.1-55, and 4.2.3.1-60).

High-speed turbulent skin-friction values are not well defined at the present time. A theory that has had wide acceptance is that of reference 42. The limited experimental data (e.g., reference 43) substantiate this theory reasonably well.

Figures 4.2.3.1-66 and 4.2.3.1-67 are based upon Newtonian impact values at $M \to \infty$ and should give reasonable results for bodies at these speeds. The charts of reference 44 give the drag of bodies of revolution composed of cone frustums and spherical noses based on Newtonian flow. A similar set of charts is contained in reference 45. A more comprehensive set of charts based on Newtonian flow is available in reference 46 for arbitrary bodies of revolution.

DATCOM METHODS

Method 1.   Hypersonic Similarity

The method described as method 2 of paragraph C can be used at hypersonic Mach numbers, but with the body skin-friction drag coefficient calculated as outlined in method 2 that follows (see equation 4.2.3.1-j).

Method 2.   Newtonian Flow Plus Skin Friction

The zero-lift drag (based on the maximum frontal area) of bodies composed of cone-cylinder frustums and pointed or spherical noses is estimated by adding the pressure-drag coefficient of each segment to the body skin-friction drag coefficient.

$$C_{D_0} = C_{D_f} + \sum_{n=1}^{m} C_{D_{P_n}} \left(\frac{d_n}{d_{max}} \right)^2 \qquad \qquad 4.2.3.1\text{-}i$$

The procedure to be followed in evaluating equation 4.2.3.1-i is:

Step 1   Divide the body into m segments, the first segment being the pointed conical or spherical nose and each succeeding segment a cylinder or circular cone frustum. The pressure-drag coefficient for a spherical nose is obtained from figure 4.2.3.1-66. The pressure-drag coefficient of a pointed conical nose, cylinder, or circular cone frustum is obtained from figure 4.2.3.1-67. (Note that the cylinder is considered as a cone frustum with $\theta = 0$ and $a/d = 1.0$, and that the pressure-drag coefficient is zero by Newtonian impact theory.) Figures 4.2.3.1-66 and 4.2.3.1-67 are from reference 44, and are based on Newtonian impact theory. The pressure-drag coefficients from figures 4.2.3.1-66 and 4.2.3.1-67 are based on the base area of the specific segment. The ratio $(d_n/d_{max})^2$ refers the pressure-drag coefficients to the maximum body frontal area.

Step 2   Obtain the body skin-friction drag coefficient by

$$C_{D_f} = 1.02 \, C_{f_{inc}} \frac{C_{f_c}}{C_f} \frac{S_S}{S_B} \qquad \qquad 4.2.3.1\text{-}j$$

where

$C_{f_{inc}}$ is the incompressible (M = 0), turbulent, flat-plate skin-friction coefficient, including roughness effects, as a function of Reynolds number based on the total length of the body ℓ_B. This value is obtained from figure 4.1.5.1-26 as discussed in paragraph A of Section 4.1.5.1.

$\dfrac{C_{f_c}}{C_f}$ is the ratio of compressible to incompressible skin-friction coefficient obtained from figure 4.2.3.1-68.

4.2.3.1-16

$\dfrac{S_S}{S_B}$ is the ratio of the body wetted area to maximum body frontal area, determined as outlined in paragraph A of this section.

If method 2 is applied at Mach numbers low enough so that the base drag is significant, the base drag should be added to the results obtained using equation 4.2.3.1-j. Unfortunately, the only base-drag coefficient results available which are compatible with the Newtonian-theory results (restricted to bodies with forward facing slopes or cylinders, in which case the Newtonian results are equal to zero) are those for cylindrical afterbodies. The pressure-drag coefficient for cylindrical afterbodies is presented in figure 4.2.3.1-60 for $M \leq 6$.

Sample Problem

Method 2. Newtonian Flow Plus Skin Friction

Given: A body with the following configuration (reference 54):
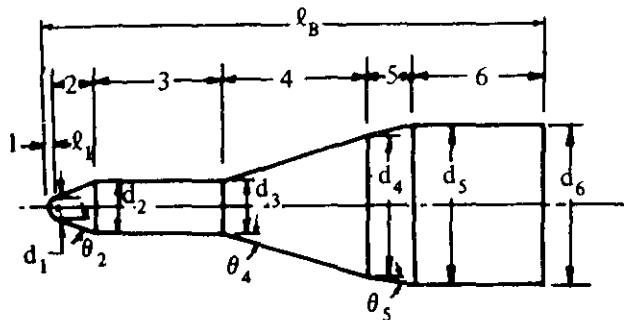
Segment 1: Spherical nose

ℓ_1 = 0.29 in. $d_1 = d_s$ = 0.58 in.

Segment 2: Cone frustum

θ_2 = 20° $a_2 = d_1$ = 0.58 in.

$\cdot d_2$ = 1.50 in.

Segment 3: Cylinder

θ_3 = 0 $a_3 = d_2$ = 1.50 in.

d_3 = 1.50 in.

Segment 4: Cone frustum

θ_4 = 16.5° $a_4 = d_3$ = 1.50 in.

d_4 = 4.10 in.

Segment 5: Cone frustum

θ_5 = 10.4° $a_5 = d_4$ = 4.10 in.

d_5 = 4.50 in.

Segment 6: Cylinder

θ_6 = 0 $a_6 = d_5$ = 4.50 in.

d_6 = 4.50 in.

Additional characteristics:

S_S/S_B = 8.14 ℓ_B = 14.4 in.   M = 4.65 R_ℓ = 7.63 x 10^6 (based on ℓ_B)

Polished metal surface; assume k = 0.08 x 10^{-3} in.

Compute:

Determine C_{D_p} of the body segments

Segment 1

$$\ell_1/(d_1/2) = (0.29)/(0.58/2) = 1.0$$

$$C_{D_{P_1}} = 1.0 \quad \text{(figure 4.2.3.1-66)}$$

Segment 2

$$a_2/d_2 = (0.58)/(1.50) = 0.387$$

$$C_{D_{P_2}} = 0.200 \quad \text{(figure 4.2.3.1-67)}$$

Segment 3

$$a_3/d_3 = (1.50)/(1.50) = 1.0$$

$$C_{D_{P_3}} = 0 \quad \text{(figure 4.2.3.1-67)}$$

Segment 4

$$a_4/d_4 = (1.50)/(4.10) = 0.366$$

$$C_{D_{P_4}} = 0.138 \quad \text{(figure 4.2.3.1-67)}$$

Segment 5

$$a_5/d_5 = (4.10)/(4.50) = 0.911$$

$$C_{D_{P_5}} = 0.010 \quad \text{(figure 4.2.3.1-67)}$$

Segment 6

$$a_6/d_6 = (4.50)/(4.50) = 1.0$$

$$C_{D_{P_6}} = 0 \quad \text{(figure 4.2.3.1-67)}$$

Determine the skin-friction drag coefficient C_{D_f}

$$\ell/k = 14.4/(0.08 \times 10^{-3}) = 0.18 \times 10^6; \quad \text{cutoff } R_\ell \simeq 7.5 \times 10^7 \quad \text{(figure 4.1.5.1-27 at M = 0)}$$

Since cutoff $R_\ell > 7.63 \times 10^6$, read C_f at $R_\ell = 7.63 \times 10^6$

$C_f = 0.00314$ (figure 4.1.5.1-26 at $M = 0$)

$C_{f_c}/C_f = 0.44$ (figure 4.2.3.1-68)

$$C_{D_f} = 1.02\, C_{f_{inc}} \frac{C_{f_c}}{C_f} \frac{S_S}{S_B} \quad \text{(equation 4.2.3.1-j)}$$

$$= (1.02)(0.00314)(0.44)(8.14) = 0.0115$$

Solution:

$$C_{D_0} = C_{D_f} + \sum_{s=n}^{m} C_{D_{P_n}} \left(\frac{d_n}{d_{max}}\right)^2 \quad \text{(equation 4.2.3.1-i)}$$

$$= C_{D_f} + C_{D_{P_1}}\left(\frac{d_1}{d_6}\right)^2 + C_{D_{P_2}}\left(\frac{d_2}{d_6}\right)^2 + C_{D_{P_3}}\left(\frac{d_3}{d_6}\right)^2 + C_{D_{P_4}}\left(\frac{d_4}{d_6}\right)^2 + C_{D_{P_5}}\left(\frac{d_5}{d_6}\right)^2 + C_{D_{P_6}}\left(\frac{d_6}{d_6}\right)^2$$

$$= 0.0115 + (1.0)\left(\frac{0.58}{4.50}\right)^2 + (0.200)\left(\frac{1.50}{4.50}\right)^2 + 0 + (0.138)\left(\frac{4.10}{4.50}\right)^2 + (0.010)\left(\frac{4.50}{4.50}\right)^2 + 0$$

$$= 0.175 \quad \text{(based on } S_B)$$

The Mach number of this example is low enough so that the base drag is significant. The base drag coefficient is obtained from figure 4.2.3.1-60 as

$$C_{D_b} = 0.055 \quad \text{(based on } S_B)$$

So, the final result is

$$C_{D_0} = C_{D_f} + C_{D_p} + C_{D_b} = 2.30 \quad \text{(based on } S_B)$$

This result compares favorably with the test value shown in reference 54.

E. RAREFIED GAS

In the discussions of aerodynamic properties presented previously, it has been assumed that the air behaves as a continuous fluid; whereas, at the very low densities encountered at extreme altitudes the actual molecular structure of the air will become important.

By accepted definition (reference 47) a rarefied gas flow is a flow in which the length of the molecular mean free path is comparable to some significant dimension of the flow field. The ratio of these two lengths is called the Knudsen number. If the characteristic length is chosen to be the body dimension used in the definition of Reynolds number, then the Knudsen number can be shown to be given approximately by

$$Kn \approx M/R_\varrho$$

By the definition given above, the flow can be considered as rarefied if $Kn > 1$. If the flow is very rarefied, say $Kn > 3$ (reference 47) then individual gas molecules strike the surface of the body without interacting with surrounding gas molecules; this flow regime is called free-molecule flow. Between the regime of free-molecule flow and that of continuous gas dynamics (where $Kn \approx 10^{-4}$ or 10^{-5}) lies a large transition region that is not yet clearly defined as to its characteristics.

It is apparent that, if $Kn = 3$ defines the limit for the free-molecule flow regime, the aerodynamics of bodies in this type of flow is of interest only in its application to satellite studies. A Knudsen number of three corresponds to an altitude of roughly 100 miles, if the reference length used is only one foot, with increasing altitude for larger reference dimensions. It seems unlikely that anything resembling a full-size aircraft will attempt to utilize the tenuous atmosphere at these extreme altitudes for a useful purpose without flying at essentially orbital speeds. It is not possible to make any clearcut statements regarding the transition regime. The region likely to be of most interest in aircraft and missile work is that where the flow is just slightly rarefied, that is, where the continuous flow equations are just beginning to become questionable. This is called the slip-flow regime. In the slip-flow regime either the Mach number is large or the Reynolds number is small, by continuum standards. Analysis of the slip-flow regime is difficult, because its characteristics are likely to be masked by compressibility and viscosity effects.

An excellent discussion is presented by Hayes and Probstein (reference 48) concerning the validity of continuum theory as applied to rarefied gas flow. It is concluded that, when properly applied, continuum gas dynamics and viscous flow theory can be useful far into the regime of what is normally considered the domain of kinetic theory.

At the other end of the spectrum, free-molecule flow theory is important for several problems dealing with satellites. Since satellites generally operate in the free-molecule flow regime, it is necessary to estimate the drag coefficient under these conditions in order to predict the perturbations and decay of the orbit, and to use satellite measurements to estimate atmospheric density.

There are many analyses in the literature on the lift and drag of bodies in free-molecule flow (references 47, 49, 50, and 51), since the problem is amenable to analytical solution. In the discussion of reference 47, expressions for the local pressure and shear forces are given in general form, so that these forces can be computed for any type of interaction of the atmospheric molecules with the body surface. At the present, very little is known of the nature of this interaction, and more research is required to establish the type of interaction that may be expected in a specific problem.

Jastrow and Pearse (reference 52) have discussed an additional drag that arises in the flight of a body through a medium containing ions and electrons, as in the ionosphere. The satellite tends to acquire a negative equilibrium electrostatic potential. As a result, atmospheric ions that would otherwise have missed the satellite are drawn into collisions with it, thus increasing the drag.

Integrated drag forces for the simple shapes of the cylinder and sphere are given in reference 47. These data are shown in figure 4.2.3.1-69 for the simplified case in which the surface temperature is equal to the ambient temperature, and for the extremes of specular and fully diffuse reflection.

REFERENCES

1. Hoerner, S.F.: Fluid-Dynamic Drag. Published by Author, 1958. (U)

2. Kurzweg, H.H.: Interrelationship Between Boundary Layer and Base Pressure. Jour. Aero. Sci., Vol. 18, No. 11, Nov. 1951. (U)

3. Morrow, J.D., and Nelson, R.L.: Large-Scale Flight Measurements of Zero-Lift Drag of 10 Wing-Body Configurations at Mach Numbers from 0.8 to 1.6. NACA RM L52D18a, 1953. (U)

4. Hart, R.G.: Effects of Stabilizing Fins and a Rear-Support Sting on the Base Pressures of a Body of Revolution in Free Flight at Mach Numbers from 0.7 to 1.3. NACA RM L52E06, 1952. (U)

5. Chapman, D.R.: An Analysis of Base Pressure at Supersonic Velocities and Comparison with Experiment. NACA TN 2137, 1950. (U)

6. Blakeslee, D.J., Johnson, R.P., and Skavdahl, H.: A General Representation of the Subsonic Lift-Drag Relation for an Arbitrary Airplane Configuration. Rand RM 1593, 1955. (U)

7. Spreiter, J.R.: Aerodynamics of Wings and Bodies at Transonic Speeds. Jour. Aero. Sci., Vol. 26, No. 8, August 1959. (U)

8. Stoney, W.E., Jr.: Collection of Zero-Lift Drag Data on Bodies of Revolution from Free-Flight Investigations. NACA TN 4201, 1958. (U)

9. Kelly, T.C.: Transonic Wind-Tunnel Investigation of the Effects of Body Indentation for Boattail and Cylindrical Afterbody Shapes on the Aerodynamic Characteristics of an Unswept-Wing-Body Combination. NACA RM L54A08, 1954. (U)

10. Morgan, F.G., Jr., and Carmel, M.M.: Transonic Wind-Tunnel Investigation of the Effects of Taper Ratio, Body Indentation, Fixed Transition, and Afterbody Shape on the Aerodynamic Characteristics of a 45° Sweptback Wing-Body Combination. NACA RM L54A15, 1954. (U)

11. Katz, E., and Stoney, W.E., Jr.: Base Pressures Measured on Several Parabolic-Arc Bodies of Revolution in Free Flight at Mach Numbers from 0.8 to 1.4 and at Large Reynolds Numbers. NACA RM L51F29, 1951. (U)

12. Peck, R.F.: Flight Measurements of Base Pressure on Bodies of Revolution With and Without Simulated Rocket Chambers. NACA RM L50I28a, 1950. (U)

13. Gollos, W.W.: Transonic and Supersonic Pressure Drag for a Family of Parabolic Type Fuselages at Zero Angle of Attack. Rand Report RM 982, 1952. (C) Title Unclassified

14. Morris, D.N.: A Summary of the Supersonic Pressure Drag of Bodies of Revolution. Jour. Aero. Sci., Vol. 28, No. 7, July 1961. (U)

15. Fraenkel, L.E.: The Theoretical Wave Drag of Some Bodies of Revolution. RAE Aero 2420, 1951. (U)

16. Fraenkel, L.E.: Supersonic Flow Past Slender Bodies of Elliptic Cross-Section. ARC R&M 2954, 1955. (U)

17. Moeckel, W.E.: Experimental Investigation of Supersonic Flow with Detached Shock Waves for Mach Numbers Between 1.8 and 2.9. NACA RM E50D05, 1950. (U)

18. Sommer, S.C., and Stark, J.A.: The Effect of Bluntness on the Drag of Spherical-Tipped Truncated Cones of Fineness Ratio 3 at Mach Numbers 1.2 to 7.4. NACA RM A52B13, 1952. (U)

19. Hart, R.E.: Flight Investigation of the Drag of Round-Nosed Bodies of Revolution at Mach Numbers from 0.6 to 1.5 Using Rocket-Propelled Test Vehicles. NACA RM L51E25, 1951. (U)

20. Anon.: The Drag Coefficient of Very High Velocity Spheres. New Mexico School of Mines, Research and Development Division, Oct. 1949. (U)

21. Chauvin, L.T.: Pressure Distribution and Pressure Drag for a Hemispherical Nose at Mach Numbers 2.05, 2.54, and 3.04. NACA RM L52K06, 1952. (U)

22. Wood, G.P., and Gooderum, P.B.: Method of Determining Initial Tangents of Contours of Flow Variables Behind a Curved, Axially Symmetric Shock Wave. NACA TN 2411, 1951. (U)

23. Winkler, E.M., and Danberg, J.E.: Heat Transfer Characteristics of a Hemispheric Cylinder at Hypersonic Mach Numbers. IAS Preprint 622, Jan. 1956. (U)

24. Stine, H.A., and Wanlass, K.: Theoretical and Experimental Investigation of Aerodynamic-Heating and Isothermal Heat-Transfer Parameters on a Hemispherical Nose with Laminar Boundary Layer at Supersonic Mach Numbers. NACA TN 3344, 1954. (U)

25. Crawford, D.H., and McCauley, W.D.: Investigation of the Laminar Aerodynamic Heat-Transfer Characteristics of a Hemisphere-Cylinder in the Langley 11-Inch Hypersonic Tunnel at a Mach Number of 6.8. NACA TN 3706, 1956. (U)

26. Korobkin, I.: Local Flow Conditions, Recovery Factors and Heat Transfer Coefficients on the Nose of a Hemispheric Cylinder at a Mach Number of 2.8. Navord 2865, May 1953. (U)

27. Ferri, A.: The Influence of Reynolds Numbers at High Mach Numbers. (Abstract) p. 623. Jour. Roy. Aero. Soc., Nov. 1943. (U)

28. Seiff, A., et al: Aerodynamic Characteristics of Bodies at Supersonic Speeds. NACA RM A51J25, 1951. (U)

29. Love, E.S.: The Base Pressure at Supersonic Speeds on Two-Dimensional Airfoils and Bodies of Revolution (With and Without Fins) Having Turbulent Boundary Layers. NACA RM L53C02, 1953. (U)

30. Cubbage, J.M., Jr.: Jet Effects on Base and Afterbody Pressures of a Cylindrical Afterbody at Transonic Speeds. NACA RM L56C21, 1956. (U)

31. Piland, R.O.: Drag Measurements on a 1/6-Scale, Finless, Sting-Mounted NACA RM-10 Missile in Flight at Mach Numbers from 1.1 to 4.04 Showing Some Reynolds Number and Heating Effects. NACA RM L54H09, 1954. (U)

32. Solomon, G.E.: Transonic Flow Past Cone Cylinders. NACA TN 3213, 1954. (U)

33. Seiff, A., and Sommer, S.C.: Experimental Investigation of the Drag of 30°, 60°, and 90° Cone Cylinders at Mach Numbers Between 1.5 and 8.2. NACA RM A52A14b, 1952. (U)

34. Drougge, G.: The Flow Around Conical Tips in the Upper Transonic Range. The Aeronautical Research Institute of Sweden Report No. 25, 1948. (U)

35. Stoney, W.E., Jr.: Transonic Drag Measurements of Eight Body-Nose Shapes. NACA RM L53K17, 1954. (U)

36. Mauersberg, J.D., Thomas, R.E., Ward, V.G., and Von Eschen, G.L.: Blockage and Interference Effects of a Cone-Cylinder Model at Mach Numbers from 0.80 to 1.30. OSU Research Foundation Report SR-4, Jan. 1955. (U)

37. Yoshihara, H.: On the Flow Over a Cone-Cylinder Body at Mach Number One. WADC TR-52-295, 1952. (U)

38. Hieser, G., Henderson, J.H., and Swihart, J.M.: Transonic Aerodynamic and Loads Characteristics of a 4-Percent-Thick Unswept-Wing-Fuselage Combination. NACA RM L54B24, 1954. (U)

39. Johnston, J.F., and Lopatoff, M.: Study by NACA Wing-Flow Method of Transonic Drag Characteristics of a Blunt-Nose Body of Revolution and Comparison with Results for a Sharp-Nose Body. NACA RM L9C11, 1949. (U)

40. Gray, J.D.: Transonic Interference Effects Upon Lift and Drag Measurements in a Slotted Test Section. AEDC-TR-54-47, 1955. (U)

41. Jack, J.R.: Theoretical Pressure Distributions and Wave Drags for Conical Boattails. NACA TN 2972, 1953. (U)

42. VanDriest, E.R.: Turbulent Boundary Layer with Variable Prandtl Numbers. NAA AL 1914, 1951. (U)

43. Sommer, S.C., and Short, B.J.: Free-Flight Measurements of Turbulent-Boundary-Layer Skin Friction in the Presence of Severe Aerodynamic Heating at Mach Numbers from 2.8 to 7.0. NACA TN 3391, 1955. (U)

44. Fisher, L.R.: Equations and Charts for Determining the Hypersonic Stability Derivatives of Combinations of Cone Frustums Computed by Newtonian Impact Theory. NACA TN D-149, 1959. (U)

45. Gray, J.D.: Drag and Stability Derivatives of Missile Components According to the Modified Newtonian Theory. AEDC-TN-60-191, 1960. (U)

46. Rainey, R.W.: Working Charts for Rapid Prediction of Force and Pressure Coefficients on Arbitrary Bodies of Revolution by Use of Newtonian Concepts. NACA TN D-176, 1959. (U)

47. Schaaf, S.A., and Chambre, P.L.: Flow of Rarefied Gases; Section H of Fundamentals of Gas Dynamics; Vol. III of High Speed Aerodynamics and Jet Propulsion: Princeton University Press, 1958. (U)

48. Hayes, W.D., and Probstein, R.F.: Hypersonic Flow Theory. Academic Press, 1959. (U)

49. Stalder, J.R., and Zurick. V.J.: Theoretical Aerodynamic Characteristics of Bodies in a Free Molecule Flow Field. NACA TN 2423, 1951. (U)

50. Ashley, H.: Applications of the Theory of Free Molecule Flow to Aeronautics. Jour. Aero. Sci., Vol. 16, No. 2, Feb. 1949. (U)

51. Schamberg, R.: A New Analytic Representation of Surface Interaction for Hyperthermal Free-Molecule Flow with Application to Neutral-Particle Drag Estimates of Satellites. The Rand Corporation RM 2313, 1959. (U)

52. Jastrow, R., and Pearse, C.A.: Atmospheric Drag on the Satellite. Jour. of Geophysical Research, Vol. 62, No. 3, Sept. 1957. (U)

53. McDevitt, J.B., and Taylor, R.A.: Force and Pressure Measurements at Transonic Speeds for Several Bodies Having Elliptical Cross Sections. NACA TN 4362, 1958. (U)

54. Lust, R.M.: Investigation of the Static Longitudinal Stability Characteristics of a Model of an Intermediate-Range Ballistic Missile at Mach Numbers Between 1.57 and 4.65. NASA TM X-289, 1960. (C) Title Unclassified.

55. Welsh, C.J., and deMoraes, C.A.: Results of Flight Tests to Determine Drag of Parabolic and Cone-Cylinder Bodies of Very Large Fineness Ratios at Supersonic Speeds. NACA RM L51E18, 1951. (U)
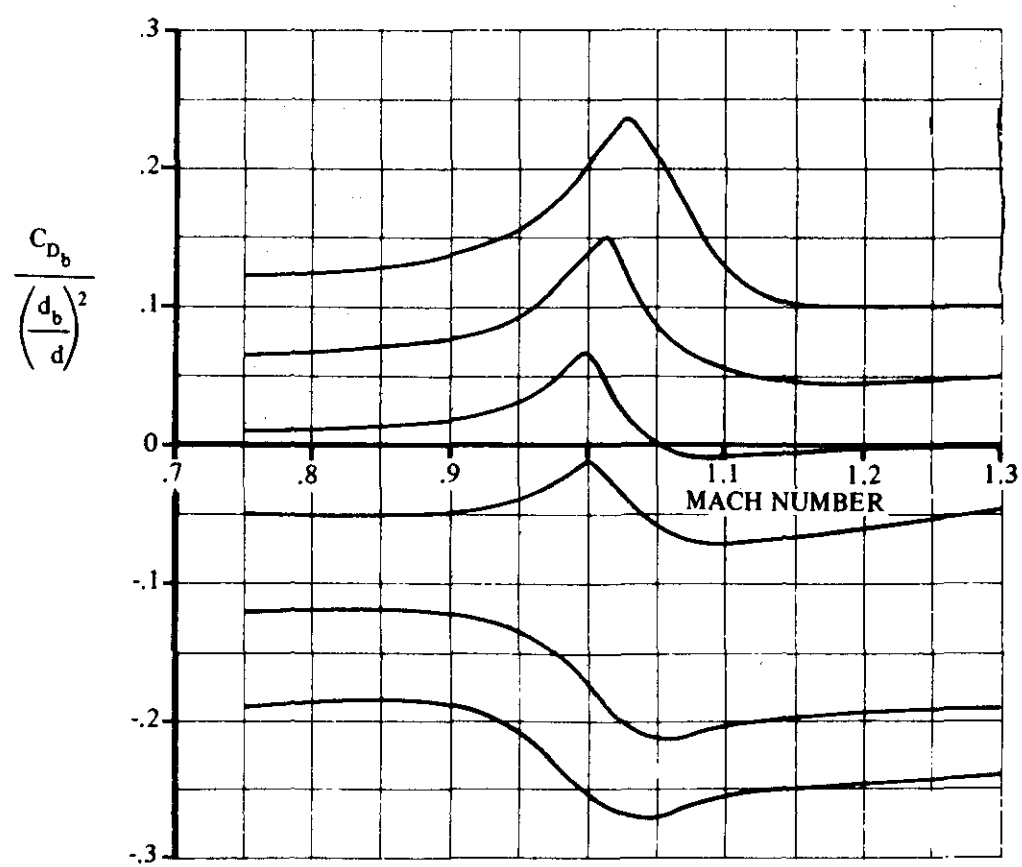
FIGURE 4.2.3.1-24 TRANSONIC FAIRING FOR BASE-PRESSURE COEFFICIENT

DRAG
DIVERGENCE
MACH
NUMBER
M_D

Chart valid for maximum diameter between
40% and 60% of body length

FINENESS RATIO, ℓ_B/d
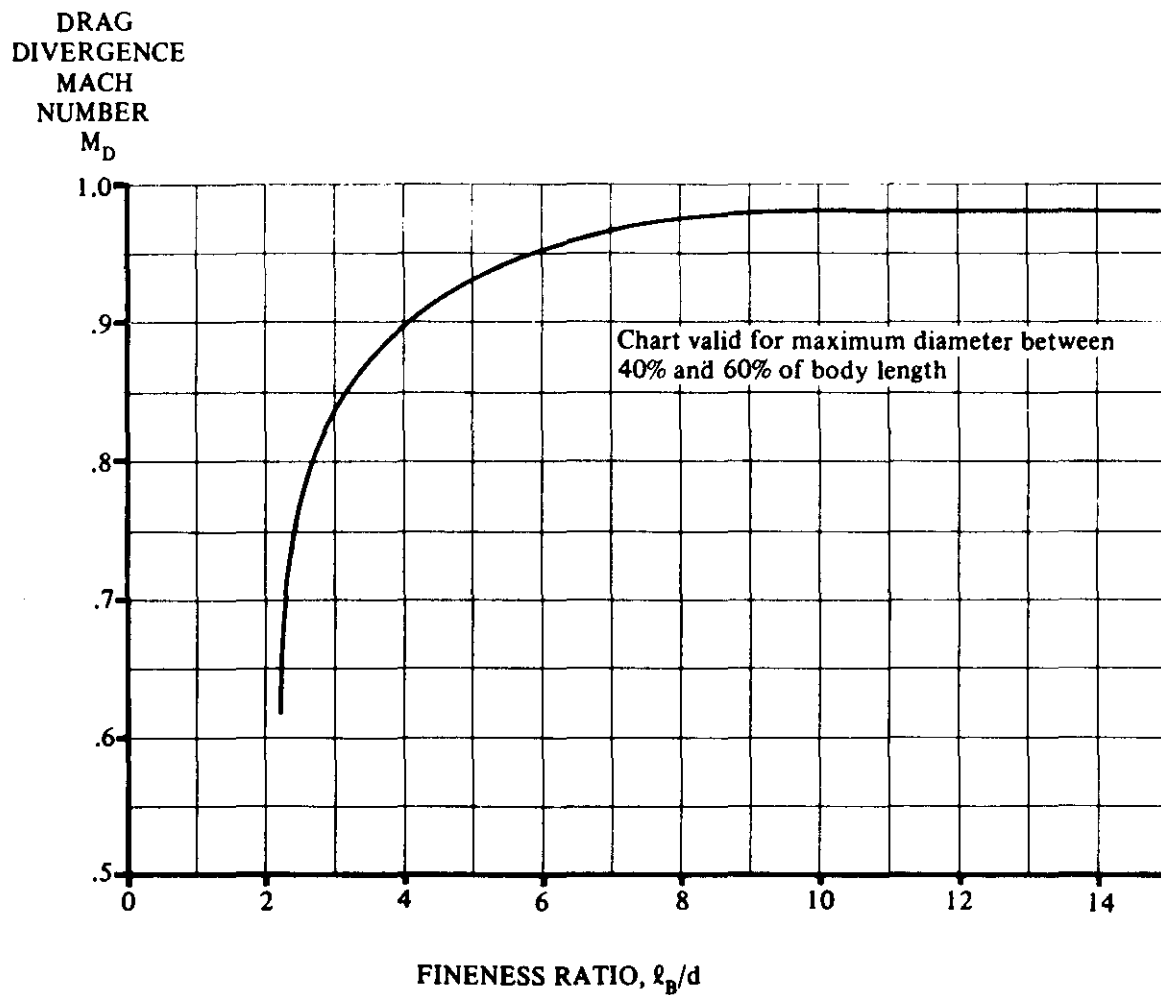
FIGURE 4.2.3.1-25 DRAG-DIVERGENCE MACH NUMBER FOR CLOSED-NOSED BODIES
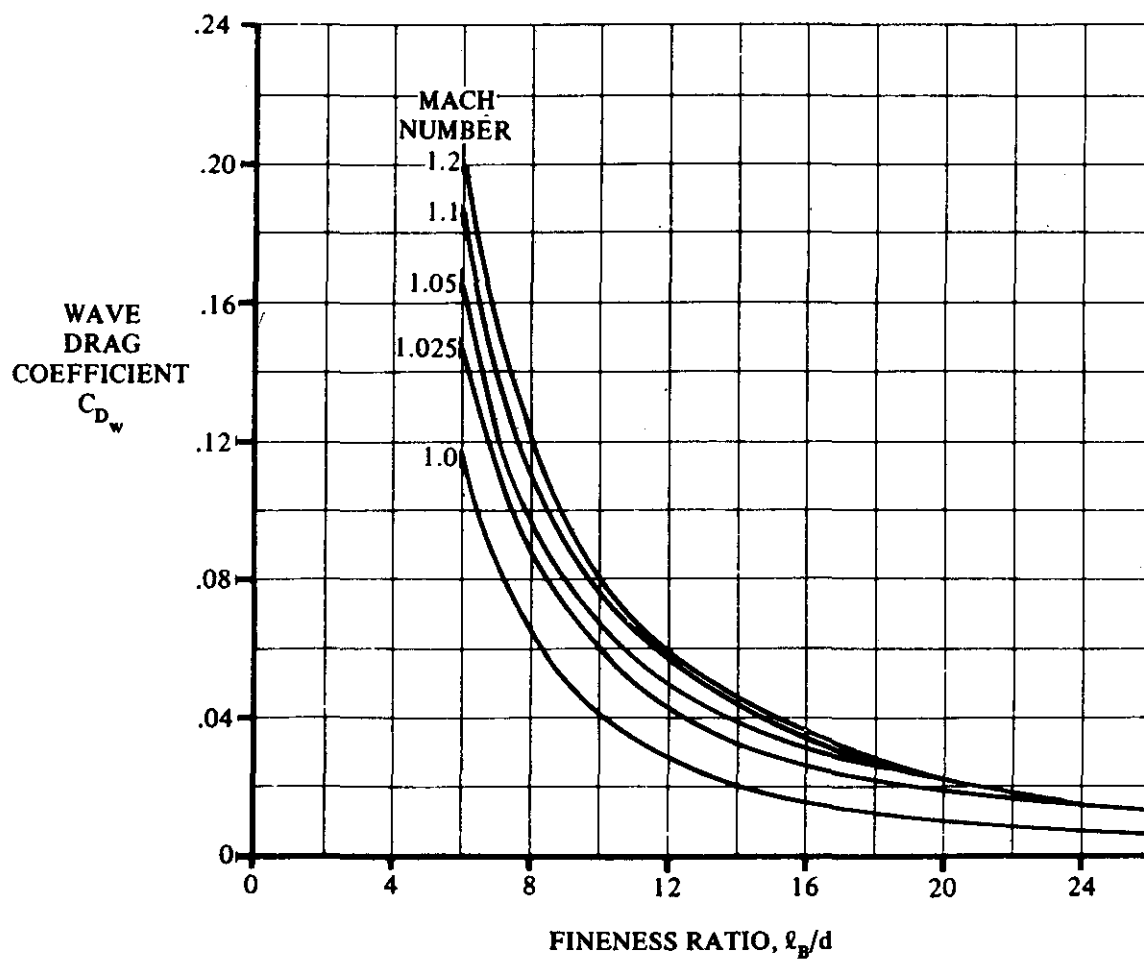
FIGURE 4.2.3.1-26 WAVE DRAG FOR PARABOLIC-TYPE FUSELAGE

Note:
a   is the nose diameter of forebody or base diameter of afterbody
d   is the maximum diameter of forebody or afterbody
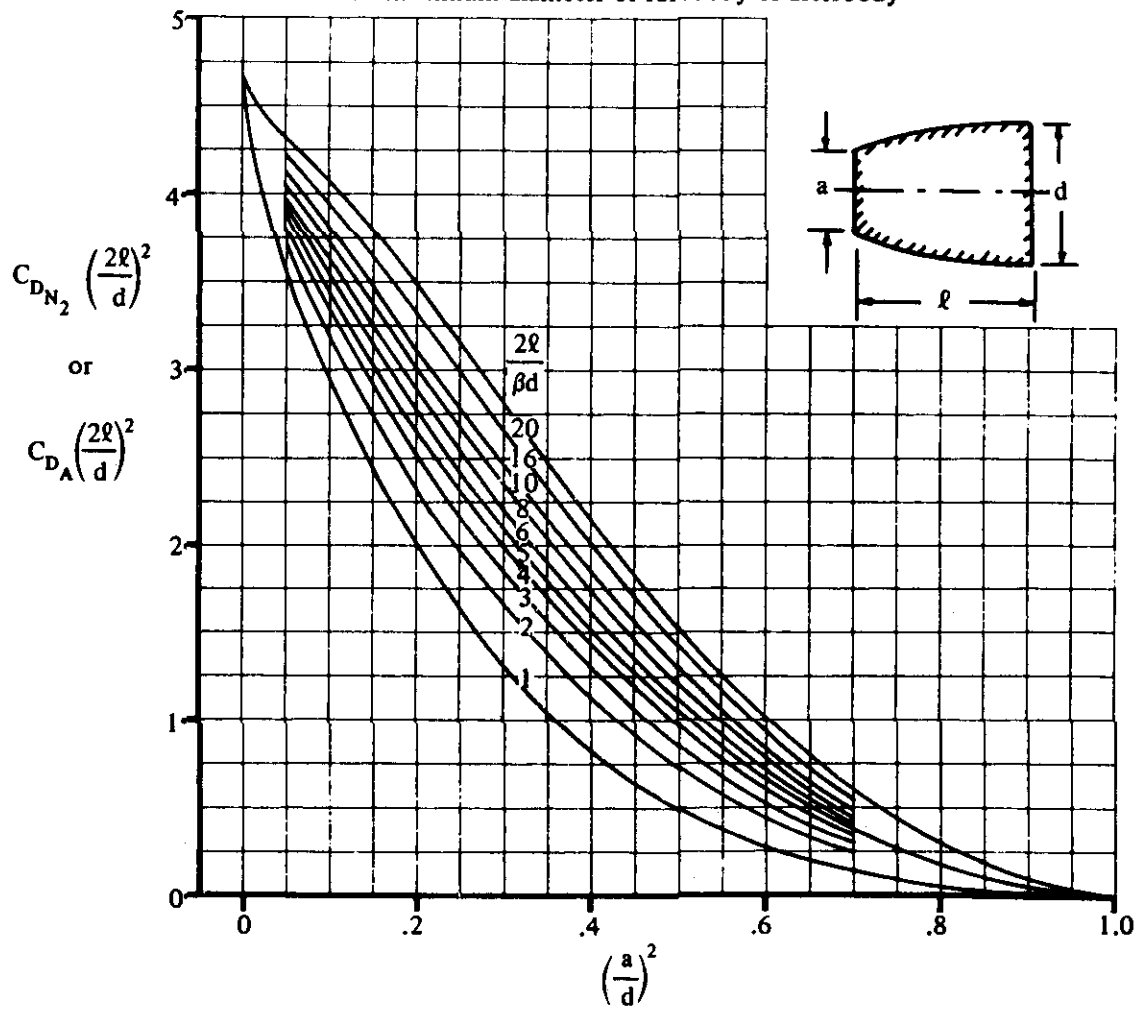
FIGURE 4.2.3.1-27 DRAG OF (SLENDER) FOREBODIES OR AFTERBODIES OF PARABOLIC PROFILE

Note:
  a   is the nose diameter of forebody or base diameter of afterbody
  d   is the maximum diameter of forebody or afterbody
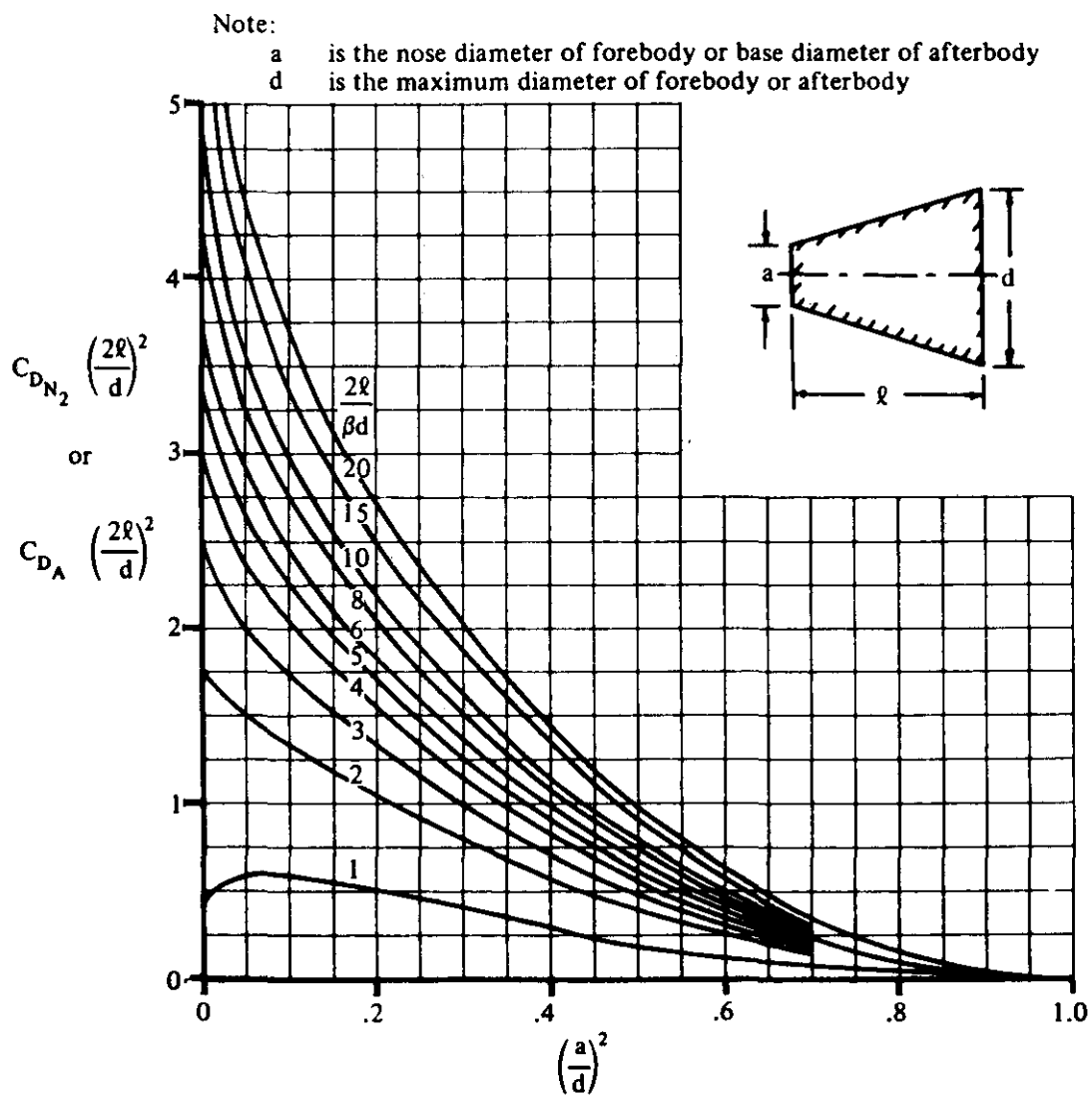
FIGURE 4.2.3.1-28 DRAG OF (SLENDER) CONICAL FOREBODIES OR AFTERBODIES
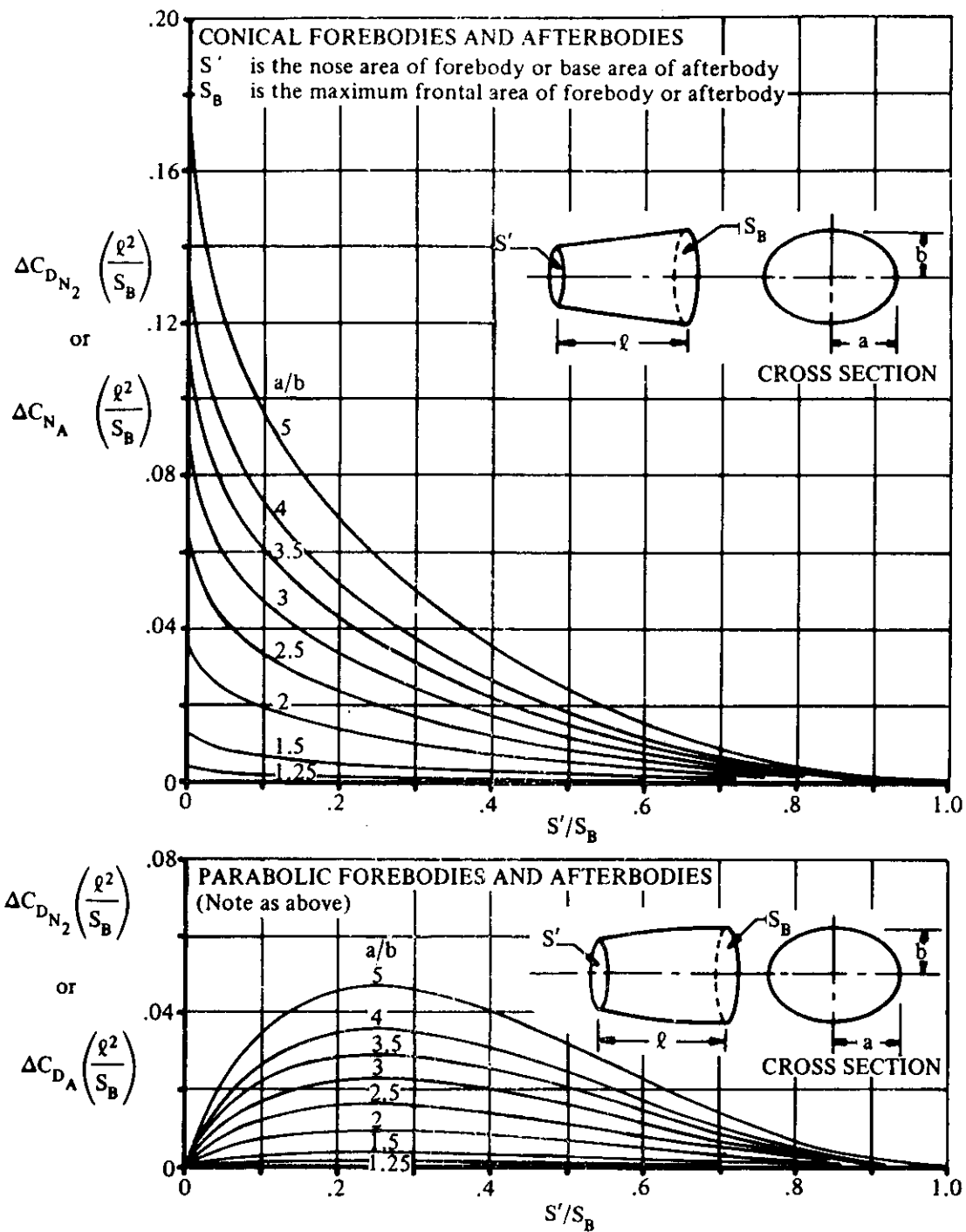
FIGURE 4.2.3.1-29 REDUCTION IN WAVE-DRAG COEFFICIENT DUE TO NONCIRCULAR CROSS SECTION
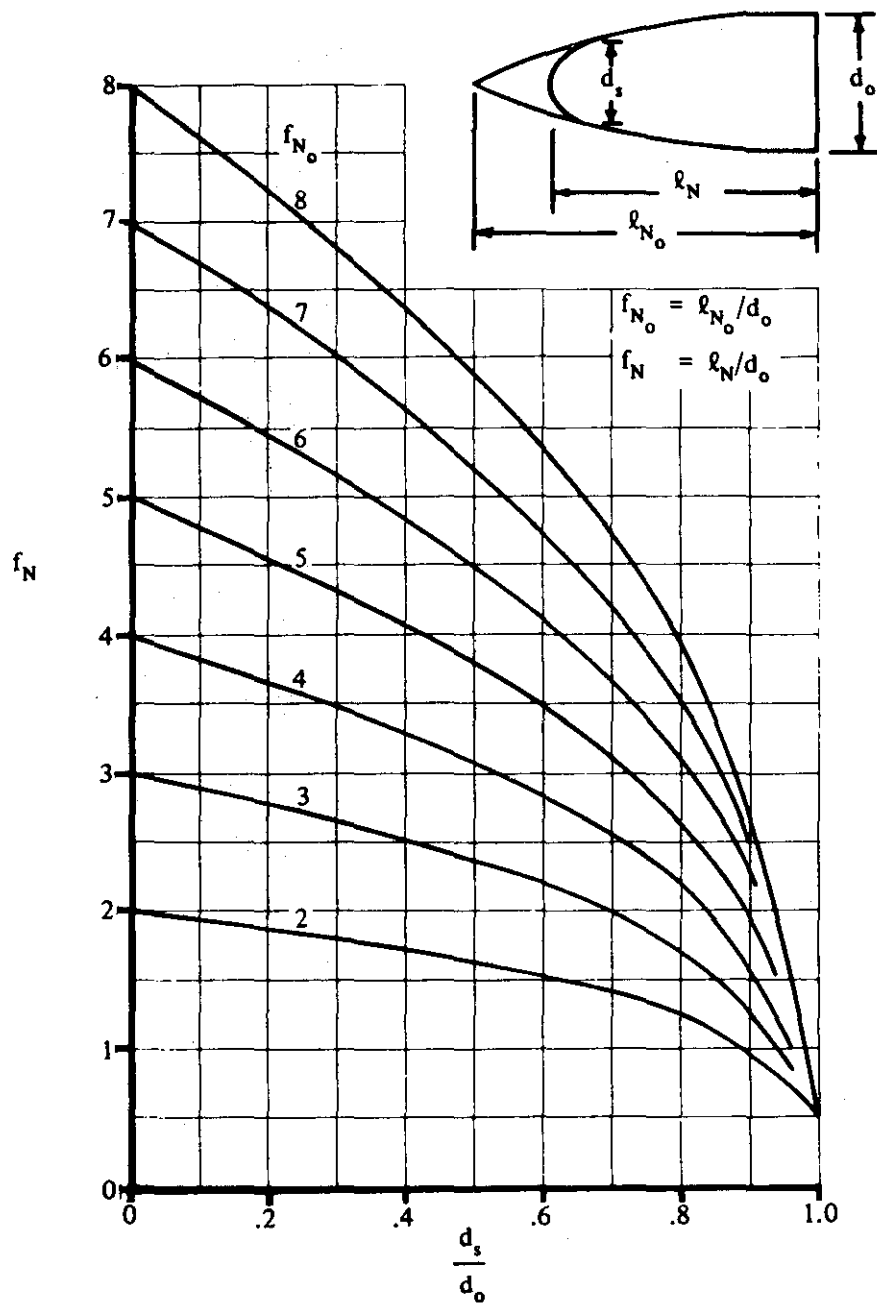
FIGURE 4.2.3.1-30 FINENESS RATIO OF SPHERICALLY BLUNTED OGIVE NOSES
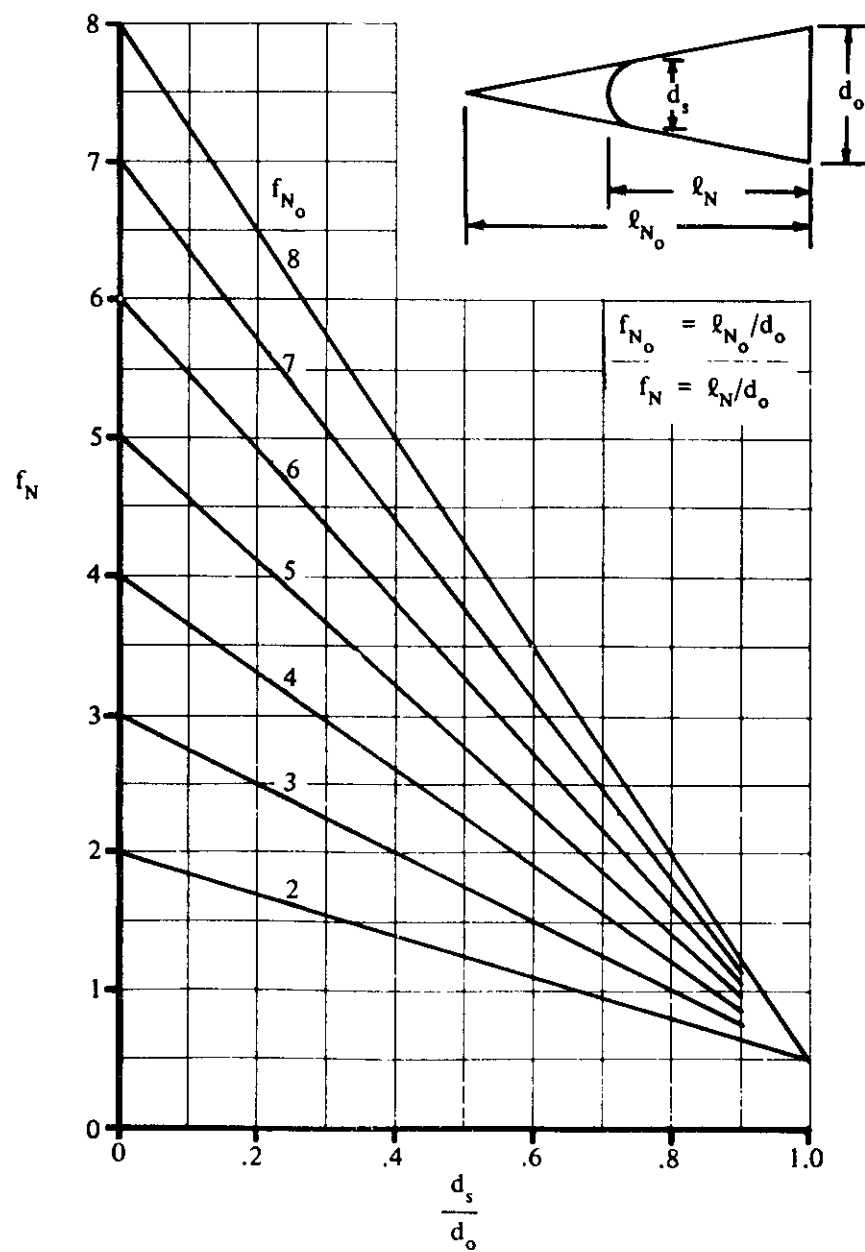
FIGURE 4.2.3.1-31 FINENESS RATIO OF SPHERICALLY BLUNTED CONICAL NOSES
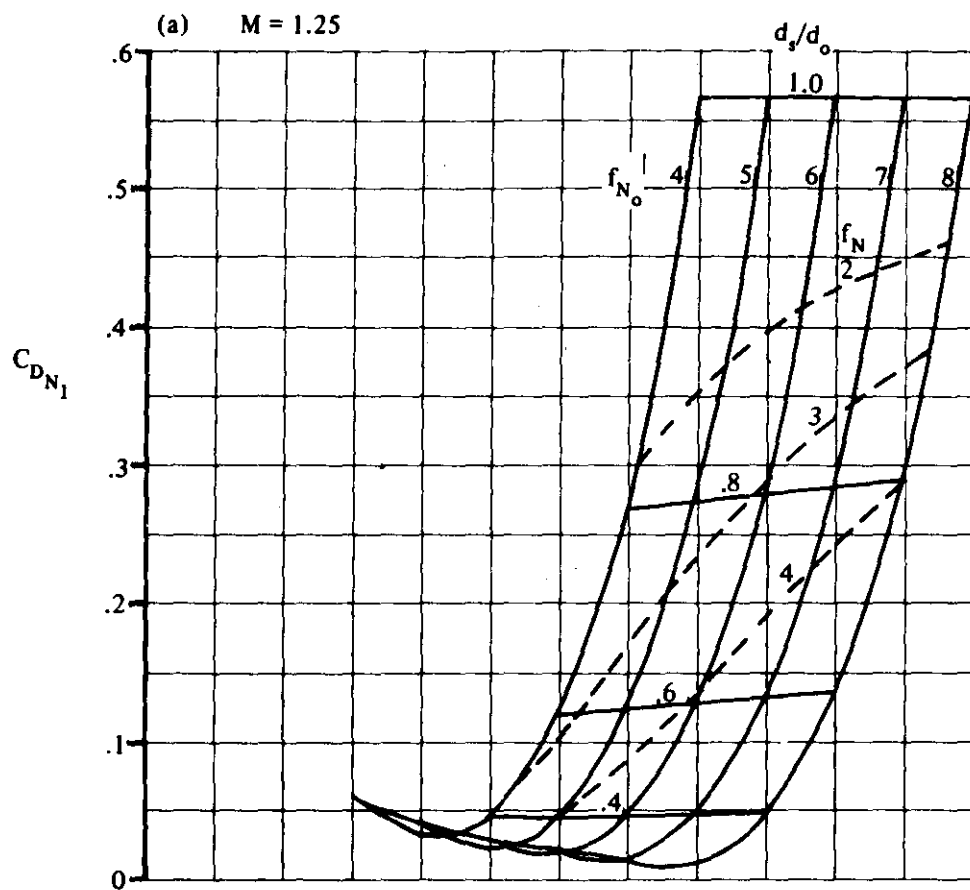
FIGURE 4.2.3.1-32 EFFECT OF BLUNTNESS ON SUPERSONIC PRESSURE DRAG OF
SPHERICALLY BLUNTED OGIVES

(b)   M = 1.5

FIGURE 4.2.3.1-32 (CONTD)

(c) M = 1.75
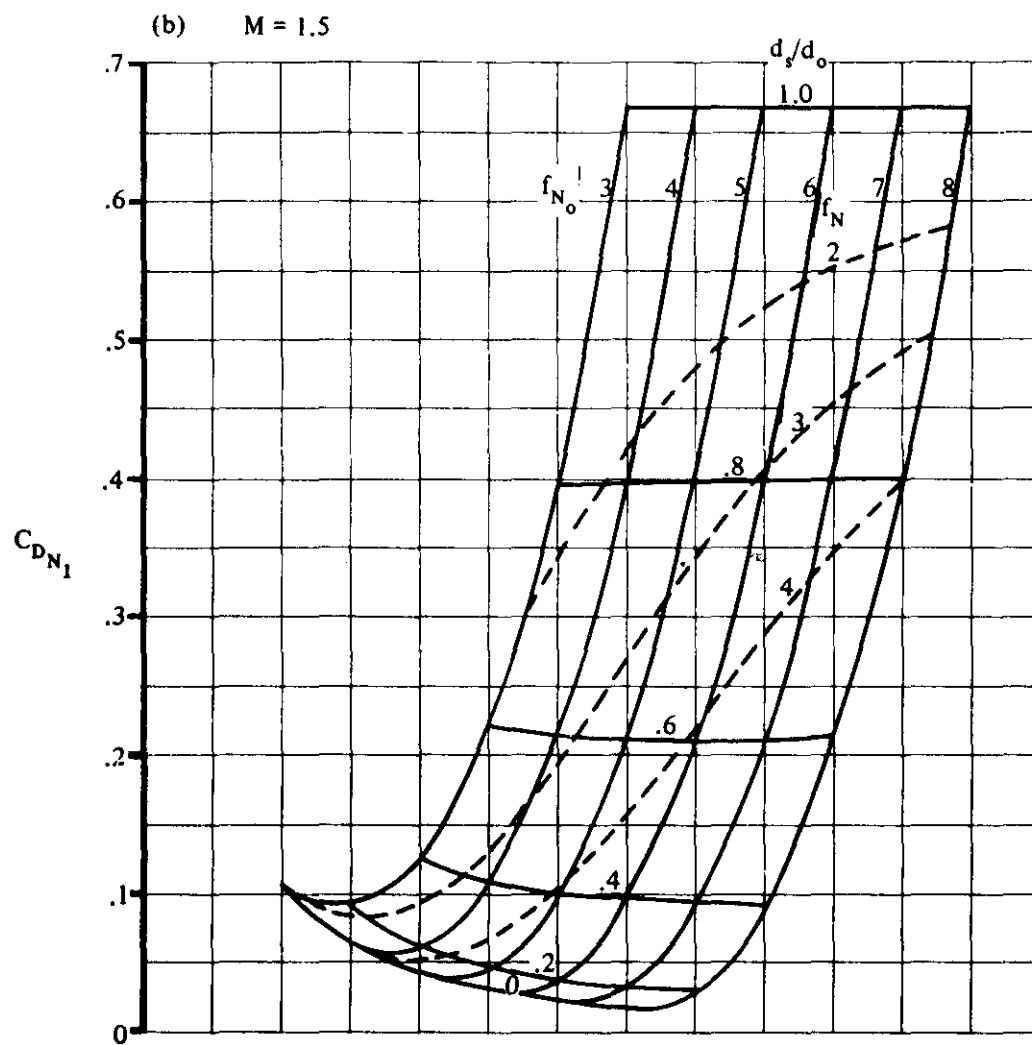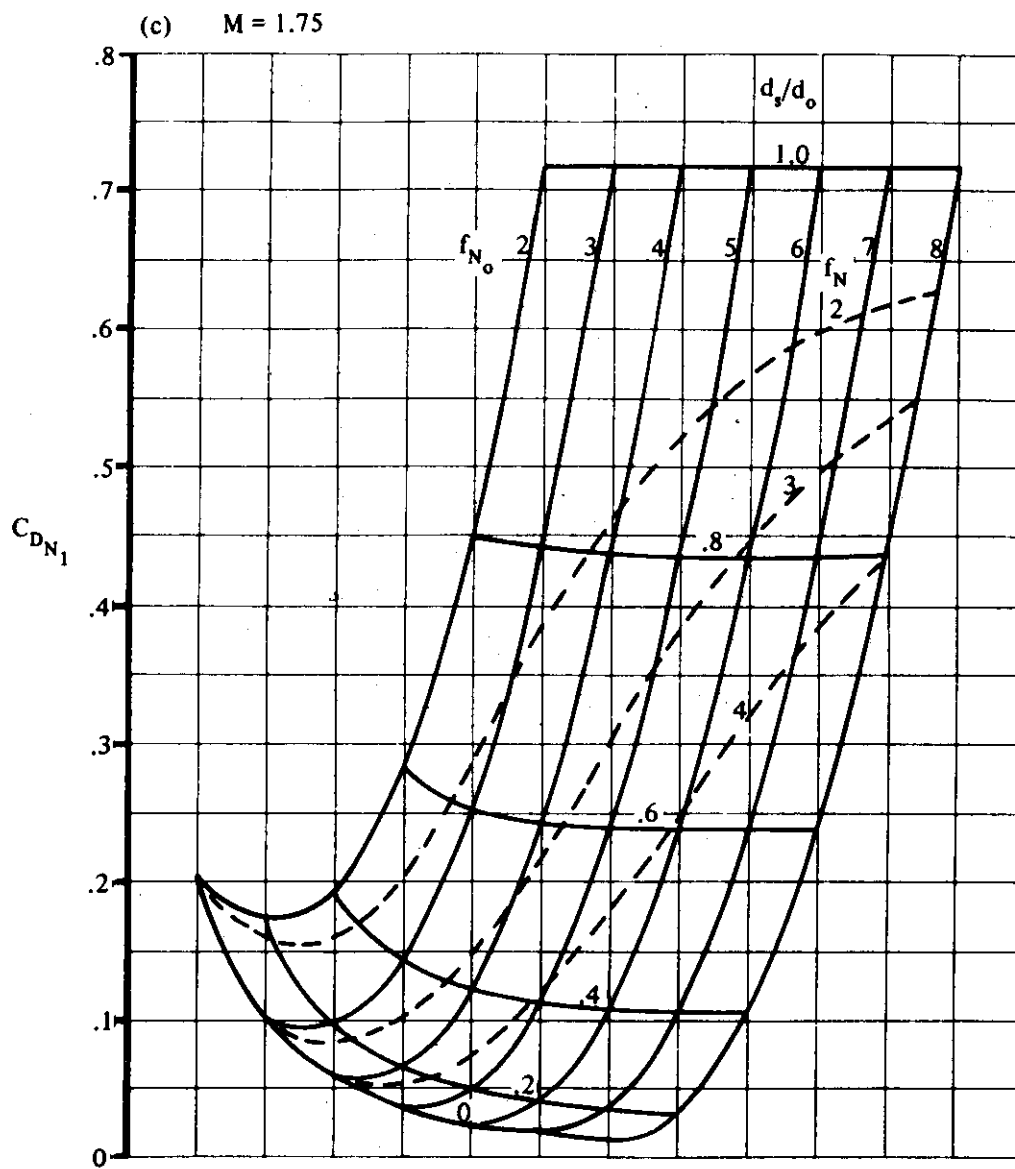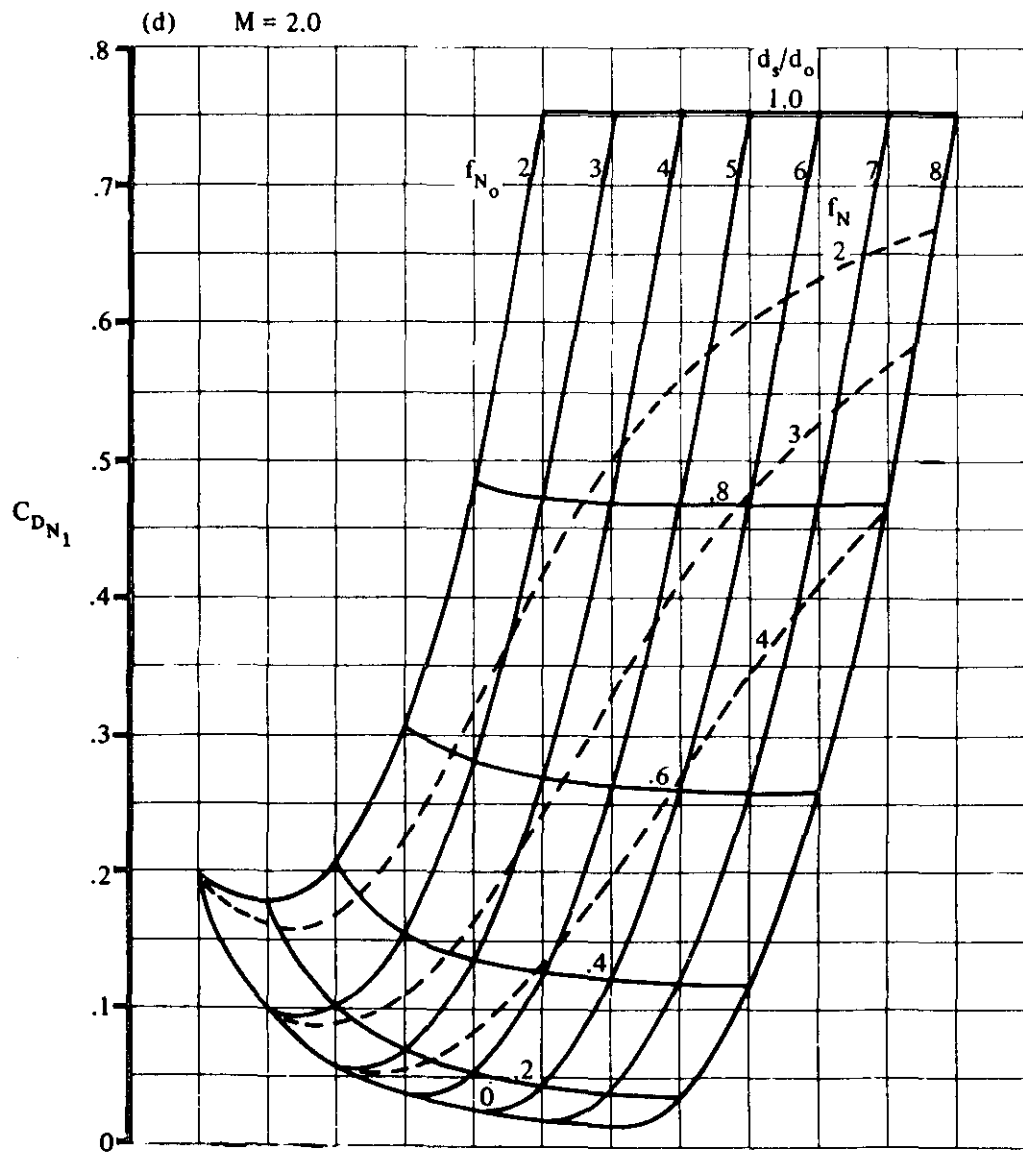
FIGURE 4.2.3.1-32 (CONTD)

FIGURE 4.2.3.1-32 (CONTD)

(e) M = 3.0

FIGURE 4.2.3.1-32 (CONTD)

(f)   M = 4.0
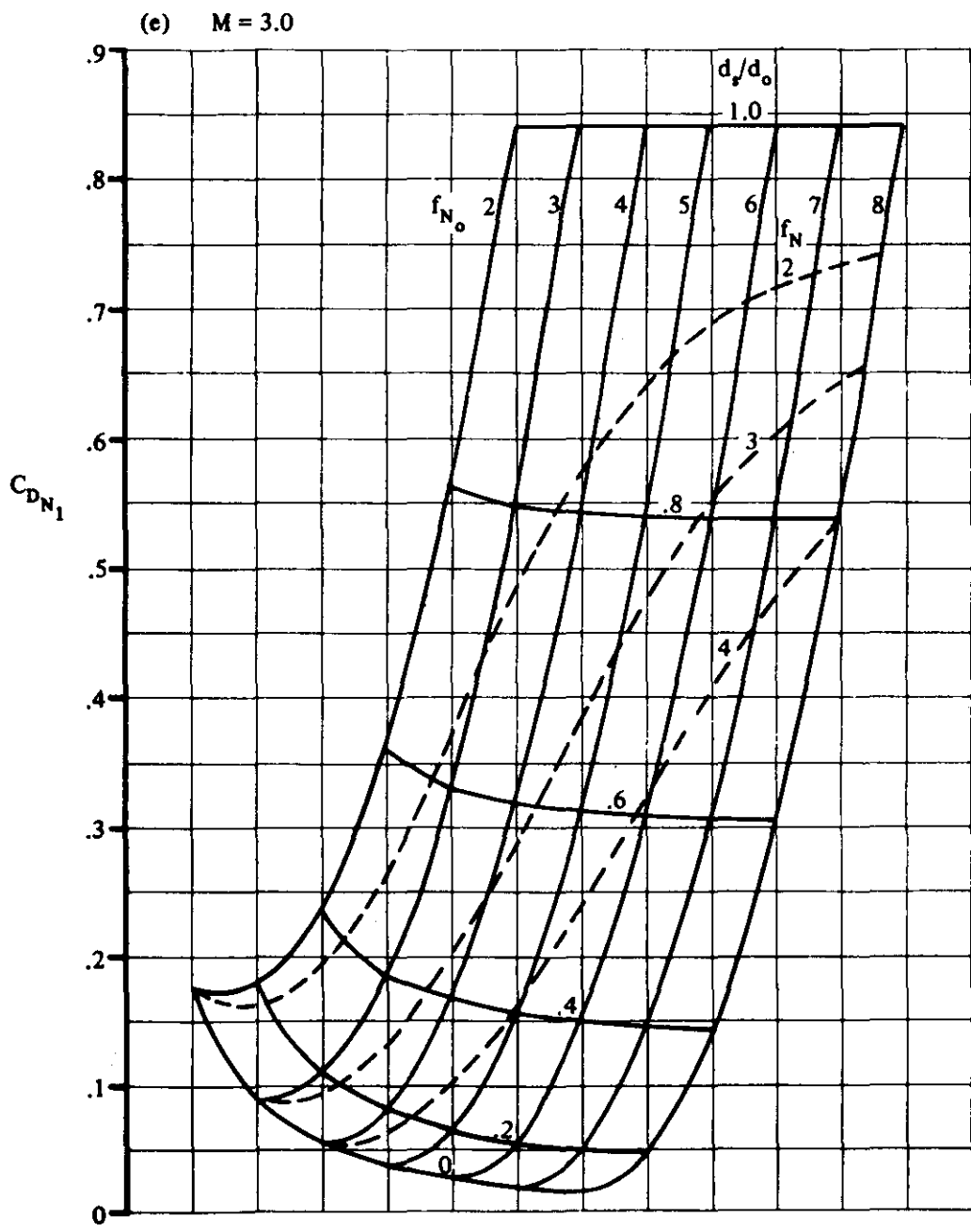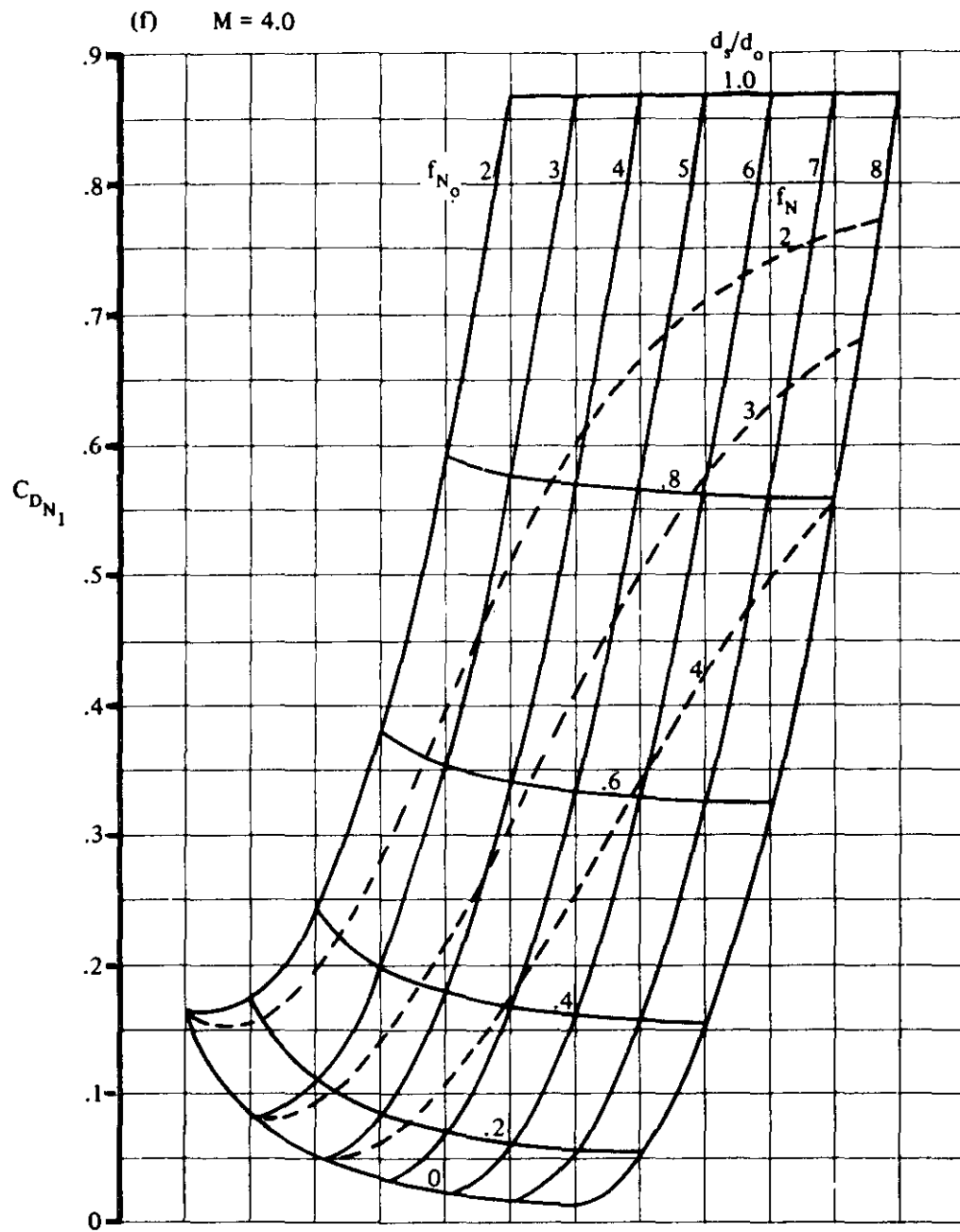
FIGURE 4.2.3.1-32 (CONTD)
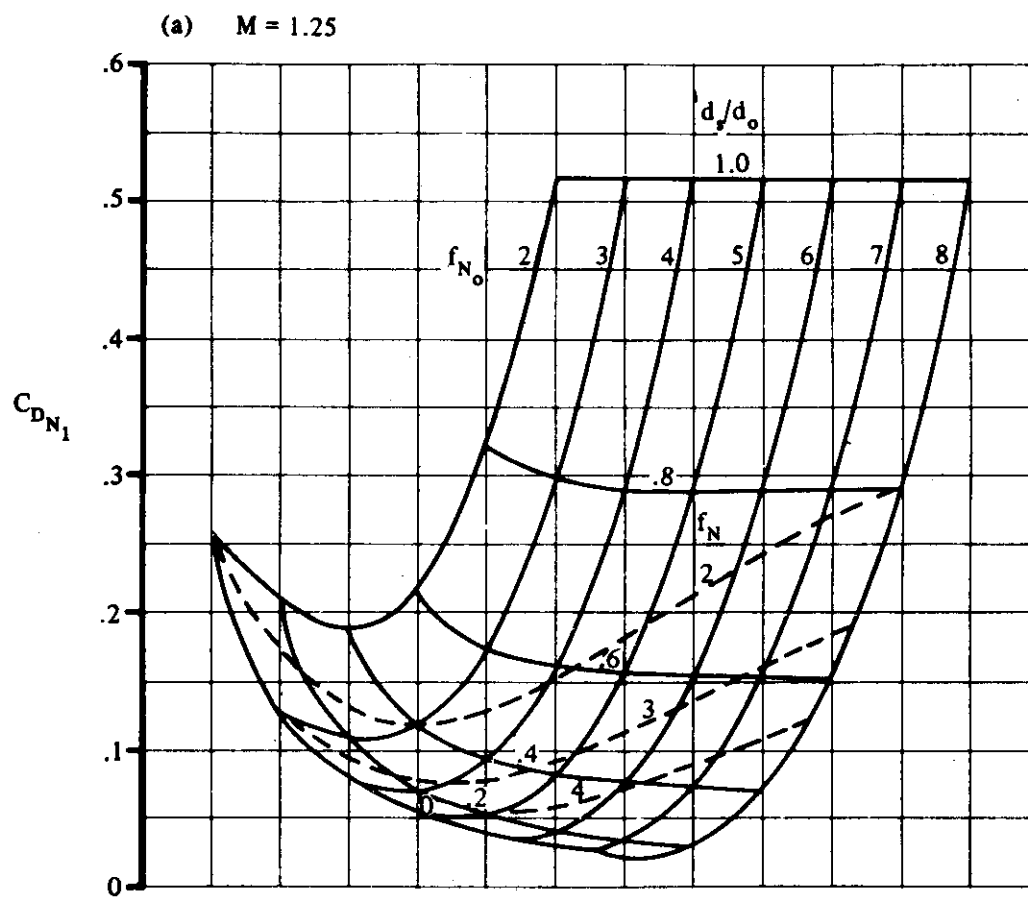
FIGURE 4.2.3.1-38 EFFECT OF BLUNTNESS ON SUPERSONIC PRESSURE DRAG OF
SPHERICALLY BLUNTED CONES

(b) M = 1.5

FIGURE 4.2.3.1-38 (CONTD)

(c)   M = 1.75

FIGURE 4.2.3.1-38 (CONTD)

(d) M = 2.0

FIGURE 4.2.3.1-38 (CONTD)

(e)   M = 3.0

FIGURE 4.2.3.1-38 (CONTD)

(f)   M = 4.0
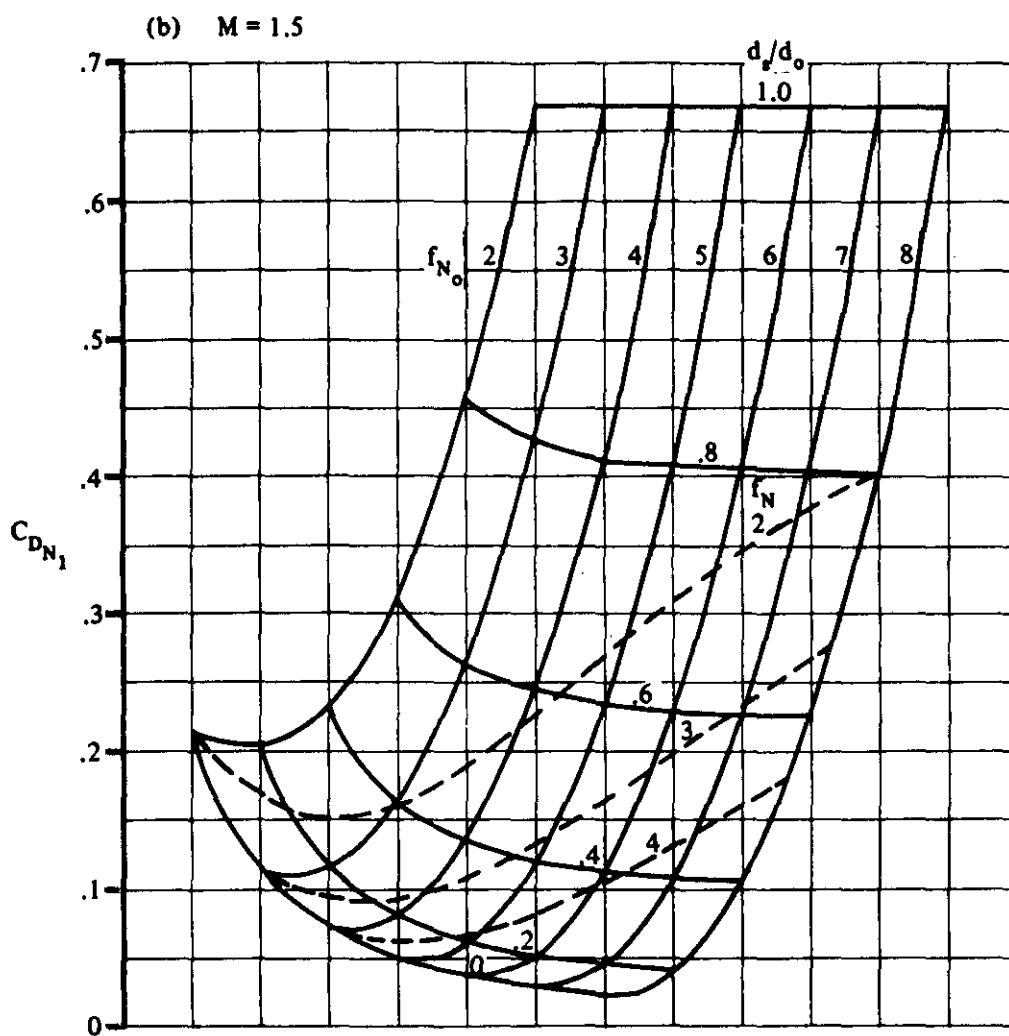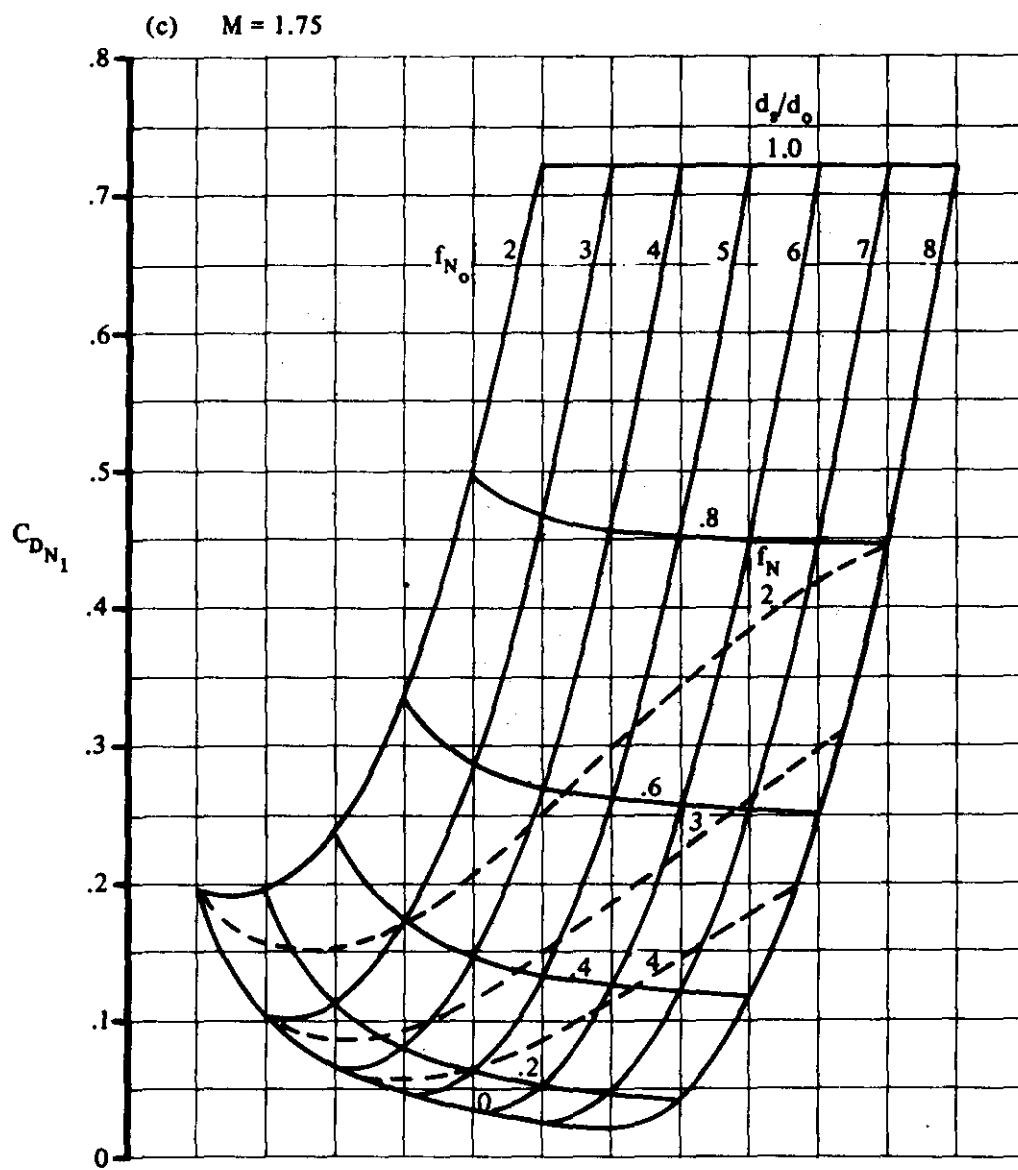
FIGURE 4.2.3.1-38 (CONTD)
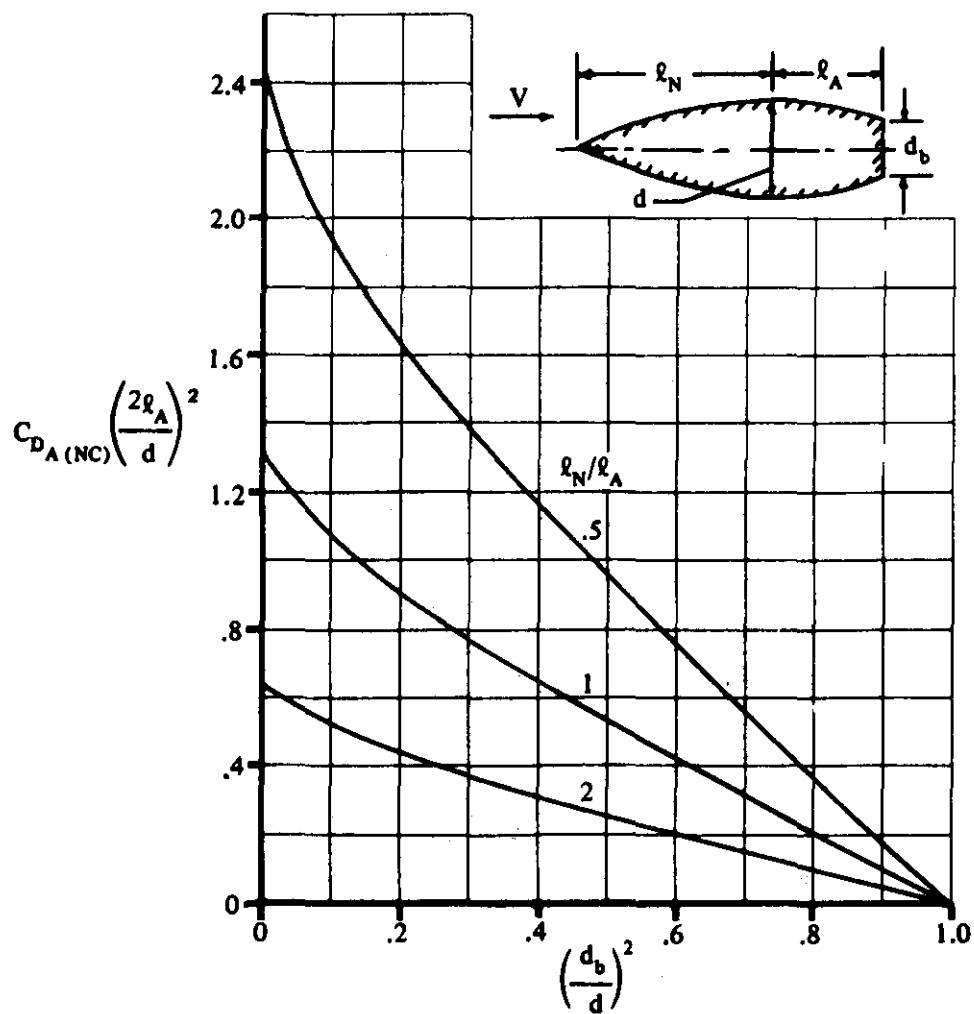
FIGURE 4.2.3.1-44a INTERFERENCE DRAG OF TRUNCATED AFTERBODIES BEHIND POINTED
FOREBODIES (PARABOLIC PROFILES: NO PARALLEL PORTION)
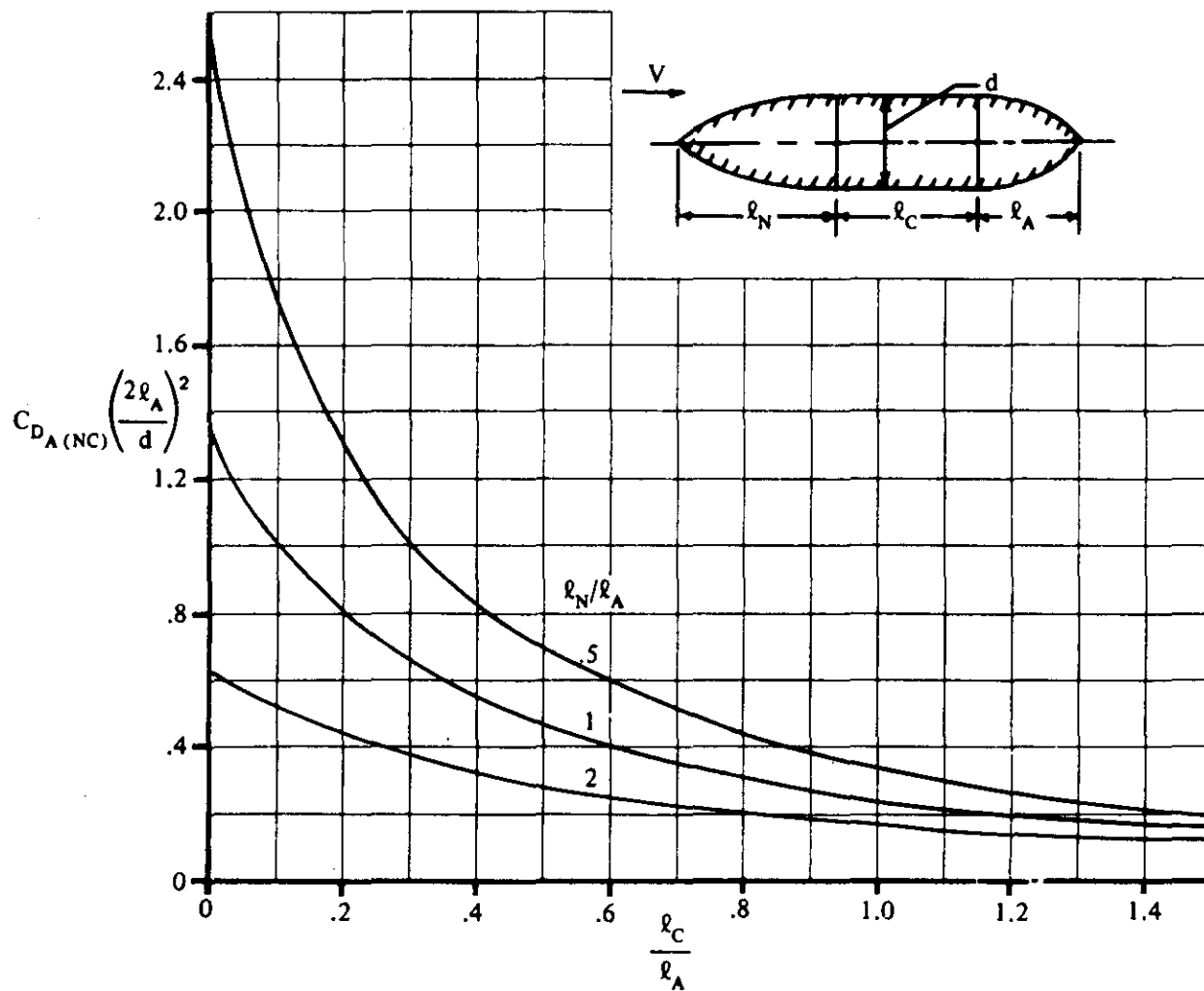
FIGURE 4.2.3.1-44b INTERFERENCE DRAG FOR POINTED BODIES OF PARABOLIC PROFILE
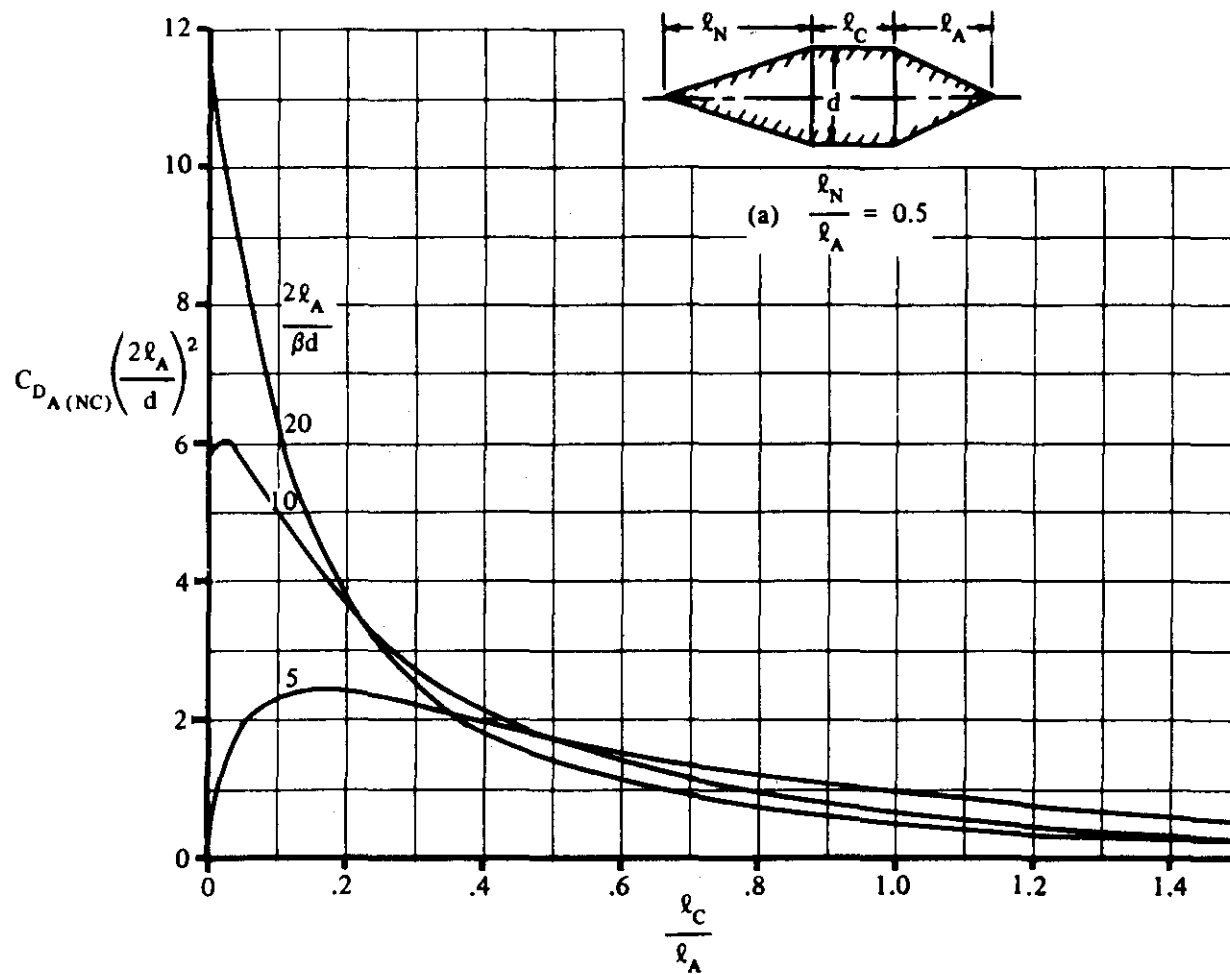
FIGURE 4.2.3.1-46 INTERFERENCE DRAG OF POINTED CONICAL BODIES
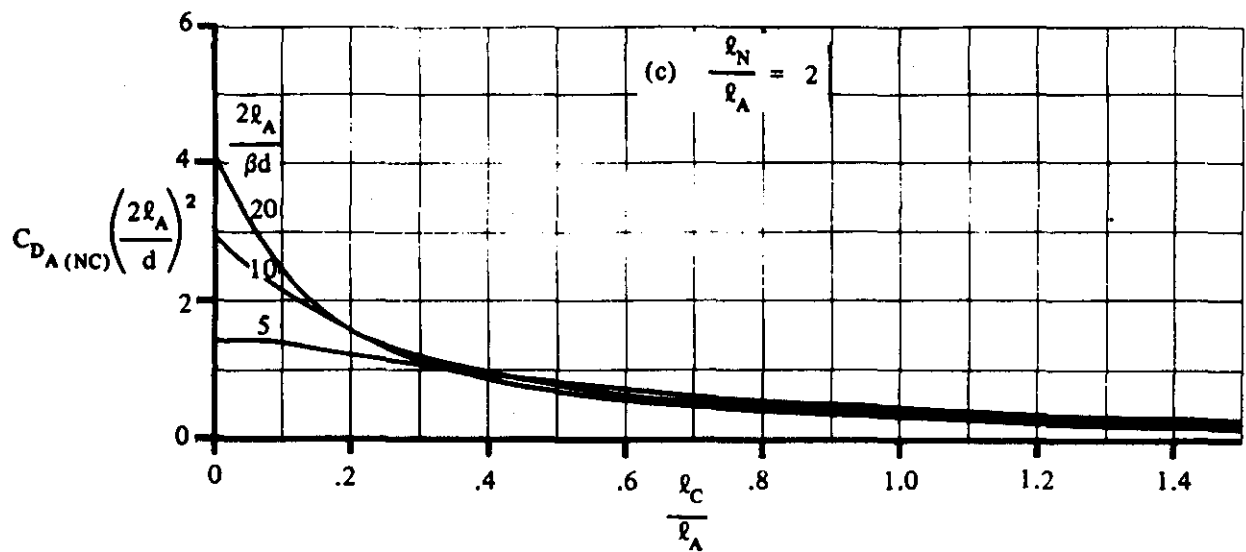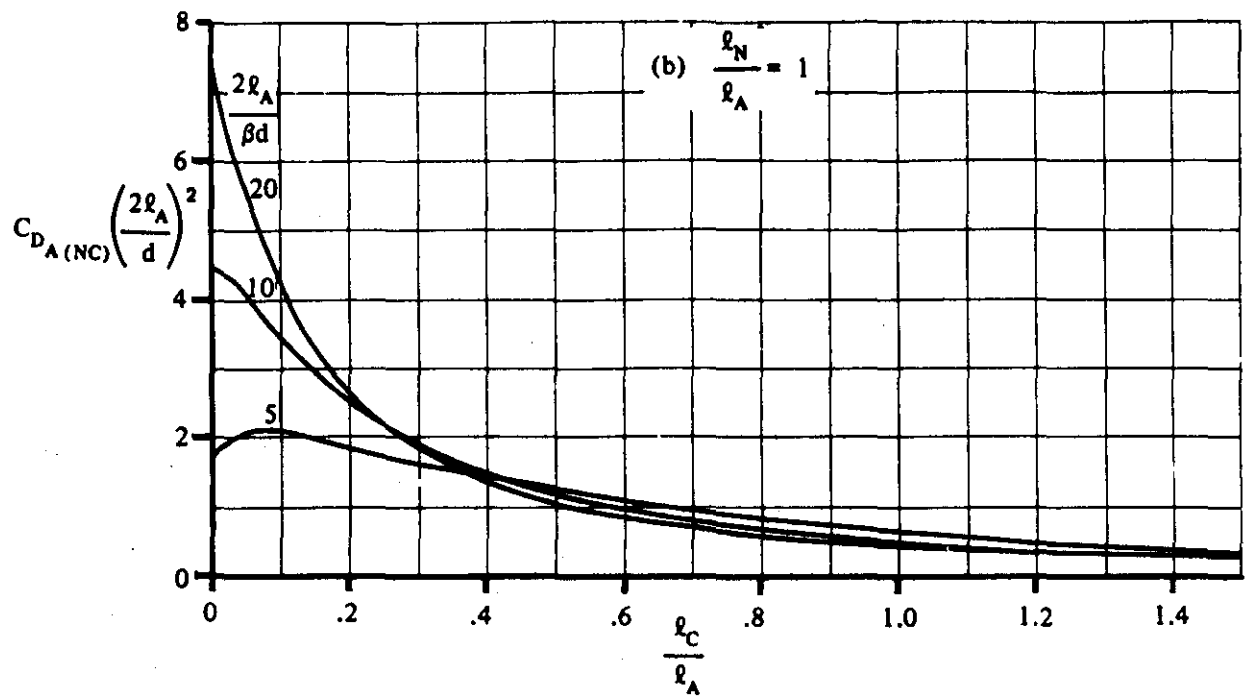
FIGURE 4.2.3.1-46 (CONTD)

S′   is the nose area of forebody or base area of afterbody
S_B is the maximum frontal area of forebody or afterbody
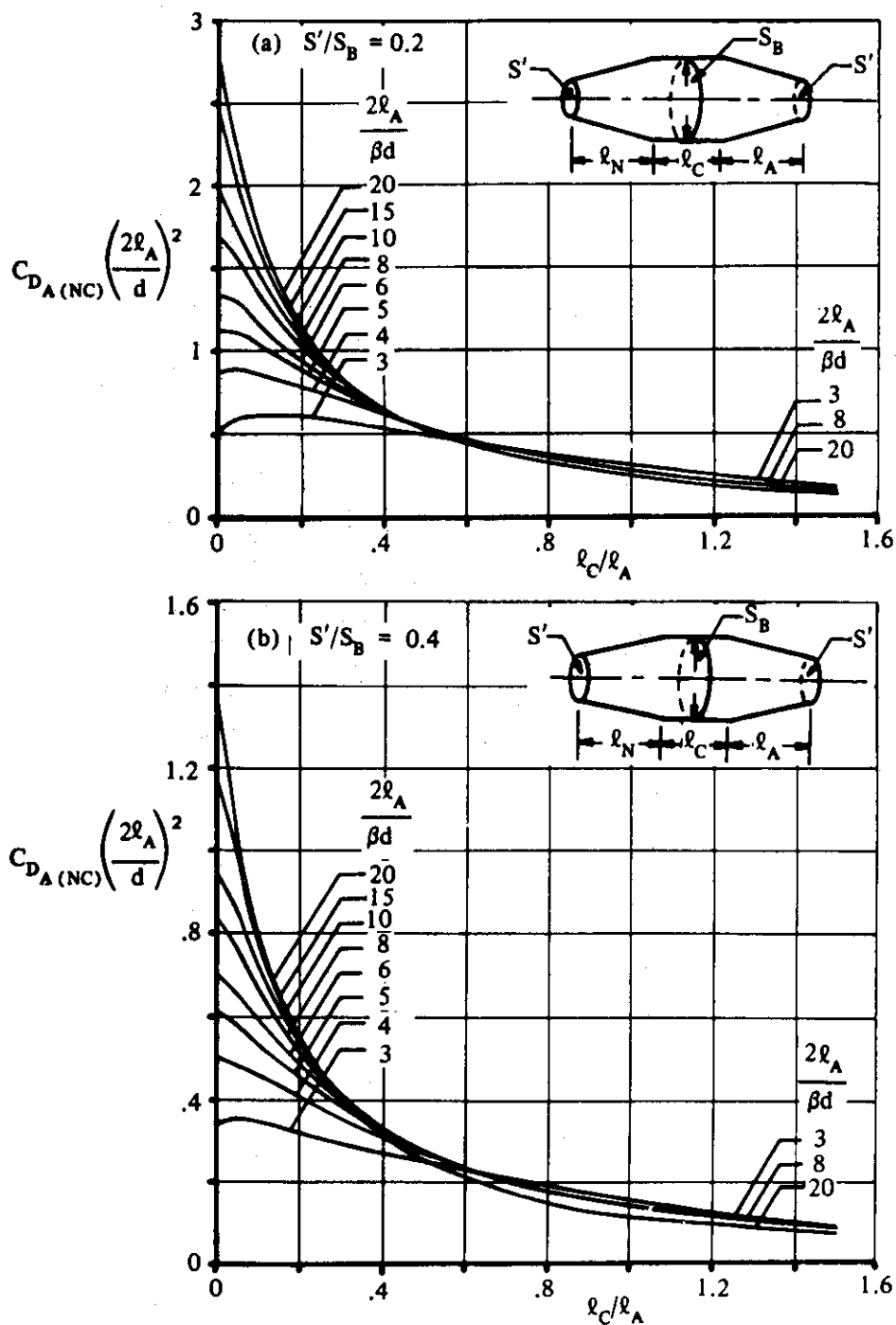
FIGURE 4.2.3.1-48 INTERFERENCE DRAG OF DUCTED CONICAL PROFILES

S '   is the nose area of forebody or base area of afterbody

S_B is the maximum frontal area of forebody or afterbody

(c) S'/S_B = 0.6
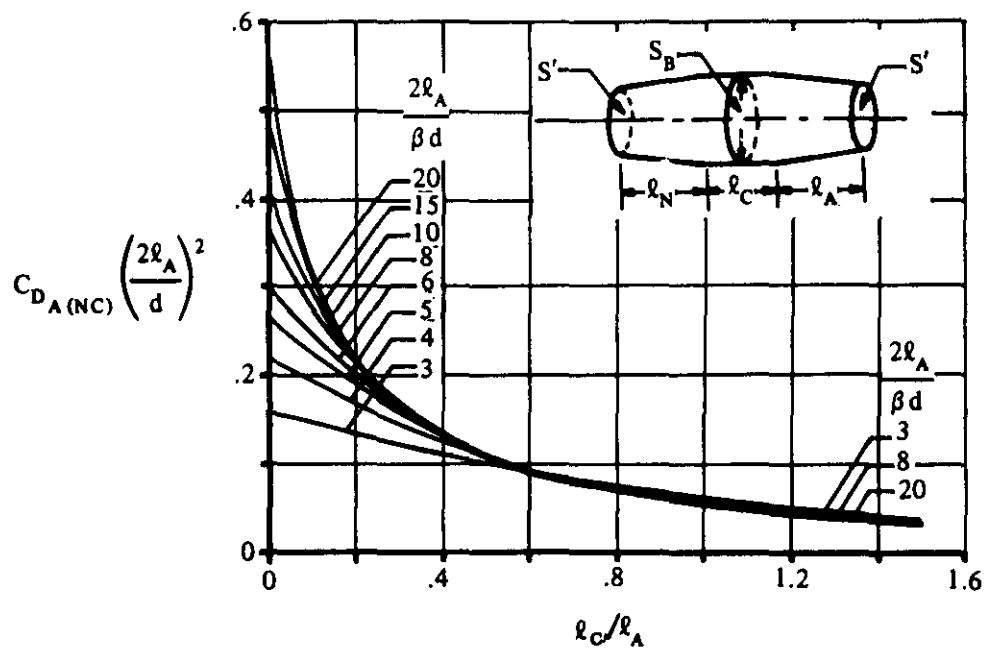
FIGURE 4.2.3.1-48 (CONTD)
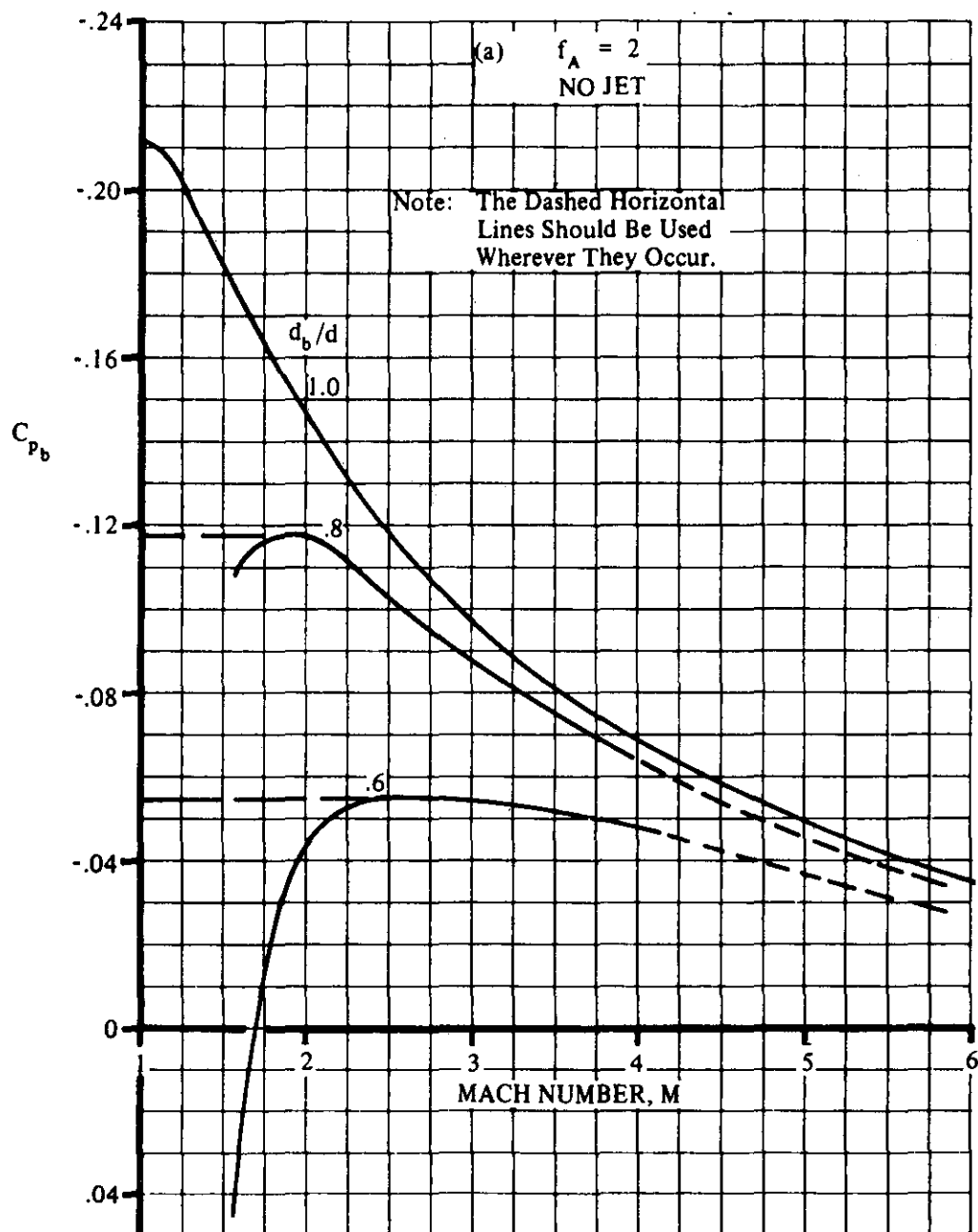
FIGURE 4.2.3.1-50 BASE-PRESSURE COEFFICIENT FOR OGIVE BOATTAILS
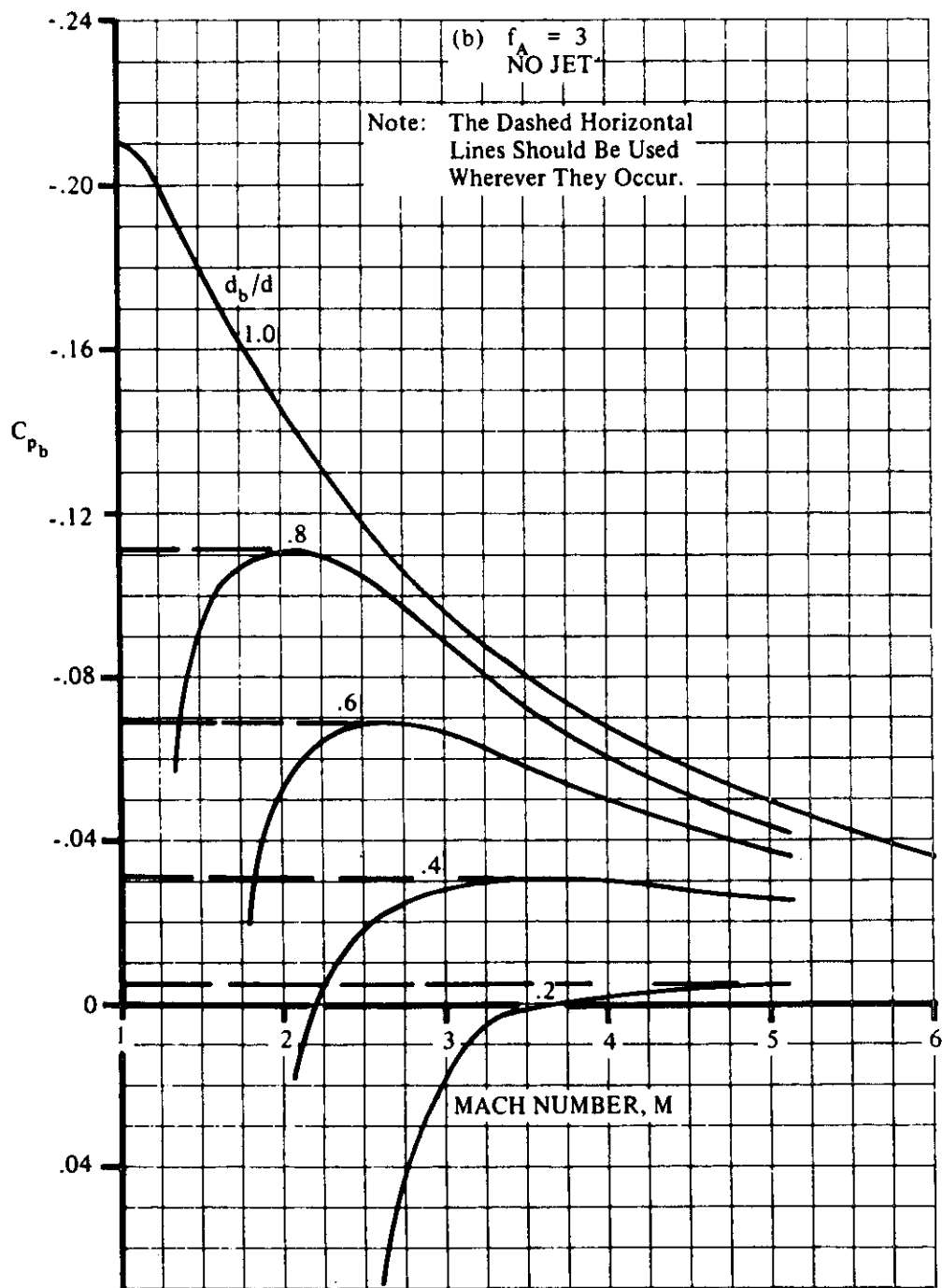
FIGURE 4.2.3.1-50 (CONTD)
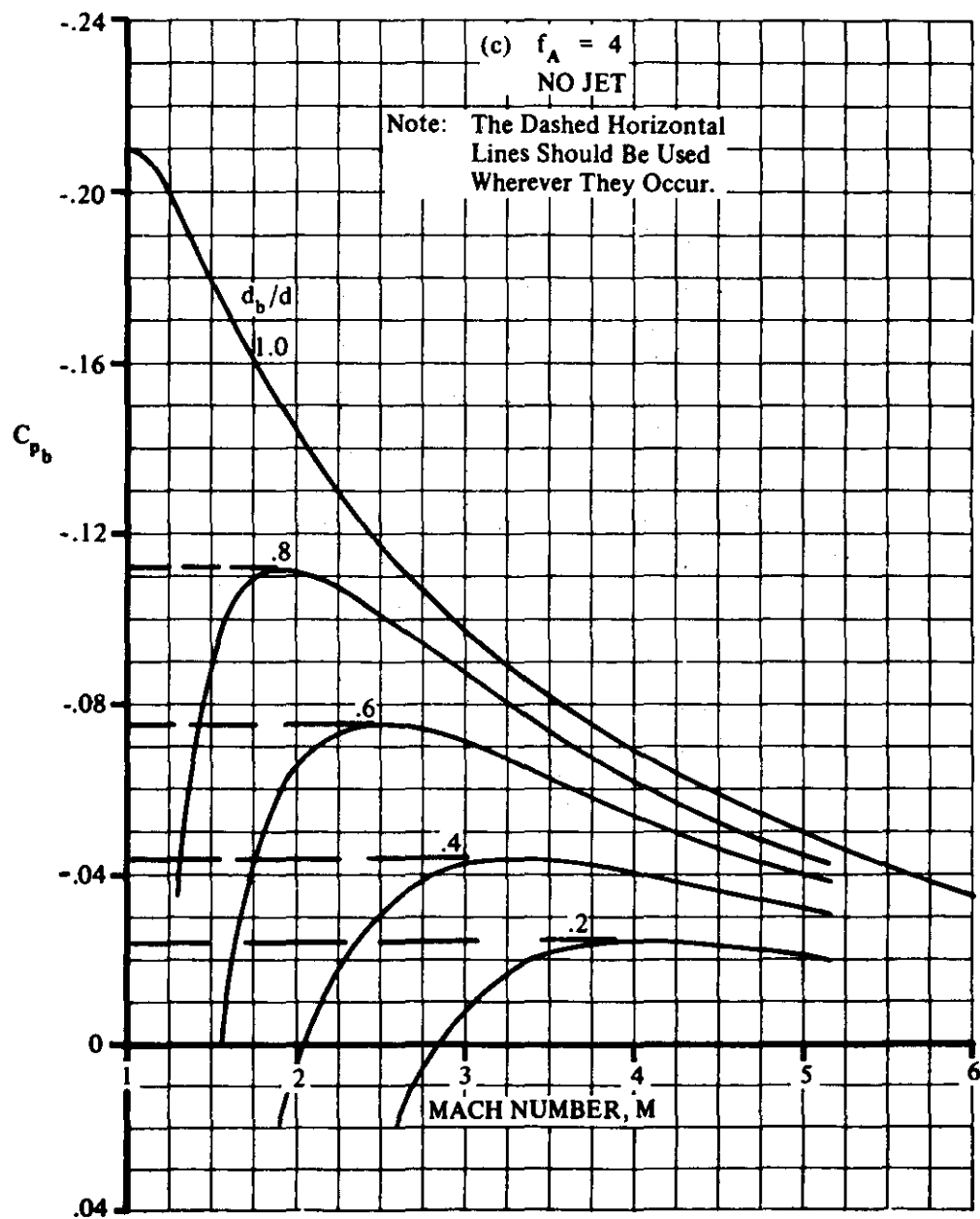
FIGURE 4.2.3.1-50 (CONTD)
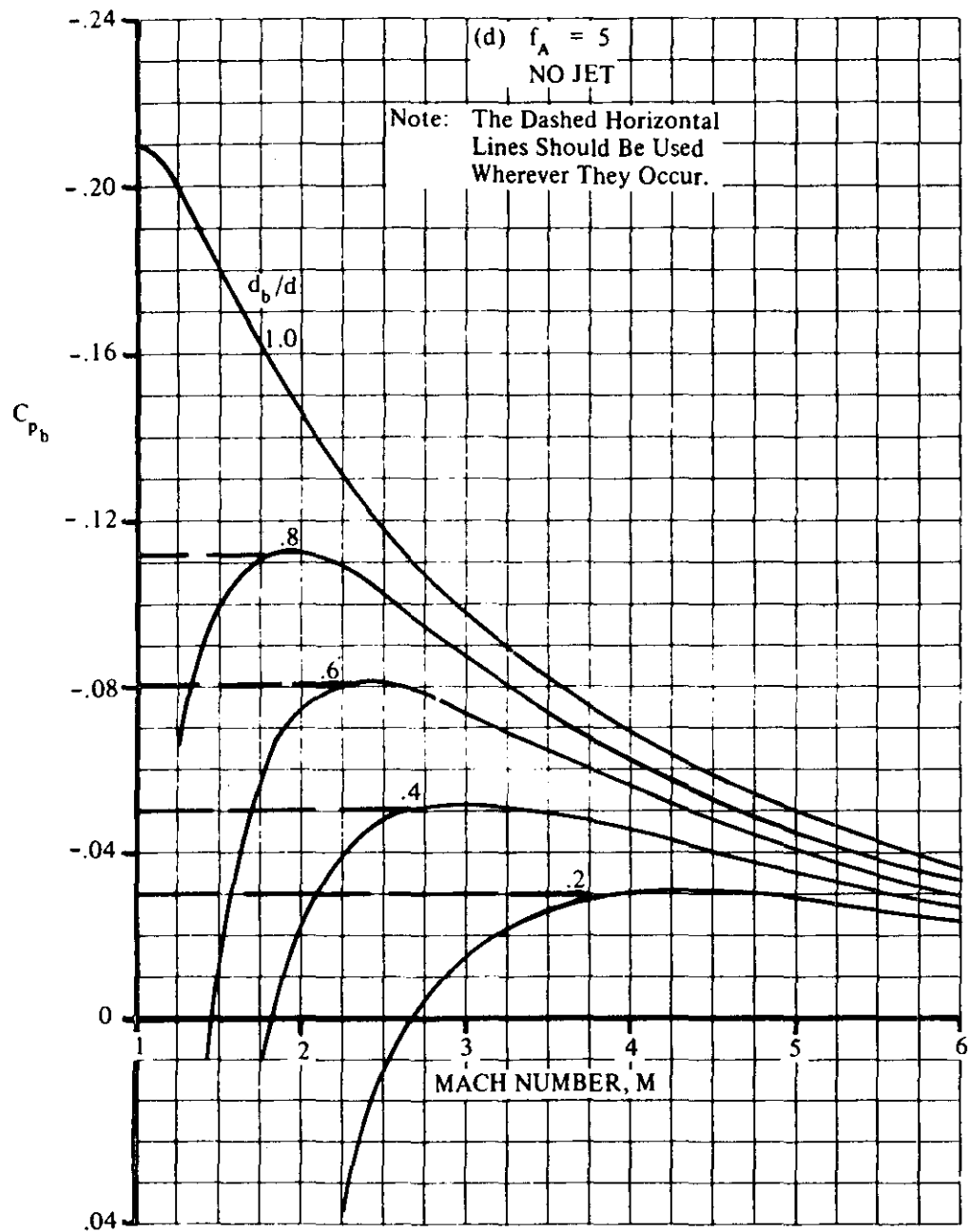
FIGURE 4.2.3.1-50 (CONTD)
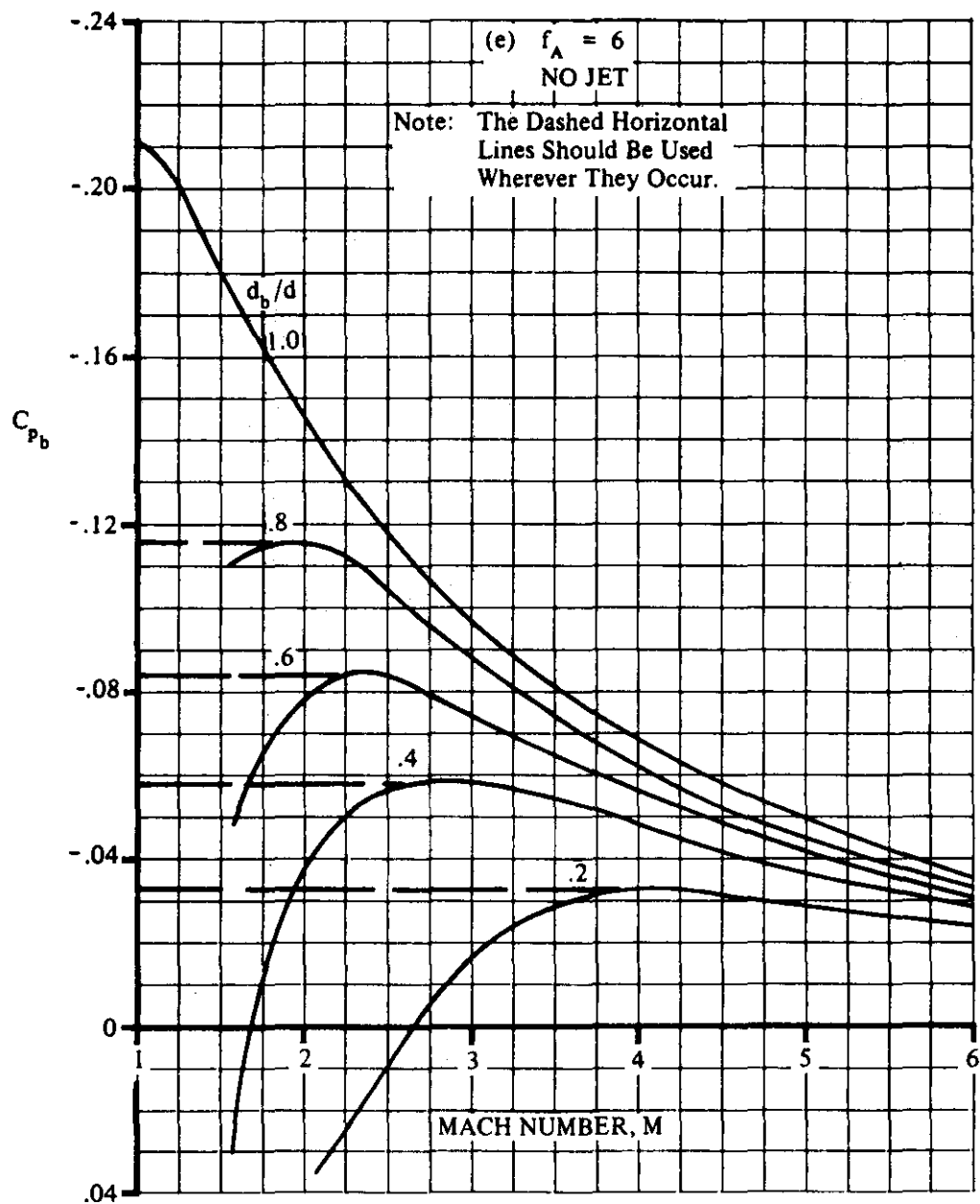
FIGURE 4.2.3.1-50 (CONTD)
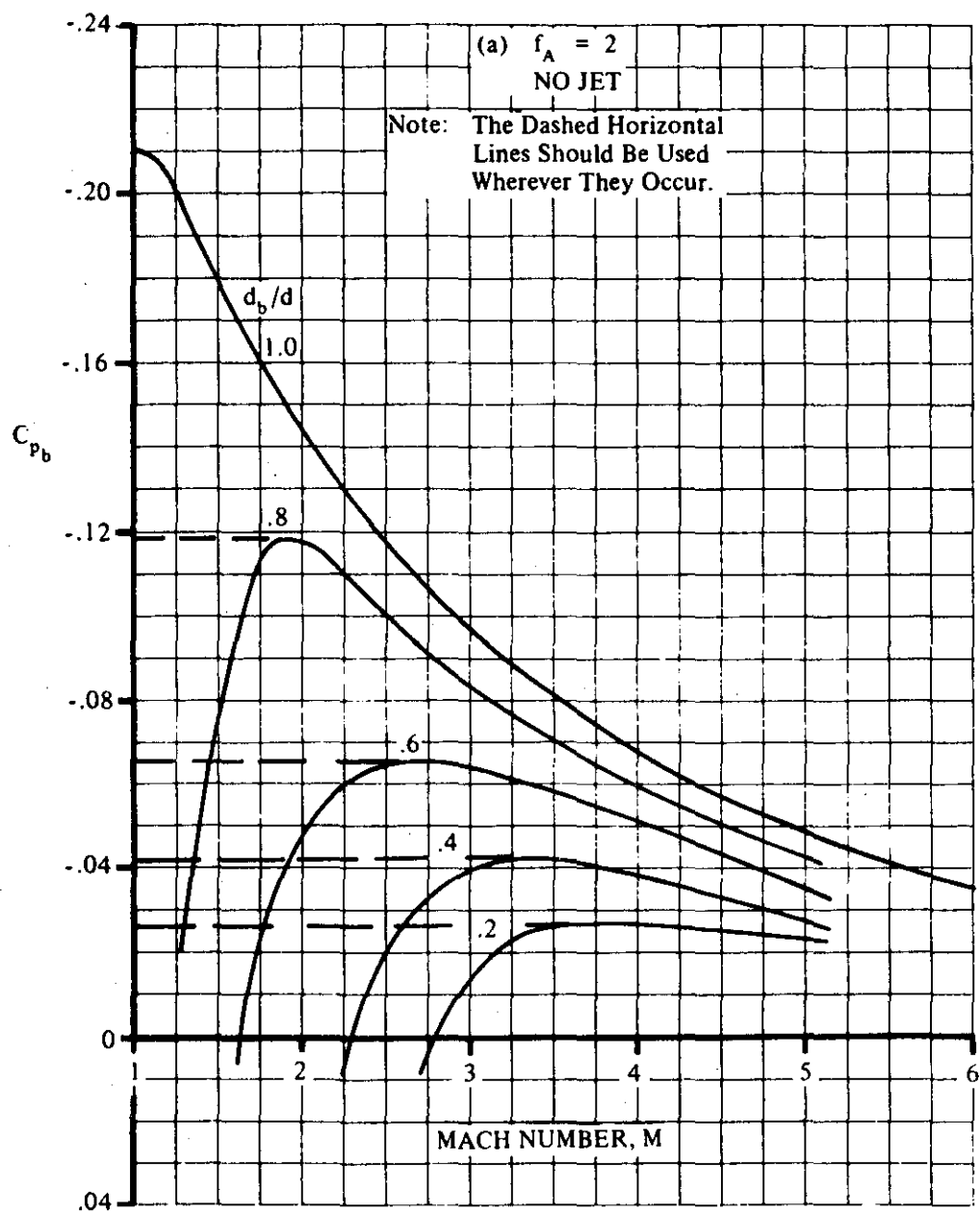
FIGURE 4.2.3.1-55 BASE-PRESSURE COEFFICIENT FOR CONICAL BOATTAILS
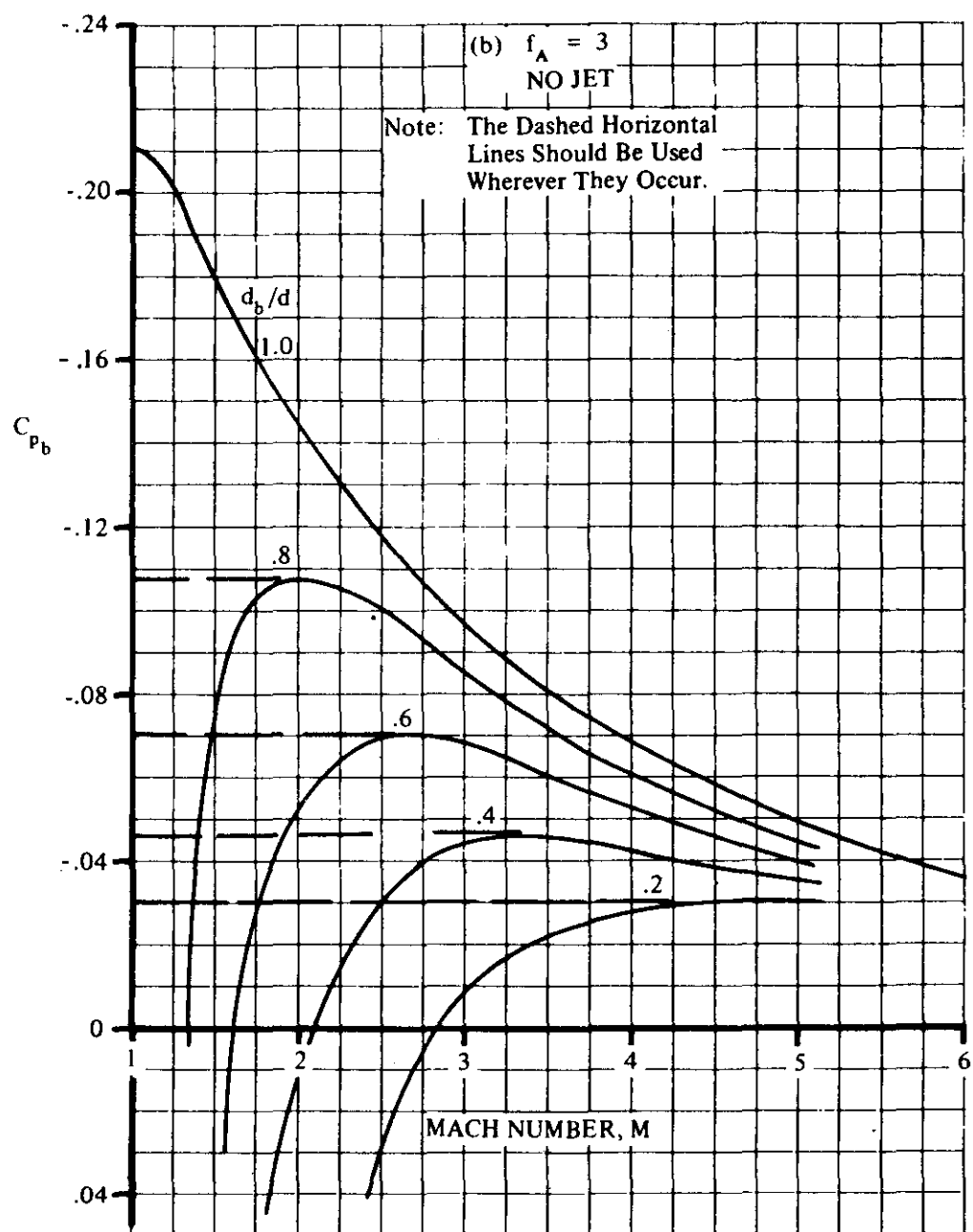
FIGURE 4.2.3.1-55 (CONTD)
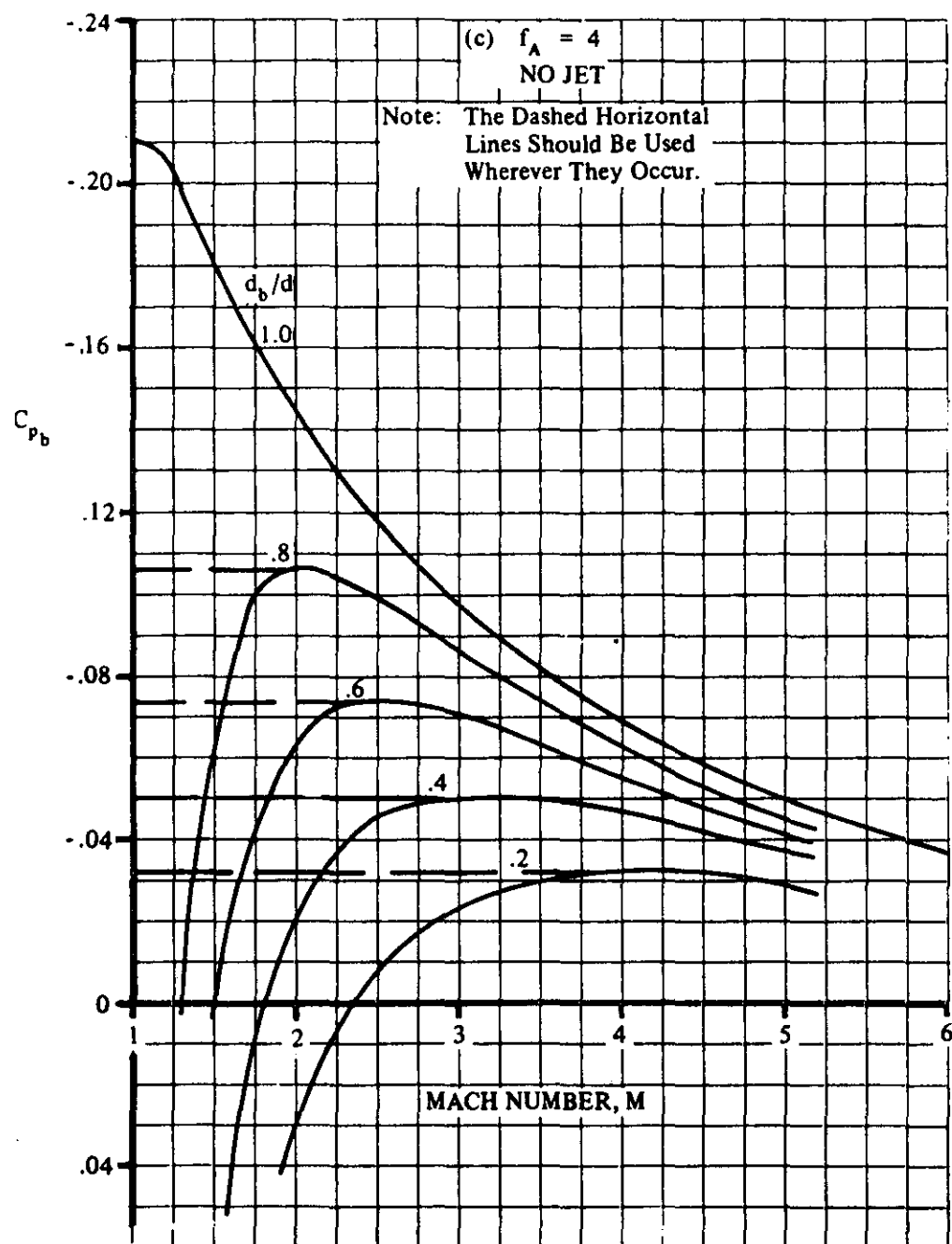
FIGURE 4.2.3.1-55 (CONTD)
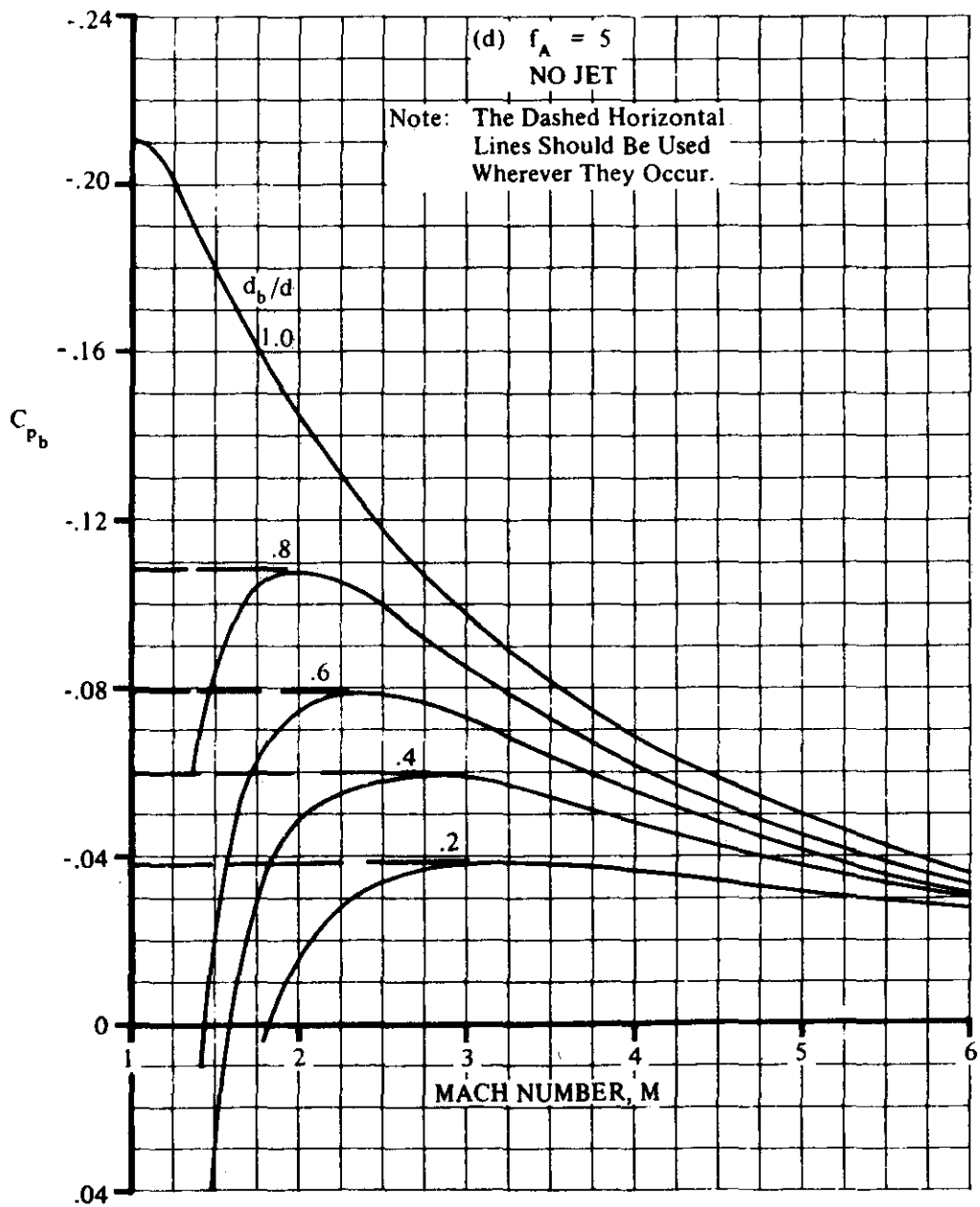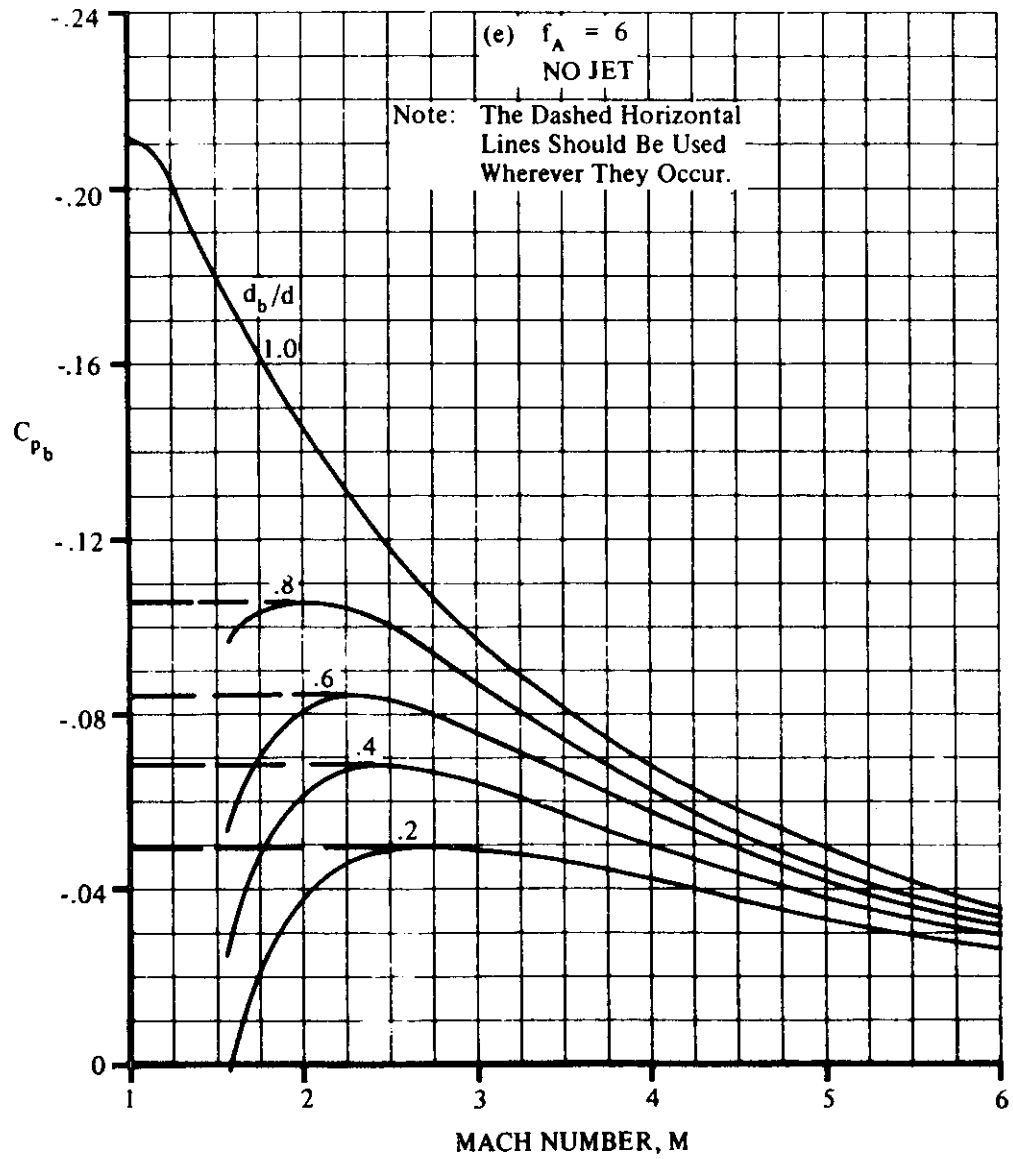
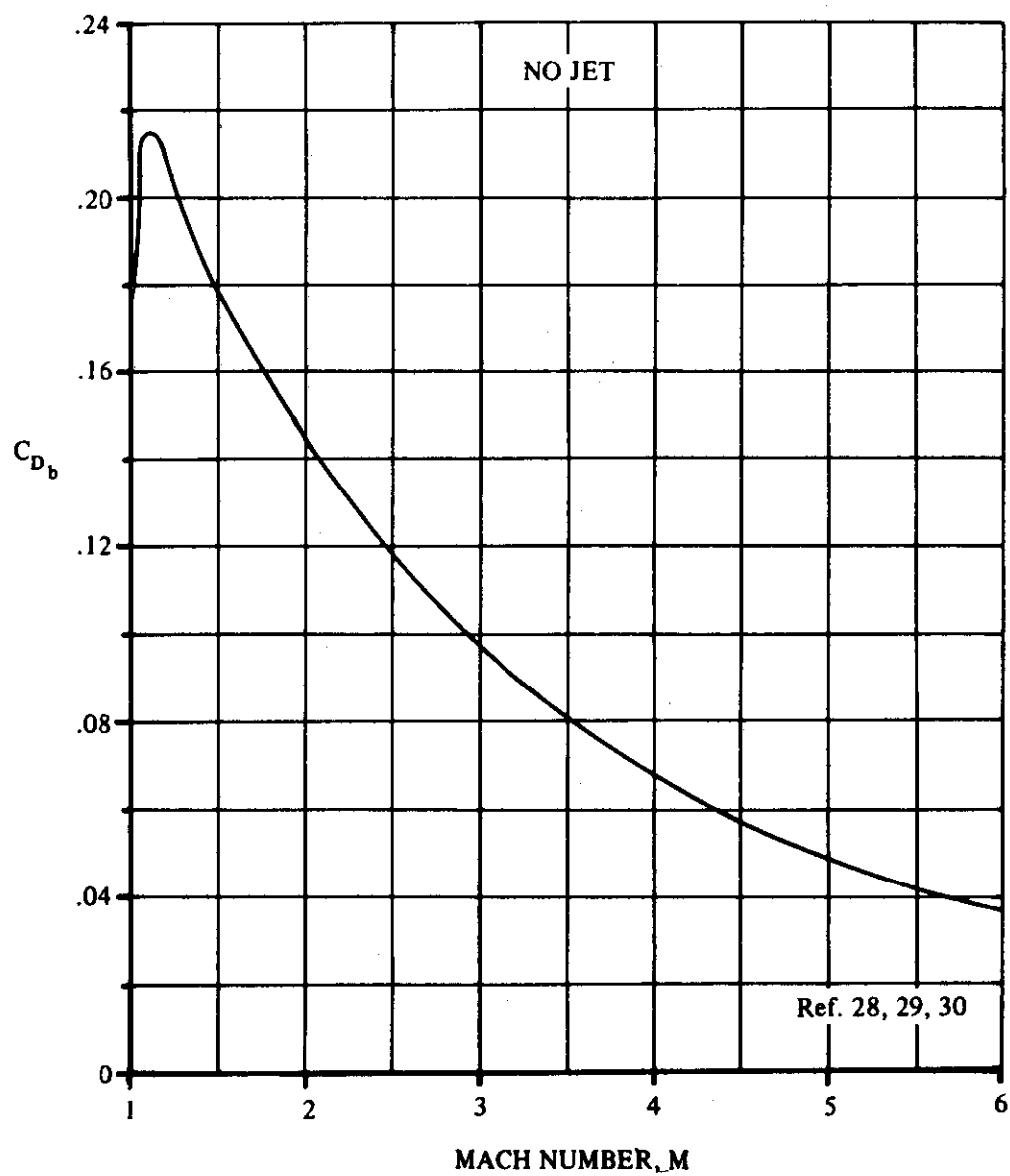FIGURE 4.2.3.1-55 (CONTD)

FIGURE 4.2.3.1-55 (CONTD)

FIGURE 4.2.3.1-60 BASE DRAG COEFFICIENT FOR BODIES OF REVOLUTION WITH NO BOATTAIL

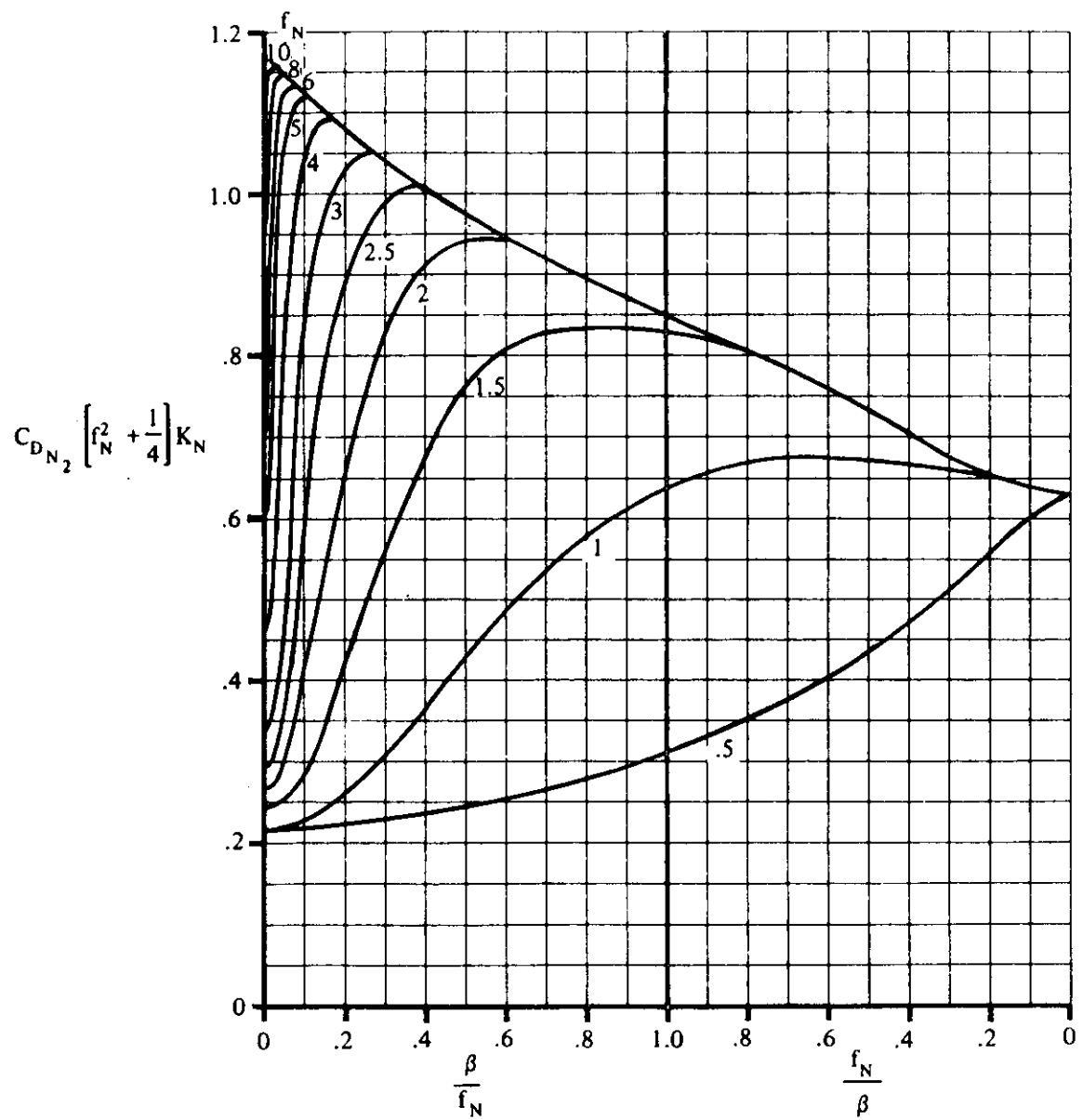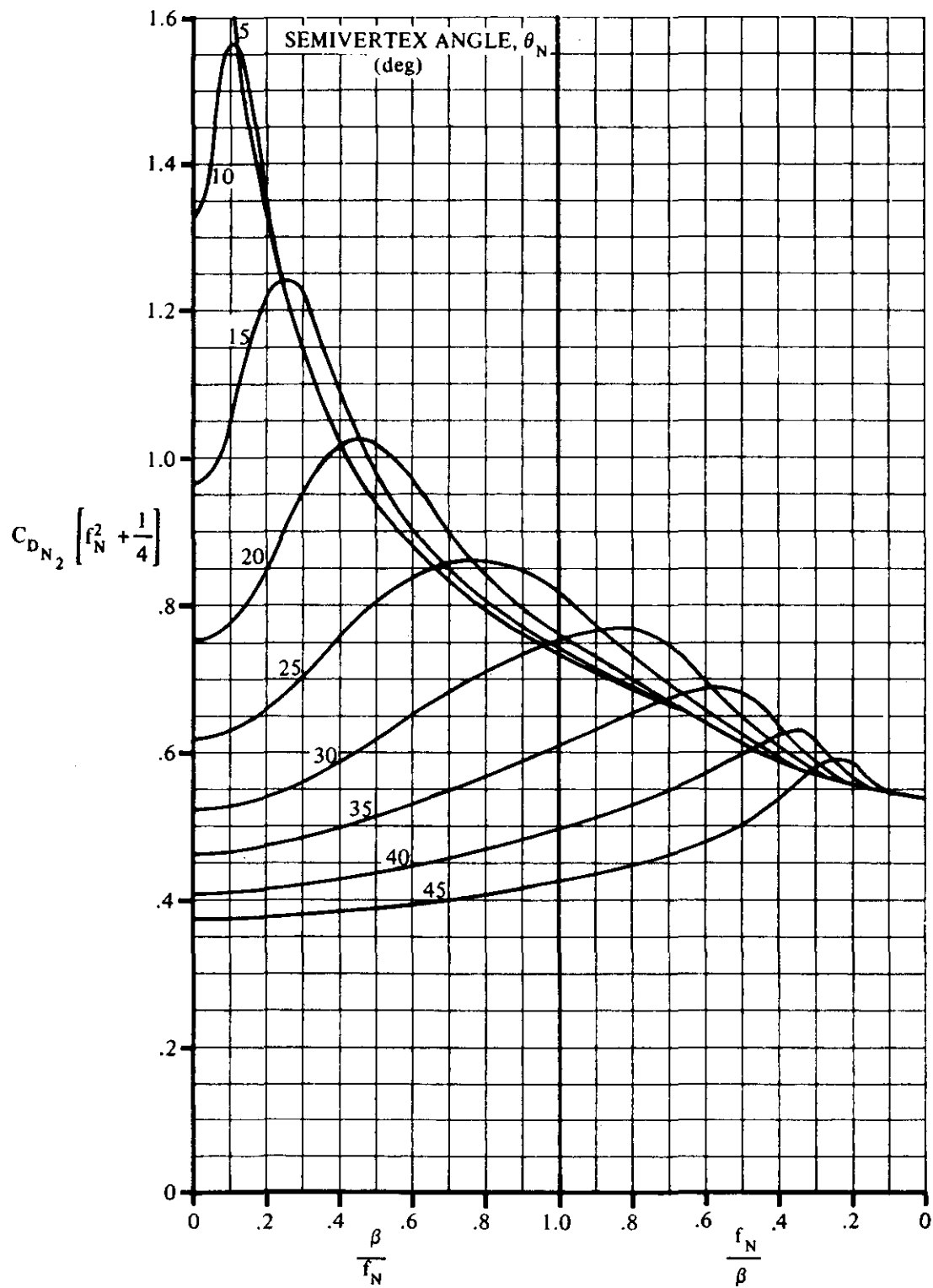FIGURE 4.2.3.1-61 SUPERSONIC PRESSURE DRAG OF OGIVE NOSES

FIGURE 4.2.3.1-62 SUPERSONIC PRESSURE DRAG OF CONICAL NOSES

4.2.3.1-62

The graph shows K_N on the vertical axis plotted against SEMIVERTEX ANGLE, θ_N (deg) on the horizontal axis, with the equation:

$$K_N = \frac{C_{D_{N_2}} \left[f_N^2 + \frac{1}{4} \right]_o}{C_{D_{N_2}} \left[f_N^2 + \frac{1}{4} \right]_\theta} \quad \text{as } M \rightarrow \infty$$
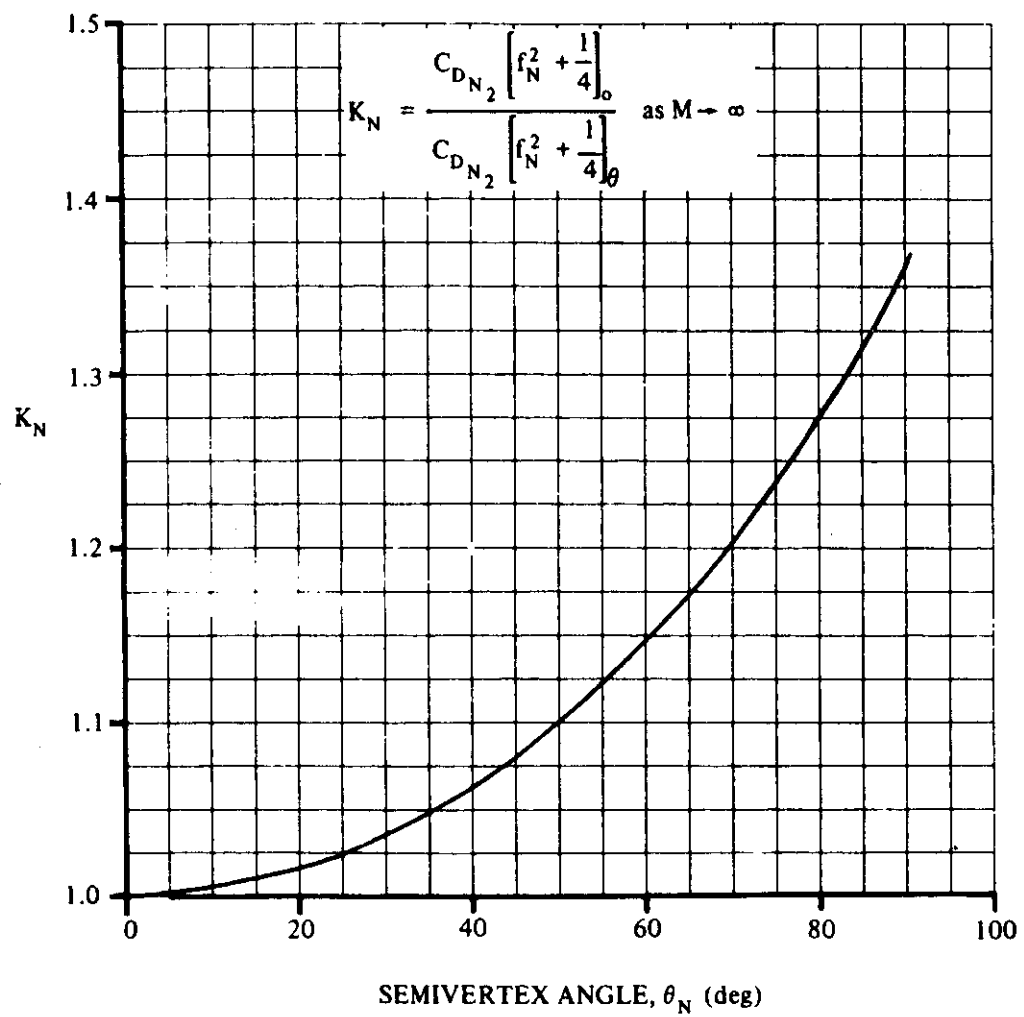
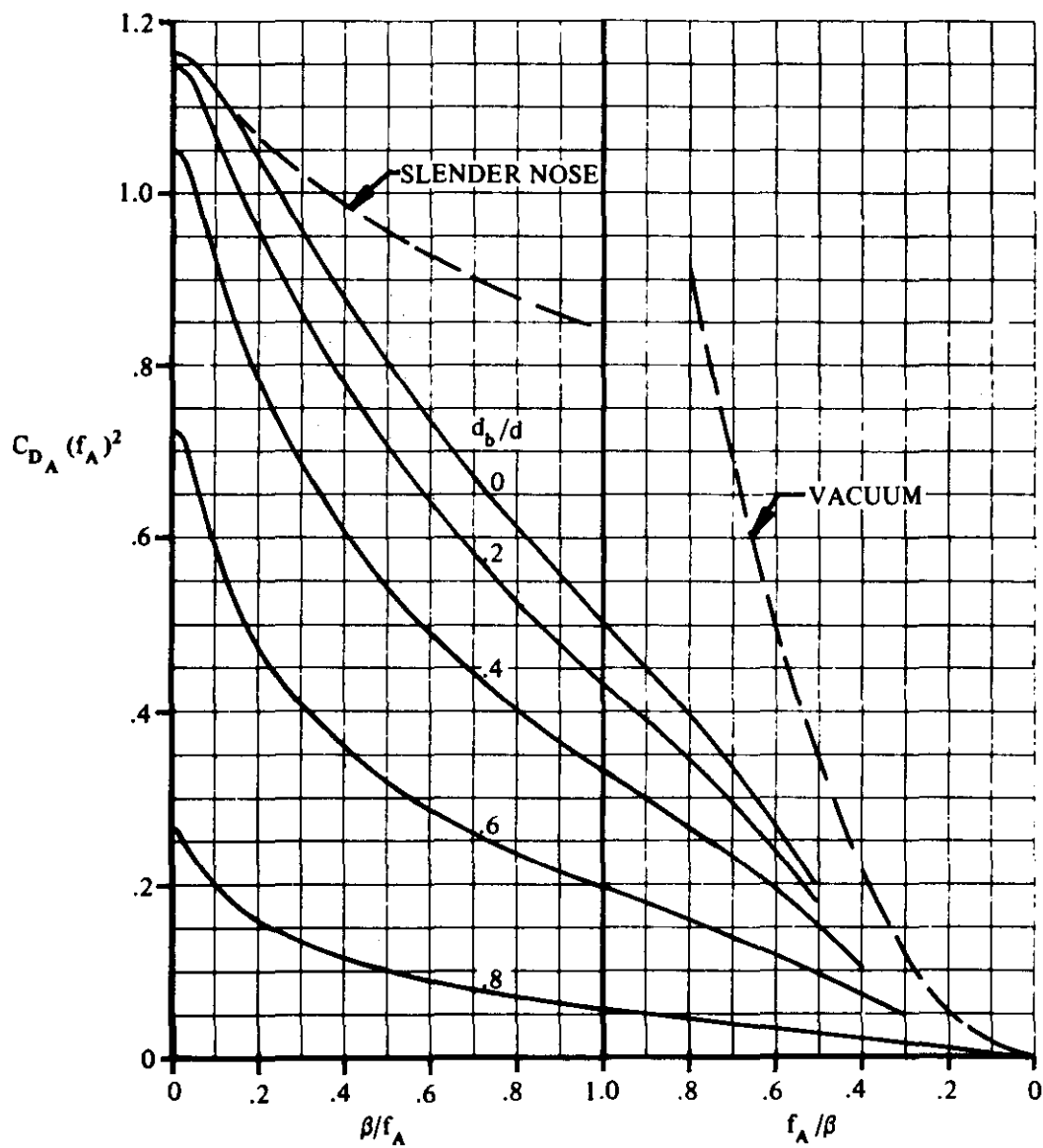FIGURE 4.2.3.1-63 CORRELATION FACTOR FOR PRESSURE DRAG OF OGIVE NOSES

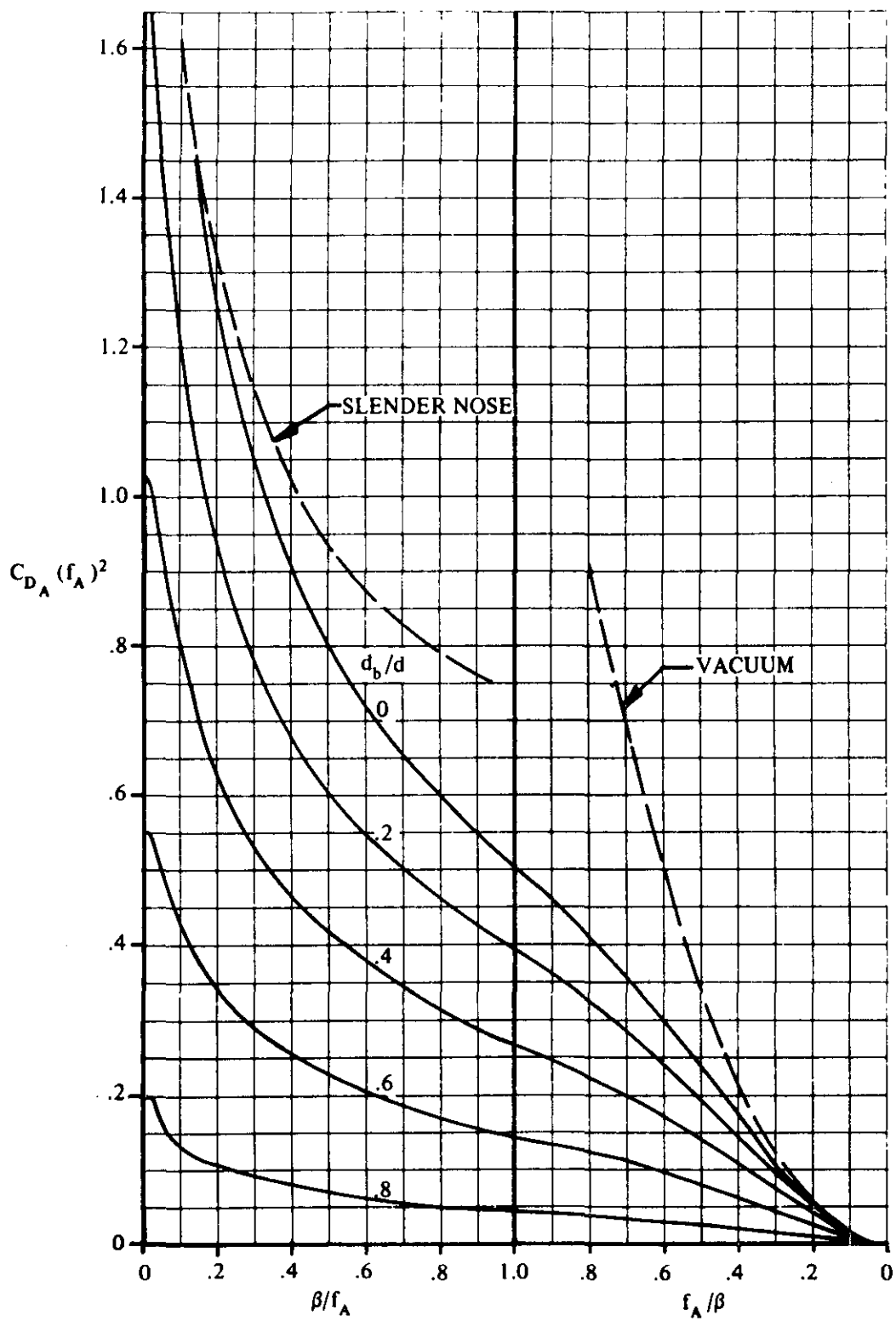FIGURE 4.2.3.1-64 SUPERSONIC PRESSURE DRAG OF OGIVE BOATTAILS

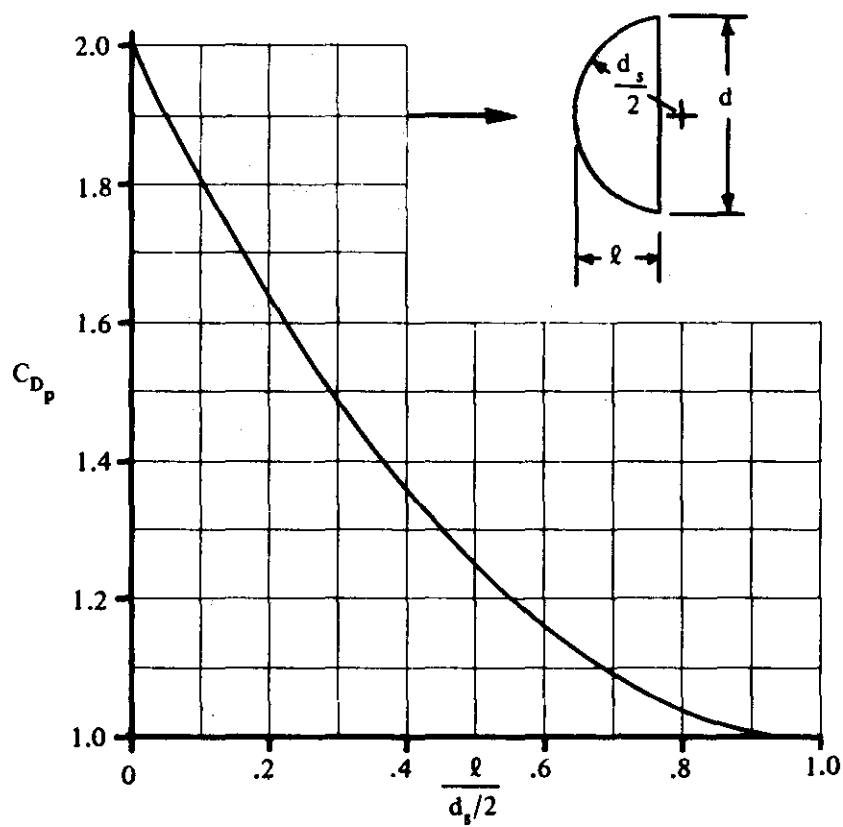FIGURE 4.2.3.1-65 SUPERSONIC PRESSURE DRAG OF CONICAL BOATTAILS

FIGURE 4.2.3.1-66 NEWTONIAN DRAG COEFFICIENT FOR SPHERICAL SEGMENTS
REFERRED TO BASE AREA OF SEGMENT
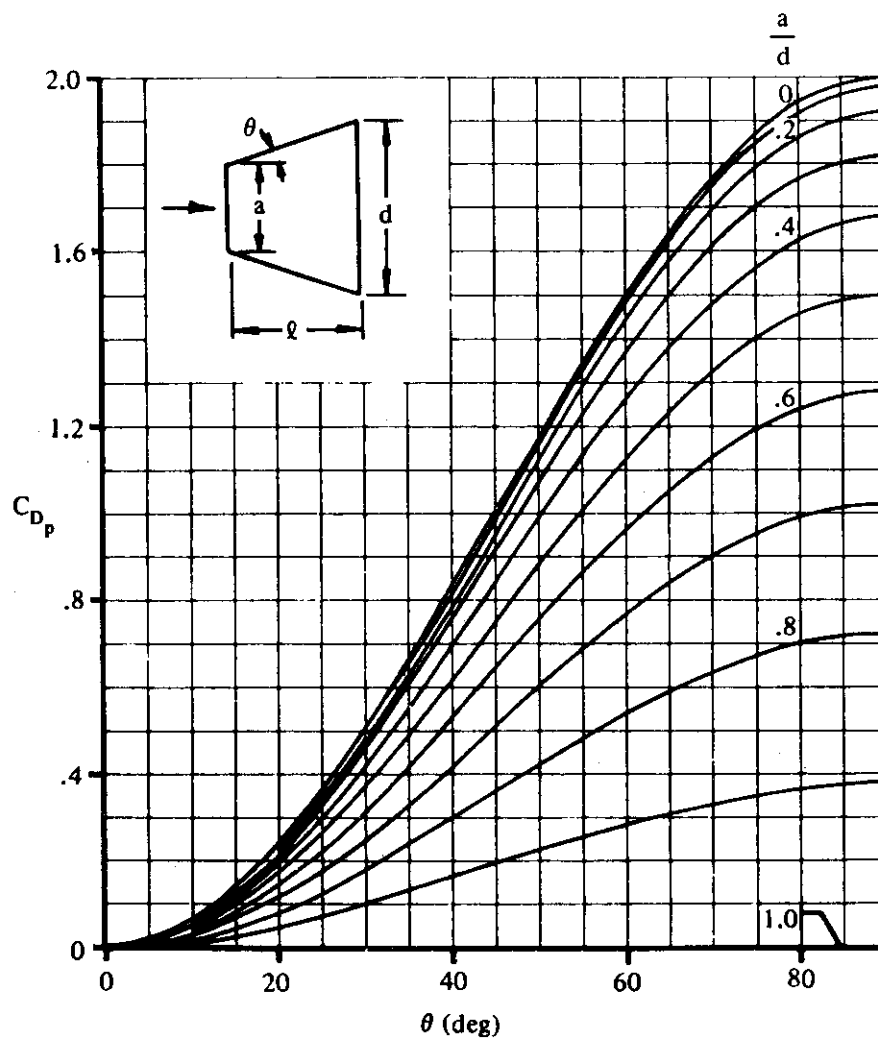
FIGURE 4.2.3.1-67 DRAG-FORCE COEFFICIENT DUE ONLY TO THE INCLINED SIDES OF A CONE
FRUSTUM CALCULATED BY NEWTONIAN THEORY.
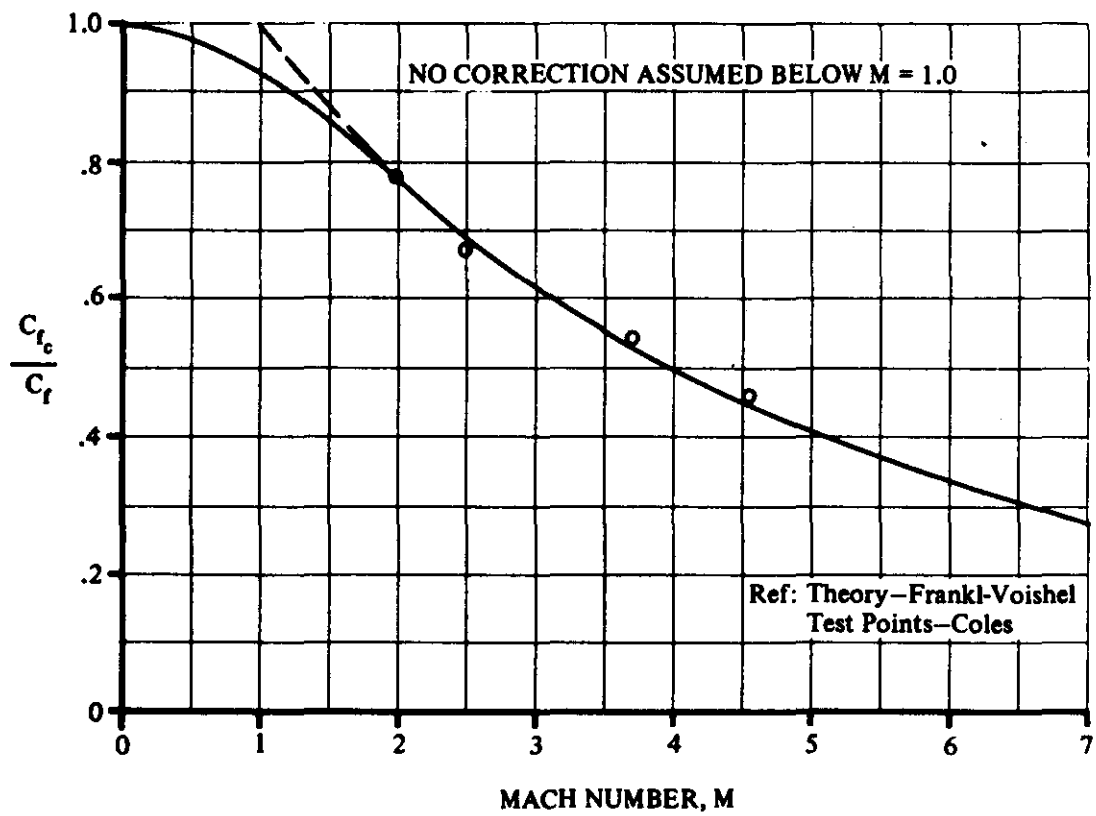C_D IS BASED ON BODY BASE AREA S_b.

FIGURE 4.2.3.1-68 COMPRESSIBILITY EFFECT ON TURBULENT SKIN FRICTION
(ZERO HEAT TRANSFER)

Reference Area:

Cylinder (axis normal to flow direction) — Cylindrical Surface Area
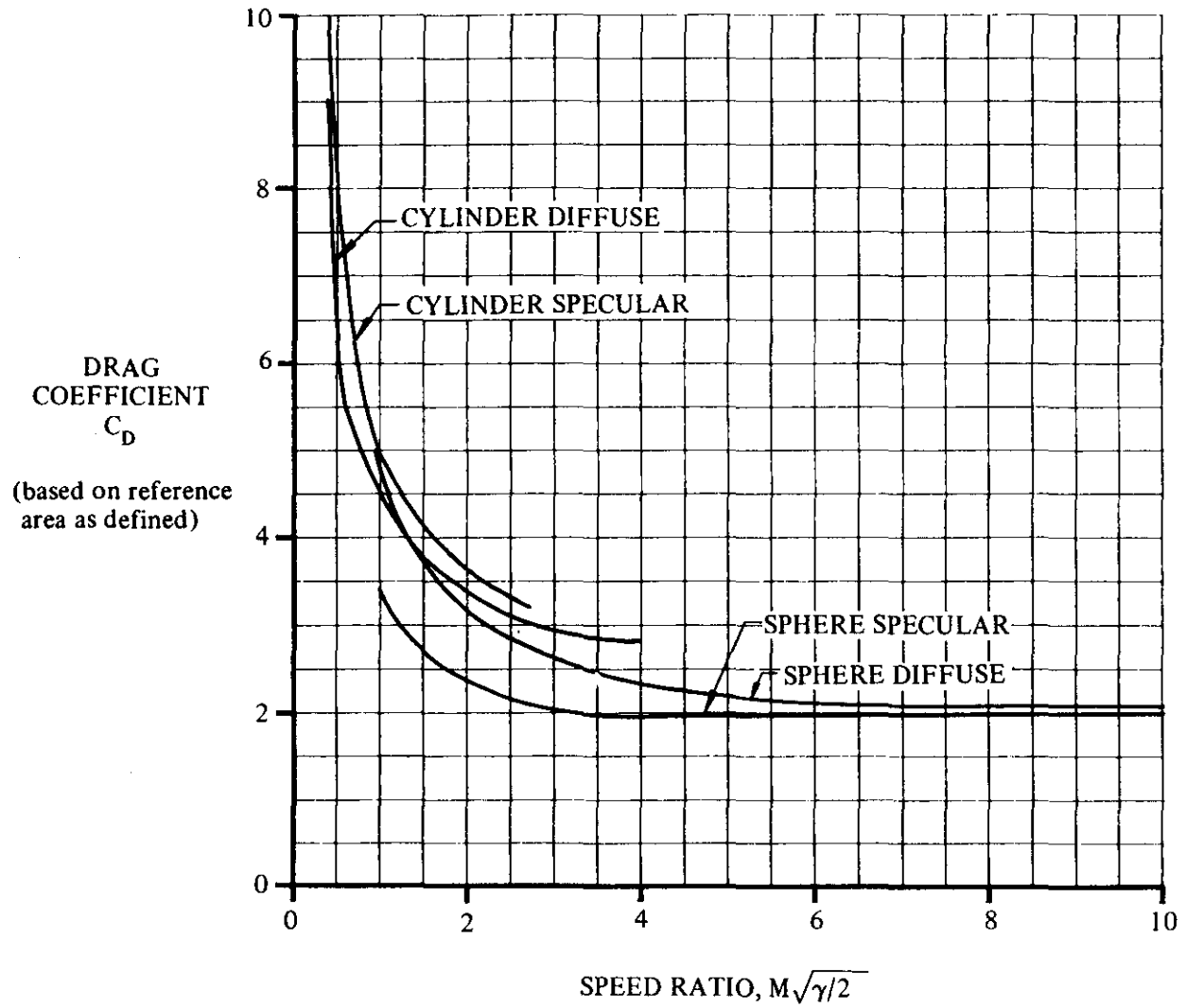Sphere — Surface Area

FIGURE 4.2.3.1-69 DRAG COEFFICIENTS FOR SPHERE AND CYLINDER IN FREE-MOLECULE FLOW

4.2.3.2 BODY DRAG AT ANGLE OF ATTACK

The drag of bodies at angle of attack is closely related to their lift and drag at zero angle of attack. The total drag of a body at angle of attack can be expressed as

$$C_D = C_{D_0} + C_D(\alpha) \qquad 4.2.3.2\text{-a}$$

where C_{D_0} is the body zero-lift drag, as developed in Section 4.2.3.1, and $C_D(\alpha)$ is the drag due to angle of attack as determined in this section. Discussions of the various applicable theories are given in Sections 4.2.1.1 and 4.2.1.2 and will not be repeated here.

A. SUBSONIC

Four methods are presented for estimating body drag due to angle of attack. The first method is taken from Reference 1 and is quite general since it applies to both short and long bodies of revolution. This method assumes that the flow is potential over the forward part of the body and has no viscous contribution in this region. On the aft part of the body, the flow is assumed to be entirely viscous, with lift arising solely from cross-flow drag. The second method, taken from Reference 2, is accurate to within ±10 percent for bodies of high fineness ratio but is not accurate for bodies of low fineness ratio. This method assumes that the viscous contribution at each station along the body is equal to the steady-state drag of a section of an infinite cylinder placed normal to a flow with velocity V sin α. This method is included for bodies of high fineness ratio because of its ease of application. The third method, taken from Reference 3, is also given because of its ease of application. This method is limited in application to small angles of attack and moderate fineness ratios. The fourth method, taken from Reference 4, presents a method of computing axial-force coefficient. This method (based on slender-body theory) applies to the angle-of-attack range of 0 to 180° for bodies with circular cross sections. It is recommended that one of the first three methods be used in the low-angle-of-attack range.

DATCOM METHODS

Method 1. General

The subsonic drag due to angle of attack of a body of revolution, based on $(V_B)^{2/3}$, is given in Reference 1 as

$$C_D(\alpha) = \frac{(k_2 - k_1)}{(V_B)^{2/3}} 2\alpha^2 S_o + \frac{2\alpha^3}{(V_B)^{2/3}} \int_{x_o}^{\ell_B} \eta \, r \, c_{d_c} \, dx \qquad 4.2.3.2\text{-b}$$

where

$$\frac{(k_2 - k_1)}{(V_B)^{2/3}} 2\alpha^2 S_o$$

is the potential-flow solution for C_{L_α} from Paragraph A of Section 4.2.1.1, multiplied by α^2

$\dfrac{2\alpha^3}{(V_B)^{2/3}} \displaystyle\int_{x_o}^{\ell_B} \eta\, r\, c_{d_c}\, dx$ is the viscous solution for C_L at angle of attack from Paragraph A of Section 4.2.1.2, multiplied by α.

α is the body angle of attack in radians.

All the parameters required to solve Equation 4.2.3.2-b are defined in Sections 4.2.1.1 and 4.2.1.2.

Method 2. Bodies of High Fineness Ratio

The subsonic drag due to angle of attack of a body of revolution, based on $(V_B)^{2/3}$, is given in Reference 2 as

$$C_D(\alpha) = 2\alpha^2\,\frac{S_b}{(V_B)^{2/3}} + \eta c_{d_c}\,\frac{S_p}{(V_B)^{2/3}}\,\alpha^3 \qquad\qquad 4.2.3.2\text{-}c$$

where

S_b is the body base area.

V_B is the total body volume.

S_p is the body planform area.

α is the body angle of attack in radians.

η is the ratio of the drag on a finite cylinder to the drag on an infinite cylinder, obtained from Figure 4.2.1.2-35a as a function of the body fineness ratio ℓ_B/d.

c_{d_c} is the experimental steady-state cross-flow drag coefficient of a circular cylinder of infinite length, obtained from Figure 4.2.1.2-35b as a function of the cross-flow Mach number at a given angle of attack.

Comparisons between results obtained by this method and test results (Reference 2) show that the body drag due to angle of attack is, in general, fairly accurately predicted up to moderate angles of attack for bodies with fineness ratios as low as about 6. For bodies with fineness ratios of about 15 and greater, the method should predict the drag due to angle of attack quite accurately over the angle-of-attack range of practical interest.

Method 3. $\alpha < 10^\circ$ and $2f \tan\alpha < 5$

For the range of parameters $\alpha < 10^\circ$ and $2f\,\tan\alpha < 5$, the simplified method of Reference 3 indicates that the subsonic drag due to angle of attack of a body of revolution, based on body base area, may be given as

4.2.3.2-2

$$C_D(\alpha) = \alpha^2 + 0.49 f^2 \; \frac{c_{d_c}}{S_b} \alpha^4 \qquad\qquad 4.2.3.2\text{-d}$$

where α is the body angle of attack in radians, f is the body fineness ratio, and the remaining parameters are defined in Method 2 above.

The first three sample problems illustrate the accuracy of the above methods applied to the same configuration.

Method 4. High Angles of Attack

The method of Reference 4 is applicable to the angle-of-attack range of 0 to 180°. Due to the complexity of calculating drag for bodies with noncircular cross sections, the Datcom method is limited to bodies with circular cross sections. For noncircular cross-section bodies, the user is referred to the treatment presented in References 4 and 5. The Datcom method predicts axial-force coefficient C_X based on body base area. Sketch (a) shows how this term may be used in conjunction with the C_N calculated in Section 4.2.1.2 to obtain C_D ($C_D = C_N \sin\alpha - C_X \cos\alpha$).
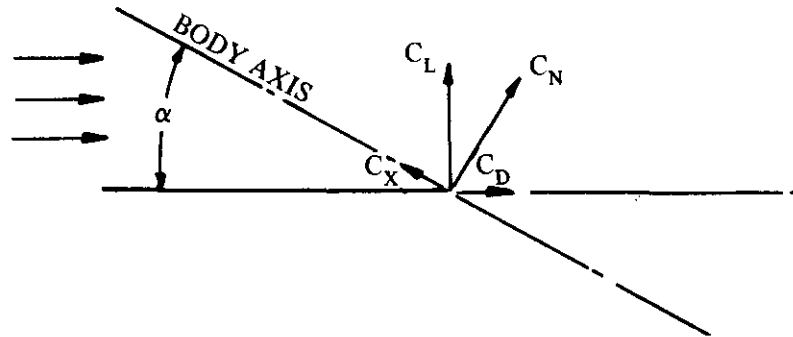
SKETCH (a)

The axial force C_X of a circular-cross-section body at an angle of attack, based on the body base area, is given by

$$C_X = C_{X_{\alpha=0}} \cos^2\alpha' \quad \text{(for } 0 \leqslant \alpha \leqslant 90^\circ\text{)} \qquad\qquad 4.2.3.2\text{-e}$$

$$C_X = C_{X_{\alpha=180^\circ}} \cos^2\alpha' \quad \text{(for } 90^\circ \leqslant \alpha \leqslant 180^\circ \qquad\qquad 4.2.3.2\text{-f}$$

and

$$C_{X_{\alpha=0}} = -(C_f + C_{D_b}) \qquad\qquad 4.2.3.2\text{-g}$$

$$C_{X_{\alpha=180^\circ}} = C_f + C_{D_b} \qquad\qquad 4.2.3.2\text{-h}$$

where

$C_{X_{\alpha=0}}$ is the axial-force coefficient at $\alpha = 0$.

α' is an incidence angle defined as $\alpha' = \alpha$ for $0 \leqslant \alpha \leqslant 90^{\circ}$, and $\alpha' = 180^{\circ} - \alpha$ for $90^{\circ} \leqslant \alpha \leqslant 180^{\circ}$.

$C_{X_{\alpha=180^{\circ}}}$ is the axial-force coefficient at $\alpha = 180^{\circ}$.

C_f is the turbulent flat-plate skin-friction coefficient based on the reference length. This value is obtained from Figure 4.2.3.2-27 as a function of Reynolds number (based on body length) and Mach number.

C_{D_b} is the base-drag coefficient based on the maximum body frontal area, given by Equation 4.2.3.1-b.

It is recommended that this method be used only in the high-angle-of-attack range where other Datcom methods are not applicable. No substantiating test data are available for this method in the subsonic speed range.

Sample Problems

1. Method 1

Given: The parabolic body of revolution of Reference 10.
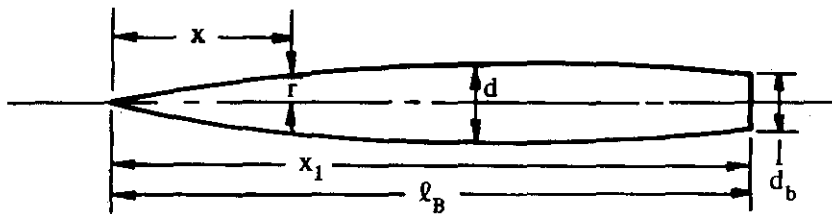
$\ell_B = 5.04$ ft $d = 0.510$ ft $d_b = 0.376$ ft $f = 9.87$

$V_B = 0.687$ cu ft; $(V_B)^{2/3} = 0.7786$ sq ft $M = 0.40$ $0 \leq \alpha \leq 18^{\circ}$

Body ordinates: $r = 0.255 \left[1 - \left(1 - \dfrac{2x}{6.375} \right)^2 \right]^{3/4}$

Compute:

Potential Flow Term   (Section 4.2.1.1)

$x_1 = 5.04$ ft*

$x_1/\ell_B = 5.04/5.04 = 1.0$

---

* x_1 may be determined by inspection for this case

4.2.3.2-4

$x_o / \ell_B = 0.903$ (Figure 4.2.1.1-20b)

$x_o = (0.903)(5.04) = 4.55$ ft

$$S_o = \pi(r_o)^2 = \pi \left\{ 0.255 \left[1 - \left(1 - \frac{2x_o}{6.375} \right)^2 \right]^{3/4} \right\}^2 = \pi \left\{ 0.255 \left[1 - \left(1 - \frac{(2)(4.55)}{6.375} \right)^2 \right]^{3/4} \right\}^2$$

$$= 0.151 \text{ sq ft}$$

$(k_2 - k_1) = 0.938$ (Figure 4.2.1.1-20a)

$$\frac{(k_2 - k_1)}{(V_B)^{2/3}} 2\alpha^2 S_o = \frac{(0.938)}{(0.7786)} 2\alpha^2 (0.151) = 0.364 \, \alpha^2$$

Viscous Term   (Section 4.2.1.2)

$\eta = 0.685$ (Figure 4.2.1.2-35a)

$c_{d_c} = f(M_c); \quad M_c = M \sin \alpha$

M_c varies between $0.40 \sin (0)$ to $0.40 \sin 18^\circ$; $\quad 0 \le M_c \le 0.1236$

$c_{d_c} = 1.20$ (constant)   (Figure 4.2.1.2-35b)

$$\int_{x_o}^{\ell_B} \eta \, r \, c_{d_c} \, dx = (0.685)(1.20) \int_{x_o}^{\ell_B} r \, dx = 0.822 \sum_{x_o}^{\ell_B} r \, \Delta x$$

x	r*	Δx	rΔx
$x_o = 4.55$			
	0.2136	0.20	0.043
4.75			
	0.2010	0.20	0.040
4.95			
	0.1906	0.09	0.017
$\ell_B = 5.04$			

$\Sigma r \Delta x = 0.100$

$$\int_{x_o}^{\ell_B} \eta \, r \, c_{d_c} \, dx = (0.822)(0.100) = 0.0822$$

---

* r is taken to be at the midpoint of each body segment.

$$\frac{2\alpha^3}{(V_B)^{2/3}} \int_{X_o}^{\ell_B} \eta \, r \, c_{d_c} \, dx = \frac{2\alpha^3}{(0.7786)} (0.0822) = 0.211 \, \alpha^3$$

Solution:

$$C_D(\alpha) = \frac{(k_2 - k_1)}{(V_B)^{2/3}} 2\alpha^2 S_o + \frac{2\alpha^3}{(V_B)^{2/3}} \int_{X_o}^{\ell_B} \eta \, r \, c_{d_c} \, dx \quad \text{(Equation 4.2.3.2-b)}$$

$$= 0.364 \, \alpha^2 + 0.211 \alpha^3$$

①	②	③	④	⑤
α (deg)	α (rad)	α^2 (rad^2)	α^3 (rad^3)	$C_D(\alpha)$ 0.364 ③ + 0.211 ④
0	0	0	0	0
2	0.0349	0.00122	0.00004	0.0005
4	0.0698	0.00487	0.00034	0.0018
6	0.1047	0.01096	0.00115	0.0042
8	0.1396	0.01949	0.00272	0.0077
10	0.1745	0.03045	0.00531	0.0122
12	0.2094	0.04385	0.00918	0.0179
14	0.2443	0.05968	0.01458	0.0248
16	0.2792	0.07795	0.02176	0.0330
18	0.3141	0.09866	0.03099	0.0425

The calculated results are compared with test values from Reference 10 in Sketch (b).

2. Method 2

Given: The same configuration as in Sample Problem 1.

Additional Characteristics:

$$S_b = 0.111 \text{ sq ft} \qquad S_p = 2.016 \text{ sq ft}$$

Compute:

Potential Flow Term

$$2\alpha^2 \frac{S_b}{(V_B)^{2/3}} = 2\alpha^2 \left(\frac{0.111}{0.7786}\right) = 0.285 \, \alpha^2$$

Viscous Term

$$\eta = 0.685$$
$$c_{d_c} = 1.20 \quad \Big\} \text{(Sample Problem 1)}$$

$$\eta \, c_{d_c} \frac{S_p}{(V_B)^{2/3}} \, \alpha^3 = (0.685)(1.20)\frac{2.016}{0.7786}\alpha^3 = 2.128 \, \alpha^3$$

Solution:

$$C_D(\alpha) = 2\alpha^2 \frac{S_b}{(V_B)^{2/3}} + \eta \, c_{d_c}\frac{S_p}{(V_B)^{2/3}}\alpha^3 \quad \text{(Equation 4.2.3.2-c)}$$

$$= 0.285\,\alpha^2 + 2.128\,\alpha^3$$

①	②	③	④	⑤
α (deg)	α (rad)	α^2 (rad^2)	α^3 (rad^3)	$C_D(\alpha)$ $0.285 \, ③ + 2.128 \, ④$
0	(See calculation table, Sample Problem 1)			0
2				0.0004
4				0.0021
6				0.0056
8				0.0113
10				0.0200
12				0.0320
14				0.0480
16				0.0685
18				0.0941

The calculated results are compared with test values from Reference 10 in Sketch (b).

3. Method 3

Given: The same configuration as in Sample Problems 1 and 2.
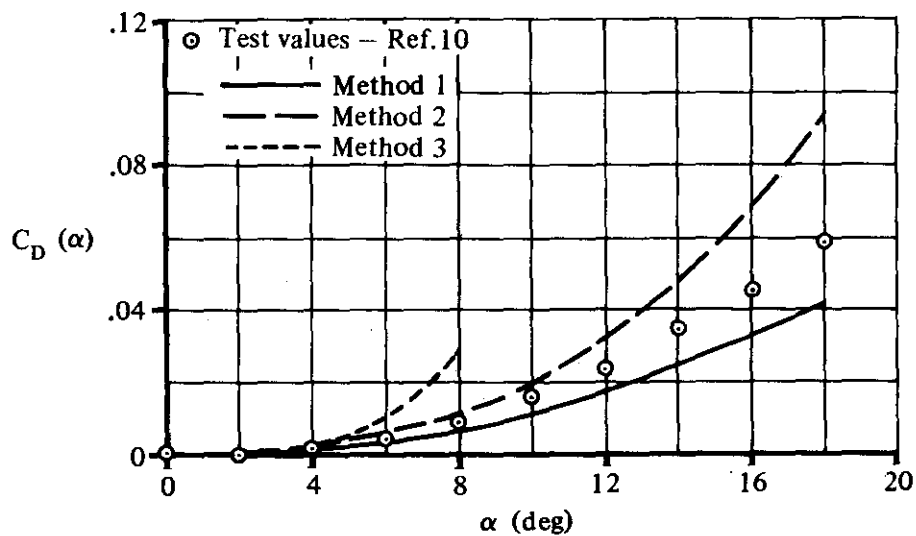
Compute:

$$c_{d_c} = 1.20 \text{ (Sample Problem 1)}$$

2f tan α > 5 for α > 14.2°; therefore, the problem is limited to angles of attack < 10°.

Solution:

$$C_D(\alpha) = \alpha^2 + 0.49 \, f^2 \frac{c_{d_c}}{S_b} \, \alpha^4 \quad \text{(Equation 4.2.3.2-d)}$$

$$= \alpha^2 + (0.49)(9.87)^2 \frac{1.20}{0.111} \alpha^4$$

$$= \alpha^2 + 516 \, \alpha^4$$

①	②	③	④	⑤	⑥
α (deg)	α (rad)	α^2 (rad^2)	α^4 (rad^4)	$C_D(\alpha)$ (based on S_b) ③ + 516 ④	$C_D(\alpha)$ (based on $(V_B)^{2/3}$) ⑤ $S_b/(V_B)^{2/3}$
0	0	0	0	0	0
2	0.0349	0.00122	0.000001	0.00173	0.0002
4	0.0698	0.00487	0.000024	0.01725	0.0025
6	0.1047	0.01096	0.00012	0.07286	0.0104
8	0.1396	0.01949	0.00038	0.21549	0.0307

The calculated results from Column 6 are compared with test values from Reference 10 in Sketch (b)

SKETCH (b)